Mycosynthesis of Inorganic Nanoparticles and their Evaluation in Catalysis and Nano-fertilization

THESIS

Submitted in partial fulfilment
of the requirements for the degree of
DOCTOR OF PHILOSOPHY

by

ARPIT BHARGAVA

Under the Supervision of
Prof. Jitendra Panwar

BIRLA INSTITUTE OF TECHNOLOGY AND SCIENCE, PILANI

2016

Mycosynthesis of Inorganic Nanoparticles and their Evaluation in Catalysis and Nano-fertilization

THESIS

Submitted in partial fulfilment
of the requirements for the degree of
DOCTOR OF PHILOSOPHY

by

ARPIT BHARGAVA

Under the Supervision of
Prof. Jitendra Panwar

BITS Pilani
Pilani | Dubai | Goa | Hyderabad

BIRLA INSTITUTE OF TECHNOLOGY AND SCIENCE, PILANI
2016

BIRLA INSTITUTE OF TECHNOLOGY AND SCIENCE, PILANI

CERTIFICATE

This is to certify that the thesis entitled "**Mycosynthesis of Inorganic Nanoparticles and their Evaluation in Catalysis and Nano-fertilization**" submitted by **Arpit Bhargava, ID. No. 2009PHXF411P** for award of Ph.D. Degree of the Institute embodies original work done by him under my supervision.

_____

Signature of the Supervisor

Name   : **JITENDRA PANWAR**

Date: Designation: **Associate Professor**

अनेकसंशयोच्छेदि, परोक्षार्थस्य दर्शकम् ।

सर्वस्य लोचनं शास्त्रं, यस्य नास्ति अन्धैव सः ॥

That which foresees what isn't obvious, that which obliterates
doubts, science is the eye, without which one is blind

ACKNOWLEDGEMENTS

ABSTRACT

  The impact of nanotechnology is increasing at tremendous pace due to its remarkable potential. Nanoparticles are considered as the protagonist of the nanotechnology revolution. Amid nanoparticles, inorganic nanoparticles are of special interest due to their unique and tuneable properties. In recent years, the surging demand of nanoparticles has boosted unprecedented expansion of research for the development of high yielding and sustainable synthesis methods which can deliver nanomaterials with desired characteristics. Unlike the well-established physico-chemical methods which have various limitations, biological methods inspired by mimicking natural biomineralization processes have great potential for nanoparticle synthesis. Of special interest, microorganisms isolated from metal rich regions develop resistance mechanism for their survival which can be exploited for synthesis of metal or metal oxide nanoparticles. Among various metal tolerant microorganisms, fungi represents a favourable natural machinery due to its large and most diverse secretome making it highly anticipated for on-cell/ extracellular synthesis of nanoparticles. Following this rationale and the hypothesis that "well adapted fungi isolated from native metal rich soil conditions can be a better source for bio-inspired synthesis of metal nanoparticles" the present work serves as the initial step in development of an eco-friendly method for synthesis of iron oxide and gold nanoparticles (IONPs and Au NPs) by selecting a promising fungal isolate.

  Soil samples were collected from two metal rich regions across India to isolate fungi. All the fungal isolates were identified at molecular level followed by their screening for metal tolerance ability against iron and gold ions. Fungal isolates exhibiting prominent metal tolerance were further evaluated for their potential for synthesis of IONPs and Au NPs. Among various isolates, *Aspergillus japonicus* AJP01 showed ability for extracellular synthesis of IONPs by hydrolyzing the precursor salt solution under ambient conditions. The synthesized particles were cubic in shape with a size range of 60-70 nm with crystal structure corresponding to magnetite. FTIR spectroscopy confirmed the presence of proteins on as-synthesized IONPs. SDS-PAGE analysis of extracellular proteins demonstrated the possibility of substrate dependent protein expression advocating the role of one or more proteins in coprecipitation, controlled nucleation and/or stabilization of nanoparticles.

  Among the various fungal isolates screened to test their ability of Au NPs synthesis, *Aspergillus japonicus* AJP01 was found to synthesize spherical Au NPs on its surface. Extracellular synthesis of Au NPs was achieved using two indigenous fungi, *Cladosporium oxysporum* AJP03 and *Lichtheimia ramosa* AJP11. The as-synthesized nanoparticles were characterized by standard techniques to confirm their size, shape, distribution and crystallinity. A series of experiments were conducted to study the effect of various process parameters on particle size and yield during extracellular synthesis. Investigations were also performed to elucidate the mechanism involved in extracellular

synthesis of Au NPs by *Lichtheimia ramosa* AJP11. The obtained results provided appreciable evidence supporting the role of extracellular proteins in the reduction of gold ions followed by their nucleation and stabilization.

The efficacy and efficiency of mycosynthesized Au NPs was explored in the field of catalysis. Supported and unsupported Au NPs synthesized using fungi were used as heterogeneous and homogenous catalyst, respectively. The catalytic efficiency of fungal biomass supported Au NPs was tested by catalysing the A^3 coupling reactions to synthesize propargylamine. The nanoparticle-fungal hybrid was also found to catalyse sodium borohydride mediated reduction reaction of 4-nitophenol and hexacyanoferrate (III). Free and unsupported protein capped Au NPs were employed for the reduction of environmentally hazardous organic dyes viz., rhodamine B, bismark brown, methyl orange and methylene blue. Owing to the presence of surface proteins, the nanoparticles exhibited excellent dye degradation efficiency.

Assessment of iron oxide nanoparticle as a source of micronutrient in plants was evaluated. For this, a systematic comparison of various iron forms viz., ionic, bulk and nanoparticles (chemically and biologically synthesised) at different metal concentrations were made using wheat and spinach as test plants. Seed germination assay and a sub-pilot experimental field study using foliar spray approach was conducted to determine the effect of various iron forms on wheat plant growth and grain yield. In addition, pot study was carried out to determine the effect of foliar spray of various iron forms on growth and biomass production of spinach. The results advocated the possibility of using iron oxide nanoparticles as potential nano-fertilizers.

First of a kind of study for the assessment of toxicological potential of nanotechnology derived food in rodents was carried out. The effect of wheat sprayed with magnetite nanoparticles on female Wistar rats was evaluated using 90-day sub-acute repeated dose oral toxicity experiment. The toxicity of test substance was compared with other experimental variables. Essential checkpoints like monitoring of health status, food and water intake by animals was carried out throughout the feeding trial followed by measurement of haematological and clinical biochemistry parameters, examination of gross necroscopy and histopathology of selected tissues at terminal sacrifice. In conclusion, results showed lack of toxicity of test substance under experimental conditions.

Overall, the present research work revolves around mycosynthesis and application of inorganic nanoparticles. Commercially important metals (iron and gold) were chosen for synthesis of nanoparticles using biological approaches, particularly by exploiting the potential of metal tolerant soil fungi. Attempts were made to increase the efficiency of the synthesis protocol by optimizing various reaction parameters and understanding the involved molecular mechanism. Application of Au NPs were explored in the field of catalysis for fine chemical synthesis and dye remediation. IONPs were assessed to test

their potential as nano-fertilizer by conducting sub-pilot field and pot scale experiments using wheat and spinach plants, respectively. The as-obtained nanotechnology derive food (wheat) was evaluated for its toxicological potential in rodents on the basis of recommended guidelines.

TABLE OF CONTENTS

LIST OF TABLES

LIST OF FIGURES

LIST OF ABBREVIATIONS

Symbol	Abbreviation
μg	Microgram
μL	Microliter
μm	Micrometer
μmol	Micromole
4-AP	4-aminophenol
4-NP	4-nitrophenol
AAS	Atomic Absorption Spectroscopy
ABTS	2,2'-Azino-di-[3-ethylbenzthiazoline sulphonate]
ALP	Alkaline phosphatase
ALT	Alanine aminotransferase
am	After meridian
ANOVA	Analysis of Variance
AST	Aspartate aminotransferase
B.C	Before Christ
BCA	Bicinchoninic acid
B-Fe3O4	Biologically synthesized magnetite nanoparticles
BITS	Birla Institute of Technology and Science
BLAST	Basic Local Alignment Search Tool
bp	Base pair
C	Celsius
Cat	Catalogue
CAZRI	Central Arid Zone Research Institute
CBB	Coomassie Brilliant blue
Cfu	Colony forming unit
Chem	Chemical
cm	Centimeter
CV	Column volume
d.nm	Diameter in nanometer
DLS	Dynamic Light Scattering
DNA	Deoxyribonucleic acid
dS	DeciSiemens
EC	Electrical conductivity
EC number	Enzyme commission number
EDS	Energy dispersive spectroscopy
EDTA	Ethylenediaminetetraacetic acid
EFSA	European Food Security Authority
EU	Enzyme unit
eV	Electron volt
FAOSTAT	Food and agriculture organization statistical database
Fcc	Face centered cubic
FDA	Food and Drug Administration
FTIR	Fourier transform infrared
FWHM	Full width half maximum
GIXRD	Grazing incidence X-ray diffraction
GM	Genetically modified
h	Hour
ha	Hectare

Symbol	Abbreviation
HCT	Haematocrit
HGB	Haemoglobin
HR-TEM	High Resolution Transmission Electron microscopy
IAEC	Institutional Animal Ethics Committee
ICCD	International Centre for Diffraction Data
IM	Inner membrane
IONPs	Iron oxide nanoparticles
IR	Infrared
IRB	Iron reducing bacteria
ITS	Internal transcribed spacer
JCPDS	Joint Committee on Powder Diffraction Standards
kDa	Kilo Dalton
KeV	Kilo electron Volt
Kg	Kilogram
kV	Kilovolt
L	Liter
LDH	Lactate dehydrogenase
Ltd	Limited
m	Meter
M	Molar
mA	Milliampere
MALDI-MS	Matrix Assisted Laser Desorption/Ionisation Mass spectrometry
mbar	Millibar
MCHC	Mean corpuscle haemoglobin concentration
MCV	Mean corpuscle volume
MDH	Malate dehydrogenase
mg	Milligram
MGYP	Malt Glucose Yeast extract Peptone
min	Minute
ml	Milliliter
mm	Millimeter
mM	Millimolar
mmol	Millimolar
MPa	Megapascal
MRI	Magnetic resonance imaging
MTB	Magnetotactic bacteria
MTC	Maximum tolerable concentration
MTCC	Microbial Type Culture Collection
N	Normal
n	Number of replicates
NADH	Nicotinamide adenine dinucleotide
NBT	Nitroblue tetrazolium
NCBI	National Center for Biotechnology Information
$N\text{-}Fe_2O_3$	Maghemite nanoparticles
$N\text{-}Fe_3O_4$	Magnetite nanoparticles
ng	Nanogram
nm	Nanometer
NMR	Nuclear magnetic resonance
No	Number

Symbol	Abbreviation
NPs	Nanoparticles
ns	Non-significant
OD	Optical density
OECD	Organization for Economic Co-operation and Development
OM	Outer membrane
PAGE	Polyacrylamide gel electrophoresis
PBS	Phosphate buffered saline
PCR	Polymer chain reaction
PDA	Potato dextrose agar
PDI	Polydispersity index
PLT	Blood platelet
pm	Post meridian
pmol	Picomole
PVDF	Polyvinylidene difluoride
QTOF	Quadrupole Time-of-Flight
RBC	Red blood cell
Rf	Retention factor
ROS	Reactive oxygen species
rpm	Rotations per minute
rRNA	Ribosomal ribonucleic acid
S.D	Standard Deviation
SAED	Selected area electron diffraction
SDS	Sodium dodecyl sulphate
SEC	Size exclusion chromatography
SEM	Scanning electron microscope
SPM	Scanning Probe Microscopy
SPR	Surface plasmon resonance
T	Type strain
TAC	Total anti-oxidant capacity
TEM	Transmission Electron Microscopy
TLC	Thin layer chromatography
UK	United Kingdom
USA	United States of America
USEPA	United States Environmental Protection Agency
UV	Ultra violet
V	Volt
v/v	volume/volume
w/v	weight/volume
w/w	weight/weight
WBC	White blood cell
XPS	X-ray photoelectron spectroscopy
XRD	X-ray diffraction

Chapter I

General Introduction

Preface

This chapter represents a general introduction to the research work carried out in this thesis. It gives a brief overview of nanotechnology and nanoparticles. The potential of various top-down and bottom-up approaches for the synthesis of nanoparticles has been discussed. Further, potential applications of nanoparticles have been described with special emphasis on gold and iron oxide nanoparticles. Finally, the gap in the existing research is presented along with the thesis objectives.

1.1 Nanotechnology

The term "Nanotechnology" literally means a technology performed at or on nanoscale. The idea of nanotechnology was first presented by physicist and Nobel Laureate Richard Feynman on December 29, 1959 during his lecture entitled "There is plenty of room at the bottom" at the annual meeting of the American Physical Society, California Institute of Technology, USA. He speculated the possibility and potential of nanosized materials and proposed the concept of manipulating individual atoms to make new small structures having very different properties. In his own words *"The principles of physics, as far as I can see, do not speak against the possibility of maneuvering things atom by atom. It is not an attempt to violate any laws; it is something, in principle, that can be done; but in practice, it has not been done because we are too big"*. Japanese scientist Norio Taniguchi coined the term "Nanotechnology" in 1974. Eric Drexler introduced this term in his book "Engineer of Creation" published in 1986 and brought it into the public domain. Today as we know, nanotechnology encompasses the synthesis, characterization, exploration and application of nanosized materials by integrating principles of physical, chemical, and biological sciences. The resulting product deals with scales ranging from individual atoms or molecules to submicron dimensions, as well as the integration of the resulting nanostructures into larger systems (Kaehler 1994). Nanotechnology cannot be considered as a single discipline but is a domain in science and technology. The field of nanotechnology is too vast, too interdisciplinary and too rapidly changing to cover exhaustively. The interdisciplinary nature of the field makes it somewhat difficult for researchers in one field to understand and draw on developments in another area (Pool and Owens 2006). There have been impressive developments in the field of nanotechnology in the recent past, with numerous methodologies developed to synthesize nanomaterial of particular characteristics depending on specific requirements. New applications of these nanomaterials are increasing rapidly. The developments are strictly due to the improvement of characterization and synthesis techniques on the nanometer scale. This allowed the release of scientist's innate curiosity toward a field generous of new physical phenomena and synthetic opportunities.

Nanotechnology is likely to have a profound impact on our economy and society in the early twenty-first century (Nel et al. 2015). Research in nanotechnology promises breakthroughs in areas as materials and manufacturing, nanoelectronics, medicine and healthcare, energy, biotechnology, information technology, and space technology. It is widely felt that nanotechnology will be the next industrial revolution. In terms of fiscal statistics, the global market for nanotechnology products was valued at $22.9 billion in 2013 which increased to about $26 billion in 2014. This market is expected to reach about $64.2 billion by 2019 with a compound annual growth rate of 19.8% from 2014 to 2019 (Nanotechnology: A Realistic Market Assessment, BCC Research).

1.2 Nanoparticles and their unique features

Nanoparticle can be defined as particles with at least one dimension in the range of 1-100 nm (Mohanraj and Chen 2007). Nanoparticles are known to exist in diverse shapes such as spherical, triangular, cubical, pentagonal, rod-shaped, shells, ellipsoidal and so forth. They are used as building blocks to construct complex nanostructures such as nanochains, nanowires, nanoclusters and nanoaggregates. Nanoparticles serve as a bridge between molecular and micron world. Nanoparticles contain small enough number of atoms to inherit reasonably similar properties of their bulk counterparts as well as contain a high enough number of individual atoms which behave independently showing properties somewhat similar to their molecular counterparts (Nguyen 2013). Therefore, nanoparticles exhibit optical (e.g. colour, transparency), electrical (e.g. conductivity), physical (e.g. melting point, magnetism), mechanical (e.g. hardness and tensile strength) and chemical (e.g. reactivity, reaction rates) properties that are very different from both the bulk and the constituent atoms or molecules.

The most typical example of change in optical property is the striking red or ruby colour of gold nanoparticle solution as compared to the yellow or golden colour of bulk gold. This is due the phenomenon of surface plasmon resonance (SPR) wherein occurs a red shift of the plasmon band to visible frequencies at the nanoscale, unlike that for bulk metals where the plasmon absorption is in the UV region (Eustis and El-Sayed 2006). In addition, optical properties of gold nanoparticles also depend on their size and shape due to which gold nanorods exhibit different optical properties than their spherical counterparts. Physical property like magnetism in iron oxide nanoparticles is another remarkable example wherein magnetic nanoparticles with size less than 20 nm show unique property of superparamagnetism (Jun et al. 2008). A superparamagnetic material is composed of small ferromagnetic clusters (e.g. crystallites), small enough that they can randomly flip direction under thermal fluctuations. As a result, the material as a whole is not magnetized except in an externally applied magnetic field. Changes in the mechanical properties can be highlighted with the example of carbon nanotubes. Unlike bulk carbon which has very limited use, carbon nanotubes, long and thin cylinders of carbon are unique for their size, shape, and remarkable properties (Bernholc et al. 2002). These molecules can be manipulated chemically and physically in very useful ways. Nanotubes show extraordinary high mechanical strength, electrical and heat conductivity. These properties change depending on the different kinds of nanotube (defined by its diameter, length, and chirality, or twist). A few intrinsic properties like melting point, also change when the size of the bulk material reduces to nano scales (Zhang et al. 2000). Melting-point depression is a term which refers to the phenomenon of reduction of the melting point of a material with reduction of its size. This phenomenon is very prominent in nanoscale materials which melt at temperatures hundreds of degrees lower than bulk materials. Changes in melting point occur because nanoscale materials have a much larger surface-to-volume ratio than

bulk materials, drastically altering their thermodynamic and thermal properties. In addition, the catalytic efficiency also increases at nanoscales as surface area to volume ratio increases which increases the probability of substrate interaction at the catalyst surface. Advantages of using a nanocatalyst includes precise selectivity, extremely high activity, low energy consumption and long lifetime (Chaturvedi et al. 2012). These advantages are result of difference in size, shape, spatial distribution, surface composition, electronic structure, thermal and chemical stability of the nanocatalyst as compared to their bulk counterparts.

1.3 Synthesis of nanoparticles

Methods for the synthesis of nanoparticles can be broadly categorized as physical, chemical and biological methods. These methods utilize either the top-down or bottom-up approach of synthesis (Ghorbani et al. 2011). The top-down approach involves division of massive solid by breaking and dismantling using mechanical tools and ablations to fabricate nano-sized materials. On the other hand, bottom-up approach builds nano-entities by combining smaller components such as atoms and single molecules, which are held together by covalent forces. With obvious reasons, bottom-up approach is much advantageous as the covalent bonds holding a single molecule together are far stronger than the weak interactions that hold more than one molecule together. Various physico-chemical methods used in top-down synthesis approach viz., micropatterning, pyrolysis, laser ablation and attrition (milling) suffer from a number of limitations which include stringent conditions for monodisperse nanoparticle synthesis, optimization of time and process temperature, employment of complex and hi-tech instrumentation, enormous energy requirement etc. While physicochemical methods in the bottom-up approach viz., chemical reduction, microemulsion, electrochemical and microwave suffer from various disadvantages like difficulty in controlling experimental conditions, feeble reproducibility, polydispersity, costly chemicals/ catalyst and recovery as well as energy intensive and eco-hazardous processes. Although physical and chemical methods promise high productivity with considerable ease in upgrading to industrial scale, a major drawback which limits their employment in biomedical applications is the use of potentially hazardous capping material, generation of toxic by-products and yield of particles in non-polar organic solvent (Gericke and Pinches 2006).

All these limitations can be potentially overcome by using bio-inspired approach for nanoparticle synthesis. Bio inspired approach circumvents these limitations by enabling synthesis at mild pH, temperature and pressure along with substantially lower cost. Biological systems have been making functional nanoparticles like magnetosomes since the beginning of life (Poole and Owens 2006). The bio-inspired approach uses biological building blocks to assemble nanostructures with exceptional accuracy. Biological methods for nanoparticle synthesis are broadly based on either the use of live/ dead biomass or their

cellular/ extra cellular extract. In recent years, inspired from natural biological systems, researchers have been able to develop an alternative approach for nanoparticle synthesis using microorganisms. Among various microorganisms used for biosynthesis of nanoparticles, bacteria and fungi have been most immensely investigated. Though other organisms like viruses, algae and cyanobacteria have also been employed for nanoparticle synthesis, the extent of research with these microbes is limited as reviewed by Park et al. (2016). Fungi have emerged out as potential candidate for biosynthesis of nanoparticles because of their ease in handling, low cost maintenance and higher biomass production (Gade et al. 2010). Additionally, being a eukaryotic organism, fungi have been reported to contain large and versatile biomolecules which play vital role in nanoparticle synthesis; and helpful in achieving significantly higher and desired productivity (Dhillon et al. 2011).

1.4 Characterization of nanoparticles

Evaluation and application of nanoparticles requires concrete data with reference to nanoparticles size, shape, morphology, crystallinity, dispersity, elemental composition, surface coating and charge (Rao and Biswas 2009). Thus, nanoparticle characterization is necessary to establish understanding and control of their synthesis and use in various applications. In this regard, although individual technique suffers from one or more disadvantages, a cumulative collection of results by use of various techniques fulfils the purpose. Recent yet dynamic progress in the field of characterization techniques is providing newer and better aids as well as cutting down the cost as well. However, there still remains a need for the ultimate characterization technique due to which the development of novel tools and instruments is one of the greatest challenges in the field of nanotechnology. Table 1.1 summarizes various spectroscopic, crystallographic and microscopic techniques used for the characterization of nanoparticles along with the information that can be acquired by each technique.

1.5 Application of Nanoparticles

The impact of nanotechnology is increasing at tremendous pace due to its remarkable potential. Most applications of nanotechnology are based on the fact that nanoscale provides great freedom for manipulation (Stark et al. 2015). Using nanotechnology, it is possible to manipulate the bulk material and make them stronger, lighter, durable, extremely conductive and reactive (Figure 1.1).

Nanoparticles are considered as the protagonist of the nanotechnology revolution. Amid nanoparticles, metal and metal oxides nanoparticles are of special interest due to their unique and tuneable properties, flexibility in functionalization and supple biological interactivity. Gold nanoparticles (Au NPs) are one such example of metallic nanoparticles with versatile applications (Daniel and Astruc 2004). Due to their excellent current transfer

ability they are used as conductors in products ranging from printable inks to electronic chips. Photodynamic therapy which utilizes Au NPs to produce heat when excited by the Near-IR light is employed to eradicate targeted tumors. The large surface area of Au NPs and their non-toxic behaviour with living cell is the basis of their use in therapeutics delivery. The optical property of Au NPs is utilized to develop colorimetric sensors for real time detection of various chemicals, pathogens and contaminants. With this, a variety of Au NPs based microscopic probes and diagnostic kits have also been developed. Among various applications of Au NPs, catalysis has been one of the most sought after because of its commercial significance. In addition to the selective oxidation of carbon monoxide, reduction of nitrogen oxides and fine chemical synthesis, the catalytic properties of Au NPs have also been explored for the degradation of environmentally hazardous chemicals (Tsukuda et al. 2011; Zhang et al. 2011).

Table 1.1 Techniques routinely used for nanoparticle characterization.

	Technique	Information
Spectroscopic techniques	UV-visible spectroscopy	Size, aggregation, structure, surface chemistry, concentration
	Fourier transform infrared spectroscopy	Surface composition
	Atomic absorption spectroscopy	Quantitative determination of chemical elements
X-ray based techniques	Energy dispersive X-ray spectroscopy	Elemental composition
	X-ray powder diffraction	Crystallographic and elemental composition
	X-ray photoelectron spectroscopy	Surface-sensitive quantitative elemental composition
	X-ray fluorescence	Qualitative and quantitative measurement of elements
Microscopic techniques	Atomic force microscopy	Size, morphology, surface texture, electrical and mechanical properties
	Scanning tunneling microscope	Elemental and molecular composition
	Scanning electron microscope	Morphology, surface, size, shape
	Transmission electron microscopy	Size, shape, crystallographic composition
	Dynamic light scattering	Particle size and distribution
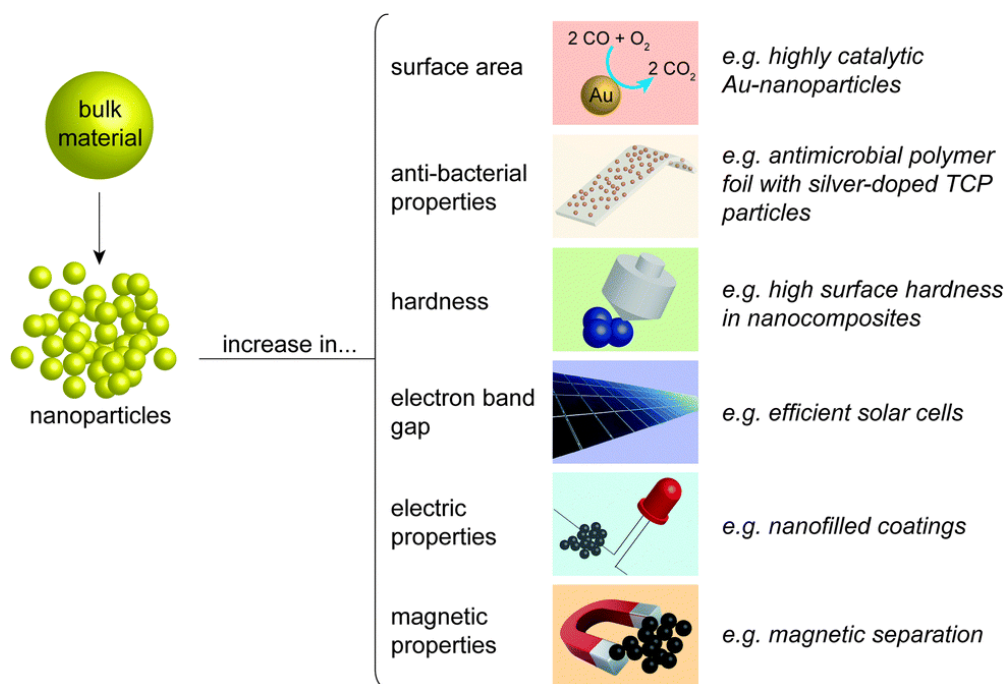
Figure 1.1 Role of nanotechnology in manipulation of various material properties and their respective applications (Adapted with permission from Stark et al. 2015)

Another important class of metallic nanoparticles is iron oxide nanoparticles (IONPs). Recent developments in the field of IONPs have diversified the scope of their application. IONPs are now routinely used to tackle problems like climate change and pollution control, clean water technology, energy generation, information storage and biomedical applications (Teja and Koh 2009). Within biomedical applications, they are used for separation of biomolecules and cells, detection and diagnostics, imaging, hyperthermia, drug and therapeutic delivery, nucleic acid delivery and transfer, cell manipulation, tissue engineering (Lin 2015). A new yet interesting application of IONPs is in the agriculture field. In the present scenario, agriculture demands for greater efficiency in the food production due to growing population; and shrinking arable land and water resources (Mastronardi et al. 2015). In the past few decade, agriculture has seen overriding revolution with the introduction of hybrid crops and use of plants as expression system. Nanotechnology also extends its relevance in agricultural field with the development of nanoscale technology for improvement in crop yield qualitatively and quantitatively. Nanoparticles like IONPs have high surface area, sorption capacity and controlled release kinetics which make them a "smart delivery system" (Sasson et al. 2007). Nanostructured fertilizers have been projected to increase the nutrient use efficiency through mechanisms such as targeted delivery, slow or controlled release and efficient nutrient management (Cui et al. 2010). Studies are ongoing to explore the possibilities to implement nanoparticles of physiologically important elements to enhance photosynthesis, biomass production and harvest quality (Solanki et al. 2015).

Since the inception of nanotechnology, one of the major questions faced by the world was whether the unknown risks of nanotechnology/ nanoparticles involving their environmental and health impact, prevail over their potential benefits (Colvin 2003). These concerns deepen when nanoparticles come directly in contact with biological systems for example, when used as "nano-fertilizers". As being an infant technology, the ethical and safety issues surrounding the use of nanoparticles in plant productivity are limitless and must be very carefully evaluated before being adapted for use (Bouwmeester et al. 2009). This highlights the importance of systematic and thorough quantitative studies regarding the potential health impacts, environmental clearance and safe disposal of nanoparticles which can lead to improvements in designing further applications of nanotechnology (Meng et al. 2009).

1.6 Gaps in Existing Research

Ever increasing use of nanotechnology in various fields is escalating the demand of nanomaterials. Technologies for synthesis of nanoparticles are undergoing constant development to cope up with the demand in the present scenario, and recent synthesis methods are replacing the conventional methods. Increasing awareness towards ecosystem restoration has influenced researchers to develop eco-friendly yet cost effective and efficient methodologies for nanoparticle synthesis. Biological methods for nanoparticle synthesis particularly using microorganisms, presents a desirable alternate to the conventional physical and chemical synthesis methods. However, even after several decades, biological approaches are still practiced at the laboratory level only and have not been profitably scaled-up to the industrial level. The primary reason for this delay is the random selection of microbial species for nanoparticle synthesis without suitable rationale. In order to achieve enhanced synthesis rate, well defined size, shape and crystallinity of nanoparticles, it is imperative to choose an appropriate microbial species. Another crucial reason is low particle yield and lesser understanding of factors affecting properties of nanoparticles. Hence, there is a need to develop new protocols for biosynthesis of nanoparticles which shall be eco-friendly, efficient and up-scalable.

Once synthesized, the nanoparticles can be used in various commercial applications such as catalysis for fine chemical synthesis as well as environmental management. Increased use of nanoscale material in present times has increased the chances of exposure of nanoparticles to plants and animals. Incorporation of NPs in food chain is a considerable threat to eco-system and should be investigated critically. Although, nanoparticles of toxic and heavy elements have negative effect on plants as reported by many studies, nanoparticles of physiologically important elements can have positive and growth promoting effect on plants, if applied thoughtfully. There is urgent and necessary need to analyse the effect of these nanoparticles on the food chain. Therefore, it is essential to assess the effect of inorganic nanoparticles on plant system and subsequently the effect of

nanotechnology-derived food material on animal system. Conclusively, detailed study on the effect of nanoparticles in plant and animal systems is a pre-requisite for taking advantage of nanomaterials in agriculture leading to the development of sustainable agro-nanotechnology.

1.7 Objectives

Based on the above mentioned considerations, the present thesis aims to fulfil following objectives:

1. Screening and identification of potential microorganisms for synthesis of inorganic nanoparticles.
2. Development of an optimized protocol for biosynthesis of inorganic nanoparticles.
3. Assessment of catalytic potential of nanoparticles for chemical synthesis and environmental remediation.
4. Evaluation of nanoparticles as potential "nano-fertilizers" in plant system.
5. Toxicological assessment of nanotechnology derived food in animal system.

1.8 References

Bernholc, J., Brenner, D., Buongiorno Nardelli, M., Meunier, V. and Roland, C. (2002). Mechanical and electrical properties of nanotubes. *Annual Review of Materials Research* 32: 347-375.

Bouwmeester, H., Dekkers, S., Noordam, M. Y., Hagens, W. I., Bulder, A. S., de Heer, C., ten Voorde, S. E. C. G., Wijnhoven, S. W., Marvin, H. J. and Sips, A. J. (2009). Review of health safety aspects of nanotechnologies in food production. *Regulatory Toxicology and Pharmacology* 53: 52-62.

Chaturvedi, S., Dave, P. N. and Shah, N. K. (2012). Applications of nano-catalyst in new era. *Journal of Saudi Chemical Society* 16: 307-325.

Colvin, V. L. (2003). The potential environmental impact of engineered nanomaterials. *Nature Biotechnology* 21:1166-1170.

Cui, H. X., Sun, C. J., Liu, Q., Jiang, J. and Gu, W. (2010). Applications of nanotechnology in agrochemical formulation, perspectives, challenges and strategies. *International Conference on Nanoagri*, Sao pedro, Brazil, 28-33.

Daniel, M. C. and Astruc, D. (2004). Gold nanoparticles: assembly, supramolecular chemistry, quantum-size-related properties, and applications toward biology, catalysis, and nanotechnology. *Chemical Reviews* 104: 293-346.

Dhillon, G. S., Brar, S. K., Kaur, S. and Verma, M. (2011). Green approach for nanoparticle biosynthesis by fungi: current trends and applications. *Critical Reviews in Biotechnology* 32: 49-73.

Eustis, S. and El-Sayed, M. A. (2006). Why gold nanoparticles are more precious than pretty gold: noble metal surface plasmon resonance and its enhancement of the radiative and nonradiative properties of nanocrystals of different shapes. *Chemical Society Reviews* 35: 209-217.

Gade, A., Ingle, A., Whiteley, C. and Rai, M. (2010). Mycogenic metal nanoparticles: progress and applications. *Biotechnology Letters* 32: 593-600.

Gericke, M. and Pinches, A. (2006). Biological synthesis of metal nanoparticles. *Hydrometallurgy* 83: 132-140.

Ghorbani, H. R., Safekordi, A. A., Attar, H. and Sorkhabadi, S. M. (2011). Biological and non-biological methods for silver nanoparticles synthesis. *Chemical and Biochemical Engineering Quarterly* 25: 317-326.

Jun, Y. W., Seo, J. W. and Cheon, J. (2008). Nanoscaling laws of magnetic nanoparticles and their applicabilities in biomedical sciences. *Accounts of Chemical Research* 41: 179-189.

Kaehler, T. (1994). Nanotechnology: basic concepts and definitions. *Clinical chemistry* 40: 1797-1799.

Lin, W. (2015). Introduction: nanoparticles in medicine. *Chemical Reviews* 115: 10407-10409.

Mastronardi, E., Tsae, P., Zhang, X., Monreal, C. and DeRosa, M. C. (2015). Strategic role of nanotechnology in fertilizers: potential and limitations. In: Rai, M., Ribeiro, C., Mattoso, L. and Duran, N. (Eds.) Nanotechnologies in food and agriculture. Springer International Publishing, Switzerland. p. 25-67.

Meng, H., Xia, T., George, S. and Nel, A. E. (2009). A predictive toxicological paradigm for the safety assessment of nanomaterials. *ACS Nano* 3: 1620-1627.

Mohanraj, V. J. and Chen, Y. (2007). Nanoparticles-a review. *Tropical Journal of Pharmaceutical Research* 5: 561-573.

Nel, A. E., Parak, W. J., Chan, W. C., Xia, T., Hersam, M. C., Brinker, C. J., Zink, J. I., Pinkerton, K. E., Baer, D. R. and Weiss, P. S. (2015). Where are we heading in nanotechnology environmental health and safety and materials characterization? *ACS Nano* 9: 5627-5630.

Nguyen, T. D. (2013). From formation mechanisms to synthetic methods toward shape-controlled oxide nanoparticles. *Nanoscale* 5: 9455-9482.

Park, T. J., Lee, K. G. and Lee, S. Y. (2016). Advances in microbial biosynthesis of metal nanoparticles. *Applied Microbiology and Biotechnology* 100: 521-534.

Poole, C. P. Jr. and Owens, F. J. (2006). Introduction to nanotechnology. John Wiely & Sons (Asia) Pte. Ltd. pp. 388.

Rao, C. N. R. and Biswas, K. (2009). Characterization of nanomaterials by physical methods. *Annual Review of Analytical Chemistry* 2: 435-462.

Sasson, Y., Levy-Ruso, G., Toledano, O. and Ishaaya, I. (2007) Nanosuspensions: emerging novel agrochemical formulations In: Ishaaya, I., Horowitz, A. R. and

Nauen, R. (Eds.) Insecticides design using advanced technologies. Springer Berlin Heidelberg, pp 1-39.

Solanki, P., Bhargava, A., Chhipa, H., Jain, N. and Panwar, J. (2015). Nano-fertilizers and their smart delivery system. In: Rai, M., Ribeiro, C., Mattoso, L. and Duran, N. (Eds.) Nanotechnologies in food and agriculture. Springer International Publishing, Switzerland. p. 81-101.

Stark, W. J., Stoessel, P. R., Wohlleben, W. and Hafner, A. (2015). Industrial applications of nanoparticles. *Chemical Society Reviews* 44: 5793-5805.

Teja, A. S. and Koh, P. Y. (2009). Synthesis, properties, and applications of magnetic iron oxide nanoparticles. *Progress in Crystal Growth and Characterization of Materials* 55: 22-45.

Tsukuda, T., Tsunoyama, H. and Sakurai, H. (2011). Aerobic oxidations catalyzed by colloidal nanogold. *Chemistry-An Asian Journal* 6: 736-748.

Zhang, M., Efremov, M. Y., Schiettekatte, F., Olson, E. A., Kwan, A. T., Lai, S. L., Greene, W. J. E. and Allen, L. H. (2000). Size-dependent melting point depression of nanostructures: nanocalorimetric measurements. *Physical Review B* 62: 10548-10557.

Zhang, Y., Cui, X., Shi, F. and Deng, Y. (2011). Nano-gold catalysis in fine chemical synthesis. *Chemical Reviews* 112: 2467-2505.

Chapter II

Isolation, Identification and Metal Tolerance Profile of Fungi Isolated from Metal Rich Region

Preface

In recent years, the surging demand of nanomaterials has boosted unprecedented expansion of research for the development of high yielding and sustainable synthesis methods which can deliver nanomaterials with desired characteristics. Unlike the well-established physico-chemical methods which have various limitations, biological methods inspired by mimicking natural biomineralization processes have great potential for nanoparticle synthesis. Taking inspiration from the phenomenon of metal resistance and its associated mechanisms, the present chapter demonstrates isolation and identification of metal tolerant fungal isolates. The work serves as the initial step in development of an eco-friendly method for synthesis of nanoparticles by selection of a promising microorganism on the hypothesis that "well adapted microbes isolated from native metal rich soil conditions can be a better source for bio-inspired synthesis of metal nanoparticles".

2.1 Introduction

The ever-increasing use of nanotechnology is escalating the demand of nanomaterials. A myriad variety of nanoparticles are being manufactured, which are anticipated to foster various sectors viz., electronics, information technology, aerospace, fine chemical synthesis, cosmetics, bio-medicine and several commercial products (Bhushan 2010). The size, shape and composition of nanoscopic materials play a vital role in controlling their physical, chemical, optical and electronic properties (Cao 2004). Thus, in the recent years, there has been an unprecedented expansion in research for the development of new synthesis methods which can deliver nanomaterials with well-defined properties. Technologies for synthesis of nanomaterials are undergoing constant advancement to cope up with the demand in the present scenario, and recent synthesis methods are replacing the conventional 'low-yielding, unprofitable and hazardous' ones. An ideal synthesis approach must utilize cost effective materials and generate no or minimal by-products in addition of being highly productive (Thakkar et al. 2010). Fortunately, end of the 20th century witnessed evolution of synthesis strategies inspired by natural biological systems which were closer to being an ideal method for nanoparticle synthesis unlike the physical and chemicals methods (Klaus et al. 1999). This amalgam of biology and material science illustrated incredible potential to replace the conventionally used processes for nanoparticle synthesis (Komeili 2007). Some examples of natural amalgams in higher organisms include bone and tooth tissues in vertebrates, carapaces of crustacean and shells in molluscs (Sanchez et al. 2005). Likewise, a number of microorganisms produce inorganic crystalline nanostructures like magnetosome synthesis by magnetotactic bacteria (Lovley et al. 1987); silica nanomaterial synthesis by diatoms (Kröger et al. 1999), proteinaceous surface layer in some bacteria (Pum and Sleytr 1999), etc.

Biomineralization has been a significant process which leads to the formation of variety of complex structures of metal and metal oxides. Metals directly or indirectly interact with various aspects of microbial growth, metabolism and reproduction. The biochemistry of metal-microbe interaction varies with every metal and microorganism. Despite the fact that all metals, even the essential ones, above a threshold concentration are toxic to cells, many microbes grow and even flourish in apparently metal-polluted locations, and a variety of mechanisms, both active and incidental, contribute to the resistance (Gadd 2010). Most of the mechanisms depend on executing change in metal speciation leading to decreased or increased mobility. These include redox transformations, production of metal-binding peptides and proteins, organic and inorganic precipitation, active transport, efflux and intracellular compartmentalization, while cell walls and other structural components have significant metal-binding abilities (Gadd 2009; Figure 2.1).

Importantly, one of the mechanisms is the cell mediated reduction of ions into respective metals and their transformation into ordered crystalline structure. This process indirectly demonstrates the capability of metal tolerant organisms to act as natural nanoparticle synthetic machinery (Salvadori et al. 2014). However, in-depth knowledge of the biochemical and molecular aspect of the process involved suggests that the ability of nanoparticle synthesis varies among microorganisms. Earlier studies have suggested that high metal stress may affect various biochemical activities in microorganisms (Giller et al. 2009). Translating knowledge gained by understanding natural biomineralization process at laboratory scale, recently a number of microorganisms like bacteria, yeast, algae and fungi have been used for the synthesis of nanoparticles (Narayanan and Sakthivel 2010; Yadav et al. 2015). Table 2.1 summarizes selected reports wherein metal tolerance property of microorganisms has been utilized for the synthesis of various nanoparticles. These observations further strengthen the positive correlation between metal tolerance potential and ability for the nanoparticle synthesis and encourages the rationale that mimicking natural processes *in vitro* may serve as platform for development of efficient nanoparticle synthesis protocols (Sarikaya et al. 2003).
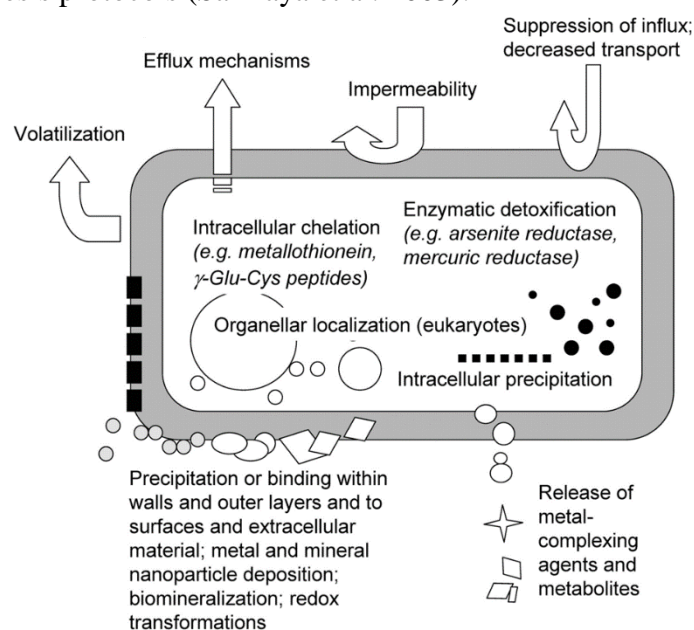
Figure 2.1 Mechanisms involved in the detoxification and transformation of metals, including mechanisms that restrict entry into the cell and intracellular detoxification or organellar compartmentation, the latter occurring in some eukaryotes, e.g. algae and fungi. (Adapted with permission from Gadd 2009)

The aim of the present study was to select metal tolerant soil fungal isolates that can be used for economical, controlled, efficient and up-scalable synthesis of nanoparticles. Among various microorganisms, fungi was chosen for the study as it is reported to have the largest and most diverse secretome making it highly anticipated for on-cell/extracellular synthesis of nanoparticles (Dhillon et al. 2011; Jain et al. 2013). The

selection was accomplished by isolating fungi from soil collected from metal rich regions followed by their molecular characterization. Later on, the metal tolerance profile of all fungal isolates was obtained and most tolerant isolates were screened for nanoparticle synthesis as discussed in next chapters.

Table 2.1 Selected reports of metal tolerant microorganisms utilized for synthesis of nanoparticles.

Organism	Metal	Mode of synthesis	References
Pseudomonas stutzeri	Ag	On-cell	Klaus et al. (1999)
Desulfobacteriaceae (family)	(Zn,Fe)S	Intracellular	Labrenz et al. (2000)
Morganella sp.	Ag	Extracellular	Parikh et al. (2008)
Stenotrophomonas maltophilia	Au	Intracellular	Nangia et al. (2009)
Lactobacillus sporogens	ZnO	On-cell	Prasad and Jha (2009)
Aspergillus flavus	Ag	Extracellular	Jain et al. (2011)
Aspergillus aeneus	ZnO	Extracellular	Jain et al. (2013)
Aspergillus sp.	ZnO	Extracellular	Jain et al. (2014)

2.2 Materials and methods

2.2.1 Materials

The microbiological media ingredients were acquired from HiMedia (HiMedia Laboratories, India). Molecular biology kits and reagents used in PCR reactions were obtained from Qiagen (Qiagen, Germany) and Promega (Promega, Germany), respectively. The primers used for amplification of ITS region were purchased from Sigma-Aldrich (Sigma-Aldrich USA) while all other primers were obtained from Eurofins (Eurofins MWG Operon, Germany). All others chemicals were purchased from Merck Chemicals (Merck KGaA, Germany) unless otherwise stated. Milli-Q$^®$ water was obtained from a Milli-Q Biocel water purification system manufactured by Merck Millipore (Merck KGaA, Germany).

Experimental handling of all the fungal isolates was carried out following the guidelines issued by Institutional Biosafety Committee in compliance with "Rules for manufacture, use/import/export and storage of hazardous microorganisms/genetically engineered organisms or cells, 1989" notified by Ministry of Environment and Forests, Government of India under Environmental (Protection) Act, 1986.

2.2.2 Sampling site and isolation of fungi

Soil samples were collected from two different metal (iron) rich regions:

(A) *Nathara Ki Pal region*: Soil samples were collected in the month of March 2010 from Nathara Ki Pal area (24°14' N 73°82' E) located in the Udaipur district of Rajasthan, India. The deposit is situated near Nathara Ki Pal village in Sarada tehsil and lies 57 km south-east of Udaipur city. Investigations carried out by the Department of Mines & Geology, Rajasthan has revealed that iron ore extends over a strike length of about 800 m with approximate width of 30 m. It persists up to 130 m in depth. A reserve of 14.2 million tonnes with 48 to 62% Fe has been estimated to be present in the iron ore as per the record (http://www.dmg-raj.org/about-dmg.html). The region has a seasonally tropical climate with all three main seasons, summer, monsoon and winter respectively, dominating the weather. Being located in desert lands of Rajasthan, the climate of Udaipur is usually hot.

(B) *Sonshi mining region*: Soil samples were collected in the month of March 2011 from the Sonshi mining region of Bicholim-Pale area (15° 29' N, 74° 4' E) located in the North Goa district of Goa, India. Iron ore reserves in Goa are variously estimated to be around 1000 million tonnes as per the record of Department of Mines and Geology, Goa (http://www.goadmg.gov.in/IronInfo.aspx). Around 80% of the deposits are fines and the rest lumps. The iron ore deposits are distributed over the northern, southern and central blocks of Goa. The northern block deposits are richer both in terms of quantity and quality of the ore. All the large mines which produce over one million tonnes are situated in the northern block. The Sonshi mining region is one of the oldest open casted mines of iron ore and is majorly operated by Sesa Sterlite Pvt. Ltd. The region being in the tropical zone and near the Arabian Sea, maintains hot and humid climate for most of the year.

A total of five sampling sites were studied at both regions. At each sampling site, three spatially distant points with a minimum of 5 m distance were selected for the collection of rhizospheric soil from naturally growing plants mainly *Calotropis procera*. Briefly, the upper soil layers were scraped off in order to remove plant debris, foreign particles and litter. The soil firmly adhered to the plant roots was collected and immediately packed in self-sealing plastic bags which were placed in an insulated carrier during transport and immediately refrigerated at 4 °C. All samples were processed within three days of their collection. Before processing, large stones and coarse roots were removed by sieving the soil samples through a 2 mm mesh sieve. A subsample of each soil was air dried and used for estimation of various physico-chemical properties mentioned below. In order to rule out the possibility of seasonal variation, an additional set of soil samples was also collected after a 6-month interval from the respective sites and processed separately.

Isolation of fungi was performed by plating the inoculum on rose bengal agar medium (pH 7.2) supplemented with 30 µg mL^{-1} of chloramphenicol (Sigma-Aldrich, USA) after serial dilutions of pooled soil samples (homogenized soils of three samples

taken per sampling site) during both first and second collection time. After incubating the plates for 5-6 days at 28° C under dark conditions, individual fungal colonies were selected and further purified by repeated sub-culturing on potato dextrose agar (PDA) medium. Preliminary identification of fungal isolates was performed on the basis of morphological and microscopic characters. Glycerol stock of all the morphologically distinct fungi were formulated and stored at -80˚ C for future use. The fungal isolates were stained with lactophenol cotton blue stain and slides were observed at ×1000 magnification using oil immersion objective.

2.2.3 Physico-chemical characteristics of rhizosphere soil

Rhizospheric soil samples were analysed for pH and electrical conductivity on 1:2.5 soil: water suspension using a digital pH and EC meter, respectively. Organic carbon was estimated by the method of Walkley and Black (1934) using 1.0 N potassium dichromate for titration and 0.5 N ferrous ammonium sulphate for back titration. Available phosphorus (Olsen P) in soil samples was determined by chlorostannus-reduced molybdophosphoric blue colour method (Olsen et al. 1954) after extraction with 0.5 M sodium bicarbonate for 30 min. Available N, K and micronutrients (Zn, Cu, Fe, Mn) in soil samples were estimated as described by Jackson (1967). The samples were analysed in replicates of 30 containing 15 samples from the first and 15 samples from the second collection of soils.

2.2.4 Molecular characterization of fungal isolates

In order to prepare fresh cultures, the fungal isolates were inoculated separately in 25 mL of Czapek's dox broth medium (pH 7.3) in 100 mL Erlenmeyer flasks. The flasks were incubated at 28 ˚C for 72 h under dark conditions. The grown mycelia were separated from the medium by centrifugation at 8000 rpm at 4 °C for 10 min. The obtained mycelia were washed thrice with autoclaved MilliQ® water followed by their mechanical crushing in liquid nitrogen using pre-chilled mortar and pestle. Fungal genomic DNA was extracted using Himedia HiPurA™ plant genomic DNA miniprep purification spin kit according to manufacturer's instructions.

Amplification of the internal transcribed spacer (ITS) regions of ribosomal DNA for all fungal isolates was performed using primers ITS1(5'TCCGTAGGTGAACCTGCGG) and ITS4(5'TCCTCCGCTTATTGATATGC) (White et al. 1990). Wherever necessary, amplification of other genes was also performed for conclusive species level identification. B-tubulin (*benA*) gene was partially amplified using primers Bt2a(5'GGTAACCAAATCGGTGCTGCTTTC) and Bt2b(5'ACCCTCAGTGTAGTGACCCTTGGC) (Glass and Donaldson 1995). Partial amplification of calmodulin (*cdl*) gene was carried out using primers CL1(5'GARTWCAAGGAGGCCTTCTC) and CL2A(5'TTTTTGCATCATGAGTTGGAC) (O'Donnell et al. 2000). In addition, elongation factor-1alpha (*EF1α*) gene was partially amplified using primers M1(5'GCTGGTATCTCCAAGGATGG) and M2(5'CGACGGACTTGACTTCRGTGG) (Woo et al. 2012). Polymerase chain reaction (PCR) was carried out in total volumes of 50 µL containing Taq Buffer A (10 mM Tris-HCl, 50 mM

KCl, and 1.5 mM MgCl$_2$, pH 8.3), 50 µM each of deoxynucleoside triphosphates, 50 pmol of each primers (30 pmol in case of *benA* and *EF1α* gene amplification), 1 unit of TaqDNA polymerase and 100-150 ng of template genomic DNA. The reactions were carried out on an Veriti® Thermal Cycler (Applied Biosystems, USA) using optimized PCR conditions (Table 2.2). The PCR products were separated on 1.0 % (w/v) agarose gel along with DNA ladder SM0241 (Fermentas Life Sciences, Canada) and purified using a Himedia HiPurA^{TM} PCR product purification spin kit. The purified PCR products were sequenced using an ABI prism DNA sequencer by BigDye terminator method (Applied Biosystems, USA). The obtained nucleotide sequences were compared using Basic Local Alignment Search Tool (BLAST) network services of the National Center for Biotechnology Information (NCBI) database (http://www.ncbi.nlm.nih.gov/). The most closely related species were determined based on the existing type strain entries. The sequences were further submitted to GenBank and the accession numbers were obtained.

Table 2.2 PCR conditions used for amplification of various regions/genes for molecular identification of fungal isolates.

Stages	ITS region	*benA* gene	*cdl* gene	*EF1α* gene
Initial Denaturation	94 ˚C (2 min)	94 ˚C (5 min)	94 ˚C (10 min)	94 ˚C (3 min)
Denaturation	94 ˚C (1 min)	94 ˚C (1 min)	94 ˚C (0.83 min)	94 ˚C (0.75 min)
Annealing	57 ˚C (1.5 min)	60 ˚C (0.75 min)	58 ˚C (0.83 min)	55 ˚C (0.75 min)
Extension	72 ˚C (2 min)	72 ˚C (1 min)	72 ˚C (1 min)	72 ˚C (1.5 min)
Final elongation	72 ˚C (4 min)	72 ˚C (7 min)	72 ˚C (7 min)	72 ˚C (4 min)
Cycles	30	35	35	30

2.2.5 Metal tolerance profiles of fungal isolates

Maximum tolerable concentration (MTC) assay was performed to determine the iron and gold metal tolerance ability of all the fungal isolates. For this purpose, experimental petri dishes were poured with Czapek's Dox agar medium supplemented with varying amounts of respective metal ions. Gold (III) chloride trihydrate (HAuCl$_4$.3H$_2$O) was used to determine the gold tolerance profile, while a mixture of Fe^{+3} (ferric chloride; FeCl$_3$) and Fe^{+2} (Ferrous sulphate heptahydrate; FeSO$_4$.7H$_2$O) in the ratio of 2:1 was used to determine the iron tolerance profile. The salts were added to the medium to obtain a final concentration of iron/gold ions in the range of 0 to 1000 µg mL^{-1} with an increment of 25 µg mL^{-1}. An inoculum of test fungus (10^6 cfu mL^{-1}) was streaked

on the medium surface of each plate. Plates without iron and gold ions were used as controls. After inoculation, the plates were incubated at 28 °C for 4 days under dark conditions to allow the fungal growth. The experiment was performed in triplicate. The maximum concentration of iron/gold ions in the medium which allowed the growth of fungus in all three replicates was considered as the MTC value.

2.3 Results and discussion

2.3.1 Physico-chemical characteristics of soil samples

The soil samples used for isolation of fungi were collected from two different regions viz., Nathara Ki Pal, Udaipur and Sonshi Mining Region, Goa. The regions were selected owing to their inherent metal rich soil. Sampling sites within the metal rich region was selected based on random sampling design approach. Even though the highest metal concentration would have been in the core of the geological mining area, the sampling sites were selected near the mining area wherein natural vegetation was present. The rhizospheric soil was used as a source of isolation for fungi as it is well known to exhibit high microbial populations (diversity) due to the availability of organic content from plants (Griffiths et al. 2001). The results for the physico-chemical analysis have been shown in Table 2.3. The soil pH at both the regions was found to be near neutral. In general, a significant variation was observed in EC, available P and various micronutrient concentrations in the soil of both sampling sites. Iron was found to be abundant at both regions with nearly four times higher concentration in the soil samples collected from Sonshi mining regions.

Table 2.3 Physico-chemical characteristics of soil collected from metal rich regions (n = 30).

Parameter	Nathara Ki Pal	Sonshi Mining Region
pH	7.06 ± 0.065	7.13 ± 0.035
EC (dS m^{-1})	0.049 ± 0.018	1.34 ± 0.64
Available N*	63.39 ± 11.00	66.0 ± 6.95
Available P*	23.0 ± 0.37	9.30 ± 0.78
Available K*	116.83 ± 3.04	137.33 ± 10.25
Zn*	8.6 ± 0.29	3.095 ± 0.29
Cu*	0.869 ± 0.24	1.067 ± 0.09
Fe*	23.55 ± 1.05	98.09 ± 4.36
Mn*	3.4 ± 0.89	28 ± 0.29

* mg kg^{-1}

2.3.2 Identification of fungal isolates

2.3.2.1 Morphological identification

Preliminary identification of fungi was performed on the basis of morphological and microscopic characteristics. Morphological parameters like form, size, elevation, margin/border, surface, opacity, colour, back pigmentation and microscopic parameters like hyphal branching pattern and spore shape, size and arrangement etc. were recorded for all isolates. Based on these parameters, a total of 11 morphologically distinct fungal isolates were observed (Table 2.4).

Table 2.4 Morphology (as observed on PDA medium) of axenic fungal isolates derived from selected metal rich regions.

Isolate	Morphology	Texture
AJP01	Deep black conidia with a cream reverse	Granular
AJP02	Yellow-green conidia with white reverse	Granular
AJP03	Olive green colony with floccose at the centre, dark green reverse	Velvety
AJP04	Pale brown rhizoids with white hairy aerial hyphae, cream reverse	Cottony
AJP05	Pale brown centre with white periphery, cream reverse	Velvety
AJP06	Straw yellow rhizoids with white hairy aerial hyphae, yellow reverse	Velvety
AJP07	Pale green centre with white periphery, cream reverse	Velvety
AJP08	White/cream mycelia with orange pigmentation, orange reverse	Cottony
AJP09	Radially sulcate growth with greyish-turquoise centre and white periphery, cream reverse	Velvety
AJP10	Yellowish-green conidia with floccose at the centre, pale white reverse	Granular
AJP11	White long hairy growth, white reverse	Woolly

2.3.2.2 Molecular identification

Molecular characterization was performed by the comparative sequence analysis of ITS regions of ribosomal DNA for most of the fungal isolates. The rRNA operon sequence are the most widely used candidate in molecular phylogenetic studies. Amplification of the ITS regions resulted in PCR products of 488-805 bp with considerable variation. The

resulting sequences were submitted to the GenBank database of NCBI and accession numbers were obtained (Table 2.5). In cases wherein the ITS region sequence was not adequate, the comparative sequence analysis of partial *benA* gene, partial *cdl* gene and partial *EF1α* gene was also adopted for conclusive characterization. The obtained sequences were duly submitted at GenBank database of NCBI and accession numbers were obtained (Table 2.6).

Except *Penicillium rubens* AJP07, culture of all the fungal isolates were deposited Microbial Type Culture Collection and Gene Bank, Institute of Microbial Technology, Chandigarh, India and their respective MTCC accession numbers were obtained (Table 2.7). These cultures are available at public domain.

Table 2.5 Analysis of ITS region complex sequences of fungal isolates with their reference sequences from NCBI GenBank database.

Fungus	Isolate	Accession Number	Sequence length					Blast Results				
			18s	ITS1	5.8S	ITS2	28s	Max. Score	Query Coverage	Max. Identity	Closest Match	Reference
Aspergillus japonicus	AJP01	JF770435	< 17	175	163	149	36 >	998	100%	100%	AJ876880	Gonzalez et al. 2005
Aspergillus flavus	AJP02	JF770436	< 20	180	158	169	62 >	948	91%	98%	JX456198	El Mahgubi et al. 2013
Cladosporium oxysporum	AJP03	KF245937	< 33	156	158	149	56 >	1002	99%	99%	AJ300332	Wirsel et al. 2002
Paraphaeosphaeria arecacearum	AJP04	KM873041	< 580 >					1033	97%	99%	JX496043	Verkley et al. 2014
Penicillium shearii	AJP05	KM873042	< 20	172	157	169	47 >	1011	98%	99%	AF033420[T]	Peterson 2000
Trichoderma longibrachiatum	AJP06	KM873043	< 619 >					1127	100%	99%	NR_120298	Kuhls et al. 1996
Penicillium rubens	AJP07	KM873044	< 22	175	157	163	54 >	1051	99%	100%	NR_111815	Houbraken et al. 2012
Fusarium solani	AJP08	KM873045	< 21	150	157	175	49 >	1002	100%	99%	FJ345352	Khot et al. 2009
Penicillium citrinum	AJP09	KM873046*	-	114	158	166	50 >	900	99%	100%	NR_121224	Peterson and Horn 2009
Aspergillus tamarii	AJP10	KM873047	< 30	181	157	175	50 >	1090	100%	99%	AY373870	Haugland et al. 2004
Lichtheimia ramosa	AJP11	KP340433	< 7	339	128	314	17 >	1424	100%	99%	GQ342848	Alastruey et al. 2010

Incomplete ITS sequence; [T] *Type strain*

Table 2.6 Analysis of partial *benA*, *cdl* and *EF1α* gene sequences of selected fungal isolates with their reference sequences from NCBI GenBank database.

Fungus	Isolate	Gene	Accession Number	Coding DNA Sequence Length	Blast Results				
					Max. Score	Query Coverage	Max. Identity	Closest Match	Reference
Aspergillus japonicus	AJP01	*benA* gene (Partial)	JX103558	<1..7, 98..139, 214..268, 329..>491	881	98%	99%	HE577804	Hubka and Kolarik 2012
		cdl gene (Partial)	JX103559	<9..35, 109..124, 244..369, 422..>634	1219	97%	99%	EU021690	Peterson 2008
Cladosporium oxysporum	AJP03	*benA* gene (partial)	KF245938	<1..67, 127..181, 253..>414	553	97%	92%	EF101455	Zalar et al. 2007
Lichtheimia ramosa	AJP11	*EF1α* gene (partial)	KP340434	<1..>460	839	100%	99%	EU826400	Hoffmann et al. 2013

Table 2.7 Fungal culture submission at MTCC with their respective accession numbers.

Fungal isolate	MTCC accession number
Aspergillus ramosa AJP01	MTCC 11733
Aspergillus flavus AJP02	MTCC 12403
Cladosporium oxysporum AJP03	MTCC 12414
Paraphaseopharea arecacearum AJP04	MTCC 12439
Penicillium shearii AJP05	MTCC 12411
Trichoderma longibrachiatum AJP06	MTCC 12402
Fusarium solani AJP08	MTCC 12412
Penicillium citrinum AJP09	MTCC 12406
Aspergillus tamarii AJP10	MTCC 12404
Lichtheimia 24amose AJP11	MTCC 12413

2.3.2.3 Fungal diversity

Clustering of obtained nucleotide sequences showed presence of 11 distinct fungal isolates at species level distributed across 7 different genera (Figure 2.2). All identified fungal isolates belong to the phylum *Ascomycota* except *Lichtheimia 24amose* which belongs to the phylum *Zygomycota* (Table 2.8). *Aspergillus* and *Penicillium* were found to be the most abundant genera holding 3 species each among the fungal isolates.
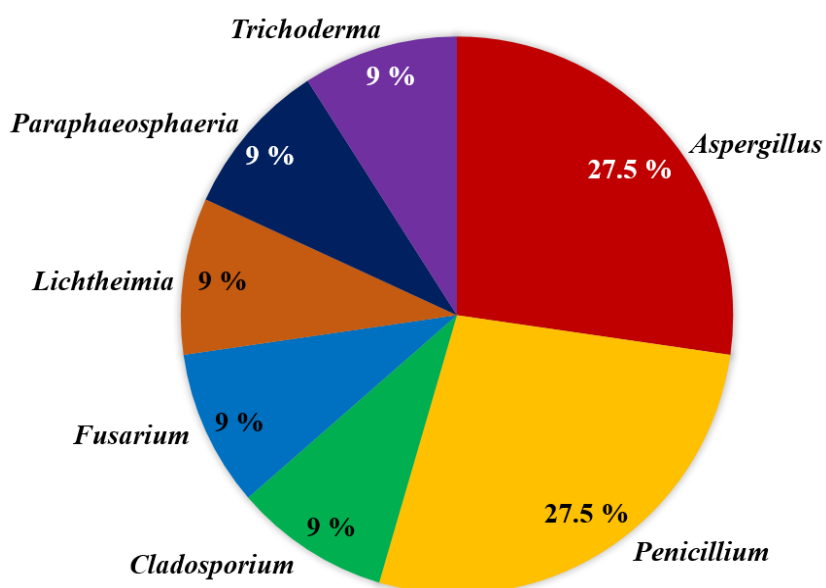
Figure 2.2 Pie chart depicting various fungal genera

Table 2.8 Phylogenetic classification of fungal isolates derived from metal rich region.

Fungus	Isolate	Classification* Kingdom[1], Phylum[2], Subphylum[3], Class[4], Subclass[5], Order[6], Family[7], Genus[8]
Aspergillus japonicus	AJP01	Fungi[1], Ascomycota[2], Pezizomycotina[3], Eurotiomycetes[4], Eurotiomycetidae[5], Eurotiales[6], Trichocomaceae[7], Aspergillus[8]
Aspergillus flavus	AJP02	Fungi[1], Ascomycota[2], Pezizomycotina[3], Eurotiomycetes[4], Eurotiomycetidae[5], Eurotiales[6], Trichocomaceae[7], Aspergillus[8]
Cladosporium oxysporum	AJP03	Fungi[1], Ascomycota[2], Pezizomycotina[3], Dothideomycetes[4], Dothideomycetidae[5], Capnodiales[6], Davidiellaceae[7], Cladosporium[8]
Paraphaeosphaeria arecacearum	AJP04	Fungi[1], Ascomycota[2], Pezizomycotina[3], Dothideomycetes[4], Pleosporomycetidae[5], Pleosporales[6], Montagnulaceae[7], Paraphaeosphaeria[8]
Penicillium shearii	AJP05	Fungi[1], Ascomycota[2], Pezizomycotina[3], Eurotiomycetes[4], Eurotiomycetidae[5], Eurotiales[6], Trichocomaceae[7], Penicillium[8]
Trichoderma longibrachiatum	AJP06	Fungi[1], Ascomycota[2], Pezizomycotina[3], Sordariomycetes[4], Hypocreomycetidae5, Hypocreales[6], Hypocreaceae[7], Trichoderma[8]
Penicillium rubens	AJP07	Fungi[1], Ascomycota[2], Pezizomycotina[3], Eurotiomycetes[4], Eurotiomycetidae[5], Eurotiales[6], Trichocomaceae[7], Penicillium[8]
Fusarium solani	AJP08	Fungi[1], Ascomycota[2], Pezizomycotina[3], Sordariomycetes[4], Hypocreomycetidae[5], Hypocreales[6], Nectriaceae[7], Fusarium[8]
Penicillium citrinum	AJP09	Fungi[1], Ascomycota[2], Pezizomycotina[3], Eurotiomycetes[4], Eurotiomycetidae[5], Eurotiales[6], Trichocomaceae[7], Penicillium[8]
Aspergillus tamarii	AJP10	Fungi[1], Ascomycota[2], Pezizomycotina[3], Eurotiomycetes[4], Eurotiomycetidae[5], Eurotiales[6], Trichocomaceae[7], Aspergillus[8]
Lichtheimia ramosa	AJP11	Fungi[1], Zygomycota[2], Mucoromycotina[3], Mucorales[6], Lichtheimiaceae[7], Lichtheimia[8]

* Source: Mycobank (http://www.mycobank.org/)

2.3.3 Metal tolerance profile of fungal isolates

All the fungal isolates were screened for their metal tolerance ability against iron and gold ions and the results were expressed in terms of MTC (Figure 2.3).
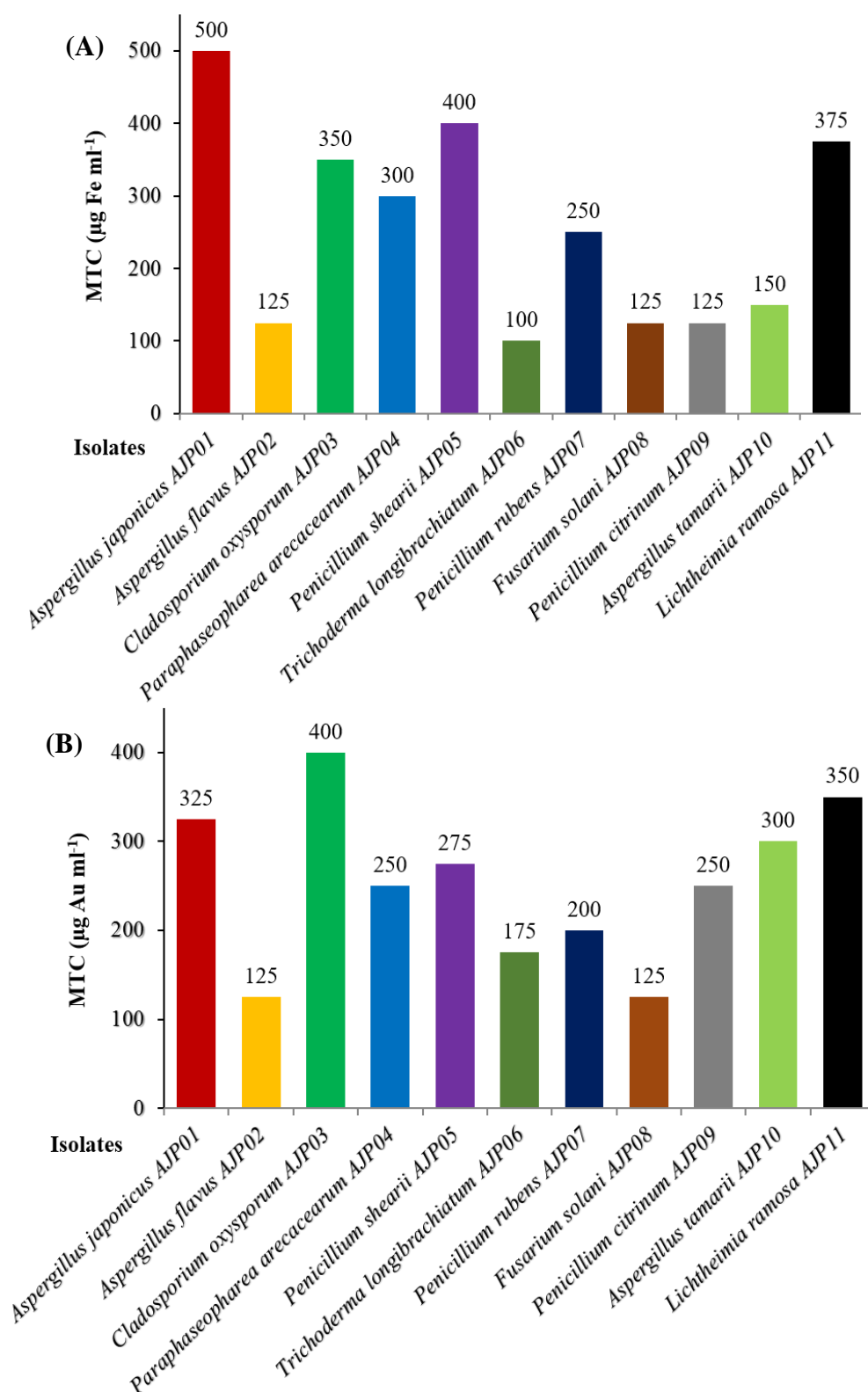
Figure 2.3 Metal tolerance profile of fungal isolates towards (A) iron and (B) gold ions

All fungal isolates were able to survive upto 100 µg mL^{-1} of iron concentration. More than 50 % isolates could withstand Fe concentration of 200 µg mL^{-1} respectively. *Aspergillus japonicus* AJP01 (MTC: 500 µg Fe mL^{-1}) was found to be the most tolerant fungus among all the isolates followed by *Penicillium shearii* AJP05 (MTC: 400 µg Fe mL^{-1}) and *Lichtheimia ramosa* AJP11 (MTC: 375 µg Fe mL^{-1}). A higher proportion (60%) of fungal isolates showed significant tolerance against gold with a varying degree of magnitude. *Cladosporium oxysporum* AJP03, *Lichtheimia ramosa* AJP11 and *Aspergillus japonicus* AJP01 exhibited highest metal tolerance against gold with a MTC value of 400, 350 and 325 µg mL^{-1} respectively. The fungal isolates exhibiting highest MTC values were subjected to screening for their potential towards iron oxide and gold nanoparticle synthesis. Similar experiments on determination of metal tolerable concentration in fungus isolated from zinc rich regions, showed enhanced resistance against zinc ions (Jain et al. 2013).

2.4 Conclusions

This chapter provides an overview of sampling and isolation of fungi from rhizospheric soil of plants naturally growing at metal rich regions of Nathara Ki Pal, Udaipur and Sonshi Mine, Goa. Soil physico-chemical characteristics revealed a high iron content at both the sampling sites. A total of 11 morphologically distinct fungi were isolated and identified at molecular level. All the fungal isolates were screened for their metal tolerance ability against iron and gold ions. *Aspergillus japonicus* AJP01 (MTC: 500 µg mL^{-1}) was found to be the most tolerant fungus against iron while *Cladosporium oxysporum* AJP03 and *Lichtheimia ramosa* AJP11 exhibited highest metal tolerance with a MTC value of 400 and 350 µg mL^{-1}, respectively against gold ions. In addition to iron, *Aspergillus japonicus* AJP01 also showed gold metal tolerance with a MTC value of 325 µg mL^{-1}. Hence, these fungal isolates were further utilized as potential candidates for respective nanoparticle (iron oxide or gold) synthesis.

2.5 References

Alastruey-Izquierdo, A., Hoffmann, K., de Hoog, G. S., Rodriguez-Tudela, J. L., Voigt, K., Bibashi, E. and Walther, G. (2010). Species recognition and clinical relevance of the zygomycetous genus *Lichtheimia* (syn. Absidia pro parte, Mycocladus). *Journal of Clinical Microbiology* 48: 2154-2170.

Bhushan, B., Ed. (2010). Springer handbook of nanotechnology. Springer, Berlin, 3rd Edition, pp.1964.

Cao, G., Ed. (2004). Synthesis, properties and applications, Taylor and Francis, London, 1st Edition, pp.616.

Dhillon, G. S., Brar, S. K., Kaur, S. and Verma, M. (2011). Green approach for nanoparticle biosynthesis by fungi: current trends and applications. *Critical Reviews in Biotechnology* 32: 49-73.

El Mahgubi, A., Puel, O., Bailly, S., Tadrist, S., Querin, A., Ouadia, A., Oswald, I. P. and Bailly, J. D. (2013). Distribution and toxigenicity of *Aspergillus* section *Flavi* in spices marketed in Morocco. *Food Control* 32: 143-148.

Gadd, G. M. (2009). Heavy metal pollutants: environmental and biotechnological aspects. *Encyclopedia of Microbiology* 2: 351-360.

Gadd, G. M. (2010). Metals, minerals and microbes: geomicrobiology and bioremediation. *Microbiology* 156: 609-643.

Giller, K. E., Witter, E. and McGrath, S. P. (2009). Heavy metals and soil microbes. *Soil Biology & Biochemistry* 41: 2031-2037.

Glass, N. L. and Donaldson, G. C. (1995). Development of primer sets designed for use with the PCR to amplify conserved genes from filamentous ascomycetes. *Applied and Environmental Microbiology* 61: 1323-1330.

González-Salgado, A., Patiño, B., Vázquez, C. and González-Jaén, M. T. (2005). Discrimination of *Aspergillus niger* and other *Aspergillus* species belonging to section *Nigri* by PCR assays. *FEMS Microbiology Letters* 245: 353-361.

Griffiths, B. S., Ritz, K., Wheatley, R., Kuan, H. L., Boag, B., Christensen, S., Ekelund, F., Sørensen, S. J., Muller, S. and Bloem, J. (2001). An examination of the biodiversity-ecosystem function relationship in arable soil microbial communities. *Soil Biology and Biochemistry* 33: 1713-1722.

Haugland, R. A., Varma, M., Wymer, L. J. and Vesper, S. J. (2004). Quantitative PCR analysis of selected *Aspergillus*, *Penicillium* and *Paecilomyces* species. *Systematic and Applied Microbiology* 27: 198-210.

Hoffmann, K., Pawłowska, J., Walther, G., Wrzosek, M., de Hoog, G. S., Benny, G. L., Kirk, P. M. and Voigt, K. (2013). The family structure of the Mucorales: a synoptic revision based on comprehensive multigene-genealogies. *Persoonia* 30: 57-76.

Houbraken, J., Frisvad, J. C., Seifert, K. A., Overy, D. P., Tuthill, D. M., Valdez, J. G. and Samson, R. A. (2012). New penicillin-producing *Penicillium* species and an overview of section Chrysogena. *Persoonia* 29: 78-100.

Hubka, V. and Kolarik, M. (2012). β-tubulin paralogue tubC is frequently misidentified as the benA gene in *Aspergillus* section *Nigri* taxonomy: primer specificity testing and taxonomic consequences. *Persoonia* 29: 1-10.

Jackson, M. L., Ed. (1967). Soil Chemical Analysis. Prentice Hall, New Delhi, 1st Edition pp. 498.

Jain, N., Bhargava, A. and Panwar, J. (2014). Enhanced photocatalytic degradation of methylene blue using biologically synthesized "protein-capped" ZnO nanoparticles. *Chemical Engineering Journal* 243: 549-555.

Jain, N., Bhargava, A., Majumdar, S., Tarafdar, J. C. and Panwar, J. (2011). Extracellular biosynthesis and characterization of silver nanoparticles using *Aspergillus flavus* NJP08: A mechanism perspective. *Nanoscale* 3: 635-641.

Jain, N., Bhargava, A., Tarafdar, J. C., Singh, S. and Panwar, J. (2013). A biomimetic approach towards synthesis of zinc oxide nanoparticles. *Applied Microbiology and Biotechnology* 97: 859-869.

Khot, P. D., Ko, D. L. and Fredricks, D. N. (2009). Sequencing and analysis of fungal rRNA operons for development of broad-range fungal PCR assays. *Applied and Environmental Microbiology* 75: 1559-1565.

Klaus, T., Joerger, R., Olsson, E. and Granqvist, C. G. (1999). Silver-based crystalline nanoparticles, microbially fabricated. *Proceedings of the National Academy of Sciences of the United States of America* 96: 13611-13614.

Komeili, A. (2007). Molecular mechanisms of magnetosome formation. *Annual Review of Biochemistry* 76: 351-366.

Kröger, N., Deutzmann, R. and Sumper, M. (1999). Polycationic peptides from diatom biosilica that direct silica nanosphere formation. *Science* 286: 1129-1132.

Kuhls, K., Lieckfeldt, E., Samuels, G. J., Kovacs, W., Meyer, W., Petrini, O., Gams, W., Börner, T. and Kubicek C. P. (1996). Molecular evidence that the asexual industrial fungus *Trichoderma reesei* is a clonal derivative of the ascomycete *Hypocrea jecorina*. *Proceedings of the National Academy of Sciences USA* 93: 7755-7760.

Labrenz, M., Druschel, G. K., Thomsen-Ebert, T., Gilbert, B., Welch, S. A., Kemner, K. M., Logan, G. A., Summons, R. E., Stasio, G. D., Bond, P. L., Lai, B., Kelly, S. D. and Banfield, J. F. (2000). Formation of sphalerite (ZnS) deposits in natural biofilms of sulfate-reducing bacteria. *Science* 290: 1744-1747.

Lovley, D. R., Stolz, J. F., Nord, G. L. and Phillips, E. J. P. (1987). Anaerobic production of magnetite by a dissimilatory iron-reducing microorganism. *Nature* 330: 252-254.

Nangia, Y., Wangoo, N., Sharma, S., Wu, J.-S., Dravid, V., Shekhawat, G. S. and Suri, C. R. (2009). Facile biosynthesis of phosphate capped gold nanoparticles by a bacterial isolate *Stenotrophomonas maltophilia*. *Applied Physics Letters* 94: 233901-233903.

Narayanan, K. B. and Sakthivel, N. (2010). Biological synthesis of metal nanoparticles by microbes. *Advances in Colloid and Interface Science* 156: 1-13.

O'Donnell, K., Nirenberg, H., Aoki, T. and Cigelnik, E. (2000). A multigene phylogeny of the *Gibberella fujikuroi* species complex: detection of additional phylogenetically distinct species. *Mycoscience* 41: 61-78.

Olsen, S. R., Cole, C. V., Watanabe, F. S. and Dean, L. A. (1954). Estimation of available phosphorus in soils by extraction with sodium bicarbonate. *Circular 939, US Department of Agriculture: Washington, DC, USA*: 1-19.

Parikh, R. Y., Singh, S., Prasad, B. L., Patole, M. S., Sastry, M. and Shouche, Y. S. (2008). Extracellular synthesis of crystalline silver nanoparticles and molecular evidence of silver resistance from *Morganella* sp.: towards understanding biochemical synthesis mechanism. *Chembiochem* 9: 1415-1422.

Peterson, S. W. (2000). Phylogenetic analysis of *Penicillium* species based on ITS and LSU-rDNA nucleotide sequences. In: Samson, R. A. and Pitt, J. I. (Eds.) Integration of modern taxonomic methods for *Penicillium* and *Aspergillus* classification. Hargrove Academic Publishers, Amsterdam, p. 163-178.

Peterson, S. W. (2008). Phylogenetic analysis of *Aspergillus* species using DNA sequences from four loci. *Mycologia* 100: 205-26.

Peterson, S. W. and Horn, B. W. (2009). *Penicillium parvulum* and *Penicillium georgiense*, sp. nov., isolated from the conidial heads of *Aspergillus* species. *Mycologia* 101: 71-83.

Prasad, K. and Jha, A. K. (2009). ZnO nanoparticles: synthesis and adsorption study. *Natural Sciences* 1: 129-135.

Pum, D. and Sleytr, U. B. (1999). The application of bacterial S-layers in molecular nanotechnology. *Trends in Biotechnology* 17: 8-12.

Salvadori, M. R., Ando, R. A., do Nascimento, C. A. O. and Corrêa, B. (2014). Intracellular biosynthesis and removal of copper nanoparticles by dead biomass of yeast isolated from the wastewater of a mine in the Brazilian Amazonia. *PLoS One* 9: e87968.

Sanchez, C., Arribart, H. and Guille, M. M. G. (2005). Biomimetism and bioinspiration as tools for the design of innovative materials and systems. *Nature Materials* 4: 277-288.

Sarikaya, M., Tamerler, C., Jen, A. K. Y., Schulten, K. and Baneyx, F. (2003). Molecular biomimetics: nanotechnology through biology. *Nature Materials* 2: 577-585.

Thakkar, K. N., Mhatre, S. S. and Parikh, R. Y. (2010). Biological synthesis of metallic nanoparticles. *Nanomedicine* 6: 257-262.

Verkley, G. J., Dukik, K., Renfurm, R., Göker, M. and Stielow J. B. (2014). Novel genera and species of coniothyrium-like fungi in Montagnulaceae (Ascomycota). *Persoonia* 32: 25-51.

Walkley, A. J. and Black, I. A. (1934). Estimation of soil organic carbon by the chromic acid titration method. *Soil Science* 37: 29–38.

White, T. J., Bruns, T., Lee, S. and Taylor, J. (1990). Amplification and direct sequencing of fungal ribosomal RNA genes for phylogenetics. In: Innis, M. A., Gelfand, D. H., Sninsky, J. J. and White, T. J. (Eds.). PCR protocols a guide to methods and applications. Academic Press, San Diego, p. 315-322.

Wirsel, S. G., Runge-Froböse, C., Ahrén, D. G., Kemen, E., Oliver, R. P. and Mendgen, K. W. (2002). Four or more species of *Cladosporium* sympatrically colonize *Phragmites australis*. *Fungal Genetics and Biology* 35: 99-113.

Woo, P. C., Leung, S. Y., Ngan, A. H., Lau, S. K. and Yuen, K. Y. (2012). A significant number of reported *Absidia corymbifera* (*Lichtheimia corymbifera*) infections are caused by *Lichtheimia ramosa* (*syn. Lichtheimia hongkongensis*): an emerging cause of mucormycosis. *Emerging Microbes & Infections* 1: e15.

Yadav, A., Kon, K., Kratosova, G., Duran, N., Ingle, A. P. and Rai, M. (2015). Fungi as an efficient mycosystem for the synthesis of metal nanoparticles: progress and key aspects of research. *Biotechnology letters* 37: 2099-2120.

Zalar, P., de Hoog, G. S., Schroers, H. J., Crous, P. W., Groenewald, J. Z. and Gunde-Cimerman, N. (2007). Phylogeny and ecology of the ubiquitous saprobe *Cladosporium sphaerospermum*, with descriptions of seven new species from hypersaline environments. *Studies in Mycology* 58: 157-83.

Chapter III

Extracellular Synthesis, Characterization and Mechanistic Insights of Mycogenic Iron Oxide Nanoparticles

Preface

The chapter discusses the extracellular synthesis of iron oxide nanoparticles (IONPs) using *Aspergillus japonicus* AJP01. The fungal isolate demonstrated its ability to hydrolyze the precursor salt solution, a mixture of iron cyanide complexes, under ambient conditions. Hydrolysis of these complexes released ferric and ferrous ions, which underwent protein mediated coprecipitation and controlled nucleation resulting in the formation of IONPs. TEM, SAED, EDS and XRD analysis confirmed the mycosynthesis of IONPs. The synthesized particles were cubic in shape with a size range of 60-70 nm with crystal structure corresponding to magnetite. SEM analysis revealed the absence of IONPs on fungal biomass surface, indicating extracellular nature of synthesis. FTIR spectroscopy confirmed the presence of proteins on as-synthesised IONPs, which may confer their stability. On the basis of present findings, a probable mechanism for synthesis of IONPs is proposed. The simplicity and versatility of the present approach can be utilized for the synthesis of other nanomaterials.

3.1 Introduction

The advent of nanotechnology has revolutionized science, economy and everyday life. Iron oxide nanoparticles (IONPs) have been consistently used in developing technologies related to data storage, environmental remediation, energy generation, water purification etc. (Teja and Koh 2009). Narrowing our focus to applications of IONPs in biology, their amenable properties offer very useful and attractive potential in biomedicine (Lin 2015). IONPs interact efficiently with biological entities like cells [10-100µm], viruses [20-450nm], proteins [5-50nm] and genes [10-100nm] thus leading to exciting opportunities in the field of cell tagging and tracking (Becker et al. 2007; Connell et al. 2015); drug and gene delivery (Dobson 2006; Colombo et al. 2012), detection of probes (Lin et al. 2007; Hassen et al. 2008; Plank 2009), MRI imaging (Sun et al. 2008; Ling et al. 2015), hyperthermic effect (Thiesen and Jordan 2008; Singh and Sahoo 2014) as well as a prospective material to be applied in agriculture (Solanki et al. 2015).

Considering the ill-effects of physicochemical methods (like costly setup, energy intensive processes, poly-disperse particle synthesis, generation of toxic by-products, non-eco-friendly etc.), alternate methods for nanoparticle synthesis deserve merit. The increased awareness towards the development of clean, reliable and eco-friendly alternate for synthesis of IONPs has encouraged the researchers to look into newer "Greener" methods (Gao et al. 2008; Wang et al. 2009). Various multicellular as well as unicellular organisms have been known to synthesize IONPs for various functions. Among the multicellular ones, biomineralization of magnetite (Fe_3O_4), one of the most common forms of iron oxide has been shown to occur in diverse range of organisms like algae, insects, mollusks, fish and birds (Bazylinski et al. 1991). Unlike, multicellular organisms, the synthesis of IONPs has been pronouncedly studied in unicellular organisms like magnetotactic and iron reducing bacteria.

The landmark discovery of magnetotactic bacteria [MTB] by Richard Blakemore disclosed one of the most remarkable biomineralization processes in nature (Blakemore 1982). MTB are in fact the oldest reported microbial factories for IONPs fabrication. As a naturally occurring phenomenon, it involves the formation of intracellular magnetic structure, the magnetosomes, which are nanosized, membrane enclosed crystals of magnetic iron minerals composed of magnetite [Fe_3O_4] or greigite [Fe_3S_4] (Jogler et al. 2009). Magnetosome crystals have species-specific morphologies, sizes and arrangements (Figure 3.1; Arakaki et al. 2008). Their formation is genetically regulated by a complex set of genes situated mainly at magnetosome island in MTB genome (Matsunaga and Okamura 2003; Komeili 2007). Magnetosomes are involved in magnetotaxis which direct the bacterial cells to swim towards the growth favouring microoxic zones of the chemically stratified natural water (Frankel and Blakemore 1989). Almost all the reported MTB are microaerophiles which can form multiple magnetosomes within them through an oxygen sensitive process and are motile by means of flagella. The group is highly diverse in terms

of phylogeny, morphology and physiology (Amann et al. 2007). Despite their high abundance and ubiquitous occurrence in marine and fresh water habitats, most MTB are difficult to isolate and cultivate *in-vitro,* which is probably due to their adaptation to complex chemical gradients typically encountered in stratified sediments. Only a limited number of MTB strains have been isolated in pure culture (Schuler et al. 2007). Out of which species of *Magnetosiprillum* are extensively studied for elucidation of mechanism for magnetosome formation (Figure 3.2; Murat et al. 2010).
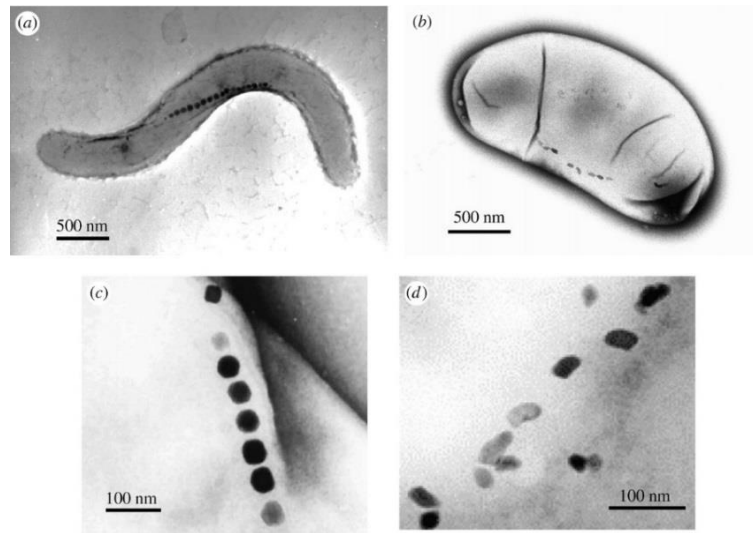
Figure 3.1 TEM images of magnetotactic bacteria. (a) *Magnetospirillum magneticum* strain AMB-1 and (b) *Desulfovibrio magneticus* strain RS-1. Magnetotactic bacteria synthesized bacterial magnetic particles of (c) the AMB-1 strain and (d) the RS-1 strain. (Adapted with permission from Arakaki et al. 2008)
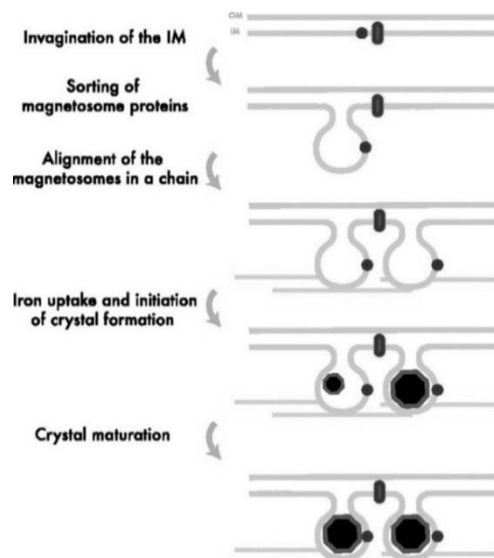
Figure 3.2 Model for step-wise assembly of magnetosomes in *Magnetospirillum magneticum* strain AMB-1 wherein IM and OM stand for inner membrane and outer membrane respectively. (Adapted with permission from Murat et al. 2010)

In general, magnetosomes are arranged along the axis showing single or multiple chains with particle size ranging between 35 to 120 nm, with single domain magnetism (Bazylinski et al. 1994). Surrounding the mineral core is the magnetosome membrane which is a lipid bilayer membrane with composition considerably similar to cytoplasmic membrane (Tanaka et al. 2006). It originates from the cytoplasmic membrane by invagination, represents a distinct subcellular compartment and has a unique biochemical composition. Roughly 20 magnetosome-specific proteins function in the vesicle formation, magnetosomal iron transport and control the crystallization and intracellular arrangement (Schuler 2008). It has been hypothesised that these membrane proteins may play functional roles like accumulation of supersaturating iron concentration, maintenance of reductive conditions and mineralization of iron either by oxidation or by partial reduction and dehydration of ferrihydrite intermediate to magnetite (Arakaki et al. 2008).

Iron reducing bacteria (IRB) is another group of microorganisms known to synthesize IONPs. Synthesis of IONPs by IRB is exclusively extracellular (Lovley et al. 1987; Glasauer et al. 2002). The precipitation of magnetite granules occurs for energy generation under strict anaerobic conditions. At biochemical level, electrons originated from oxidation of organic matter are transferred to ferric ion, mostly in the form of ferrihydrite which reduces to magnetite. The magnetite particles are usually 10-50 nm in size with round or oval shape (Lovley et al. 1990). Unlike the lipid bilayer membrane surrounding magnetosomes, magnetite granules synthesized by IRB are mostly bare "uncovered" with exception as observed in *Shewanella putrefaciens* wherein exopolysaccharides act as covering material (Dong et al. 2000). Cellular entities like membrane bound c-type cytochromes (involved in electron transport) and Fe (III) reductase (involved in ferric iron reduction) facilitate the formation of magnetite in IRBs viz., *Thiobacillus*, *Geobacter*, *Shewanella*, *Desulfovibrio*, etc. (Vali et al. 2004; Lovley et al. 1993).

Apart from the groups of MTB and IRB which synthesise IONPs in microaerophillic and anaerobic environment, respectively, recent years have observed reports of many other species synthesizing IONPs under aerobic conditions. Bacteria like acid tolerant *Leptospirillum ferriphilum* (Gao et al. 2006) and iron oxidising *Leptothrix ochracea* (Hashimoto et al. 2007) were found to produce magnetosome like iron mineral nanoparticles. Both of these bacterial species belong to the class of Chemolithotrophs which utilize iron as an energy source similar to IRBs. Bharde et al. (2005, 2008) have successfully obtained magnetite, maghemite and iron sulphide (gregite) nanoparticles from an aerobic bacterium, an Actinobacteria species using aqueous mixture of potassium ferricyanide/ferrocyanide. The nanoparticles produced by Actinobacter under aerobic conditions were found to have a protein coat. The only conclusive report of fungi producing IONPs is by Bharde et al. (2006), where *Fusarium oxysporum* and *Verticillium* sp. were challenged with mixture of potassium ferricyanide/ferrocyanide at room temperature thus

producing magnetite nanoparticles extracellularly. This research group also explored the possibility of using mixture of ferric and ferrous chloride but the particles formed were irregular in shape and had poor crystal structure.

In the present study, learning from natural biomineralization process in various microorganisms and gathering information from already published studies related to synthesis of IONPs, an indigenous protocol for extracellular mycosynthesis of IONPs was developed. Fungi isolated from metal rich region (as discussed in chapter II) were chosen as potential candidate(s) for biosynthesis because of their ease in handling, low cost maintenance as well as easy downstream processing due to predominant extracellular nature of nanoparticles synthesis (Gade et al. 2010). Additionally, being a eukaryotic organism, fungi have been reported to secrete versatile range of extracellular components yet in higher amounts as compared to prokaryotic organisms. This might be helpful in achieving significantly higher and desired productivity of various nanoparticles (Dhillon et al. 2011). Simplicity and versatility of the present approach can be utilized for extracellular biosynthesis of other nanoparticles.

3.2 Materials and methods

3.2.1 Screening of fungal isolates

All the fungal isolates were screened to check their ability to hydrolyze the precursor salt solution comprised of freshly prepared potassium ferricyanide $K_3[Fe(CN)_6]$ and potassium ferrocyanide $K_4[Fe(CN)_6]$ in a millimolar ratio of 1: 0.5. For this purpose, 20 g fresh weight of three day old fungal biomass was exposed to 100 mL of precursor salt solution in a 250 mL Erlenmeyer flask and incubated at 28 ˚C for 72 h on a rotary shaker (120 rpm). In order to prevent the photo-decomposition of ferricyanide $[Fe(CN)_6^{-3}]$ to ferrocyanide $[Fe(CN)_6^{-2}]$ ions, flasks were incubated under dark conditions. The hydrolysis of iron cyanide complex was monitored by taking UV-visible absorption spectra of the supernatant as a function of time. The isolate showing maximum hydrolysis in the recorded time was selected for further study.

3.2.2 Extracellular synthesis of IONPs

The selected fungal isolate was maintained on PDA slants (pH 5.6) with repeated sub-culturing on fresh media. From an actively growing culture, a loopful of spores was inoculated in 80 mL of MGYP medium (0.3 % malt extract, 1.0 % glucose, 0.3 % yeast extract, 0.5 % peptone; pH 7.0) in 250 mL Erlenmeyer flasks. The inoculated flasks were incubated at 28 ˚C for 72 h on a rotary shaker (120 rpm). After incubation, the fungal biomass was separated from the culture medium by centrifugation (5000 rpm) at 4 ˚C for 15 min, and washed thrice with autoclaved Milli-Q water to remove all traces of media. Typically, 20 g of biomass (fresh weight) was resuspended in 100 mL of precursor salt solution in a 250 mL Erlenmeyer flask and incubated at 28 ˚C for 96 h on a rotary shaker

(120 rpm) under dark conditions. After incubation, the biomass was separated by filtration using Whatman grade 1 filter paper (Whatman Inc., USA) and the cell-free filtrate containing IONPs was obtained for further characterization. Biomass in autoclaved Milli-Q water (without precursor salt solution) as positive control and pure precursor salt solution (without biomass) as negative control were also incubated simultaneously along with the experimental flasks in three replicates.

3.2.3 Characterization of nanoparticles

3.2.3.1 UV-visible spectroscopy

Hydrolysis of iron cyanide complex was monitored by taking UV-visible absorption spectra of the culture supernatant at different time intervals. The measurements were carried out on a V-630 UV-visible spectrophotometer instrument (Jasco Corporation, Japan) at a resolution of 1 nm in the range of 200-800 nm with a scan speed of 400 nm/min using a 1 cm path length quartz cuvette. The results were analysed using Jasco's spectra manager software and graphs were plotted using Origin 9.0 (OriginLab Corporation, USA).

3.2.3.2 Transmission electron microscopy and selected area electron diffraction

Samples for transmission electron microscopy (TEM) imaging and selected area electron diffraction (SAED) pattern determination were prepared on a carbon-coated TEM grid by drop coating the cell-free filtrate containing IONPs after 30 min sonication in a water bath sonicator (Thermo Scientific, USA). After few minutes, extra solution was removed using a lint free blotting paper and the grids were kept in a vacuum desiccator prior to measurement. TEM measurement and SAED pattern determination were carried out on a JEM-2100 instrument (JEOL, Japan) operated at an accelerating voltage of 80 kV and 200 kV for low and high resolution imaging, respectively.

3.2.3.3 Energy dispersive spectroscopy

Energy dispersive spectroscopy (EDS) analysis was carried out using a H-7650 scanning electron microscope (SEM) instrument (Hitachi High-Technologies Corporation, Japan) equipped with Quantax EDS attachment (Bruker AXS Ltd., UK) by freeze drying the cell-free filtrate containing IONPs followed by coating on a double sided carbon tape attached to the grid surface. The data was recorded using a pulse processor, which measures the signals and passes them onto an analyser for data display and analysis.

3.2.3.4 X-ray diffraction

The crystalline phase of the iron oxide was identified by grazing incidence X-ray diffraction (GIXRD) measurements of thin layer of mycosynthesised IONPs on glass substrates carried out on a X'Pert PRO X-ray diffractometer instrument (PANalytical BV, The Netherlands). The diffraction pattern was recorded between 20° and 80° (2θ) with diffractometer operated at a voltage of 40 kV and a current of 30 mA with CuKα radiation. Crystal phase was determined by comparing the calculated values of inter planar spacing

and corresponding intensities of diffraction peaks with theoretical values from the Joint Committee on Powder Diffraction Standards-International Centre for Diffraction Data (JCPDS-ICCD) database.

3.2.3.5 Fourier transform infrared spectroscopy

Fourier transform infrared (FTIR) spectroscopy measurements of the freeze-dried IONPs diluted with potassium bromide in the ratio of 1: 100 were recorded on a IR Prestige-21 FTIR instrument (Shimadzu, Japan) with a diffuse reflectance mode (DRS-8000) attachment. All measurements were carried out in wavenumber range of 400-4000 cm^{-1} at a resolution of 4 cm^{-1}.

3.2.3.6 Scanning electron microscopy

For scanning electron microscopy (SEM) analysis of the fungal biomass exposed to precursor salt solution, the biomass was fixed overnight at 4 ˚C with 2.5 % (v/v) glutaraldehyde in 0.1 M sodium phosphate buffer, pH 7.2. The specimen was rinsed in buffer, dehydrated in a series of 30-100 % ethanol and then dried in a desiccator under vacuum. An automatic Polaron OM-SC7640 sputter coater instrument (Quorum Technologies, UK) was used for coating the specimens with gold particles. The specimen was examined using EVO 40 scanning electron microscope instrument (Carl Zeiss, Germany).

3.2.4 Fungal viability assay

The growth (colony forming unit, CFU) and viability of fungus before and after exposure to precursor salt solution was checked. For determination of CFU, the fungal biomass was cut into pieces (5 × 5 mm) and shaken with 0.02 % Tween 80 for 30 min on a rotary shaker (250 rpm). Suitable dilutions were spread on the surface of PDA medium (pH 5.6). CFU on the plates were counted after incubation at 28 ˚C for 72 h under dark conditions (Schnurer 1993). The fungus viability was observed by inoculating the exposed fungal biomass on PDA medium (pH 5.6). The inoculated petri plates were incubated at 28 ˚C for 72 h under dark conditions.

3.2.5 Elucidation of the mechanism behind synthesis of IONPs

3.2.5.1 Protein purification and one dimensional gel electrophoresis

Extracellular proteins from both the test (biomass exposed to precursor salt solution) and control (biomass in autoclaved Milli-Q water) were purified using ammonium sulphate precipitation. Solid ammonium sulphate was added slowly at a final saturation of 80 % (Simpson 2004). The mixture was gently stirred for 4-5 h at 4 ˚C. The resulting precipitate was subsequently collected by centrifugation at 10,000 rpm for 20 min at 4 ˚C. The proteins obtained thereafter were resuspended in minimum amount of 50 mM phosphate buffer, pH 7.2 and purified using a 12-kDa cut off cellulose dialysis membrane (Catalogue no. D9652; Sigma -Aldrich, USA) pre-treated as per the manufacturer's instructions. Briefly, the

precipitated protein was filled in the treated dialysis bag, which was then suspended in dialysis buffer (50 mM phosphate buffer, pH 7.2) and stirred slowly at 4 ˚C. The buffer was changed 3-4 times over a 12 h period. The total protein concentration in the dialyzed samples was estimated by standard protocol of Lowry et al. (1951), using bovine serum albumin as standard.

The dialyzed protein fractions were separated on the basis of molecular weight by sodium dodecyl sulphate-polyacrylamide gel electrophoresis (SDS-PAGE) as per standard procedure with adequate modifications (Laemmli 1970). Samples were denatured in 2X sample buffer containing 60 mM Tris (pH 6.8), 25 % glycerol, 2 % SDS, 14.4 mM 2-mercaptoethanol, 0.1 % bromophenol blue and boiled for 5 min, followed by centrifugation at 8,000 rpm for 1 min at 4 ˚C. Unstained protein molecular weight marker SM0661 was run along with samples. Electrophoresis was performed on a Mini Protean® Tetra-Cell instrument (BioRad Laboratories, USA) at a constant voltage of 80 kV. After electrophoresis, the gel was stained with Coomassie Brilliant blue G-250 stain and was observed in a BioRad Gel Doc^{TM} XR imaging system. The molecular mass of the protein bands was determined by interpolation from a semi- logarithmic plot of relative molecular mass versus the R_f value (relative mobility).

3.2.5.2 Role of fungal extracellular proteins in IONPs synthesis

A separate experiment was performed to examine the possibility of IONPs synthesis, solely by the fungal extracellular proteins. For this, 20 g (fresh weight) of fungal biomass was suspended in 100 mL of autoclaved Milli-Q water and incubated for 72 h in Erlenmeyer flask in similar conditions as described earlier. After incubation, the cell-free filtrate containing extracellular proteins was recovered by filtration using Whatman grade 1 filter paper. The precursor salt solution at a final millimolar ratio of 1: 0.5 was added to the flask containing cell-free filtrate and incubated on a rotary shaker (120 rpm) at 28 ˚C for 96 h under dark conditions. Cell-free filtrate (without precursor salt solution) as positive control and pure precursor salt solution (without cell-free filtrate) as negative control were also incubated simultaneously along with the experimental flasks in three replicates.

3.2.5.3 Role of fungal extracellular proteins in IONPs stabilization

The role of extracellular proteins in nanoparticle stabilization was investigated. For this, the cell-free filtrate containing extracellular proteins from positive control flask (without precursor salt solution) was recovered by filtration using Whatman grade 1 filter paper. The commercially available magnetite nanoparticles (Cat. No. 637106; Sigma-Aldrich, USA) at a final concentration of 50 mg/mL was added to the cell-free filtrate after 3 h of vigorous sonication and incubated on a rotary shaker (150 rpm) at 28 ˚C for 72 h under dark conditions. After which dynamic light scattering and zeta potential measurements were carried out on a Zetasizer Nano ZS (Malvern Instruments Ltd, UK) at

neutral pH. Magnetite nanoparticles (50 mg/mL) suspended in water and cell-free filtrate containing extracellular proteins from positive control flask were used as control.

3.2.6 Assay for hydrolysis of iron cyanide complex

3.2.6.1 Ferrozine assay for estimation of free iron

In order to estimate the free iron content in the solution after completion of reaction, ferrozine assay was performed in the cell-free filtrate (Gibbs 1976). For this, aliquot (1 mL) was treated with ferrozine at a final concentration of 1 mM and the absorbance was recorded at 562 nm against blank (1 mM ferrozine). Ferrous sulphate solution (1 mM) was used as positive control whereas cell-free filtrate (without precursor salt solution) and pure precursor salt solution (without cell-free filtrate) were used as negative controls. The experiment was performed in triplicate.

3.2.6.2 Phenolphthalin assay for cyanide

To estimate the amount of residual cyanide in the solution after iron cyanide complex hydrolysis by the fungus, phenolphthalin assay was performed (Cacace et al. 2007). Briefly, the reaction was setup in a 50 mL volumetric flask containing 45 mL of pH adjusted borax buffer (2.5×10^{-2} M; pH 10.8). To this 100 µL of cell-free filtrate containing residual cyanide (after 96 h of biomass exposure) was added as sample. Phenolphthalin (2.0×10^{-4} M; dissolved in 0.9 % (v/v) ethanol), copper (II) (3.6×10^{-4} M (Cu) as copper (II) nitrate) and EDTA (1.8×10^{-4} M) were added in the order as mentioned. The final volume was made up to 50 mL with the buffer, incubated for 5 min at 25 ˚C and the absorbance was recorded at 553 nm against blank without sample.

3.2.7 Effect of reaction conditions on cyanide hydrolysis

For efficient and faster hydrolysis of cyanide complex, experiments were carried out to test the effect of various reaction parameters viz., reaction pH, amount of biomass and concentration of precursor salt. The hydrolysis of iron cyanide complex was monitored by taking UV-visible absorption spectra of the supernatant as a function of time. The experiments were performed in triplicate with respective control.

3.2.7.1 Effect of pH

Effect of reaction pH was studied by altering the pH of Milli-Q water before the addition of fungal biomass and precursor salt. For this, either 0.1 N HCl or 0.1 N NaOH was added to 100 mL of cell-free filtrate to adjust the final pH at 2.0, 4.0, 6.0, 8.0 and 10.0 using a Cyberscan 1100 pH meter (Eutech Instruments, Singapore).

3.2.7.2 Amount of biomass

In order to study the amount of biomass, the quantity of fungal mycelia suspended in autoclaved Milli-Q water was varied. For this purpose 20 g, 10 g, 6.66 g, 5 g and 3.33 g

of biomass (fresh weight) was suspended in 100 mL of autoclaved Milli-Q water to achieve the biomass: water ratio of 1:5, 1:10, 1:15, 1:20 and 1:30 respectively.

3.2.7.3 Effect of concentration of precursor salt

The effect of precursor salt concentration on hydrolysis of cyanide complex was studied by varying the initial concentration of $K_3[Fe(CN)_6]$ in the range of 0.1- 4.0 mM with respective variation in concentration of $K_4[Fe(CN)_6]$ to maintain their millimolar ratio of 1:0.5.

3.3 Results and discussion

3.3.1 Screening of fungal isolates

All the fungal isolates were screened to check their ability to hydrolyze the precursor salt solution. The absorption spectrum of precursor salt solution showed highly symmetric band with peak maximum at 420 nm which is attributed to the characteristic absorption maximum of potassium ferricyanide (Williams 1997). A steady decrease in intensity of peak as a function of time of reaction was observed during the reaction spanning 120 h. Change in the absorbance at 420 nm was recorded to calculate the % hydrolysis of iron cyanide complex (Figure 3.3).
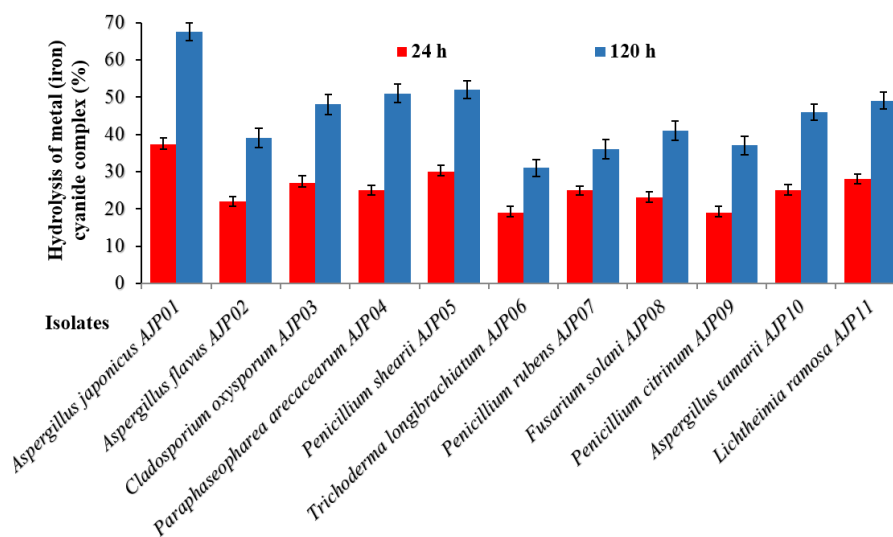
Figure 3.3 Comparative ability of various fungal isolates towards hydrolysis of precursor salt

Maximum hydrolysis of iron cyanide complex was observed in case of *Aspegillus japonicus* AJP01 which resulted in 37.28 % hydrolysis within 24 h and 67.52 % within 120 h. Among all the isolates, *Trichoderma longibrachiatum* AJP06 showed least potential for hydrolysing iron cyanide complex in the recorded time. No significant increase was

observed in the percent hydrolysis after 120 h among all the isolates. The isolate showing maximum hydrolysis of iron cyanide complex was selected for the mycosynthesis of IONPs.

3.3.2 Mycosynthesis and characterization of IONPs

The extracellular synthesis of IONPs was achieved by exposing fungal biomass of *Aspergillus japonicus* AJP01 to precursor salt solution under ambient conditions. The isolate successfully hydrolyzed the iron cyanide complexes as a steady decrease in the intensity of the peak at 420 nm as a function of time was observed during the reaction spanning 96 h (Figure 3.4). Noteworthy was the development of a broad absorption band at ca. 330 nm corresponding to formation of iron oxide (Sherman and Waite 1985). This indicates the concurrent synthesis of IONPs as the cell-free filtrate turned brown in colour at the end of the reaction (inset to Figure 3.4). Similar kind of observation regarding change in colour of the cell-free filtrate has been reported by Bharde et al. (2006), wherein synthesis of IONPs was achieved using *Fusarium oxysporum* and *Verticillium* species.
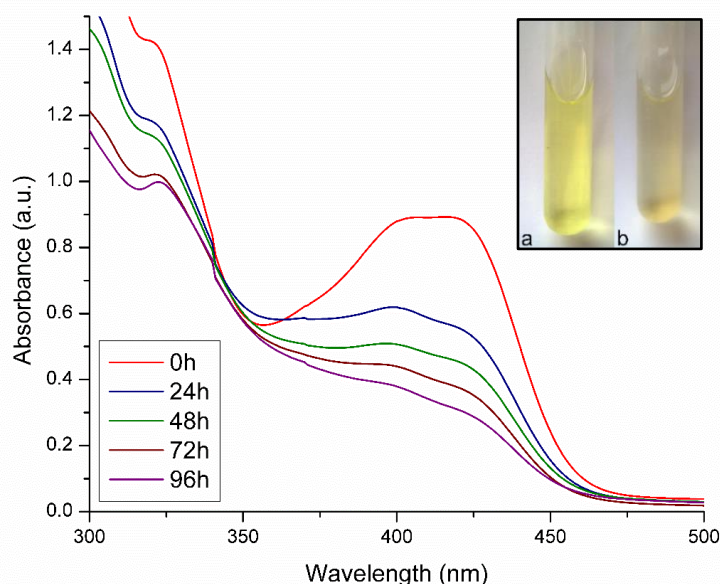
Figure 3.4 UV-visible absorption spectrum of cell-free filtrate representing gradual synthesis of IONPs as a function of time. Inset shows test tube containing cell-free filtrate exposed to precursor salts at (a) 0 hours and (b) 96 hours of reaction

Percent hydrolysis of iron cyanide complexes showed no significant increase after 96 h of reaction (Figure 3.5). The subsequent decrease in the rate of hydrolysis with time may be credited to the increase in pH towards alkaline apart from decline in substrate concentration which might have affected the fungal enzyme activity like nitrilase/cyanide hydratase. Cyanide hydratase is primarily a fungal enzyme responsible for hydrolysis of cyanide complexes forming formamide (Ebbs 2004). The hydrolysis may be attributed to cyanide biodegradation as a consequence of its availability as sole source of carbon and nitrogen for the survival of fungus under nutrient deprived stress conditions (Dumestre et al. 1997; Barclay et al. 1998a).
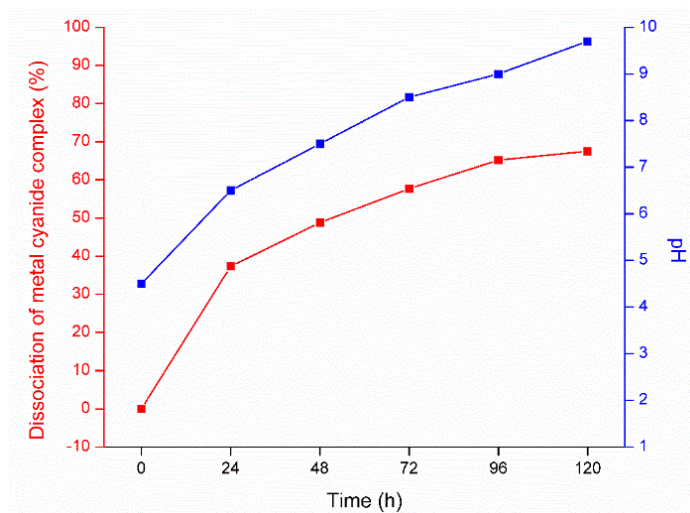
Figure 3.5 Graphical representation of increase in rate of hydrolysis of iron cyanide complex (in percent) observed at 420 nm (red) and increase in reaction pH (blue) as a function of time

The size and morphology of mycosynthesised IONPs were determined by TEM measurements. A representative TEM micrograph (Figure 3.6) revealed the particles morphology to be cubic in shape with strict control over particle size. The particle size distribution histogram obtained from TEM measurements (Figure 3.7) showed that maximum number of particles confined in the range of 60-70 nm and possess an average size of 82.25 ± 5 nm. It is notable that the size of mycosynthesised nanoparticles is less than 100 nm as characterized by TEM analysis. This amenable size makes them potential candidate for use in various bio-inspired applications, where particle size is an essential consideration (Arruebo et al. 2007).
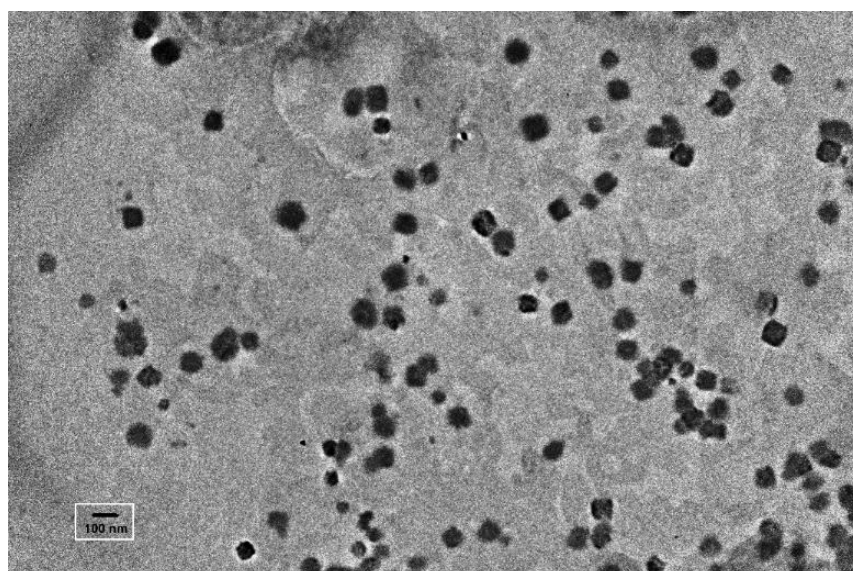
Figure 3.6 TEM micrograph of mycosynthesised iron oxide nanoparticles. (Scale bar equivalent to 100 nm)
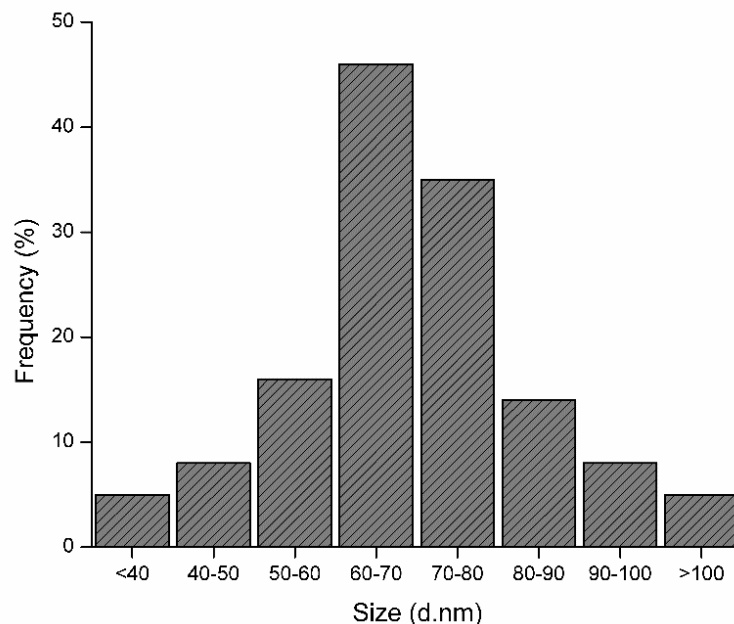
Figure 3.7 Particle size distribution histogram of IONPs extracted from TEM analysis

The SAED patterns (Figure 3.8) confirmed the nanoparticle to be crystalline and the diffraction pattern data were found to be consistent with the typical structure characteristic of iron oxide (magnetite [Fe_3O_4] and maghemite [γ-Fe_2O_3]). On the basis of calculated d-values, the diffraction pattern analysis suggested that particles belong to magnetite (Sun et al. 2004). High-resolution TEM micrograph (Figure 3.9) demonstrated the well-resolved interference fringe pattern attesting to the crystallinity of a typical magnetite nanoparticle with no sign of crystal defects.
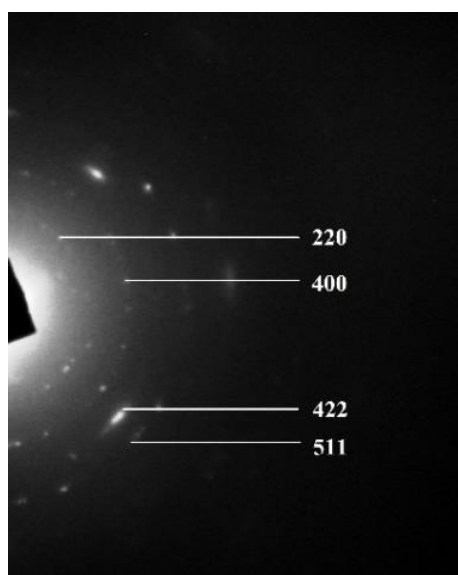
Figure 3.8 SAED pattern from a single iron oxide nanoparticle. The diffraction rings correspond to allowed (511), (422), (400) and (220) Bragg's reflections
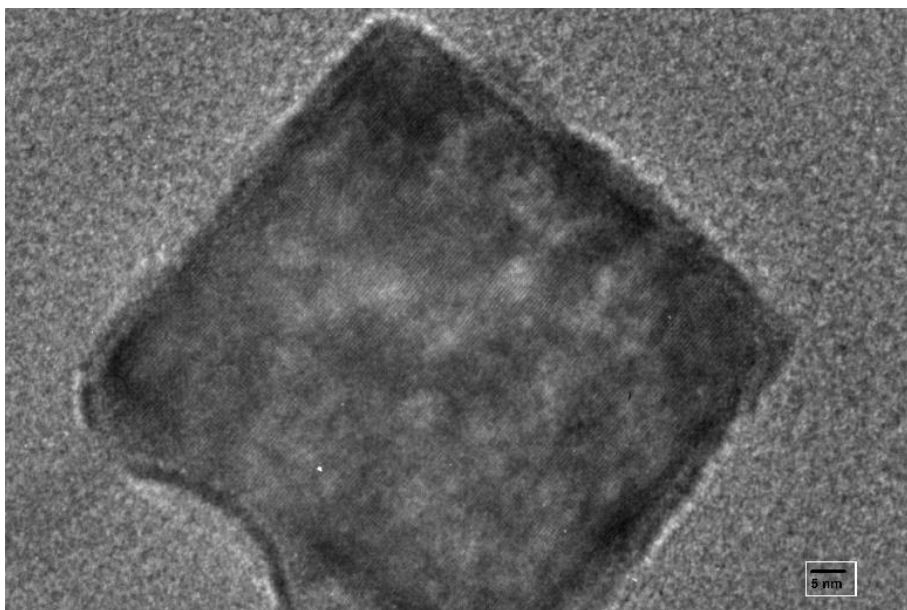
Figure 3.9 High resolution TEM micrograph of a single iron oxide nanoparticle. (Scale bar equivalent to 5 nm)

EDS analysis of freezed dried sample was performed to determine the elemental composition of nanoparticles (Figure 3.10). The EDS spectrum showed an optical absorption band at ~6.5 eV which is representative of iron (Njagi et al. 2010). Figure 3.11 shows the XRD pattern of synthesised IONPs. Analysis of XRD spectra showed characteristic Bragg's diffraction peaks which are in good agreement with the standard magnetite (JCPDS: 19-0629).
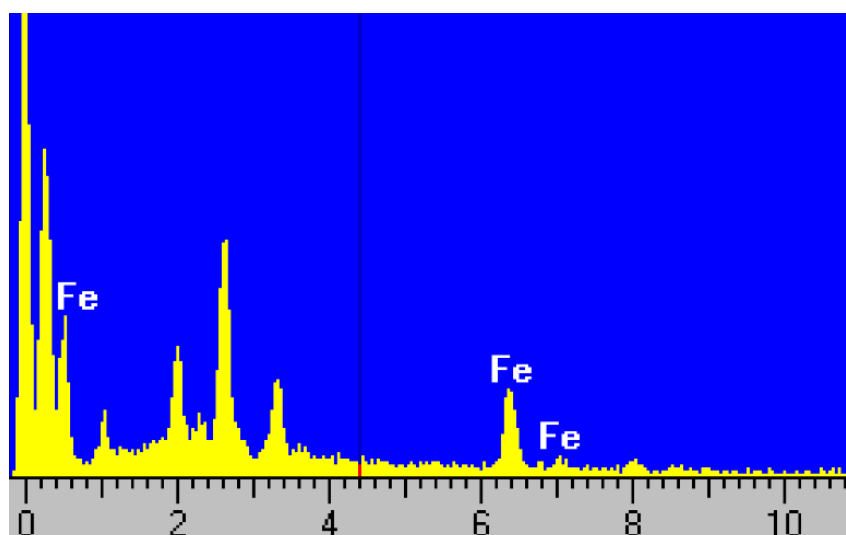
Figure 3.10 EDS spectrum of freeze dried cell-free filtrate containing mycosynthesised iron oxide nanoparticles
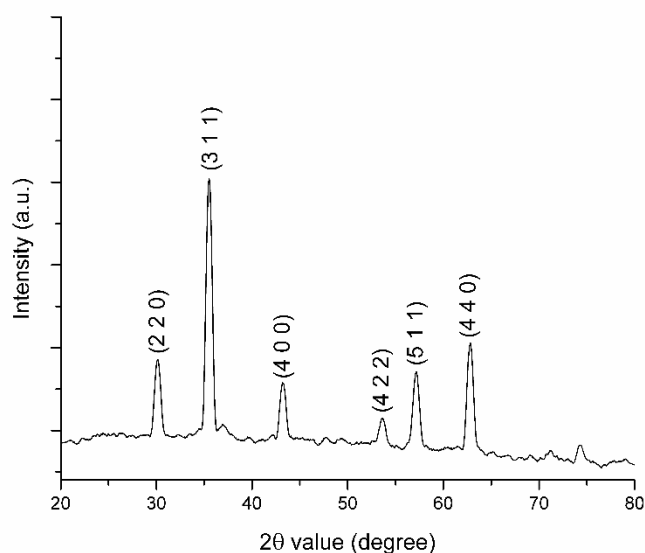
Figure 3.11 GIXRD pattern of a thin film of mycosynthesised IONPs. The XRD pattern indicates Bragg's reflections corresponding to the magnetite structure

FTIR measurements were carried out to identify the possible interaction between IONPs and bioactive molecules that may be responsible for their synthesis and stabilization (Figure 3.12). FTIR analysis of freeze dried samples showed a prominent vibration band at wavenumber 1635 cm^{-1} assigned to the amide I bond of proteins arising due to carbonyl stretch in proteins, wavenumber 1458 cm^{-1} representing –CH$_2$– bending mode characteristic of protein side chains and wavenumber 1400 cm^{-1} indicating COO$^-$stretching (Macdonald and Smith 1996; Wang et al. 2006; Yang et al. 2007). The proteins are believed to be associated to nanoparticles in their native secondary structure as indicated by vibration band at wavenumber 1635 cm^{-1} (Takekiyo et al. 2009).
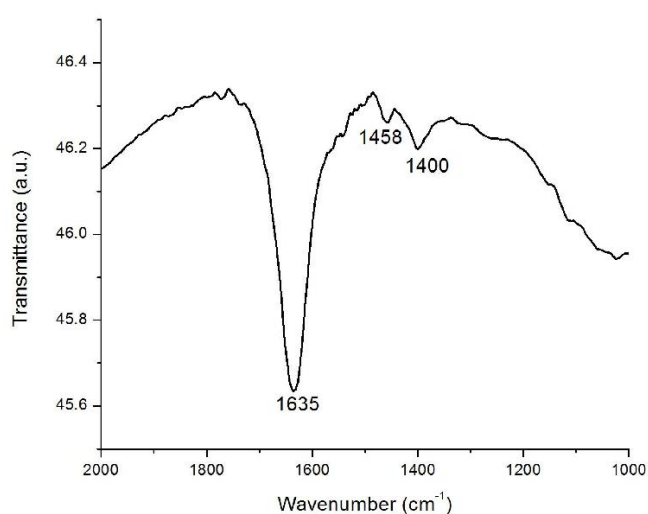
Figure 3.12 FTIR spectrum of freeze dried sample of iron oxide nanoparticles

To examine the possibility of synthesis of IONPs bounded to the fungal biomass, SEM imaging of the fungal biomass exposed to the precursor salt solution was performed after completion of reaction. A representative SEM micrograph of the exposed biomass (Figure 3.13) showed the absence of IONPs on fungal surface, signifying exclusively extracellular synthesis by this fungal isolate.
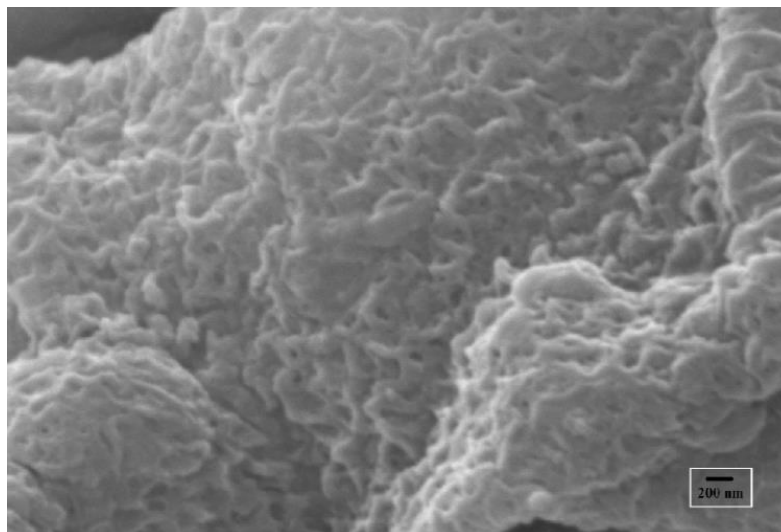
Figure 3.13 SEM micrograph of fungal biomass exposed to precursor salts showing absence of iron oxide nanoparticles on biomass surface. (Scale bar equivalent to 200 nm)

3.3.3 Fungal viability assay

The growth in terms of CFU of the fungus before and after exposure to precursor salt solution was determined to be 4×10^6 and 7×10^6, respectively. These results show that the fungus was able to maintain its growth and viability as it showed decent increase in CFU values after 96 h of exposure to precursor salt solution containing cyanide proving the utilization and degradation of cyanide as energy source. Similar results were also obtained for the viability test as carried out on PDA petri plates (Figure 3.14).
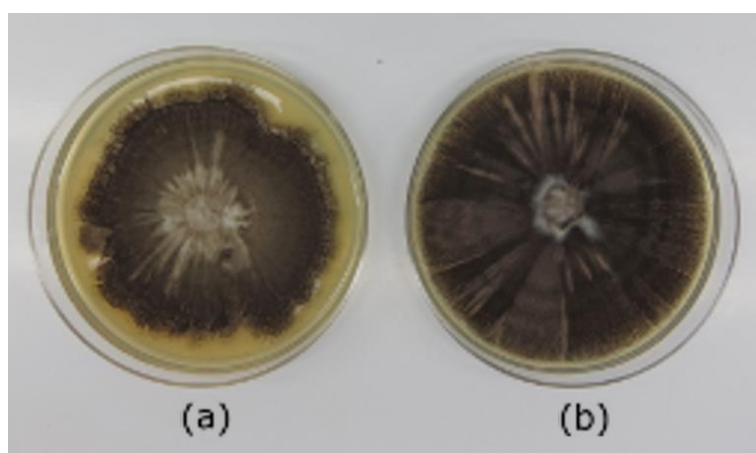
Figure 3.14 Viability of *Aspergillus japonicus* AJP01 on PDA medium (pH 5.6) (a) before and (b) after 96 h of exposure to precursor salt solution

3.3.4 Mechanism behind synthesis of IONPs

3.3.4.1 Profiling of extracellular proteins secreted from *Aspergillus japonicus* AJP01

A significant difference was observed in the concentration of various extracellular proteins expressed from biomass exposed to the precursor salt solution as compared to control (unexposed biomass). The concentration of extracellular proteins secreted by the fungal biomass exposed to precursor salt solution was determined to be 1125 ± 7.5 µg mL^{-1} which was nearly twice the concentration of extracellular proteins (587 ± 2.3 µg mL^{-1}) secreted by the unexposed biomass as estimated by Lowry's assay. To identify the active role of extracellular proteins secreted by fungal biomass in synthesis and/or stabilization of IONPs, the protein profiles were compared by one dimensional SDS-PAGE which revealed the presence of several extracellular proteins (Figure 3.15). These results indicated the elevated expression of various extracellular proteins in the presence of precursor salt solution, which may be responsible for the coprecipitation, controlled nucleation and/or stabilization of IONPs.
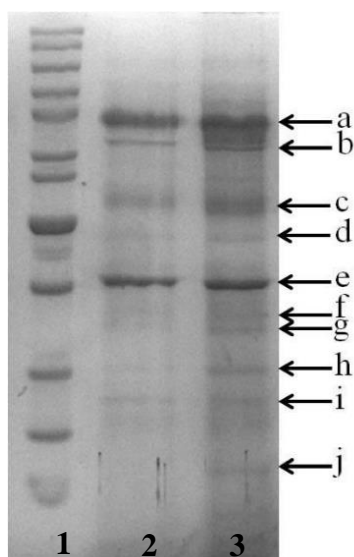
Figure 3.15 SDS-PAGE analysis of purified extracellular proteins from *Aspergillus japonicus* isolates AJP01. From left; Lane 1, 10-200 kDa molecular size marker (Fermentas SM0661; 200, 150, 120, 100, 85, 70, 60, 50, 40, 30, 25, 20, 15 and 10 kDa). Purified extracellular proteins obtained from unexposed (Lane 2) and exposed (Lane 3) fungal biomass to precursor salt solution. The arrows indicate extracellular proteins with molecular weight ca. 85 kDa (a), 76 kDa (b), 55 kDa (c), 49 kDa (d), 42 kDa (e), 38 kDa (f), 36.5 kDa (g), 31 kDa (h), 28 kDa (i) and 21 kDa (j)

3.3.4.2 Role of fungal extracellular proteins in synthesis and stabilization of IONPs

The role of fungal extracellular protein(s) in IONPs synthesis and/or stabilization was studied. For this purpose, the precursor salt solution was exposed to the cell-free filtrate of *Aspergillus japonicus* AJP01. The data obtained suggests that the hydrolysis of iron cyanide complexes may not be attributed to these extracellular proteins, as synthesis of IONPs using only cell free-filtrate (containing extracellular proteins) exclusive of biomass, failed to give positive results for hydrolysis of iron cyanide complexes. In this case, no change in the intensity at 420 nm was observed as a function of time during the course of reaction spanning 96 h. These results clearly indicate the role of fungal membrane proteins in hydrolyzing iron cyanide complexes and releasing free ferric and ferrous ions, and expectantly subsequent hydrolysis of cyanide (Barclay et al. 1998b). Fungi are well known

to degrade (hydrolyze) metal cyanide complex by the action of enzymes like cyanide hydratase or nitrilase, which hydrolyses the metal cyanide bond, releasing the free metal moiety (Barclay et al. 1998a; Ebbs 2004).

Role of fungal protein in stabilization was proved in context with commercially available magnetite nanoparticles. A zeta potential of -1.83 mV was observed in control having magnetite nanoparticles suspended in water, whereas a zeta potential value of -32.2 eV was observed for magnetite nanoparticles incubated with fungal extracellular proteins. The more negative zeta potential observed in latter case signifies that the fungal extracellular proteins play an important role in stabilization of nanoparticles making them more dispersed and stable (Patil et al. 2007).

3.3.5 Hydrolysis of iron cyanide complex by fungus

The release of iron from iron cyanide complex as a result of its hydrolysis was confirmed by the ferrozine assay, wherein ferrozine specifically binds with free ferrous ions. However, it may non-specifically bind to free ferric ions as well. In our study, the precursor salt solution exposed to fungal biomass for 96 h showed positive result in ferrozine assay. However, under normal conditions the iron cyanide complex gives negative results on reaction with ferrozine as metal ions are strongly bound with cyanide and thus are unavailable for reaction. In earlier reports, it has been clearly demonstrated that complexed iron does not react with ferrozine and requires to be released from its complex form (Riemer et al. 2004). Ferrozine assay clearly indicated the degradation of cyanide complexes by fungal isolate and subsequent release of free metal ions (Barclay et al. 1998a; Dumestre et al. 1997). In the absence of free metal ions and only cell free filtrate negative results were observed.

The hydrolysis of iron cyanide complex was further confirmed using phenolphthalin as indicator. The method is based on the oxidation of phenolphthalin to phenolphthalein (pink) by cyanide in presence of copper (Haj-Hussein et al. 1997). As the assay requires immediate measurement of colour due to its instability, the method was modified by adding EDTA as a stabilizing agent (Cacace et al. 2007). In our study, the cyanide present in the precursor salt solution comprising of $K_3[Fe(CN)_6]$ and $K_4[Fe(CN)_6]$ in a millimolar ratio of 1: 0.5 respectively before exposure to fungal biomass was found to be nearly twice as compared to the one after exposure. This observation suggests the hydrolysis (breakdown) of cyanide by the fungal biomass resulting in its decreased availability to oxidize phenolphthalin.

3.3.6 Effect of various process parameters on hydrolysis of metal cyanide complex

Extracellular mycosynthesis of IONPs by *Aspergillus japonicus* AJP01 using $K_3[Fe(CN)_6]$ and $K_4[Fe(CN)_6]$ as source of ferric and ferrous ion depends upon a key step which involves the release of these ions from their complexes. The release of these ions from their respective cyanide complex is performed by fungus by the hydrolysis of metal cyanide

bond. In this regard, it can be conjectured that the extent of hydrolysis will be directly proportional to the IONPs yield. Therefore, in order to optimize the efficient synthesis of IONPs, various parameters which may influence the fungal hydrolytic activity were studied.

The effect of various reaction parameters were studied on hydrolysis of iron cyanide complex (Table 3.1). The effect of reaction pH was studied in the pH range of 2 to 10. The % hydrolysis as determined by recording the absorbance at 420 nm after 96 h of biomass exposure ranged between 63.70 to 81.57 %. The maximum hydrolysis was recorded at pH 8.0. The microbial degradation of cyanide which results into formation of carbon and nitrogen involves various enzymatic pathways wherein specific conditions like pH, temperature, concentration of cyanide, etc play an important role (Ebbs 2004). Reports related to cyanide degradation suggest that the optimal pH for the hydrolytic enzymes is in the range of 7.0-9.0 (Martinkova et al. 2015). Changes towards the higher alkaline range have comparatively more adverse effect on enzymatic activity as compared to the ones towards the higher acidic range (Gupta et al. 2010). However, the toxicity of free cyanide (if present) increases with decreasing pH (acidic) which may lead to increased cyanide toxicity thus reducing cell viability and percent hydrolysis as well (Huertas et al. 2010).

A positive correlation was observed between the amount of suspended biomass and % cyanide hydrolysis. At lowest biomass: water ratio (1:5), presence of higher concentration of extracellular hydrolytic enzymes resulted in maximum hydrolysis of iron cyanide complex. Contrasting results were obtained at higher biomass: water ratios, wherein decreased amount of fungal extracellular metabolites (enzymes) caused decreased hydrolysis. The effect of salt concentration on cyanide hydrolysis was also investigated by varying the initial concentration of $K_3[Fe(CN)_6]$ in the range of 0.1-4.0 mM with respective variation in the concentration of $K_4[Fe(CN)_6]$ to maintain their millimolar ratio of 1:0.5. Increase in the concentration of precursor salt adversely affected the extent of hydrolysis of iron cyanide complex. However, it is worth mentioning that the fungus was able to hydrolyse 1.5 mM of salt ($K_3[Fe(CN)_6]$: $K_4[Fe(CN)_6]$; 1:0.5) with admirable performance.

Table 3.1 Effect of reaction conditions on hydrolysis of iron cyanide complex observed at 420 nm (n=3, ± SD).

Parameter	Conditions	Hydrolysis of iron cyanide complex (%)
Reaction pH	2.0	64.62 ± 0.08
	4.0	65.69 ± 2.79
	6.0	79.68 ± 0.384
	8.0	81.57 ± 1.074
	10.0	63.70 ± 1.79
	Physiological* (9.8)	67.52 ± 0.82
Biomass : water ratio	1:5	67.52 ± 0.82
	1:10	46.46 ± 6.64
	1:15	34.20 ± 2.65
	1:20	17.50 ± 1.62
	1:30	5.14 ± 1.48
Salt concentration (mM) $K_3[Fe(CN)_6]$: $K_4[Fe(CN)_6]$	0.1:0.05	79.81 ± 0.50
	0.5:0.25	77.60 ± 0.19
	1:0.5	67.52 ± 0.82
	2:1	17.33 ± 1.2
	4:2	11.84 ± 0.89

*Unaltered reaction pH

3.3.7 Possible mechanism suggesting mycosynthesis of iron oxide nanoparticles.

Based on the present experimental findings, a schematic presentation of possible mechanism for synthesis of IONPs is speculated (Fig. 3.16).
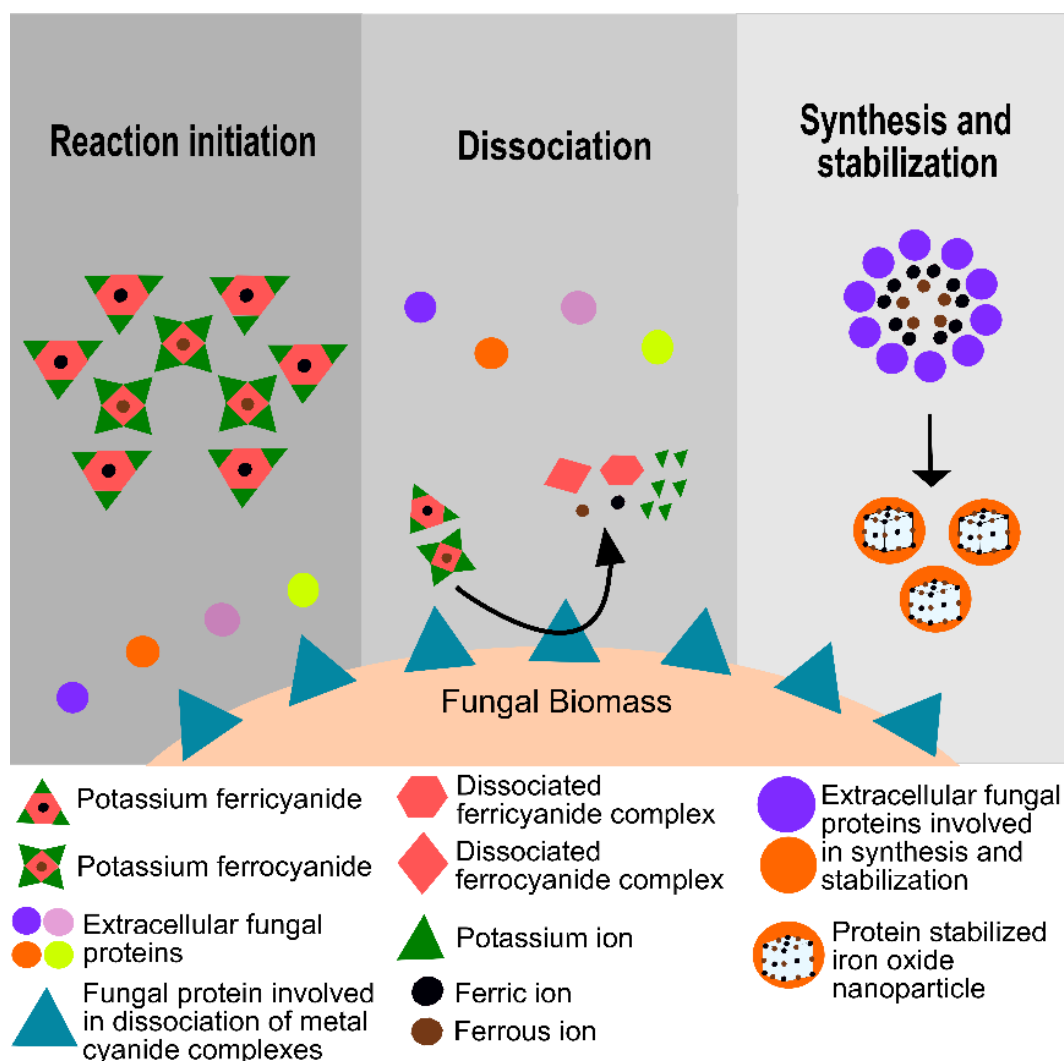
Figure 3.16 Possible mechanism suggesting mycosynthesis of IONPs by *Aspergillus japonicus* AJP01

We hypothesize that the synthesis process occurs in three steps. The first step involves the immediate release of potassium ions from the ferricyanide and ferrocyanide complexes soon after addition of precursor salts in solution. In the second step, the ferricyanide and ferrocyanide complexes undergo hydrolysis as supported by the UV-visible spectroscopic analysis. This is possibly mediated by one or more of the fungal membrane proteins releasing ferric and ferrous ions as determined by the ferrozine assay during the present study. Expectantly, hydrolysis of cyanide may take place as being the only nutrient source for growth and survival of fungi under nutrient deprived stress conditions during the experiment. The role of extracellular proteins in hydrolysis of iron cyanide complexes can be disqualified as no observable results were obtained in the reaction with only cell free-

filtrate. The third step involves the IONPs 'synthesis' by coprecipitation and controlled nucleation of ferric and ferrous ions available at millimolar ratio of 1: 0.5, respectively. Progressing alkaline pH and interaction of one or more extracellular proteins may mediate the 'synthesis', followed by stabilization of mycosynthesised IONPs by others proteins as suggested by the FTIR studies.

3.4 Conclusions

The present chapter discusses the extracellular mycosynthesis of IONPs by fungus *Aspergillus japonicus* AJP01 isolated from an iron rich region. The mycosynthesised IONPs were characterized using various techniques viz. UV-visible spectroscopy, TEM, SAED, EDS and XRD. SEM analysis of fungal biomass exposed to precursor salt solution confirmed that the nanoparticle synthesis was exclusively extracellular since no particles were found bounded to the fungal biomass surface. FTIR analysis revealed that the mycosynthesised IONPs were coated with proteins, which confers their stability. SDS-PAGE analysis of extracellular proteins both from the biomass exposed to precursor salt solution and unexposed biomass demonstrated the possibility of substrate dependent protein expression advocating the role of one or more proteins in coprecipitation, controlled nucleation and/or stabilization of nanoparticles. Further investigations at the biochemical level using ferrozine and phenolphthalin assay which proved the role of fungus in hydrolysis of iron cyanide complexes and release of free iron for IONPs synthesis and protein/polypeptide mediated stabilization of IONPs has been discussed. On the basis of present experimental findings, the probable mechanism for synthesis of IONPs is suggested.

3.5 References

Amann, R., Peplies, J. and Schuler, D. (2007). Diversity and taxonomy of Magnetotactic bacteria. In: Schuler, D. (Ed.). Magnetoreception and magnetosomes in bacteria. Springer, Berlin, 3rd Volume, p. 25-33.

Arakaki, A., Nakazawa, H., Nemoto, M., Mori, T. and Matsunaga, T. (2008). Formation of magnetite by bacteria and its application. *Journal of the Royal Society Interface* 5: 977-999.

Arruebo, M., Fernández-Pacheco, R., Ibarra, M. R. and Santamaria, J. (2007) Magnetic nanoparticles for drug delivery. *Nano Today* 2: 22-32.

Barclay, M., Hart, A., Knowles, C. J., Meeussen, J. C. L. and Tett V. A. (1998a). Biodegradation of metal cyanides by mixed and pure cultures of fungi. *Enzyme and Microbial Technology* 22: 223-231.

Barclay, M., Tett, V. A., and Knowles, C. J. (1998b). Metabolism and enzymology of cyanide/metallocyanide biodegradation by *Fusarium solani* under neutral and acidic conditions. *Enzyme and Microbial Technology* 23: 321-330.

Bazylinski, D. A., Frankel, R. B., Garratt-Reed, A. and Mann, S. (1991). Biomineralization of iron sulfides in Magnetotactic bacteria from sulfidic environments. In: Frankel, R. B. and Blakemore, R. P. (Eds.). Iron biominerals. Eds. Springer, New York, p. 239-255.

Bazylinski, D. A., Garratt-Reed, A. J. and Frankel, R. B. (1994). Electron microscopic studies of magnetosomes in Magnetotactic bacteria. *Microscopy Research and Technique* 27: 389-401.

Becker, C., Hodenius, M., Blendinger, G., Sechi, A., Hieronymus, T., Schulte, D. M., Rode, T. S. and Zenke, M. (2007). Uptake of magnetic nanoparticles into cells for cell tracking. *Journal of Magnetism and Magnetic Materials* 311: 234-237.

Bharde, A., Wani, A., Shouche, Y., Joy, P. A., Prasad, B. L. and Sastry, M. (2005). Bacterial aerobic synthesis of nanocrystalline magnetite. *Journal of the American Chemical Society* 127: 9326-9327.

Bharde, A., Rautaray, D., Bansal, V., Ahmad, A., Sarkar, I., Yusuf, S. M., Sanyal, M. and Sastry, M. (2006). Extracellular biosynthesis of magnetite using fungi. *Small* 2: 135-141.

Bharde, A., Parikh, R. Y., Baidakova, M., Jouen, S., Hannoyer, B., Enoki, T., Prasad, B. L., Shouche, Y. S., Ogale, S. and Sastry, M. (2008). Bacteria-mediated precursor-dependent biosynthesis of superparamagnetic iron oxide and iron sulfide nanoparticles. *Langmuir* 24: 5787-5794.

Blakemore, R. P. (1982). Magnetotactic bacteria. *Annual Review of Microbiology* 36: 217-238.

Cacace, D., Ashbaugh, H., Kouri, N., Bledsoe, S., Lancaster, S. and Chalk, S. (2007). Spectrophotometric determination of aqueous cyanide using a revised phenolphthalin method. *Analytica Chimica Acta* 589: 137-141.

Colombo, M., Carregal-Romero, S., Casula, M. F., Gutiérrez, L., Morales, M. P., Bohm, I. B., Heverhagen, J. T., Prosperi, D. and Parak, W. J. (2012). Biological applications of magnetic nanoparticles. *Chemical Society Reviews* 41: 4306-4334.

Connell, J. J., Patrick, P. S., Yu, Y., Lythgoe, M. F. and Kalber, T. L. (2015). Advanced cell therapies: targeting, tracking and actuation of cells with magnetic particles. *Regenerative medicin*e 10: 757-772.

Dhillon, G. S., Brar, S. K., Kaur, S. and Verma, M. (2011). Green approach for nanoparticle biosynthesis by fungi: current trends and applications. *Critical Reviews in Biotechnology* 32: 49-73.

Dobson, J. (2006). Magnetic micro- and nano-particle-based targeting for drug and gene delivery. *Nanomedicine* 1, 31-37.

Dong, H., Fredrickson, J. K., Kennedy, D. W., Zachara, J. M., Kukkadapu, R. K. and Onstott, T. C. (2000). Mineral transformations associated with the microbial reduction of magnetite. *Chemical Geology* 169: 299-318.

Dumestre, A., Chone, T., Portal, J., Gerard, M. and Berthelin, J. (1997). Cyanide degradation under alkaline conditions by a strain of *Fusarium solani* isolated from contaminated soils. *Applied Environmental Microbiology* 63: 2729-2734.

Ebbs, S. (2004) Biological degradation of cyanide compounds. *Current Opinion in Biotechnology* 15: 231-236.

Frankel, R. B. and Blakemore, R. P. (1989). Magnetite and magnetotaxis in microorganisms. *Bioelectromagnetics* 10: 223-237.

Gade, A., Ingle, A., Whiteley, C. and Rai, M. (2010) Mycogenic metal nanoparticles: progress and applications. *Biotechnology Letters* 32: 593-600.

Gao, J., Xie, J. P., Ding, J. N., Kang, J., Cheng, H. N. and Qiu, G. Z. (2006). Extraction and purification of magnetic nanoparticles from strain of *Leptospirillum ferriphilum. Transactions of Nonferrous Metals Society of China* 16: 1417-1420.

Gao, S., Shi, Y., Zhang, S., Jiang, K., Yang, S., Li, Z. and Takayama-Muromachi, E. (2008). Biopolymer-assisted green synthesis of iron oxide nanoparticles and their magnetic properties. *The Journal of Physical Chemistry C* 112: 10398-10401.

Gibbs, C. R. (1976). Characterization and application of ferrozine iron reagent as a ferrous iron indicator. *Analytical Chemistry* 48: 1197-1201.

Glasauer, S., Langley, S. and Beveridge, T. J. (2002). Intracellular iron minerals in a dissimilatory iron-reducing bacterium. *Science* 295: 117-119.

Gupta, N., Balomajumder, C. and Agarwal, V. K. (2010). Enzymatic mechanism and biochemistry for cyanide degradation: a review. *Journal of Hazardous Materials* 176: 1-13.

Haj-Hussein, A. T. (1997). Flow injection spectrophotometric determination of cyanide by the phenolphthalin method. *Talanta* 44: 545-551.

Hashimoto, H., Yokoyama, S., Asaoka, H., Kusano, Y., Ikeda, Y., Seno, M., Takada, J., Fujii, T., Nakanishi, M. and Murakami, R. (2007). Characteristics of hollow microtubes consisting of amorphous iron oxide nanoparticles produced by iron oxidizing bacteria, *Leptothrix ochracea. Journal of Magnetism and Magnetic Materials* 310: 2405-2407.

Hassen, M. W., Chaix, C., Abdelghani, A., Bessueille, F., Leonard, D. and Jaffrezic-Renault, N. (2008). An impedimetric DNA sensor based on functionalized magnetic nanoparticles for HIV and HBV detection. *Sensors and Actuators B: Chemical* 134: 755-760.

Huertas, M. J., Sáez, L. P., Roldán, M. D., Luque-Almagro, V. M., Martínez-Luque, M., Blasco, R., Castillo, F., Moreno-Vivián, C. and García-García, I. (2010). Alkaline cyanide degradation by *Pseudomonas pseudoalcaligenes* CECT5344 in a batch reactor. Influence of pH. *Journal of Hazardous Materials* 179: 72-78.

Jogler, C., Lin, W., Meyerdierks, A., Kube, M., Katzmann, E., Flies, C., Pan, Y., Amann, R., Reinhardt, R. and Schuler, D. (2009). Toward cloning of the magnetotactic metagenome: identification of magnetosome island gene clusters in uncultivated

magnetotactic bacteria from different aquatic sediments. *Applied Environmental Microbiology* 75:3972-3979.

Komeili, A. (2007). Molecular mechanisms of magnetosome formation. *Annual Review of Biochemistry* 76: 351-366.

Laemmli, U. K. (1970). Cleavage of structural proteins during the assembly of the head of bacteriophage T4. *Nature* 227: 680-685.

Lin, P. C., Tseng, M. C., Su, A. K., Chen, Y. J. and Lin, C. C. (2007). Functionalized magnetic nanoparticles for small-molecule isolation, identification, and quantification. *Analytical Chemistry* 79: 3401-3408.

Lin, W. (2015). Introduction: Nanoparticles in Medicine. *Chemical Reviews* 115: 10407-10409.

Ling, D., Lee, N. and Hyeon, T. (2015). Chemical synthesis and assembly of uniformly sized iron oxide nanoparticles for medical applications. *Accounts of Chemical Research* 48: 1276–1285

Lovley, D. R., Stolz, J. F., Nord, G. L. and Phillips, E. J. (1987). Anaerobic production of magnetite by a dissimilatory iron-reducing microorganism. *Nature* 330: 252-254.

Lovley, D. R. (1990). Magnetite formation during microbial dissimilatory iron reduction. In: Frankel, R., B. and Blackmore, R., P. (Eds.). Iron biominerals. Eds. Springer, New York, p. 151-166.

Lovley, D. R. (1993). Dissimilatory metal reduction. *Annual Reviews in Microbiology* 47: 263-290.

Lowry, O. H., Rosebrough, N. J., Farr, A. L. and Randall, R. J. (1951). Protein measurement with the folin phenol reagent. *Journal of Biological Chemistry* 193: 265-275.

Macdonald, I. D. G. and Smith, W. E. (1996). Orientation of cytochrome c adsorbed on a citrate-reduced silver colloid surface. *Langmuir* 12: 706-713.

Martinkova, L., Vesela, A. B., Rinagelova, A. and Chmatal, M. (2015). Cyanide hydratases and cyanide dihydratases: emerging tools in the biodegradation and biodetection of cyanide. *Applied Microbiology and Biotechnology* 99: 8875-8882.

Matsunaga, T. and Okamura, Y. (2003). Genes and proteins involved in bacterial magnetic particle formation. *Trends in Microbiology* 11: 536-541.

Murat, D., Quinlan, A., Vali, H. and Komeili, A. (2010). Comprehensive genetic dissection of the magnetosome gene island reveals the step-wise assembly of a prokaryotic organelle. *Proceedings of the National Academy of Sciences* 107: 5593-5598.

Njagi, E. C., Huang, H., Stafford, L., Genuino, H., Galindo, H. M., Collins, J. B., Hoag, G. E. and Suib, S. L. (2010). Biosynthesis of iron and silver nanoparticles at room temperature using aqueous *Sorghum bran* extracts. *Langmuir* 27: 264-271.

Patil, S., Sandberg, A., Heckert, E., Self, W. and Seal, S. (2007). Protein adsorption and cellular uptake of cerium oxide nanoparticles as a function of zeta potential. *Biomaterials* 28: 4600-4607.

Plank, C. (2009). Nanomedicine: Silence the target. *Nature Nanotechnology* 4: 544-545.

Riemer, J., Hoepken, H. H., Czerwinska, H., Robinson, S. R., Dringen, R. (2004). Colorimetric ferrozine-based assay for the quantitation of iron in cultured cells. *Analytical Biochemistry* 331: 370-375.

Schnurer, J. (1993). Comparison of methods for estimating the biomass of three food-borne fungi with different growth patterns. *Applied Environmental Microbiology* 59: 552-555.

Schuler, D. and Bazylinski, D. A. (2007). Techniques for studying uncultured and cultured Magnetotactic bacteria. In: Hurst, C. J., Crawford, R. L., Garland, J. L., Lipson, D. A., Mills, A. L. and Stetzenbach, L. D. (Eds.). Manual of environmental microbiology. ASM Press, Washington, p.1129-1136.

Schuler, D. (2008). Genetics and cell biology of magnetosome formation in magnetotactic bacteria. *FEMS Microbiology Reviews* 32: 654-672.

Sherman, D. M. and Waite, T. D. (1985). Electronic spectra of Fe (super 3+) oxides and oxide hydroxides in the near IR to near UV. *American Mineralogist* 70: 1262-1269.

Simpson, R. J. Ed. (2004). Purifying proteins for proteomics: a laboratory manual. Cold Spring Harbor Laboratory Press, New York, pp.750.

Singh, A. and Sahoo, S. K. (2014). Magnetic nanoparticles: a novel platform for cancer theranostics. *Drug Discovery Today* 19: 474-481.

Solanki, P., Bhargava, A., Chhipa, H., Jain, N. and Panwar, J. (2015). Nano-fertilizers and their smart delivery system. In: Rai, M., Ribeiro, C., Mattoso, L. and Duran, N. (Eds.) Nanotechnologies in food and agriculture. Springer International Publishing, Switzerland. p. 81-101.

Sun, Y. K, Ma, M., Zhang, Y., Gu, N. (2004). Synthesis of nanometer-size maghemite particles from magnetite. *Colloids Surfaces A* 245: 15-19.

Sun, C., Lee, J. S. and Zhang, M. (2008). Magnetic nanoparticles in MR imaging and drug delivery. *Advanced Drug Delivery Reviews* 60: 1252-1265.

Takekiyo, T., Wu, L., Yoshimura, Y., Shimizu, A., Keiderling, T. A. (2009). Relationship between hydrophobic interactions and secondary structure stability for trpzip β-hairpin peptides. *Biochemistry* 48: 1543-1552.

Tanaka, M., Okamura, Y., Arakaki, A., Tanaka, T., Takeyama, H. and Matsunaga, T. (2006). Origin of magnetosome membrane: proteomic analysis of magnetosome membrane and comparison with cytoplasmic membrane. *Proteomics* 6: 5234-5247.

Teja, A. S. and Koh, P. Y. (2009). Synthesis, properties, and applications of magnetic iron oxide nanoparticles. *Progress in Crystal Growth and Characterization of Materials* 55: 22-45.

Thiesen, B. and Jordan, A. (2008). Clinical applications of magnetic nanoparticles for hyperthermia. *International Journal of Hyperthermia* 24: 467-474.

Vali, H., Weiss, B., Li, Y. L., Sears, S. K., Kim, S. S., Kirschvink, J. L. and Zhang, C. L. (2004). Formation of tabular single-domain magnetite induced by *Geobacter metallireducens* GS-15. *Proceedings of the National Academy of Sciences* 101: 16121-16126.

Wang, C., Zhang, Y., Seng, H. S. and Ngo, L. L. (2006). Nanoparticle-assisted micropatterning of active proteins on solid substrate. *Biosensors and Bioelectronics* 21: 1638-1643.

Wang, Z., Zhu, H., Wang, X., Yang, F. and Yang, X. (2009). One-pot green synthesis of biocompatible arginine-stabilized magnetic nanoparticles. *Nanotechnology* 20: 465606.

Williams, M. (1997). The Merck index, 12th Edition. CD-Rom Version 12.1. *Drug Development Research* 41: 108-108.

Yang, T., Li, Z., Wang, L., Guo, C. and Sun, Y. (2007) Synthesis, characterization, and self-assembly of protein lysozyme monolayer-stabilized gold nanoparticles. *Langmuir* 23: 10533-10538.

Chapter IV

Biosynthesis of Gold Nanoparticles

Preface

This chapter discusses the potential of gold metal tolerant fungal isolates towards on-cell and extracellular synthesis of gold nanoparticles (Au NPs). Among the various fungal isolates screened to test their ability of Au NPs synthesis, *Aspergillus japonicus* AJP01 was found to synthesize spherical Au NPs on its surface. Extracellular synthesis of Au NPs was achieved using two indigenous fungi, *Cladosporium oxysporum* AJP03 and *Lichtheimia ramosa* AJP11. The as-synthesized nanoparticles were characterized by standard techniques to confirm their size, shape, distribution and crystallinity. A series of experiments were conducted to study the effect of various process parameters on particle size and yield during extracellular synthesis. Investigations were also performed to elucidate the mechanism involved in extracellular synthesis of Au NPs by *Lichtheimia ramosa* AJP11. The obtained results provide appreciable evidence supporting the role of extracellular proteins in the reduction of gold ions followed by their nucleation and stabilization. The present work serves as the initial step in development of "nano-factories" for efficient nanoparticle synthesis.

4.1 Introduction

The obsession for gold by mankind has always been there since time immemorial. Even after thousands of years, the appeal and charisma of gold remains undiminished. The oldest remains of gold were found at Varna Necropolis, a cemetery in present day Bulgaria and believed to be the first site of gold extraction nearly 7000 years ago. Apart from being a metal of beauty and commerce, the versatility and adaptability of gold has also made it an asset for the scientific and industrial world. As per the World Gold Council "Gold is not a new story. It is however an evolving one. Today gold's uniquely versatile qualities are seen in various applications, making it part of the fabric of our society" (http://www.gold.org). Gold is an essential component of emerging technologies like medical diagnostic, sensing, advance electronics, space engineering and nanotechnology (Emsley 2011).

Gold has always been on the fore-front of nanotechnology revolution. At the 'nano-scale', gold nanoparticles (Au NPs) can be as small as 1 billionth of a metre in diameter and exhibit completely new properties making it one of the most promising nano-materials. Owing to their intriguing opto-electronics properties, non-toxic behaviour and noble chemical reactivity, Au NPs have been utilized in high-end applications such as organic photovoltaics, sensory probes, therapeutics, drug delivery in biological and medical applications, electronic conductors and catalysis. Out of the approximately 1,20,228 research papers on 'nanoparticles' listed in PubMed since 1978, more than 16 % are related to gold, of which nearly 64 % have been published during 2011-2015 (http://www.ncbi.nlm.nih.gov/pubmed), signifying the importance of Au NPs. The oldest evidence of 'soluble' gold, dates back to the time of Touthankamon, an Egyptian King whose marvellous statue was constructed in the 5-4th century B.C. Later on, based on the French word "Colle" this "soluble" gold was termed as "colloid" by Graham in 1861 (Graham 1861). Colloidal gold, a suspension of Au NPs in a fluid, usually water and its beautiful ruby-red colour has fascinated people for many centuries. Its use can be traced back to ancient times. Perhaps the most famous example of use of colloidal gold is the Lycurgus Cup, also manufactured in the 5-4th century B.C. The medicinal value and curative powers of colloidal gold against various diseases was unravelled as detailed in the book "Panacea Aurea-Auro Potabile" published by the medical doctor and philosopher Francisci Antonii in 1618. Michael Faraday scientifically reported the formation of colloidal gold visualized as deep red solution by reduction of aqueous solution of chloroaurate using phosphorus in a two-phase system (Faraday 1857). He also investigated the optical properties of thin films prepared from dried colloidal solutions and observed reversible colour changes of the films upon mechanical compression. Later, a plethora of reports and methods for synthesis of Au NPs were published which have been beautifully reviewed by Daniel and Astruc (2004), Yeh et al. (2012) as well as Alex and Tiwari (2015).

As discussed in chapter one, various physical, chemical and biological methods have been used for nanoparticle synthesis based on the top-down or bottom-up synthesis approaches. Due to obvious reasons, biological methods inspired from natural biomineralization processes in living organisms have turned researchers to exploit biological systems as possible eco-friendly "nano-factories" (Lengke et al. 2006). Among various microorganisms, fungi have emerged out as potential candidate for biosynthesis of nanoparticles. Fungi are capable to synthesize Au NPs either on their surface (on-cell), intracellularly and/or extracellularly (Kitching et al. 2015). Irrespective of the location of synthesized nanoparticle, fungus offer highly controlled environment for metal ion reduction, atom nucleation and nanoparticle stabilization (Du et al. 2011). Furthermore, myco-synthetic machinery produces Au NPs with well-ordered shape, size and crystallinity due to the precise and extremely specific interactions between the biomolecules and inorganic chemical moiety (Das et al. 2012).

Unfortunately, even after several decades, biological synthesis approaches are still practiced at the laboratory level only and have not been profitably scaled-up to the industrial level. The primary reason for this delay is the random selection of microbial species for nanoparticle synthesis without suitable rationale which leads to low yield. However, this problem can be overcome by choosing a potential organism on the basis of its property of biomineralization (Gadd 2010). Another crucial reason is the lesser understanding of factors affecting properties of synthesized nanoparticles. Ideally, the nanoparticle yield, size and shape strongly depend on the reaction conditions such as concentration of reducing metabolites, precursor salt, and reaction pH (Gericke and Pinches, 2006; Korbekandi et al. 2009). The effect of these parameters must be well studied in order to upscale the synthesis process.

In order to further uplift the process of nanoparticle synthesis by microorganisms, apart from choosing a suitable organism and optimization of process parameters, improvement possibilities at molecular level shall also be looked into. For this, critical understanding of plausible mechanism(s) behind nanoparticle synthesis which includes identification and characterization of "active" biomolecules that controls the shape and crystal structure of nanoparticles as well as their stabilization are of immense importance. Isolation of these so-called "active" biomolecules, their identification and characterization followed by elucidation of synthesis mechanism will open new avenues for the possible genetic modification in microbes which will lead to the development of simple, efficient and fast protocol for synthesis of nanoparticles with desired shape, size and other properties (Thakkar et al. 2010; Colombo et al. 2012). Moreover, the knowledge gained will help us in improving our understanding of nanoparticle biomolecule interactions.

An appreciable work has been attempted to elucidate the actual mechanism of Au NPs synthesis by fungi. Substantial number of reports suggest the role of proteins in the synthesis of Au NPs by fungi (Parikh et al. 2008; Balaji et al. 2009; Duran et al. 2011).

However, satisfactory explanation about the mechanism is still lacking. For instance, a recent study by Das et al. (2012) highlighted the role of proteins in the reduction of Au (III) ion and subsequent formation of Au NPs by fungus *Rhizopus oryzae*. They observed induction of two stress proteins in presence of sub-toxic concentration of gold and hypothesized their role in Au NPs biosynthesis. In another vaguely designed study related to synthesis of Au NPs by *Phanerochaete chrysosporium*, Sanghi et al. (2011) observed an increase in the activity of laccase and ligninase enzymes and concluded that these enzymes were responsible for Au NPs synthesis. Similarly, Gupta and Bector (2013) hypothesized the role of enzyme in Au NPs synthesis by *Aspergillus fumigatus* on the basis of results obtained by native-PAGE profiling of extracellular metabolites followed by exposure of gel to precursor gold ions. Appearance of purple coloured band indicated the formation of Au NPs suggesting presence of active protein(s) in the cell-free filtrate. Collectively, all the above mentioned reports and many others as well suggest that proteins are the most likely "active" biomolecule involved in the mycosynthesis approach. Furthermore, a close analysis of the biomolecular composition of fungal cell-free filtrate reveals the presence of proteins (in the form of enzymes) in majority (McCotter et al. 2016).

In the present study, the selected gold tolerant fungal isolates (as detailed in chapter II) were screened to test their potential for on-cell and/or extracellular synthesis of Au NPs. In first part of the chapter, an eco-friendly, rapid and facile on-cell synthesis of Au NPs using fungus, *Aspergillus japonicus* AJP01 has been discussed. The dual role of this fungal isolate in synthesis as well as immobilization of Au NPs is the remarkable feature of the study. Second part of the chapter deals with the extracellular biosynthesis of Au NPs using two gold metal tolerant fungal isolates *Cladosporium oxysporum* AJP03 and *Lichtheimia ramosa* AJP11. The protocol utilizes fungal extracellular metabolites (cell-free filtrate) for reduction, nucleation and stabilization of nanoparticles. In order to obtain nanoparticles with well-defined properties and high yield, optimization of process parameters viz., concentration of extracellular metabolites and precursor salt; and reaction pH was carried out. The morphology, composition and crystallinity of nanoparticles were confirmed using standard techniques. Furthermore, mechanistic insights of the extracellular synthesis of Au NPs using *Lichtheimia ramosa* AJP11 have been investigated. Strong role of fungal extracellular proteins in the synthesis process has been deduced. The present findings can be used for development of an eco-friendly yet cost effective method for large scale production of other important nanoparticles challenging the presently available chemical and physical synthesis methods.

(A) On-cell Synthesis of Gold Nanoparticles

4.2 Materials and methods

4.2.1 On-cell synthesis of Au NPs

The fungal isolate *Aspergillus japonicus* AJP01 was maintained on PDA slants (pH 5.6) by repeated sub-culturing on fresh media at 28˚ C. From an actively growing culture, a loopful of spores was inoculated in 100 mL of MGYP medium (0.3 % malt extract, 1.0 % glucose, 0.3 % yeast extract, 0.5 % peptone; pH 7.0) in 250 mL Erlenmeyer flasks. The inoculated flasks were incubated at 28 ˚C for 72 h on a rotary shaker (120 rpm) under dark conditions. After incubation, the fungal biomass was separated from the culture medium by centrifugation (5000 rpm) at 4 ˚C for 15 min, and washed thrice with autoclaved Milli-Q water to remove all traces of media. Typically, 20 g (fresh weight) of biomass was resuspended in 100 mL of 1.0 mM gold (III) chloride trihydrate solution in 250 mL Erlenmeyer flask and incubated for 72 h under the similar conditions described above. After incubation, the biomass was separated by filtration using Whatman grade 1 filter paper (Whatman Inc., USA) and washed thrice with autoclaved Milli-Q water before further characterization. Biomass in autoclaved Milli-Q water (without gold (III) chloride solution) as positive control and pure gold (III) chloride solution (without biomass) as negative control were also incubated simultaneously at 28 ˚C for 72 h on a rotary shaker (120 rpm) under dark conditions along with the experimental flasks in three replicates.

4.2.2 Characterization of nanoparticles

4.2.2.1 UV-visible spectroscopy

The amount of Au (III) ions remaining in the solution after exposure to *Aspergillus japonicus* AJP01 as a function of time was monitored by measuring the UV-visible absorption spectrum of culture supernatant on a V-630 UV-visible spectrophotometer (Jasco Corporation, Japan) at 1 nm resolution in the range of 200-800 nm with a scan speed of 400 nm min^{-1} using a 1 cm path length quartz cuvette.

In order to validate the synthesis of Au NPs on the fungal biomass, extraction of trapped Au NPs was performed by sonicating 0.1 g (wet weight) of fungal biomass suspended in 1.0 mL Milli-Q water for 3 h in a water bath sonicator (Thermo Scientific, USA). After sonication, the fungal biomass was separated by centrifugation (3000 rpm, 5 min) and the supernatant containing extracted Au NPs was spectroscopically examined using UV-visible spectrophotometer as per the details mentioned above. The results were analysed using Jasco's spectra manager software and graphs were plotted using Origin 9.0 (OriginLab Corporation, USA).

4.2.2.2 Scanning electron microscopy and energy dispersive spectroscopy

The synthesis of Au NPs on the fungal biomass surface was confirmed by scanning electron microscopy (SEM) imaging. Sample for SEM was prepared by fixing the fungal

biomass bearing Au NPs in 2.5% (v/v) glutaraldehyde (prepared in 0.1 M sodium phosphate buffer, pH 7.2) at 4 °C for overnight. After fixation, the specimen was rinsed with phosphate buffer (pH 7.2) and dehydrated in a series of 30-100 % ethanol followed by drying in a vacuum desiccator. SEM micrographs were obtained by imaging the specimen on a Hitachi S-3400N SEM instrument (Hitachi High-Technologies Corporation, Japan). Energy dispersive spectroscopy (EDS) measurements of specimen were carried out using a Thermo Noran System SIX EDS (Thermo Fisher Scientific, USA) attached with the SEM instrument.

4.2.2.3 X-ray diffraction

X-ray diffraction (XRD) measurement of the freeze dried biomass was carried out to authenticate crystallinity of Au NPs using a X'Pert PRO X-ray diffractometer (PANalytical BV, The Netherlands) operated at a voltage of 40 kV and current of 30 mA with CuK_α radiation. The crystal phase was determined by comparing the calculated values of interplanar spacing and corresponding intensities of diffraction peaks with theoretical values from the Joint Committee on Powder Diffraction Standards-International Centre for Diffraction Data (JCPDS-ICCD) database. Scherrer's equation was applied to determine the size of the Au NPs using the data acquired by XRD analysis (Patterson 1939).

4.2.2.4 X-ray photoelectron spectroscopy

The chemical state of gold species within the Au NPs trapped on the surface of fungal biomass was determined by X-ray photoelectron (XPS) spectroscopy using an Omicron EA 125 instrument (Scienta Omicron GmbH, Germany) equipped with a seven-channel detection system. The sample was fixed on a small piece of conducting carbon tape and dried overnight under an ultra-high vacuum condition. Monochromatic light of Al-Kα radiation of energy 1486.7 eV was used as X-ray source. Wide scale and high resolution XPS spectra of Au 4f were obtained using energy steps of 0.1 and 1.0 eV respectively. The emission current of 15 mA and chamber base pressure below 10^{-9} mbar was used throughout the XPS measurement.

4.2.2.5 Transmission Electron microscopy

Au NPs extracted from fungal biomass by sonication were subjected to transmission electron microscopy (TEM) imaging. The solution containing extracted Au NPs was drop coated on a carbon-coated TEM grid after 30 min of sonication. After few minutes, extra solution was removed using a lint free blotting paper and the grids were kept in a vacuum desiccator prior to measurement. TEM measurements were carried out on a JEM-2100 instrument (JEOL, Japan) operated at an accelerating voltage of 80 kV and 200 kV for low and high resolution imaging, respectively.

4.3 Results and discussion

The concentration of Au (III) ions remaining in the culture supernatant was monitored by determining the absorption intensity of Au (III) at 290 nm (Badwaik et al. 2011). As shown in Figure 4.1, the highest concentration of Au (III) was observed at 0 min i.e. soon after the addition of gold (III) chloride in the culture supernatant which underwent a continuous decrease as a function of time. Figure 4.2 represents percent decrease in the concentration of Au (III) ions. It is clearly evident that nearly all the Au (III) ions were utilized within 60 min of biomass-salt exposure.
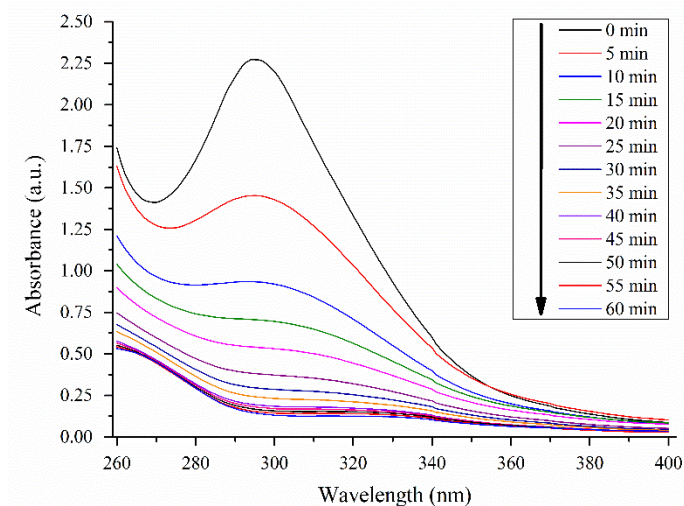
Figure 4.1 UV-visible spectra showing utilization of Au (III) ions from culture supernatant as a function of time
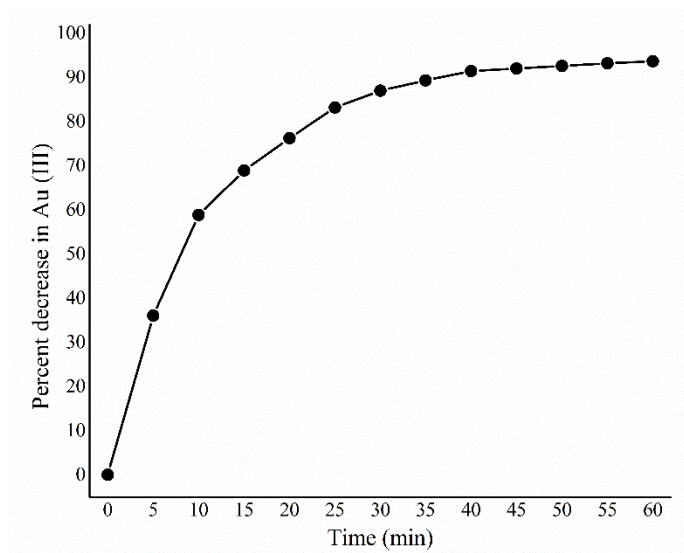
Figure 4.2 Percent decrease in concentration of Au (III) ions in the culture supernatant as a function of time

Regardless of the rapid utilization of Au (III) ions from the culture supernatant, the synthesis of Au NPs on fungal biomass was observed much later precisely after 4 h of biomass-salt exposure as evident by the change in biomass colour from pale white to vivid purple (Figure 4.3). The development of purple colour was due to the excitation of surface plasmon vibrations that absorbed light in the visible region giving a characteristic coloured appearance to Au NPs. Similar to our observation, Mukherjee et al. (2001) also reported the change in colour of fungal biomass due to surface trapping of Au NPs. Based on these results, it can be hypothesised that initially Au (III) ions were absorbed by the fungal biomass and later reduced to form Au NPs. No visual change in the colour intensity of biomass was observed after 9 h of incubation which suggested completion of nanoparticle synthesis. Notably, the reaction completion time in the present study is significantly shorter in comparison to the earlier studies on biosynthesis of Au NPs as reviewed by Kitching et al. (2015). Another distinctive feature of the present study is the exclusive surface bound synthesis of Au NPs as no purple colour was observed in the culture supernatant (Figure 4.3).

Figure 4.3 Erlenmeyer flask containing fungal biomass after 9 h exposure to gold (III) chloride (Inset shows fungal biomass before exposure)

SEM was performed to confirm the synthesis and distribution of nanoparticles on biomass surface. The representative SEM micrograph (Figure 4.4) revealed omnipresence of nanoparticles with limited aggregation on the fungal mycelia. Figure 4.5 shows the spot EDS spectrum of Au NPs trapped on biomass. The presence of a strong peak in the EDS spectrum at 2.1 KeV confirmed the presence of pure metallic Au NPs. Apart from this, the comparatively weaker signals for carbon (C), oxygen (O) and nitrogen (N) indicated the presence of fungal biomass in the vicinity of Au NPs (Song et al. 2009). Keeping this fact in mind, EDS analysis of three distinct spots of nanoparticle aggregates were carried out to determine the atomic ratio of gold with respect to carbon content. It is clearly evident that

the content of gold remained almost similar despite the location of nanoparticle aggregates confirming the homogenous synthesis of Au NPs on fungal biomass surface (Figure 4.6).

The crystalline nature of the as-synthesized Au NPs was evaluated using XRD measurements. The observed Bragg reflections indicated in Figure 4.7, exhibits fcc packing of nanoparticles with well-defined peaks at 2θ value of 38.16˚, 44.34˚, 64.67˚ and 77.62˚ corresponding to (111), (200), (220) and (311) planes, respectively. The recorded XRD pattern was found to be in good agreement with the available JCPDS-ICCD database (JCPDS file no. 00-004-0784). FWHM value of the peak at 2θ value of 38.16˚ was used in the Scherrer's equation and the particle size thus determined was found to be ~22 nm.
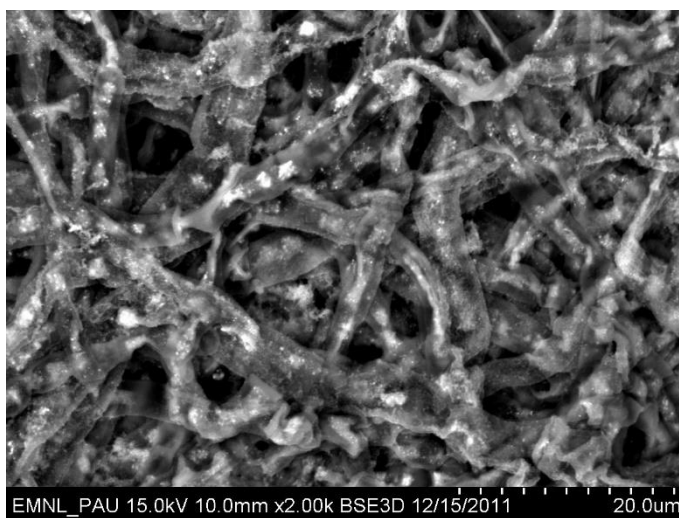
Figure 4.4 SEM micrograph of fungal biomass supporting Au NPs (Scale bar equivalent to 20 µm)
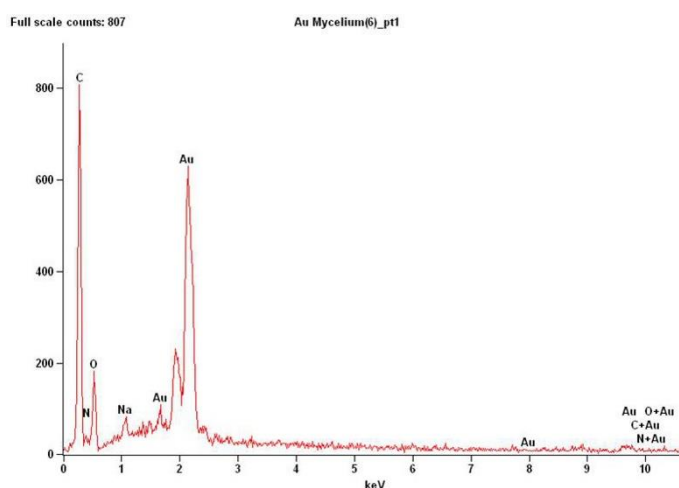
Figure 4.5 Spot EDS spectrum of Au NPs trapped on fungal biomass showing particle's elemental composition
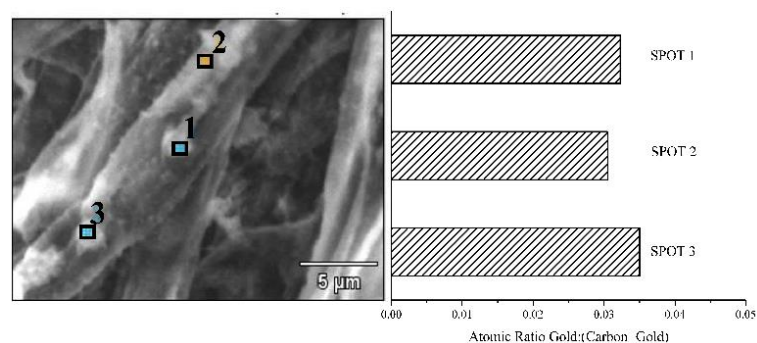
Figure 4.6 Atomic ratios of gold: (carbon + gold) obtained from EDS analysis
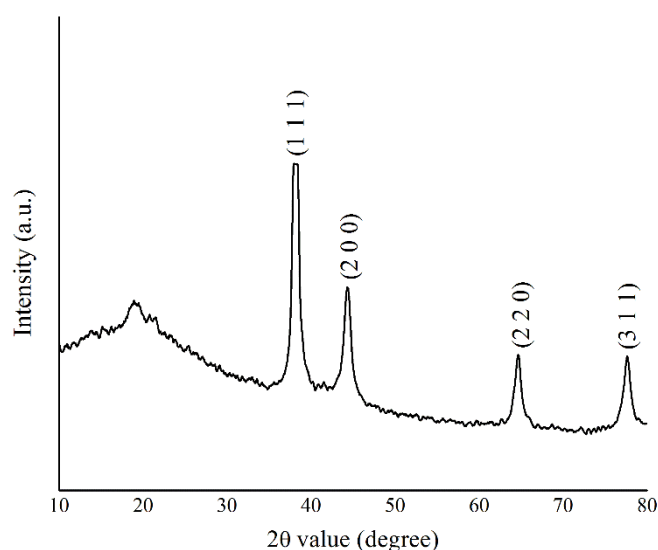
Figure 4.7 XRD pattern of freeze dried powdered fungal biomass supporting Au NPs. The peaks indicates Bragg's reflections corresponding to fcc structure of gold

XPS analysis was employed to determine the chemical as well as the oxidation state on the surface of Au NPs supported on fungal biomass. The wide scale survey scan of the vacuum dried sample showed a clear existence of gold in the form of Au 4f binding energy peaks along with the C1s, N1s and O1s peaks (Figure 4.8). This finding further confirmed the formation of Au NPs on the surface of fungal biomass. To compensate any kind of energy shift due to charging effect, XPS peak positions were calibrated against C1s binding energy of 284.5 eV. Figure 4.9 represents a high resolution XPS spectrum of Au 4f binding energy with its various deconvolution components. A linear background subtraction and Gaussian fitting were used for the deconvolution of Au 4f peak. The peaks centered around 84 eV and 87.6 eV corresponded to the spin-orbit splitting components Au $4f_{7/2}$ and Au $4f_{5/2}$, respectively and represented metallic Au (0) state. The binding energy values observed were in good agreement with the reported binding energy values of Au (0) state (Sharma et al. 2007; Das et al. 2012). Apart from this, an additional doublet of much weaker intensity towards the higher binding energy value was also observed. These

doublet peaks were found to be centred around 86.05 eV and 89.45 eV and were attributed to the spin-orbit splitting of Au (I) state. From the integral intensity ratio calculation, a small fraction of ~10% ± 3% of Au (I) oxidation state was estimated. Absence of any Au (III) components (which usually appears at even higher binding energy) confirmed that the fungal isolate successfully reduced gold (III) chloride. However, a broad peak of non-gold component centred at 81.7 eV was also observed. This might be attributed to the plasmon loss of '*Bromine*', a possible contaminant within the various chemicals used during the analysis. Similar to our interpretation, Das et al. (2012) also speculated the formation of Au (I) as an intermediate form during the reduction of Au (III) to Au (0) as reported in their study on the biomineralization mechanism of gold by *Rhizopous oryzae*.

Figure 4.8 Wide scale XPS survey spectrum of the vacuum dried fungal biomass supporting Au NPs
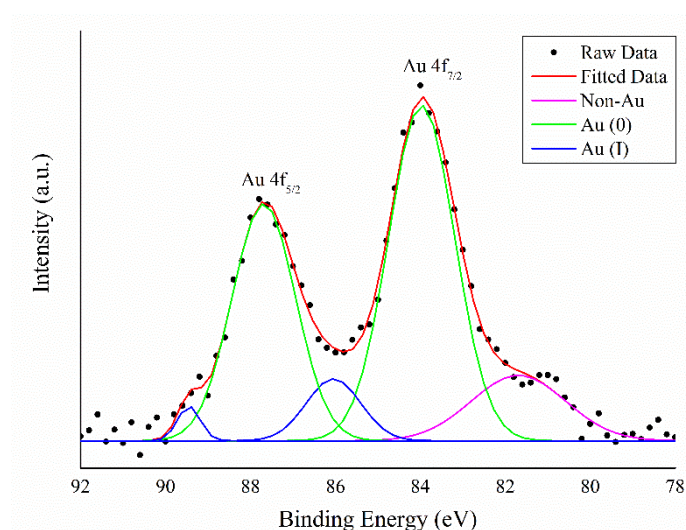
Figure 4.9 High resolution XPS spectrum of Au 4f photoelectron peaks with various deconvolution components. The scatter points refer to the raw data, while the solid lines to the curve fitting results

The UV-visible spectrum of the supernatant containing the extracted Au NPs showed appearance of a single SPR band at around 545 nm (Figure 4.10). As the characteristic SPR band may be influenced by size, shape and aggregation, presence of a single and symmetrical SPR band during the present study suggested that the as-synthesized Au NPs were isotropic in shape and size with no significant aggregation (Polte et al. 2010; Zhang et al. 2011). In order to validate these results, TEM imaging was carried out to determine size and shape of the nanoparticles. A representative TEM micrograph revealed that the particles were almost spherical in shape (Figure 4.11). The particle size histogram of Au NPs showed that the particle size ranges majorly between 15-20 nm (Figure 4.12). HR-TEM imaging of a single Au NPs demonstrated well-resolved interference fringe pattern attesting to crystallinity of the nanoparticle (Figure 4.13).
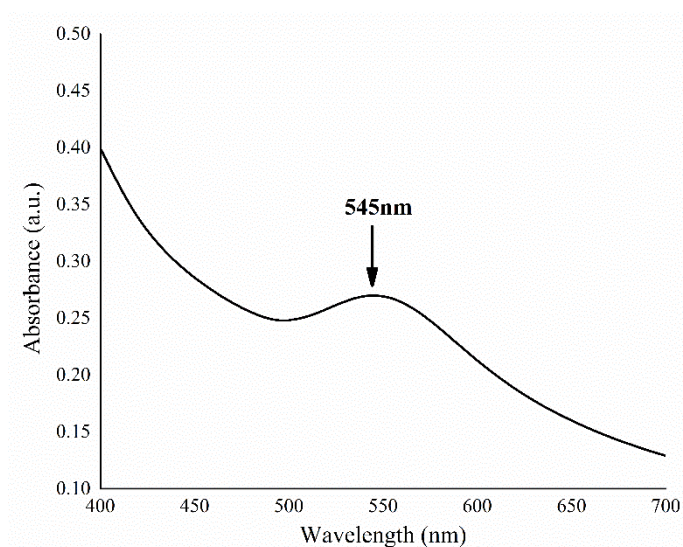
Figure 4.10 UV-visible spectra of Au NPs solution extracted from fungal biomass
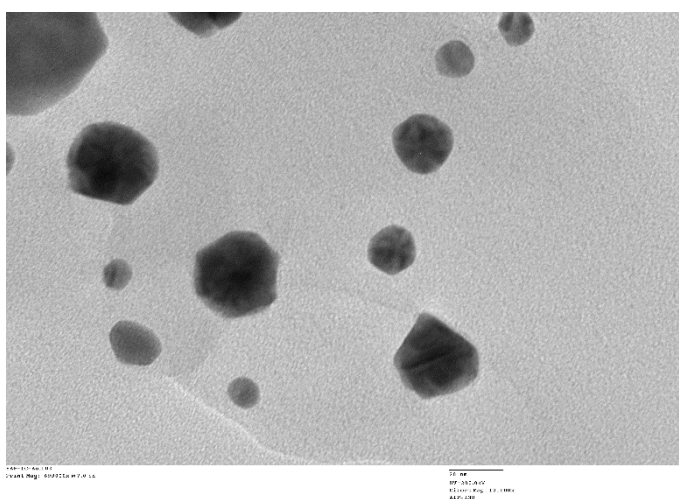
Figure 4.11 TEM micrograph of Au NPs extracted from fungal biomass (Scale bar equivalent to 20 nm)
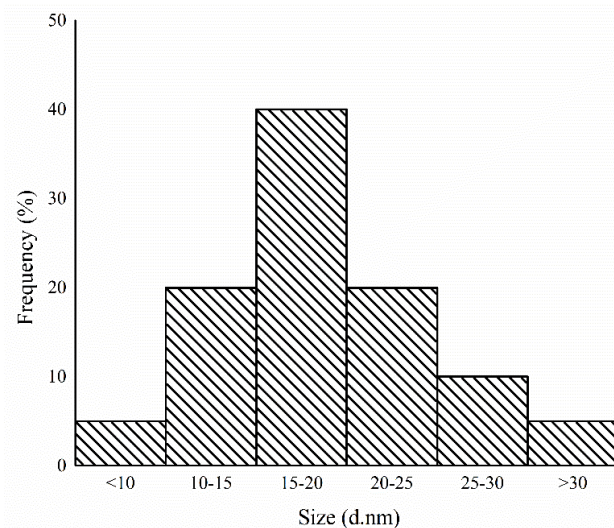
Figure 4.12 Particle size distribution histogram of Au NPs from TEM analysis
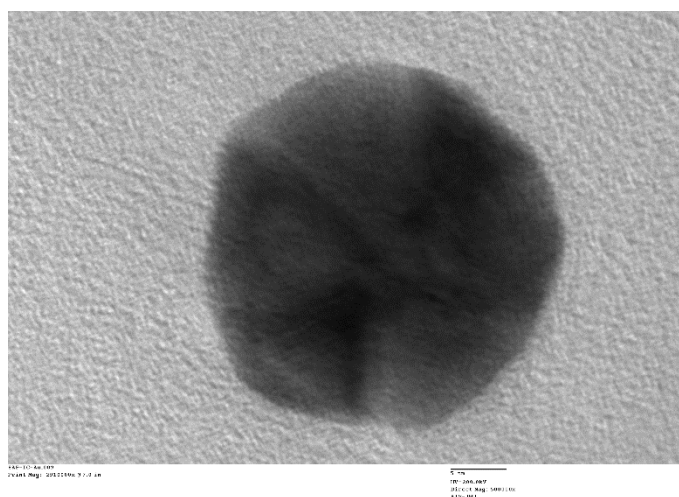
Figure 4.13 HR-TEM micrograph of single Au NPs (Scale bar equivalent to 5 nm)

4.4 Conclusions

In conclusion, the present study demonstrates on-cell synthesis of Au NPs using a soil fungus *Aspergillus japonicus* AJP01. The attractiveness of the approach lies in its simplicity and one-step procedure for the synthesis of nanoparticle-fungal hybrid which can be used in various applications like chemical and molecular sensing, bioremediation of heavy metals, catalysis, etc. Another remarkable feature of the synthesis is the dual role of fungal isolate in simultaneous synthesis and immobilization of Au NPs on its surface. The fungus was able to utilize nearly all the Au(III) ions from the culture supernatant within 60 mins of biomass-salt exposure as determined by UV-visible measurements. XPS analysis showed that the fungus successfully reduced Au (III) into Au NPs containing principally Au (0) with a small percentage of Au (I). The resulting nanoparticle exhibited the

characteristic vivid purple colour. SEM imaging coupled with EDS confirmed the synthesis and omnipresence of Au NPs on the biomass surface. XRD results attested the crystallinity of nanoparticles as the diffraction pattern was homologous to fcc gold structure. TEM analysis revealed the Au NPs to be of spherical morphology and the particle size range was predominantly between 15-20 nm with an average particle diameter of 21.54 ± 8.10 nm. The on-cell synthesis of Au NPs may have potential applications particularly in catalysis as it can serve as an excellent heterogeneous interface for reactions to proceed with added advantage of catalyst recovery and reusability.

(B) Extracellular Synthesis of Gold Nanoparticles

4.5 Materials and methods

4.5.1 Extracellular synthesis of Au NPs

The fungal isolates *Cladosporium oxysporum* AJP03 and *Lichtheimia ramosa* AJP11 were separately maintained on PDA slants (pH 5.6) with repeated sub-culturing on fresh media at 28˚ C. From an actively growing culture, a loopful of spores were inoculated in 80 mL of MGYP medium (0.3 % malt extract, 1.0 % glucose, 0.3 % yeast extract, 0.5 % peptone; pH 7.0) in 250 mL Erlenmeyer flasks. The inoculated flasks were incubated at 28 ˚C for 72 h on a rotary shaker (120 rpm). After incubation, the fungal biomass was separated from the culture medium by centrifugation (5000 rpm) at 4 ˚C for 15 min, and washed thrice with autoclaved Milli-Q water to remove all traces of media. Typically, 20 g (fresh weight) of biomass was resuspended in 100 mL autoclaved Milli-Q water in 250 mL Erlenmeyer flask and incubated for 72 h under dark at similar conditions described above. After incubation, biomass was separated using Whatman filter paper no. 1. The as-obtained cell-free filtrate was further passed through 0.22 µm nylon-66 membrane (HiMedia Laboratories, India) using vacuum in order to remove the left over fungal mycelia and spores, if any. For synthesis of nanoparticles, aqueous gold (III) chloride trihydrate at a final concentration of 0.5 mM was added to flasks containing 100 mL of respective fungal cell-free filtrate and incubated at 28 ˚C under dark conditions. Controls containing cell-free filtrate (without gold (III) chloride trihydrate; positive control) and pure gold (III) chloride trihydrate (without cell-free filtrate; negative control) were also run simultaneously along with experimental flasks in triplicate separately for both the fungal isolates. Viability of the fungal cells after incubation in Milli-Q water for 72 h was also checked. For this, the fungal mycelia were inoculated on fresh PDA plates in triplicate and incubated for 4-5 days at 28˚C in dark conditions.

4.5.2 Characterization of nanoparticles

4.5.2.1 Visual observation

The colourless cell-free filtrate developed pale yellow colour soon after the addition of gold (III) chloride trihydrate solution. The change in the colour was routinely monitored visually which would signify the bio-reduction of gold ions and formation of Au NPs.

4.5.2.2 UV-visible spectroscopy

Gradual synthesis of Au NPs was monitored by sampling 1 mL aliquot at every 24 h during the progress of reaction. UV-visible analysis was performed by measuring absorption spectra on a V-630 UV-visible spectrophotometer (Jasco Corporation, Japan) at a resolution of 1 nm with a scan speed of 400 nm min^{-1} using a 1 cm path length quartz

cuvette. Changes in the pattern of absorption spectrum and development of any peak with time were carefully observed.

4.5.2.3 Dynamic light scattering

Average hydrodynamic diameter and particle size distribution were recorded using Zetasizer Nanoseries compact scattering spectrometer (Malvern Instruments Ltd, UK). The obtained data were analyzed using Zetasizer software. Measurements were recorded at 25 °C ± 1 °C, in triplicates; each measurement was the average of 20-30 data sets acquired for 10 seconds each. Hydrodynamic diameter and polydispersity index (PDI) were calculated using the internal software analysis from the DLS intensity-weighted particle size distribution.

4.5.2.4 Transmission electron microscopy

Sample for transmission electron microscopy (TEM) imaging was prepared by drop coating of as-synthesized nanoparticle solution on to a carbon coated copper grid. The extra solution was removed using a lint free blotting paper, and the grid was vacuum dried overnight before visualization. Low and high resolution TEM micrographs were captured on JEM-2100 (JEOL Ltd., Japan) and H-7650 (Hitachi High-Technologies Corporation, Japan) instruments operated at an accelerating voltage of 80 and 200 kV, respectively.

4.5.2.5 Energy dispersive spectroscopy

Energy dispersive spectroscopy (EDS) for the elemental analysis of a single particle was carried out using Quantax EDS attachment (Bruker AXS Ltd., UK) equipped with TEM instrument. The X-ray beam of TEM was used as an electron source and energy emitted from the samples was converted into voltage signals using a Si (Li) detector which was cooled to cryogenic temperature with liquid nitrogen. The data was recorded using a pulse processor, which measures the signals and passes them onto an analyser for data display and analysis.

4.5.2.6 X-ray diffraction

X-ray diffraction (XRD) measurement of freeze dried nanoparticle sample was carried out using X'Pert PRO X-ray diffractometer (PANalytical BV, The Netherlands). The diffraction pattern was recorded between 20°- 80° (2θ) operated at a voltage of 40 kV and current of 30 mA with CuK$_\alpha$ radiation. The crystal phase was determined by comparing the calculated values of inter-planar spacing and corresponding intensities of diffraction peaks with the standard theoretical values of JCPDS-ICCD database.

4.5.2.7 Scanning probe microscopy

The surface feature of nanoparticles were studied using Surface CP-II Scanning Probe Microscope (Veeco Instruments Inc., USA) operated in atomic force mode (contact mode). The particles were sensed using a nanosized tip placed at the end of a silicon spring

which was moved across the sample as a force sensor using contact mode. A laser beam was focused at the tip edge and the deflection of the beam was measured by a photodetector. The measured tip movement was analysed to obtain the surface topography image of the sample.

4.5.2.8 X-ray photoelectron spectroscopy

The chemical state of gold species within the synthesized Au NPs was determined by X-ray photoelectron (XPS) spectroscopy using an Omicron EA 125 instrument (Scienta Omicron GmbH, Germany) equipped with a seven-channel detection system. The sample was coated on a small piece of conducting carbon tape and dried overnight under an ultra-high vacuum condition. Monochromatic light of Al-Kα radiation of energy 1486.7 eV was used as X-ray source. Wide scale and high resolution XPS spectrums of Au 4f were obtained using energy steps of 0.1 and 1.0 eV respectively.

4.5.2.9 Fourier transform infrared measurement

For FTIR measurements, the synthesized nanoparticles were freeze dried and mixed with potassium bromide in a ratio of 1:100. FTIR spectrum of sample was recorded on an IR Prestige-21 FTIR instrument (Shimadzu, Japan) with a diffuse reflectance mode (DRS-8000) in the range of 400-4000 cm^{-1} at a resolution of 4 cm^{-1}.

4.5.3 Effect of reaction conditions on particle size and yield

Reaction conditions such as concentration of extracellular metabolites in the cell-free filtrate, concentration of precursor salt and reaction pH could affect the size, rate of synthesis, overall yield and stability of as-synthesized Au NPs. A series of experiments were carried out to examine the effect of these process parameters. In addition to the visual observation, SPR peak intensity studies using UV-visible spectroscopy were carried out to determine the yield of Au NPs. DLS measurements were performed to check the average hydrodynamic particle size. In case of Au NPs synthesis using *Lichtheimia ramosa* AJP11, the results were also validated by TEM imaging. All the experiments were performed in triplicate with respective control.

4.5.3.1 Effect of concentration of extracellular metabolites

In order to study the effect of concentration of extracellular metabolites present in the cell-free filtrate, the quantity of biomass suspended in autoclaved Milli-Q water was varied. For this purpose 20 g, 10 g, 6.66 g, 5g and 3.33 g of biomass (fresh weight) was suspended in 100 mL of autoclaved Milli-Q water to achieve the biomass: water ratio of 1:5, 1:10, 1:15, 1:20 and 1:30 respectively.

4.5.3.2 Effect of concentration of precursor salt

In order to study the effect of concentration of precursor salt (gold ions), varied concentrations of gold (III) chloride trihydrate (0.1 mM, 0.5 mM, 1.0 mM, 2.0 mM and 5.0 mM) were added in the cell-free filtrate and the synthesis of Au NPs was monitored.

4.5.3.3 Effect of reaction pH

Effect of pH on synthesis of Au NPs was studied by altering the pH of cell-free filtrate before addition of precursor salt. For this, either 0.1 N HCl or 0.1 N NaOH was added to 100 mL of cell-free filtrate to adjust the final pH at 2.0, 4.0, 6.0, 8.0 and 10.0. Unaltered pH of the cell-free filtrate was used as control (pH physiological).

4.5.4 Mechanistic insights behind extracellular synthesis

Attempts were made to deduce the mechanism involved behind extracellular synthesis of Au NPs by *Lichtheimia ramosa* AJP11. For this, standard proteomic techniques were used for the isolation, purification and fractionation of extracellular proteins present in the cell-free filtrate. Subsequently, each fraction was screened for its potential for Au NPs synthesis. All the experiments were performed in triplicate.

4.5.4.1 Protein isolation, purification and one dimensional gel electrophoresis

The total protein concentration in the fungal cell-free filtrate was estimated by bicinchoninic acid (BCA) method using QuantiPro^{TM} BCA assay kit (Catalogue No. QBPCA; Sigma-Aldrich, USA) using bovine serum albumin as a standard. The methodology followed was according to the manufacturer's instructions. Extracellular proteins from cell-free filtrate were isolated using ammonium sulphate precipitation. For this, solid ammonium sulphate was gradually added to the fungal cell-free filtrate at a final saturation of 80 % (Simpson 2004). The mixture was gently stirred for overnight at 4 ˚C. The resulting precipitate was subsequently collected by centrifugation at 10,000 rpm for 20 min at 4 ˚C. The proteins obtained thereafter were resuspended in 50 mM phosphate buffer, pH 7.2 and further purified using a 12-kDa cut off cellulose dialysis membrane (Catalogue no. D9652; Sigma-Aldrich, USA) pre-treated as per the manufacturer's instructions. Briefly, the precipitated protein solution was filled in the treated dialysis bag, which was then suspended in dialysis buffer (50 mM phosphate buffer, pH 7.2) and stirred slowly at 4 ˚C. The buffer was changed 3-4 times over a period of 12 h. After dialysis, the concentration of protein was estimated by the BCA method.

The dialyzed protein fractions were separated on the basis of molecular weight by sodium dodecyl sulphate-polyacrylamide gel electrophoresis (SDS-PAGE) as per standard procedure with adequate modifications (Laemmli 1970). Samples were denatured in 2X sample buffer containing 60 mM Tris (pH 6.8), 25 % glycerol, 2 % SDS, 14.4 mM 2-mercaptoethanol, 0.1 % bromophenol blue and boiled for 5 min, followed by centrifugation at 8,000 rpm for 1 min at 4 ˚C. Electrophoresis was performed on a Mini Protean$^{®}$ Tetra-Cell instrument (BioRad Laboratories, USA) at a constant voltage of 80 kV. After electrophoresis, the gel was stained with Coomassie Brilliant blue (CBB) R-250. In another experiment, gel was stained with silver stain using ProteoSilver^{TM} kit (Catalogue No. PROT-SIL-1; Sigma-Aldrich, USA) as per the manufacturer's instructions.

The stained gels were observed in BioRad Gel Doc^TM XR imaging system and the molecular mass of protein band(s) was determined.

4.5.4.2 Protein fractionation using size exclusion chromatography

The dialyzed mixture containing fungal extracellular proteins were fractionated on the basis of their molecular weight using the size exclusion chromatography (SEC). For this purpose, Superdex™ 200 Increase 10/300 GL column and the Akta Pure 25 M chromatography system, both manufactured by GE Healthcare Pvt. Ltd., Germany were employed. All the steps were performed at 4 ˚C. The column (column volume (CV): 24 mL) was washed by 2 CV using 0.22 µm filtered, autoclaved and degassed Milli-Q water (Flow rate: 0.75 mL min^{-1}; Pre-column pressure: 3.5 MPa) followed by equilibration by 2 CV of phosphate buffer (50 mM; pH 7.2). The sample was loaded into a 500 µL capillary loop using a syringe. The proteins were eluted at a flow rate of 0.25 mL min^{-1} using the same buffer. The eluted protein fractions were collected in sterile tubes manually on the basis of appearance of 280 nm peaks as recorded by UV detector. The concentration of protein in each fraction was estimated by the BCA method.

4.5.4.3 Nanoparticle synthesis ability of various protein fractions

In order to identify the fraction(s) comprising of protein(s) responsible for Au NPs synthesis, all the eluted fractions were exposed to gold (III) chloride trihydrate solution at a final concentration of 0.5 mM and incubated at 28 ˚C under dark conditions. The raction was routinely checked. The synthesis of Au NPs was confirmed by UV-visible, DLS measurement apart from visual observation. The fraction showing fastest and/or exclusive synthesis of Au NPs was further profiled on SDS-PAGE to ascertain the active protein.

4.6 Results and discussion

4.6.1 Extracellular mycosynthesis and characterization of Au NPs

The reduction of gold ions into Au NPs was monitored by the progressive change in the colour of cell-free filtrate from pale yellow to vivid pink (Figure 4.14). In context to time, no visual change in colour was evident till 24 h of exposure after which the cell-free filtrate started to turn pale green. At later time intervals, precisely after 48 h a marked colour change to vivid pink occurred followed by increase in its intensity in case of both the tested fungal isolates. The change in the colour of cell-free filtrate was due to the surface plasmon resonance (SPR) of 6s conductive electrons at the surface of Au NPs (Noguez 2007).
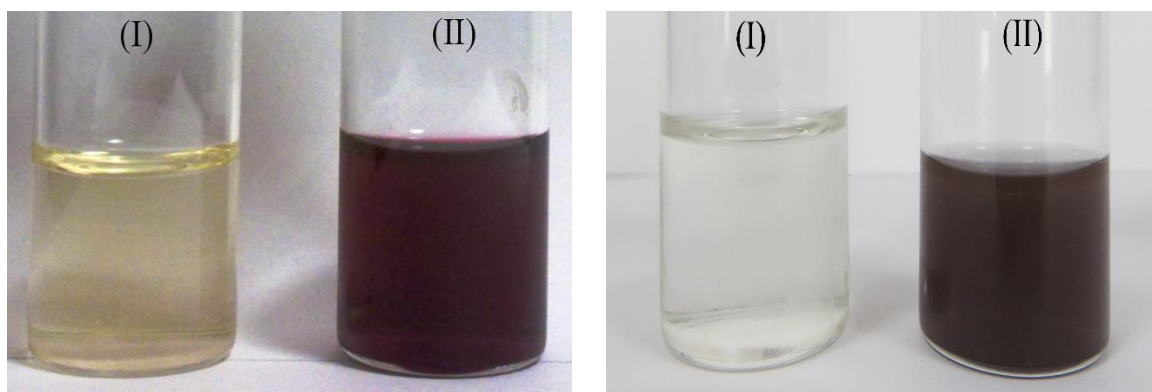
Figure 4.14 Tubes containing cell-free filtrate (I) before and (II) after formation of Au NPs using *Cladosporium oxysporum* AJP03 (left) and *Lichtheimia ramosa* AJP11 (right)

The SPR band was further quantitatively measured by recording the UV-visible absorption spectra of the reaction mixture at different time intervals (Figure 4.15). Emergence of a strong absorption peak with respect to time at 555 nm and 598 nm reflected the synthesis of Au NPs using *Cladosporium oxysporum* AJP03 and *Lichtheimia ramosa* AJP11, respectively (Mulvaney 1996; Shankar et al. 2003). Incidentally, among both the fungal isolates, no further increase in the peak intensity was recorded after 120 h of reaction signifying the complete reduction of precursor gold ions. Likewise, no shift in the absorption maxima with time indicated the monodispersity and size restriction of the synthesized nanoparticles. The negative control showed no change in the colour as well as showed no SPR peak indicating that the Au NPs synthesis was not a thermal and/ or temporal process. The stability of nanoparticle solution stored at room temperature was also determined by UV-visible spectroscopy. The presence of similar SPR peak after three months of storage confirmed the long term stability of the synthesized Au NPs.
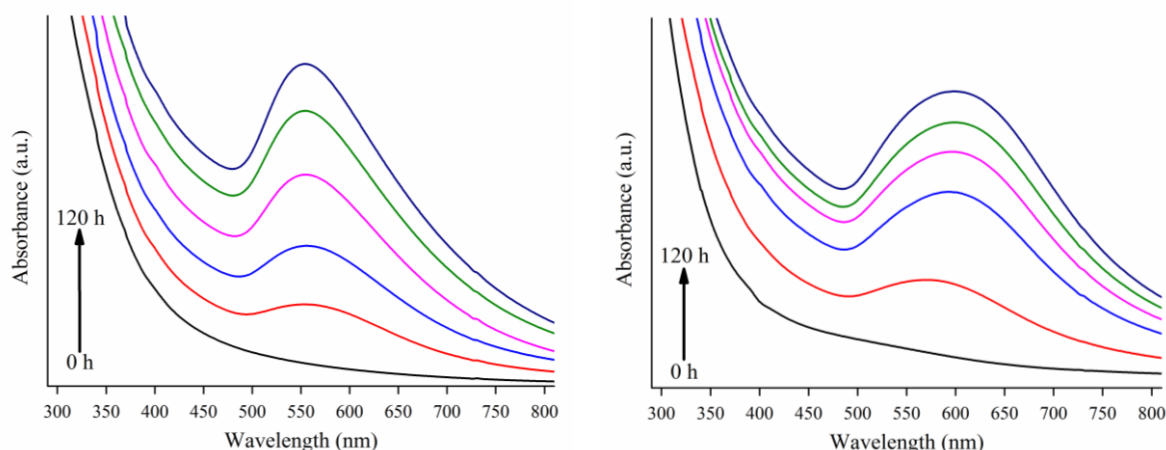
Figure 4.15 UV-visible absorption spectrum of cell-free filtrate representing time dependent gradual synthesis of Au NPs using *Cladosporium oxysporum* AJP03 (left) and *Lichtheimia ramosa* AJP11 (right). Arrow represents time of reaction (0, 24, 48, 72, 96 and 120 h) with respective curves

The frequency distribution histogram calculated using size/number relation as obtained by DLS measurement revealed that majority of particles synthesized using *Cladosporium oxysporum* AJP03 and *Lichtheimia ramosa* AJP11 were confined in the range of 40-60 nm (PDI: 0.43) and 30-50 nm (PDI: 0.39), respectively (Figure 4.16). The polydispersity index (PDI) was observed to be less than 0.7 in case of both fungal isolates indicating that all the particles were restricted to a narrow size range. Theoretically, PDI corresponds to the square of the normalized standard deviation of an underlying Gaussian size distribution and indicates the homogeneity of a sample (Liu et al. 2008).
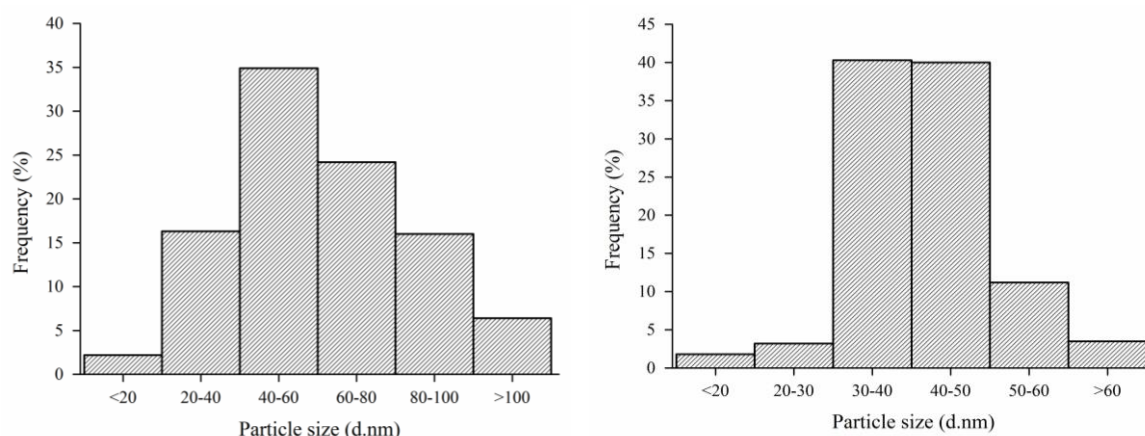
Figure 4.16 Average hydrodynamic particle size histogram determined by DLS analysis of Au NPs synthesized using *Cladosporium oxysporum* AJP03 (left) and *Lichtheimia ramosa* AJP11 (right)

The size and morphology of nanoparticles were confirmed by TEM imaging (Figure 4.17). TEM micrograph of Au NPs synthesized using *Cladosporium oxysporum* AJP03 revealed the particles to be quasi-spherical with an average particle size of 72.32 ± 21.80 nm. In comparison, *Lichtheimia ramosa* AJP11 was able to synthesize spherical Au NPs of much smaller size as the average particle size was determined to be 31.82 ± 4.28 nm. The particle size distribution histogram obtained from TEM measurement reflected similar observation that Au NPs synthesized in the latter were smaller and more monodispersed as ~50 % of nanoparticles were confined in the narrow size range of 30-35 nm (Figure 4.18).

The size distribution results obtained from TEM analysis were in agreement with the values obtained by DLS measurements. Although TEM and DLS both can be used for measurement of particle size, evidently TEM reflects the absolute dimensions of a nanoparticle unlike DLS which calculates its hydrodynamic size. The size calculation by DLS becomes more authenticated in case of spherical particles as it calculates the hydrodynamic size in terms of diameter/ radius based on the Stokes-Einstein equation of a sphere that has similar translational diffusion coefficient irrespective of nanoparticle shape

(Jiang et al. 2009). The results obtained during the present study validate the suitability of DLS as a technique for size measurement of spherical particles.
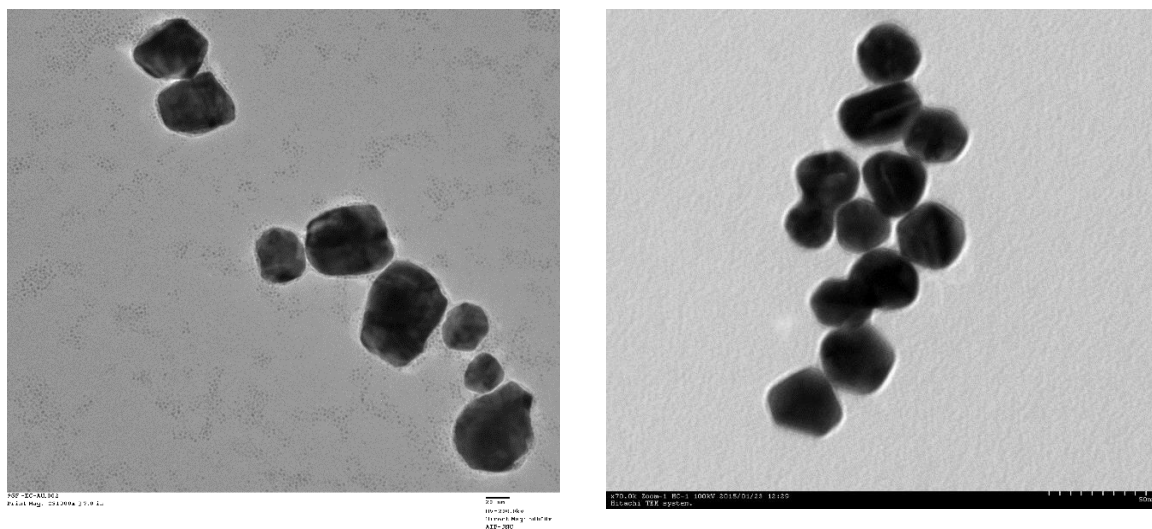
Figure 4.17 TEM micrograph of Au NPs synthesized using *Cladosporium oxysporum* AJP03 (left; scale bar equivalent to 20 nm) and *Lichtheimia ramosa* AJP11 (right; scale bar equivalent to 50 nm)
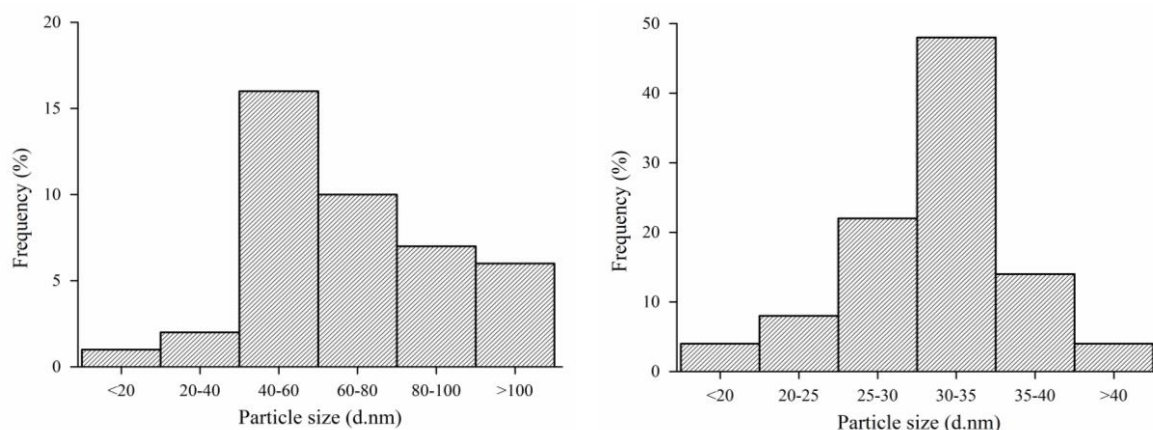
Figure 4.18 Particle size distribution histogram extracted from TEM analysis of Au NPs synthesized using *Cladosporium oxysporum* AJP03 (left) and *Lichtheimia ramosa* AJP11 (right)

The structural features of the individual nanoparticles were observed in the HR-TEM images (Figure 4.19). The particles were predominantly spherical in shape with round yet bloated edges. Careful observation of the lattice fringes in the HR-TEM micrograph demonstrated the crystalline nature of Au NPs. The micrograph also suggested preferential growth along (111) lattice plane as indicated by the presence of bloated edges (Grzelczak et al. 2008).

EDS analysis was carried out for the element characterization of the nanoparticles (Figure 4.20). The representative spot EDS spectrum recorded by bombarding a focused beam of electrons on a single nanoparticle confirmed the presence

of gold metal with distinct peaks at 9.712 and 2.120 keV corresponding to X-ray emitted from L_{α} and M shells respectively. In addition, carbon (K_{α} 0.277 keV) and copper (K_{α} 8.040 keV and L_{α} 0.930 keV) peaks were also detected as the sample was drop coated on a carbon coated copper grid (Zhang et al. 2011). The element map was obtained by progressively rastering the electron beam point by point over an area of interest. EDS mapping of a representative region containing nanoparticles clearly showed the spatial distribution of gold in the sample.
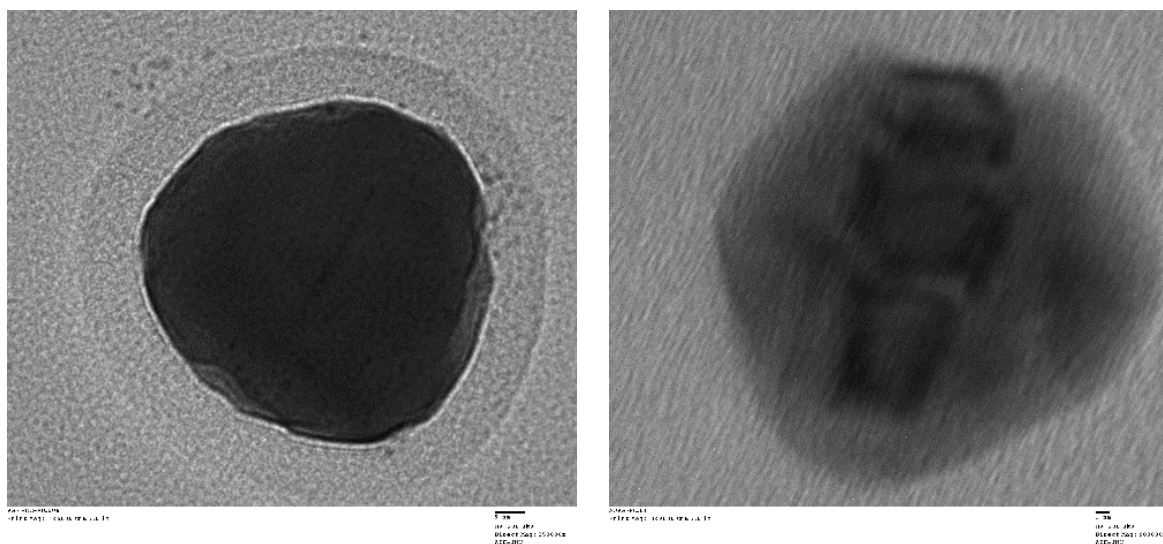
Figure 4.19 HR-TEM micrograph of a single nanoparticle synthesized using *Cladosporium oxysporum* AJP03 (left; scale bar equivalent to 5 nm) and *Lichtheimia ramosa* AJP11 (right; scale bar equivalent to 1 nm)
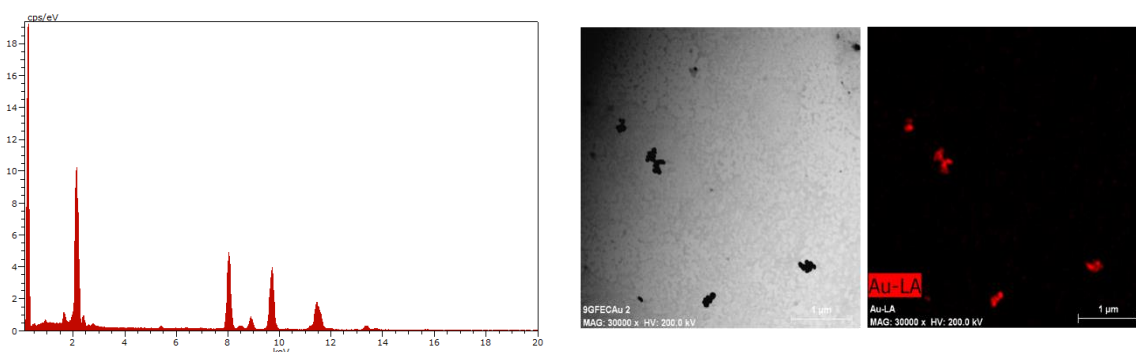
Figure 4.20 Spot EDS spectrum (left) of single nanoparticle representing the elemental composition and EDS mapping (right) showing spatial distribution of gold in the sample

The crystalline nature of nanoparticles was further validated by powder diffraction studies (Figure 4.21). Bragg reflections recorded by XRD measurement exhibited fcc crystalline structure of gold as per JCPDS file 04-0784. *Cladosporium oxysporum* AJP03 synthesized Au NPs exhibited peaks at 2θ value of 38.06˚, 44.33˚, 64.61˚ and 77.56˚ corresponding to (111), (200), (220) and (300) planes with calculated lattice constant of 4.0846 Å and intensity ratio of 0.32. Au NPs synthesized using *Lichtheimia ramosa* AJP11

exhibited peaks at 2θ value of 38.21˚, 44.36˚, 64.58˚ and 77.61˚ corresponding to (111), (200), (220) and (300) planes with calculated lattice constant of 4.0872 Å and intensity ratio of 0.26. In case of both the fungal isolates, the Bragg's reflections of as-synthesized Au NPs was found to be close to the standard value (4.079Å) of gold. As compared to the conventional intensity ratio (0.52) of (200) and (111) diffraction peak, the observed ratio suggested (111) plane to be the predominant orientation in the synthesized Au NPs (Sun and Xia 2002).
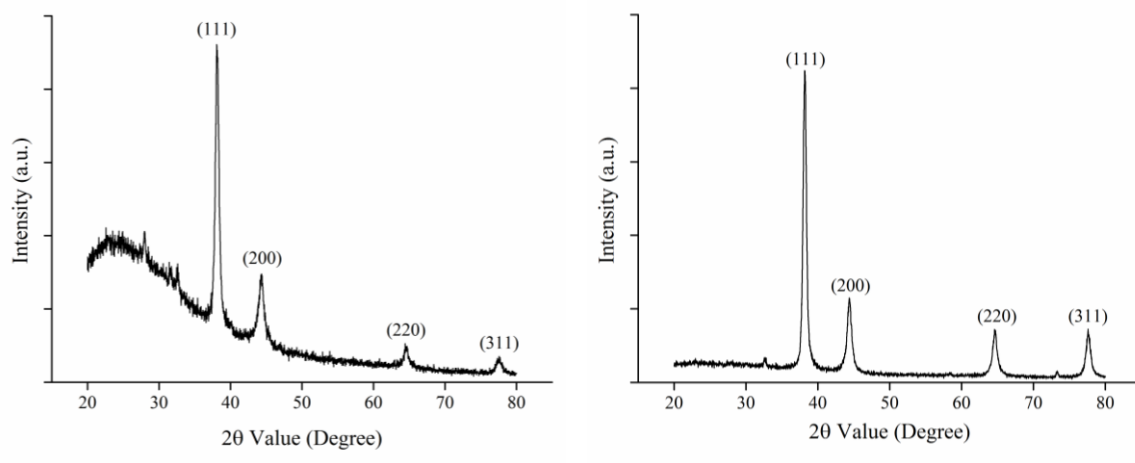
Figure 4.21 XRD spectrum with Bragg's diffraction values of Au NPs synthesized using *Cladosporium oxysporum* AJP03 (left) and *Lichtheimia ramosa* AJP11 (right)

Figure 4.22 shows representative SPM images at low and high resolution detailing the surface features of the nanoparticle which was obtained by mechanically moving a sharp probe in a raster scan over the specimen particle and recording the probe-surface interaction (Shankar et al. 2004). As seen in the figure, Au NPs present on the surface of the specimen slide have been topologically traced.
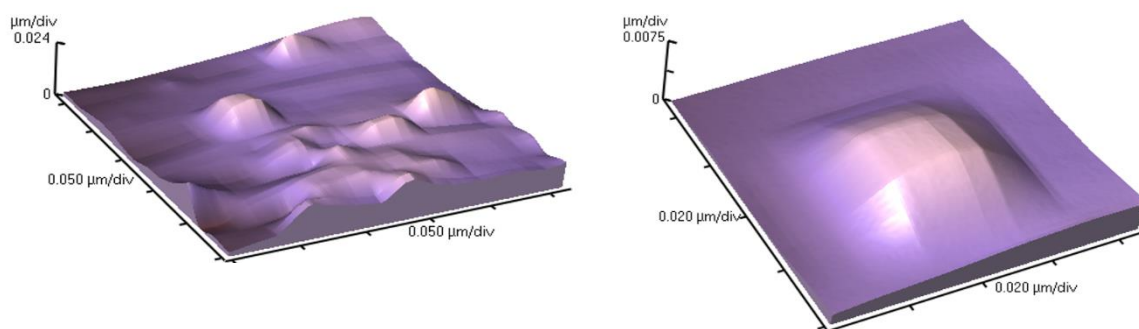
Figure 4.22 Representative SPM analysis showing topographical images of Au NPs at low (left) and high (right) resolution

The chemical composition and oxidation state of Au NPs was determined by XPS analysis (Figure 4.23). Presence of strong binding energy peak (Au 4f) observed in the

representative wide scale survey scan confirmed the presence of gold. In addition, presence of carbon and oxygen was also observed which may be due to the use of carbon tape for sample preparation and insufficient vacuum drying of the sample, respectively. The XPS peak positions were calibrated against C1s binding energy (284.5 eV), in order to compensate any kind of energy shift due to charging effect. Presence of peaks centered around 83.3 eV and 87.6 eV in the high resolution XPS spectrum corresponded to the spin-orbit splitting components Au $4f_{7/2}$ and Au $4f_{5/2}$, respectively and represented metallic Au (0) state. The binding energy values observed were in good agreement with the reported binding energy values of Au (0) state (Sharma et al. 2007; Das et al. 2012).
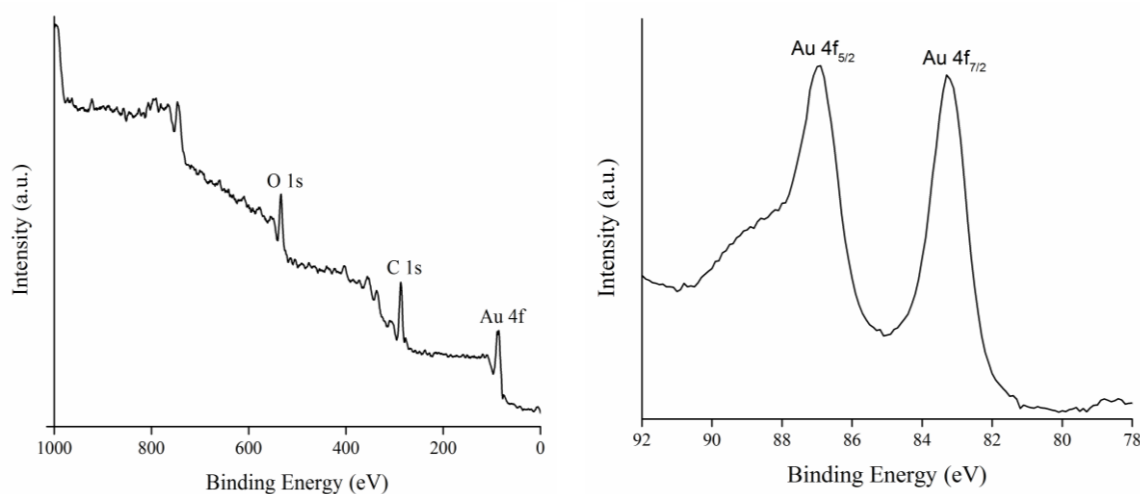
Figure 4.23 Representative XPS analysis of Au NPs showing wide scale survey (left) and high resolution Au 4f spectrum (right)

FTIR measurement of the freeze-dried samples was carried out to characterize the capping molecules present on the surface of Au NPs (Figure 4.24). FTIR analysis of nanoparticles synthesized using *Cladosporium oxysporum* AJP03 showed a prominent vibration band at wavenumber 1637 cm^{-1} corresponding to the amide I bond of proteins arising due to carbonyl stretching. Presence of transmittance bands at 1540 cm^{-1}, 1460 cm^{-1} and 1402 cm^{-1} were found to be associated with NH bending vibrations of amide II, –CH$_2$– bending mode in protein side chains and COO^{-} stretching, respectively (Macdonald and Smith 1996; Wang et al. 2006; Yang et al. 2007). FTIR spectrum of nanoparticles synthesized using *Lichtheimia ramosa* AJP11 revealed bands at wavenumber 1646 cm^{-1} and 1544 cm^{-1} corresponding to the bending vibrations of the amide I and amide II bands and corresponding stretching vibration at wave number 2926 cm^{-1}. In addition, bands at wavenumber 1381 cm^{-1} and 1032 cm^{-1} indicated C-N stretching vibrations of the aromatic and aliphatic amines, respectively (Jain et al. 2011; Vigneshwaran et al. 2006). The presence of the signature peaks of amino acids supports the presence of proteins/peptides in cell-free filtrate and strongly suggest the possibility of nanoparticle-proteins interaction resulting in particle stability.
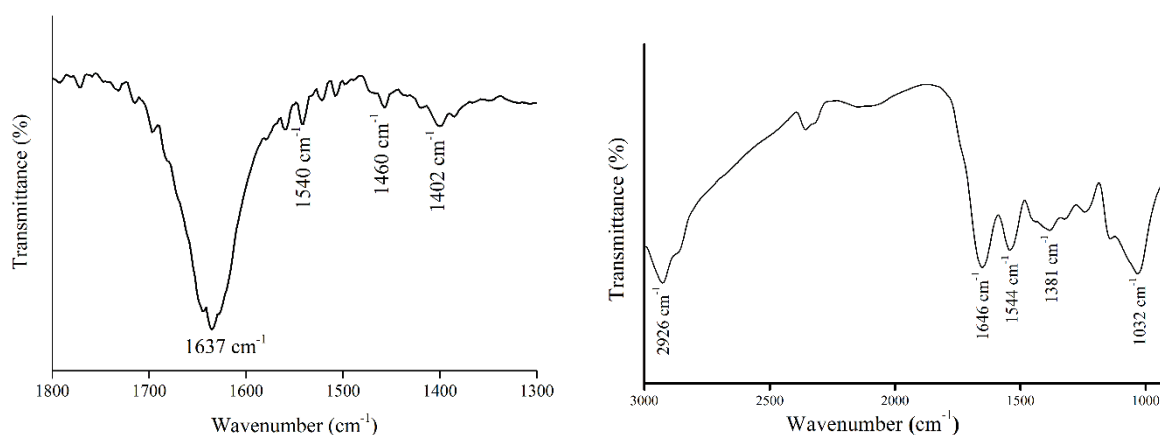
Figure 4.24 FTIR spectrum of freeze-dried powder of Au NPs synthesized using *Cladosporium oxysporum* AJP03 (left) and *Lichtheimia ramosa* AJP11 (right)

4.6.2 Effect of reaction conditions on particle size and yield

Varying biomass: water ratio (1:5, 1:10, 1:15, 1:20 and 1:30) which led to decrease in the concentration of extracellular metabolites in the cell-free filtrate were tested (Figures 4.25 and 4.26). In case of Au NPs synthesis by *Cladosporium oxysporum* AJP03, the highest concentration of extracellular metabolites (biomass: water ratio of 1:5) resulted in maximum yield whereas in *Lichtheimia ramosa* AJP11, surprisingly biomass: water ratio of 1:10 resulted in highest nanoparticle synthesis as determined by UV-visible spectroscopy. In both the fungal isolates, concentration of extracellular metabolites (1:20 and 1:30; biomass: water ratio) failed to show any SPR peak and resulted in drastic increase in average particle size. Similar results were obtained by Korbekandi et al. (2013) during their study on biosynthesis of silver nanoparticles using *Fusarium oxysporum*. DLS measurement suggested a negative correlation between the concentration of extracellular metabolites and average hydrodynamic particle size due to which biomass: water ratio of 1:5 resulted in smallest sized nanoparticles. These results can be justified by looking at the possible mechanism of nanoparticle synthesis which include bio-reduction of Au (III) ions to Au (0) followed by nucleation and stabilization. The rate of Au (III) to Au (0) conversion is directly proportional to the number of reducing bio-molecules present in the cell-free filtrate (Tripathy et al. 2010). Ideally, a higher concentration of metabolites in the cell-free filtrate leads to an increase in the number of active nucleation sites against limited number of Au (0) atoms which results in formation of smaller nanoparticles (Prozorov et al. 2007).

The effect of concentration of precursor salt was studied by adding varied volume of gold (III) chloride trihydrate solution to the cell-free filtrate (Figures 4.27 and 4.28). In both the fungal isolates, the optimum concentration of precursor salt was found to be 1.0 mM as determined by UV-visible spectroscopic measurements. Even though, the ratio of

active nucleation sites to the number of Au (0) atoms decreased with increasing concentration of ionic gold, smallest size of particles were observed at 0.5 mM instead of 0.1 mM as measured by DLS analysis (Grzelczak et al. 2008). At oversaturation (2.0 mM and 5.0 mM), no particles were synthesized suggesting an insufficient amount of reducing bio-molecules against available Au (III) ions (Pimprikar et al. 2009).

The pH of the cell-free filtrate before exposure to gold ions was varied to study the effect of reaction pH (Figure 4.29 and 4.30). In case of Au NPs synthesis by *Cladosporium oxysporum* AJP03, maximum particle yield without any flocculation was observed at physiological pH (pH 7.0). Although, nanoparticle synthesis was also visualized at pH 6.0 and 8.0, a significant reduction was observed in the SPR peak intensity. In contrast, pH 8.0 supported highest and monodispersed nanoparticle synthesis by *Lichtheimia ramosa* AJP11, followed by physiological pH (pH 7.82). At pH 6.0, the SPR peak intensity was found to be maximum but it was very broad indicating polydispersed synthesis of Au NPs. However, in both the fungal isolates, smallest particle size was observed at pH 6.0 as compared to slightly larger particles at pH 8.0 and physiological pH as determined by DLS measurements. Drastic alteration in pH at acidic condition (pH 2.0 and pH 4.0) failed to show any SPR peak along with a severe increase in the average hydrodynamic particle size in both the fungal isolates. However, marginal synthesis of Au NPs was observed at alkaline pH 10.0 in case of *Lichtheimia ramosa* AJP11. It has been proposed that reducing groups such as hydroxyl (OH-) are most reactive near neutral pH as compared to extreme acidic or alkaline conditions (Binupriya et al. 2010). It has also been hypothesized that near neutral pH favours the process of nucleation over aggregation and results in synthesis of small sized particles (Sathishkumar et al. 2009). No Au NPs were synthesized at the tested extreme pH which may be due to the denaturation of fungal extracellular metabolites.

Effect of various reaction parameters on average hydrodynamic particle size and yield of Au NPs by *Cladosporium oxysporum* AJP03 and *Lichtheimia ramosa* AJP11 have been summarized in Table 4.1 and Table 4.2, respectively.
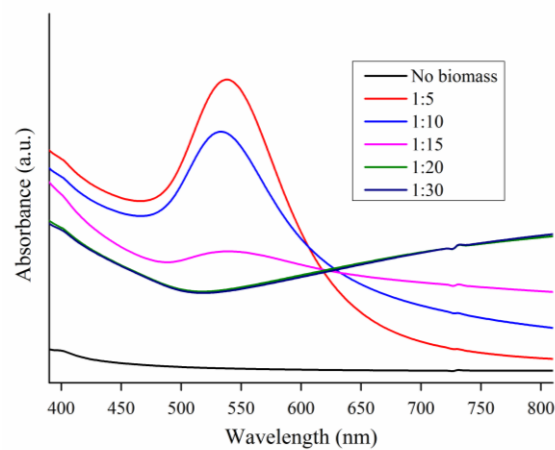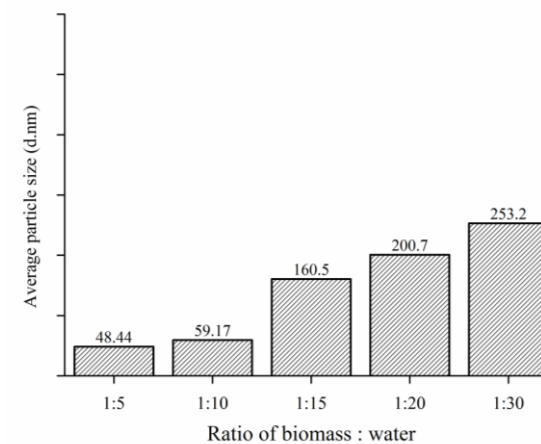
Visual observation   **UV-visible measurement**   **DLS measurement**
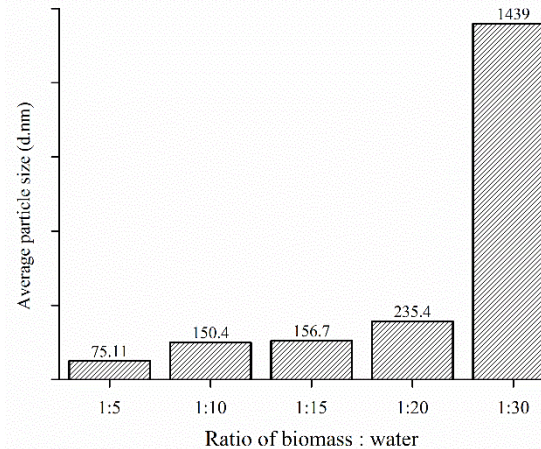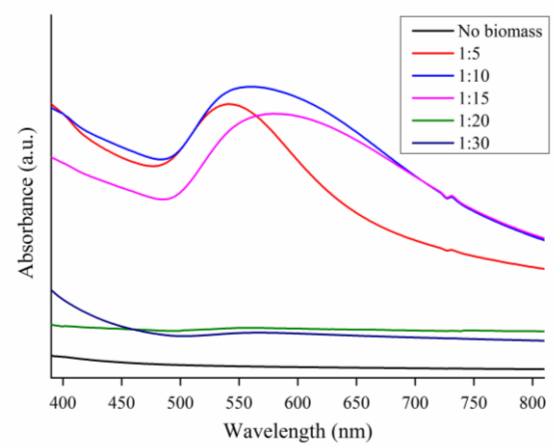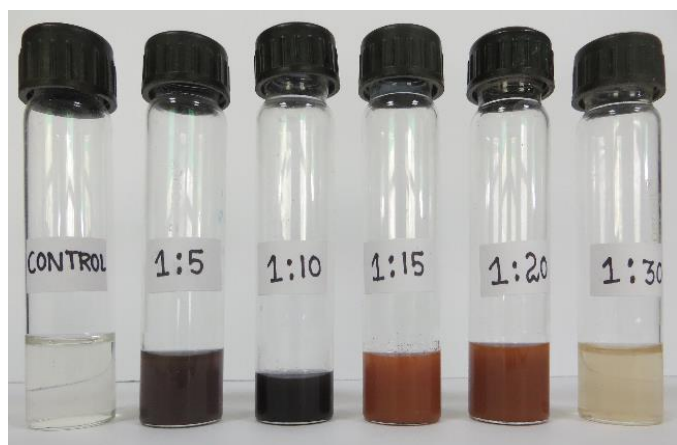
Figure 4.25 Effect of concentration of extracellular metabolite on hydrodynamic particle size and yield of Au NPs synthesized using *Cladosporium oxysporum* AJP03 (upper panel) and *Lichtheimia ramosa* AJP11 (lower panel)

	1:5	1:10	1:15	1:20	1:30
Scale bar = 50 nm	x70k	x80k	x60k	x80k	x60k
Scale bar = 100 nm	x30k	x40k	x30k	x40k	x40k
Scale bar = 200 nm	x20k	x20k	x20k	x12k	x20k
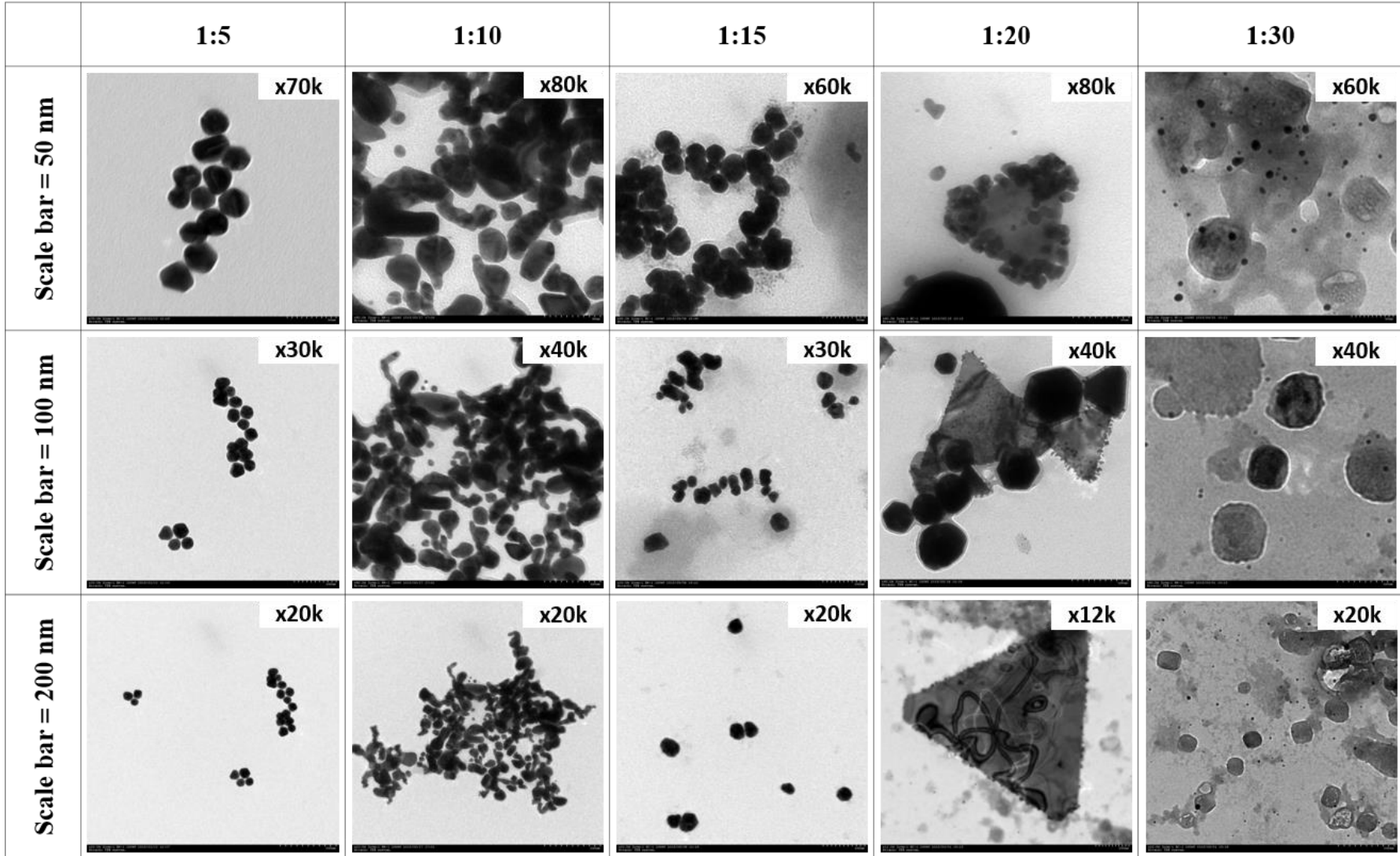
Figure 4.26 Effect of concentration of extracellular metabolite on particle size and yield of Au NPs synthesized using *Lichtheimia ramosa* AJP11
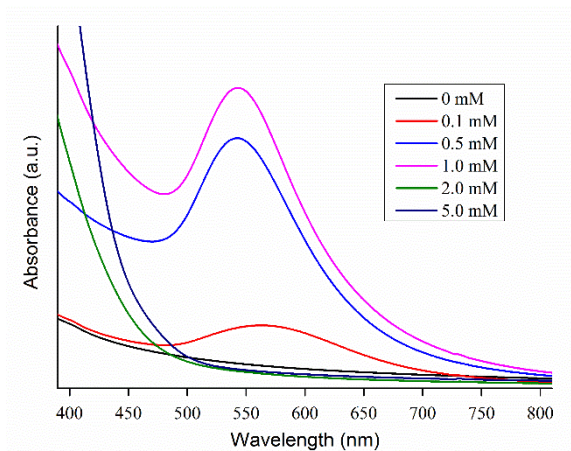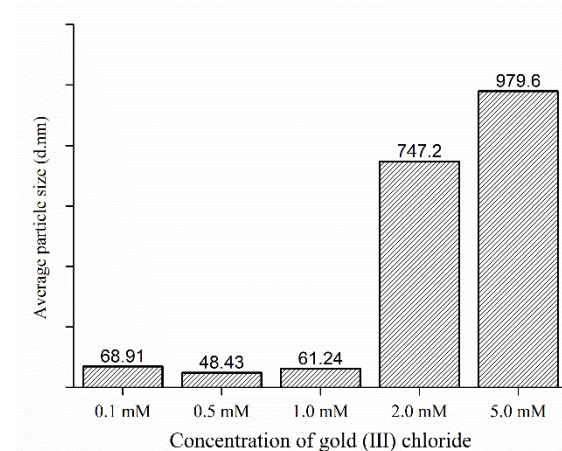
| Visual observation | UV-visible measurement | DLS measurement |
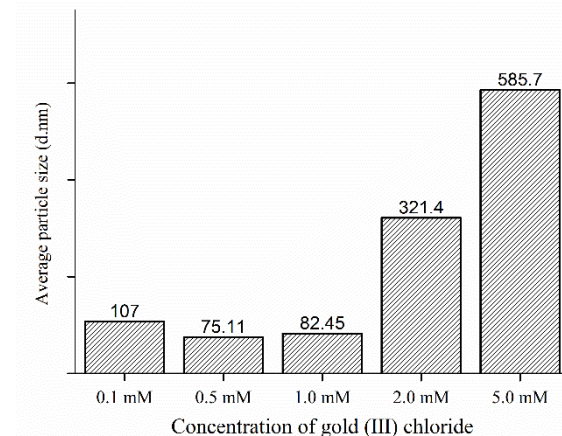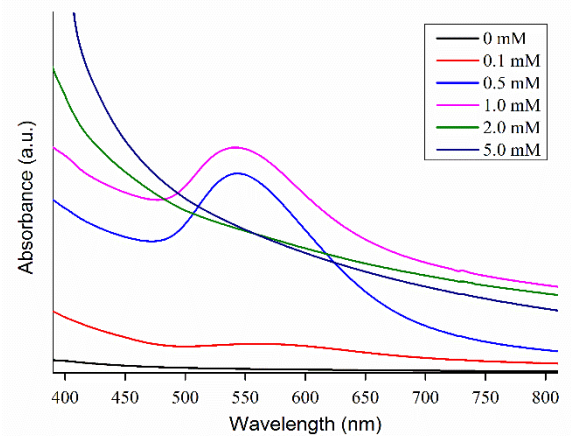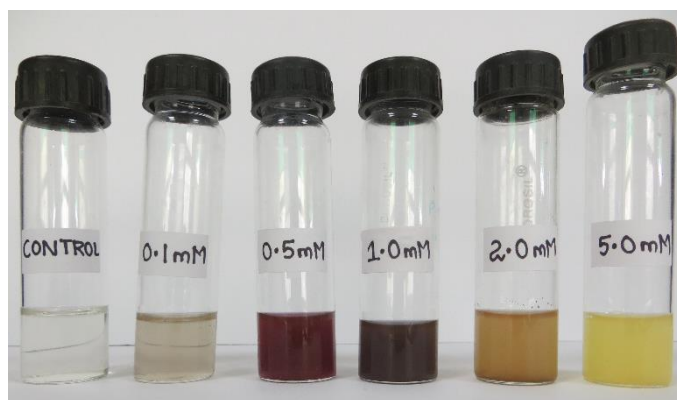
Figure 4.27 Effect of concentrations of precursor salt on hydrodynamic particle size and yield of Au NPs synthesized using *Cladosporium oxysporum* AJP03 (upper panel) and *Lichtheimia ramosa* AJP11 (lower panel)
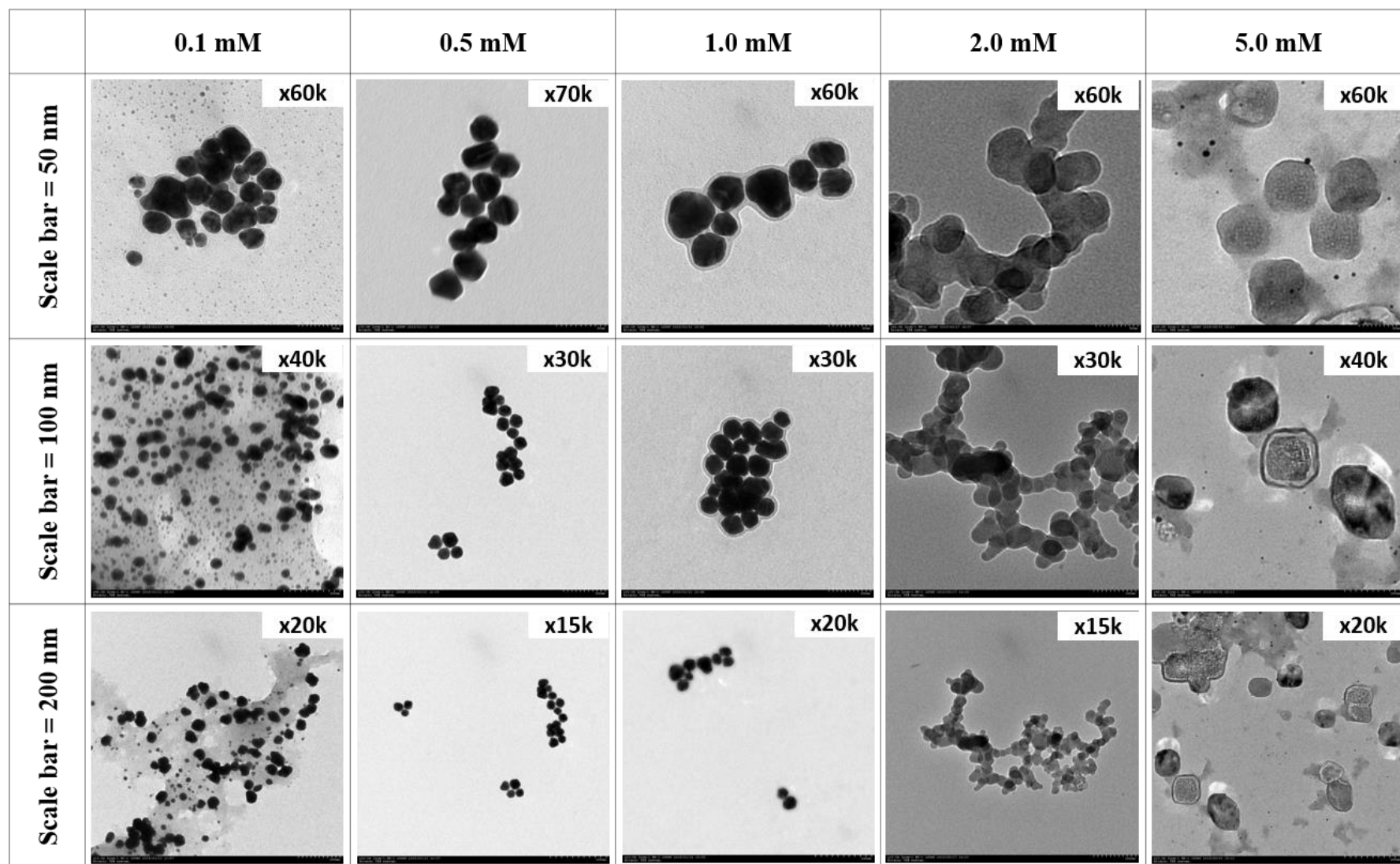
Figure 4.28 Effect of concentrations of precursor salt on particle size and yield of Au NPs synthesized using *Lichtheimia ramosa* AJP11
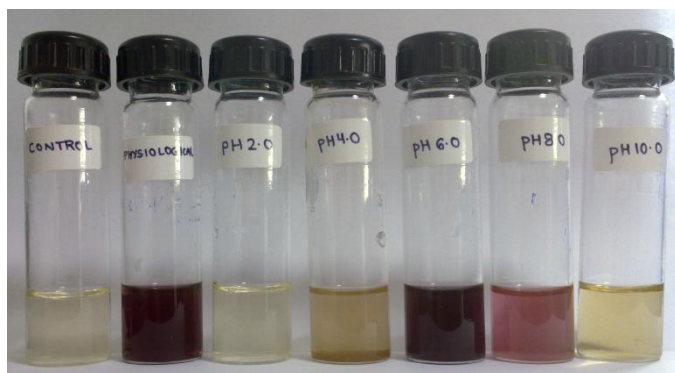
Visual observation
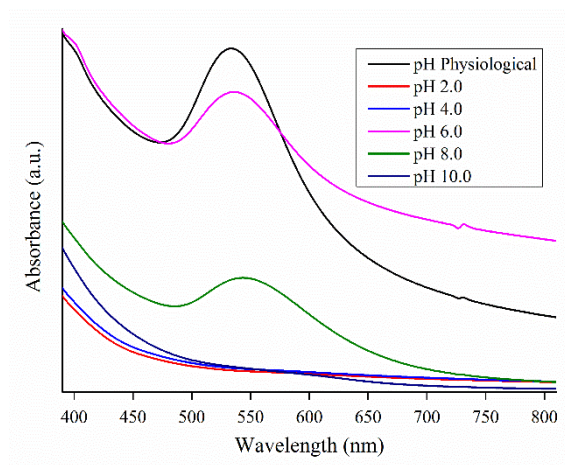
UV-visible measurement
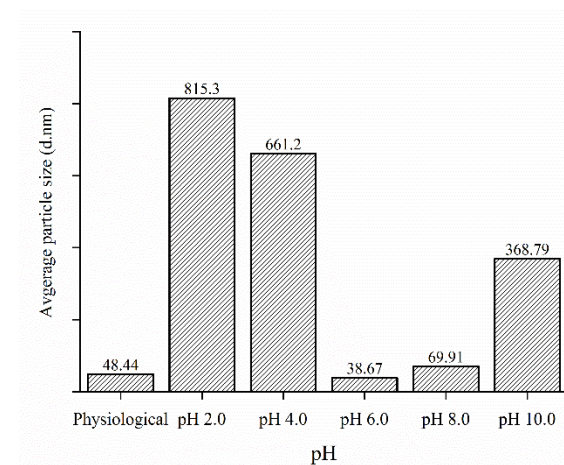
DLS measurement
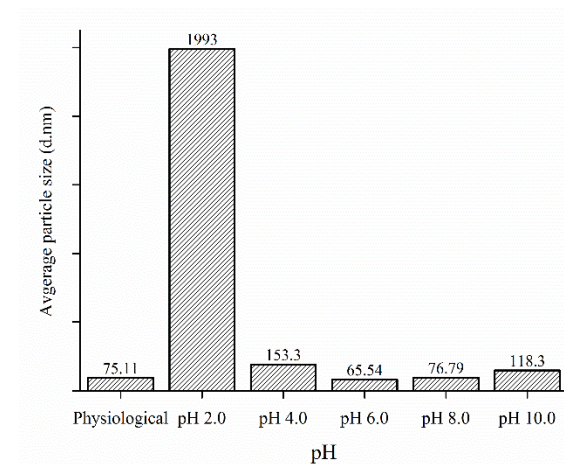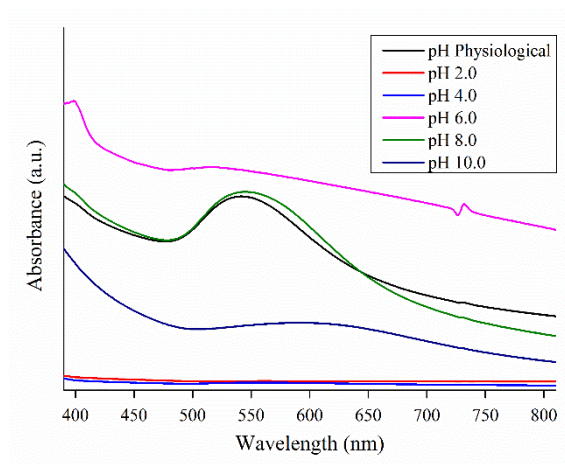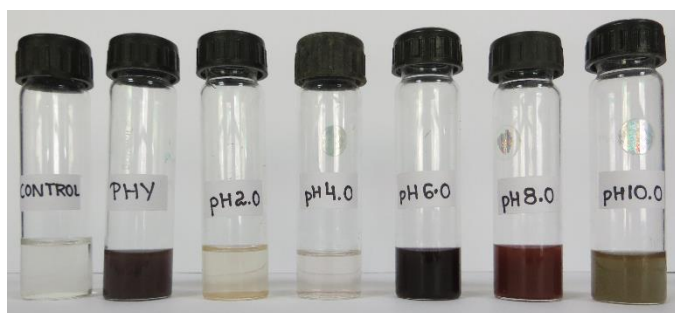
Figure 4.29 Effect of reaction pH on hydrodynamic particle size and yield of Au NPs synthesized using *Cladosporium oxysporum* AJP03 (upper panel) and *Lichtheimia ramosa* AJP11 (lower panel)
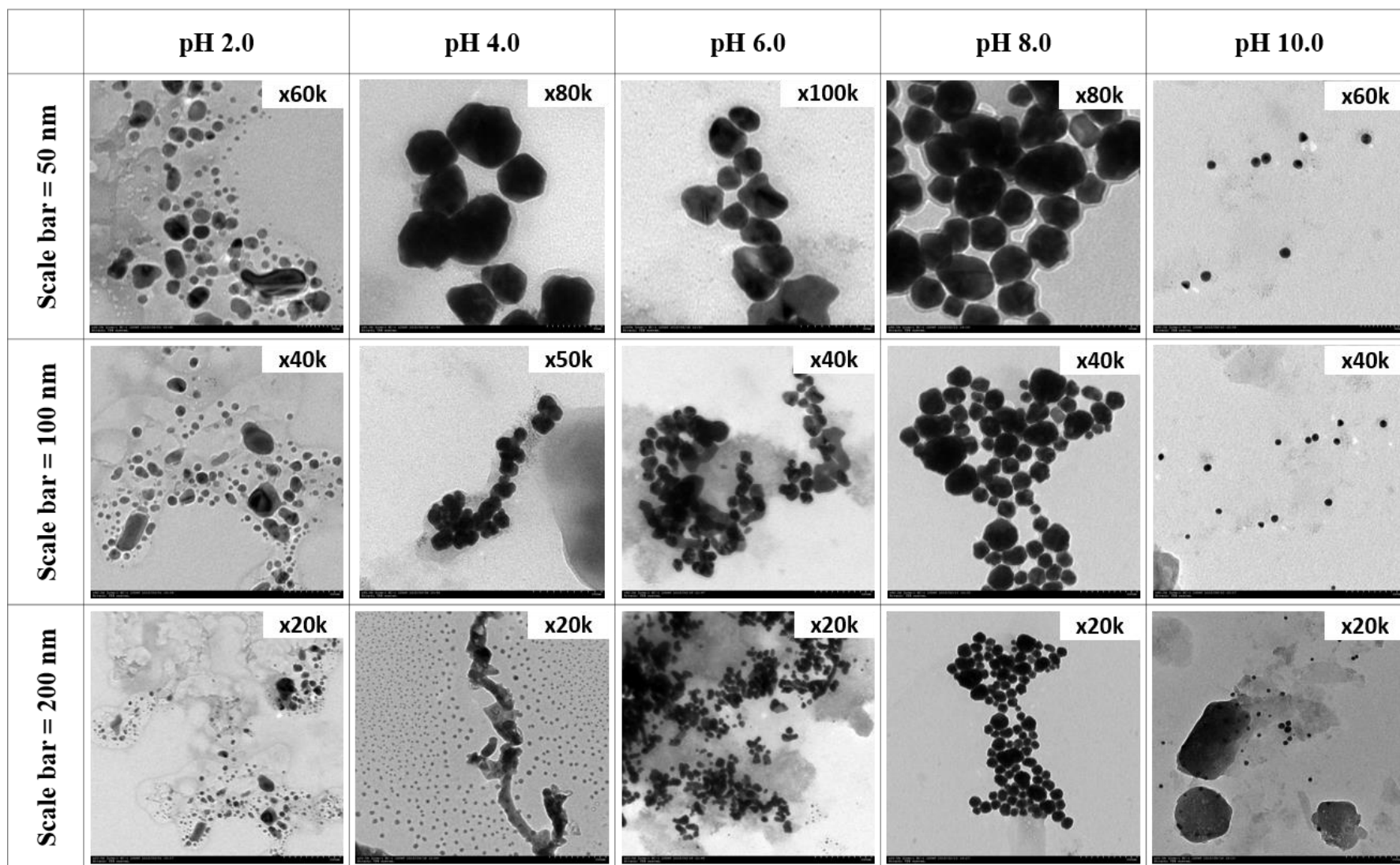
Figure 4.30 Effect of reaction pH on particle size and yield of Au NPs synthesized using *Lichtheimia ramosa* AJP11

Table 4.1 Summary of effect of various reaction parameters on size and yield of particles synthesized by *Cladosporium oxysporum* AJP03.

Condition	Variables	Visual observation of Au NPs	Relative SPR peak intensity	Average hydrodynamic particle size (d.nm)
Concentration of extracellular metabolites	Biomass: Water (1:5)	Present	+ + +	48.44
	Biomass: Water (1:10)	Present	+ +	59.17
	Biomass: Water (1:15)	Present	+	160.5
	Biomass: Water (1:20)	Absent	-	200.7
	Biomass: Water (1:30)	Absent	-	253.2
Concentration of precursor salt	0.1 mM	Present	+	68.91
	0.5 mM	Present	+ +	48.43
	1.0 mM	Present	+ + +	61.24
	2.0 mM	Absent	-	747.2
	5.0 mM	Absent	-	979.6
Reaction pH	Physiological (7.0)	Present	+ + +	48.44
	2.0	Absent	-	815.3
	4.0	Absent	-	661.2
	6.0	Present	+ +	38.67
	8.0	Present	+	69.91
	10.0	Absent	+	368.79

- = absent, + = low, ++ = moderate, +++ = high

Table 4.2 Summary of effect of various reaction parameters on size and yield of particles synthesized by *Lichtheimia ramosa* AJP11.

Condition	Variables	Visual observation of Au NPs	Relative SPR peak intensity	Average hydrodynamic particle size (d.nm)
Concentration of extracellular metabolites	Biomass: Water (1:5)	Present	+ +	75.11
	Biomass: Water (1:10)	Present	+ + +	150.4
	Biomass: Water (1:15)	Present	++	156.7
	Biomass: Water (1:20)	Absent	-	235.4
	Biomass: Water (1:30)	Absent	-	1439
Concentration of precursor salt	0.1 mM	Present	+	107
	0.5 mM	Present	+ +	75.11
	1.0 mM	Present	+ + +	82.45
	2.0 mM	Absent	-	321.4
	5.0 mM	Absent	-	585.7
Reaction pH	Physiological (7.82)	Present	+ +	75.11
	2.0	Absent	-	1993
	4.0	Absent	-	153.3
	6.0	Present	+ + +	65.54
	8.0	Present	+ +	76.79
	10.0	Partial	+	118.3

- = absent, + = low, ++ = moderate, +++ = high

4.6.3 Mechanistic insights of mycosynthesis of Au NPs by *Lichtheimia ramosa* AJP11

One of the challenges that limits the use of biological methods for industrial scale production of nanoparticles is the lack of flexibility in attaining the desired particle size/shape suitable for different applications. Although, precise modifications in the reaction parameters like concentration of extracellular metabolites, concentration of precursor salt and reaction pH may help in achieving better control over the properties of synthesized particle, strict regulation over the synthesis process can only be achieved by understanding the mechanism of biosynthesis. In agreement to the various reports discussed in the introduction section and the results obtained during the present study wherein, proteins were found to be the capping molecules conferring stability to as-synthesized Au NPs strongly indicate that among the various biomolecules present in the cell-free filtrate of *Lichtheimia ramosa* AJP11, proteins are the most likely "active" biomolecule involved in Au NPs synthesis.

Therefore, in order to elucidate nanoparticle synthesis mechanisms and understand the possible involvement of proteins, the extracellular proteins present in the cell-free filtrate of *Lichtheimia ramosa* AJP11 were isolated, purified and fractionated. Initially, the presence of proteins in the cell-free filtrate was confirmed by estimating the protein concentration using BCA method. The total protein concentration in the cell-free filtrate was determined to be 5.78 ± 2.23 µg mL^{-1}. Proteins are secreted by a fungus in response to its nutrition uptake and infectious nature (Peberdy 1994). Among these proteins, majority are hydrolytic enzymes (amylases, cellulases and proteases) secreted by the fungus to break down the complex nutrients like carbohydrate, protein and lipids into smaller subunits. Apart from this, fungus also secretes other metabolic proteins (Iwashita 2002).

To isolate the extracellular proteins in their non-denatured form, ammonium sulphate precipitation was carried out. Ammonium sulphate gradually removes the bound water molecules from the hydrophobic surfaces of the protein, increasing the hydrophobic interaction between proteins leading to their decreased solubility and subsequent precipitation (Simpson 2004). The precipitated proteins in the form of pellet was collected and subsequently dialyzed using a 12.0 kDa cut-off cellulose membrane. Dialysis eliminates small molecular weight substances such as various salts and reducing agents and also removes peptides less than 12.0 kDa from the sample by virtue of the semi-permeable nature of the membrane and process of diffusion. After dialysis, the concentration of protein in the sample was estimated to be 2.04 ± 0.43 mg mL^{-1}. Further, protein samples were resolved on a one dimensional denaturing SDS-PAGE and the gel was stained using CBB R-250 and silver staining (Figure 4.31). CBB R250 is an amino triarylmethane dye that forms strong but non-covalent complexes with proteins, most probably by a combination of van der Waals forces and electrostatic interactions with NH$^+$ groups (Sambrook et al. 1989). Practically, it binds to protein with a sensitivity of staining 10-100 ng protein on a SDS PAGE gel. To our surprise, CBB R-250 stained gel revealed

the presence of only one yet very intense band at ~ 14 kDa. However, silver staining revealed the presence of six intact bands with approximate molecular weight of 65 kDa (a), 43 kDa (b), 35 kDa (c), 22 kDa (d), 14 kDa (e) and 12 kDa (f). The process of silver staining relies on differential reduction of silver ions that are bound to the side chains of amino acids making it ~100-1000 fold more sensitive than staining with CBB R-250 (Sambrook et al. 1989). At this point, it is important to emphasize that our method does not claim to have extracted all the extracellular proteins but only those that were being released and remained stable (not degraded) under the experimental conditions of nanoparticle synthesis protocol. For instance, the incubation of fungal mycelium in nutrient deprived conditions (only Milli-Q water) for three days to collect extracellular proteins must have resulted in the liberation of proteins from fungal mycelium. It could also be possible that the presence of secreted hydrolytic enzymes may lead to degradation of proteins in substantial amounts. The viability experiment results showed that fungal cells were viable after the reaction period (72 h) which signify that intracellular proteins (cytoplasmic) were not released in the fungal cell-free filtrate.
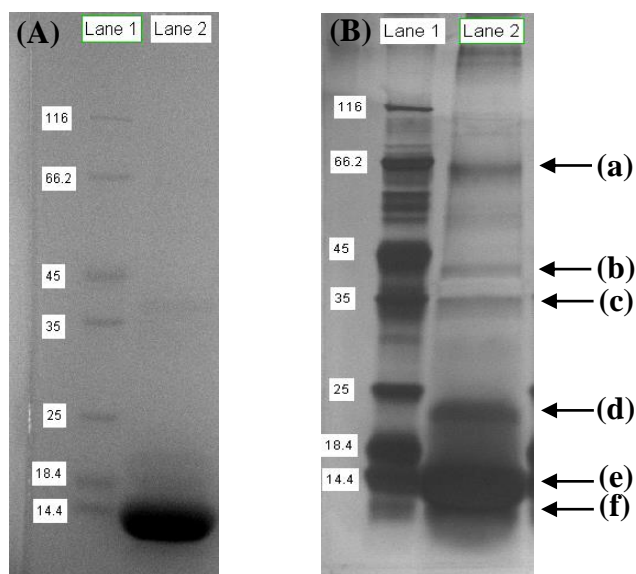
Figure 4.31 SDS-PAGE analysis of purified extracellular proteins from *Lichtheimia ramosa* AJP11. (A) CBB R250 stained gel (B) Silver stained gel Lane 1: molecular size marker (Thermo #26610; 116, 66.2, 45, 35, 25, 18.4 and 14.4 kDa) and lane 2 as sample

The fractionation of various proteins present in the dialyzed sample was performed by size exclusion chromatography using Superdex™ 200 Increase 10/300 GL column using Akta Pure 25 M chromatography system. The 10 cm wide and 30 cm long column used in our study was pre-packed with 8.6 µm beads made up of composite of cross-linked agarose and dextran (http://www.gelifesciences.com). Proteins as they flow through the column diffuse into the bead pores. Larger molecules cannot enter any pore; they flow around the beads and elute out first whereas smaller molecules get diffused into bead pores and are therefore delayed. The smaller the molecule, the longer it takes to flow through (Simpson 2004). As illustrated in Figure 4.32, the crude cell-free filtrate was resolved into six considerably distinct fractions.
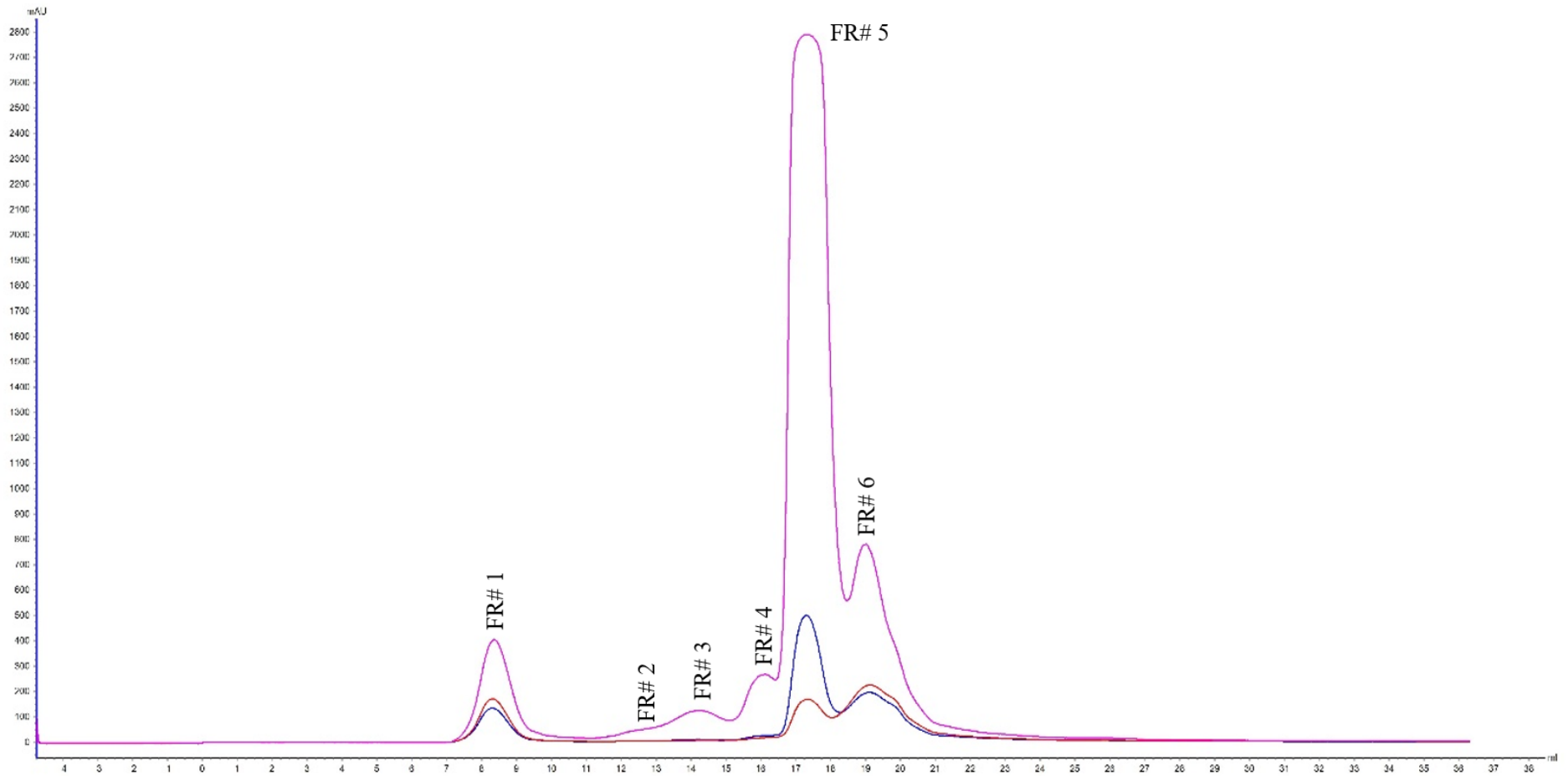
Figure 4.32 Size exclusion chromatograhic fractionation of proteins present in fungal cell-free filtrate of *Lichtheimia ramosa* AJP11. The eluted proteins were distributed in six fractions viz., FR# 1, FR# 2, FR# 3, FR# 4, FR# 5 and FR# 6. The fractions were collected on the basis of appearance of peaks corresponding to the recorded intensity at UV 280 nm (blue), UV 254 (red) and UV 214 (pink) as shown in the chromatogram

The protein(s) present in the flow through of individual fractions at equal concentration of 100 µg mL^{-1} were mixed and incubated with gold (III) chloride trihydrate at a final concentration of 0.5 mM in dark conditions at 28 ˚C in triplicates. The result of Au NPs synthesis after exposure of gold ions to individual protein fractions is shown in table 4.3.

Table 4.3 Activity of different protein fractions towards synthesis of Au NPs.

	1	2	3	4	5	6
Protein concentration* (µg mL^{-1})	98.34 ± 10.49	23.41 ± 15.38	36.82 ± 10.71	75.37 ± 12.55	200.25 ± 22.67	101.28 ± 13.65
Synthesis time	> 30 days	> 30 days	> 30 days	> 30 days	< 10 days	> 30 days
SPR peak (λ_{max}; nm)	562	565	552	543	527	536
SPR peak intensity (OD)	0.52	0.21	0.24	0.12	0.82	0.41
Average hydrodynamic size (d.nm)	82.06	187.1	86.92	265	37.81	81.98
Polydispersity Index	0.486	0.517	0.439	0.214	0.189	0.514

*Actual concentration of protein in fraction (µg mL^{-1})

Incidentally, all the fractions were able to synthesize Au NPs. However, the reaction time and magnitude of nanoparticle synthesis varied significantly (Figure 4.33). In case of fraction 5, the synthesis of Au NPs was observed within 192 hours with maximum particle yield and monodispersity, while synthesis in other fractions started after 30 days. The delayed synthesis and poor yield in other fractions indicate the possibility of non-specific reduction of gold ions by functional groups present on the amino acids which might have been exposed due to denaturation/degradation of proteins because of long incubation time.

Careful observation suggests a "red shift" in the UV-visible spectrum of other fraction showing broad peak indicating formation of large sized and polydispersed particles. This may be due to the absence of specific capping molecules in these fractions which resulted in uncontrolled growth of particles. It has been reported that protein corona surrounding nanoparticles dramatically alters the physio-chemical properties including the hydrodynamic size, surface charge and aggregation behaviour (Schottler et al. 2016).

Due to the fastest and most efficient synthesis of Au NPs by fraction 5, it was resolved on SDS-PAGE. The stained gel revealed the presence of a single protein with approximate molecular weight of 14 kDa (Figure 4.34). These results indicated the possibility of ~14 kDa protein to be the "active" biomolecule involved in extracellular synthesis of Au NPs by *Lichtheimia ramosa* AJP11. Attempts are underway in our lab to identify the protein(s) using advanced proteomic techniques. The outcome would lead to

the possibility of tracing the genes coding these proteins which will open avenues of genetic modification in the synthesis process.
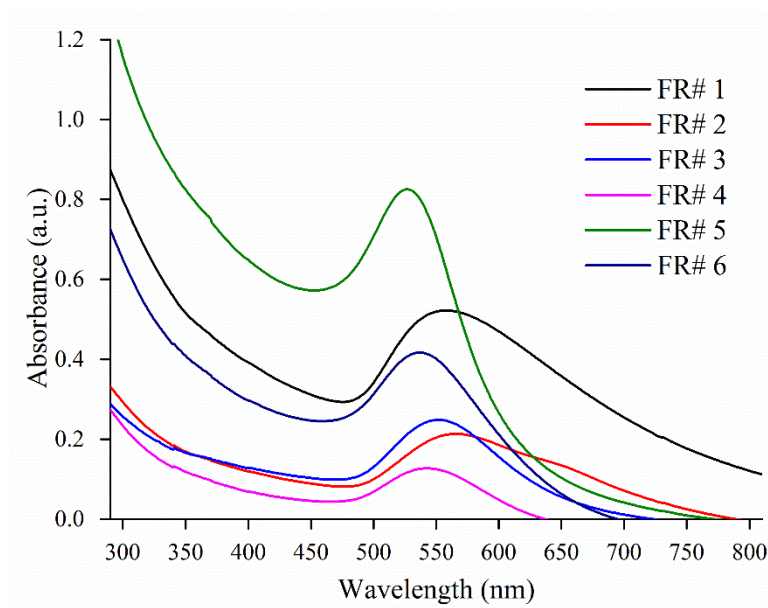
Figure 4.33 UV-visible absorption spectrum of showing Au NPs synthesis profile of various protein fractions.
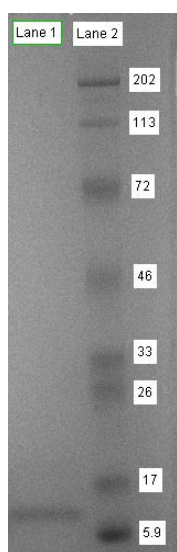
Figure 4.34 SDS-PAGE analysis of fraction 5. Lane 1 shows presence of single band at ~14 kDa. Lane 2: molecular size marker (BioRad; 202, 113, 72, 46, 33, 26, 17 and 5.9 kDa)

4.7 Conclusions

The present study divulges the potential of metal tolerant soil fungi for efficient and sustainable extracellular synthesis of gold nanoparticles. *Cladosporium oxysporum* AJP03 and *Lichtheimia ramosa* AJP11 which were found to have high gold metal tolerance ability showed potential for extracellular synthesis of Au NPs. The as-synthesized nanoparticles were spherical in shape with fcc packing having an average particle size of 72.32 ± 21.80 nm and 31.82 ± 4.28 nm in case of *Cladosporium oxysporum*

AJP03 and *Lichtheimia ramosa* AJP11, respectively. A series of experiments were conducted to study the effect of concentration of extracellular metabolites and precursor salt, and reaction pH on the particle yield and size. In general, the highest tested concentration of extracellular metabolites (1:5; biomass: water ratio) and 0.5 mM precursor salt concentration favoured the synthesis of well-defined Au NPs with smallest size. Based on the results obtained a strong role of proteins in the synthesis and stabilization of Au NPs has been speculated in *Lichtheimia ramosa* AJP11. The present approach can be extrapolated to develop controlled and up-scalable process for extracellular synthesis of gold nanoparticles for diverse applications.

4.8 References

Alex, S. and Tiwari, A. (2015). Functionalized gold nanoparticles: synthesis, properties and applications-a review. *Journal of Nanoscience and Nanotechnology* 15: 1869-1894.

Badwaik, V. D., Bartonojo, J. J., Evans, J. W., Sahi, S. V., Willis, C. B. and Dakshinamurthy, R. (2011). Single-step biofriendly synthesis of surface modifiable, near-spherical gold nanoparticles for applications in biological detection and catalysis. *Langmuir* 27: 5549-5554.

Balaji, D. S., Basavaraja, S., Deshpande, R., Mahesh, D. B., Prabhakar, B. K. and Venkataraman, A. (2009). Extracellular biosynthesis of functionalized silver nanoparticles by strains of *Cladosporium cladosporioides* fungus. *Colloids and Surfaces B: Biointerfaces* 68: 88-92.

Binupriya, A. R., Sathishkumar, M., Vijayaraghavan, K. and Yun, S. I. (2010). Bioreduction of trivalent aurum to nano-crystalline gold particles by active and inactive cells and cell-free extract of *Aspergillus oryzae* var. *viridis*. *Journal of Hazardous Material* 177: 539-545.

Colombo, M., Mazzucchelli, S., Collico, V., Avvakumova, S., Pandolfi, L., Corsi, F., Porta, F. and Prosperi, D. (2012). Protein-assisted one-pot synthesis and biofunctionalization of spherical gold nanoparticles for selective targeting of cancer cells. *Angewandte Chemie* 124: 9406-9409.

Daniel, M. C. and Astruc, D. (2004). Gold nanoparticles: assembly, supramolecular chemistry, quantum-size-related properties, and applications toward biology, catalysis, and nanotechnology. *Chemical Reviews* 104: 293-346.

Das, S. K., Liang, J., Schmidt, M., Laffir, F. and Marsili, E. (2012). Biomineralization mechanism of gold by Zygomycete Fungi *Rhizopous oryzae*. *ACS Nano* 6: 6165-6173.

Du, L., Xian, L. and Feng, J. X. (2011). Rapid extra-/intracellular biosynthesis of gold nanoparticles by the fungus *Penicillium* sp. *Journal of Nanoparticle Research* 13: 921-930.

Duran, N., Marcato, P. D., Duran, M., Yadav, A., Gade, A. and Rai, M. (2011). Mechanistic aspects in the biogenic synthesis of extracellular metal nanoparticles by peptides, bacteria, fungi, and plants. *Applied Microbiology and Biotechnology* 90: 1609-1624.

Emsley, J., Ed. (2011). Nature's building blocks: an A-Z guide to the elements. Oxford University Press, New York, 2nd Edition, pp. 720.

Faraday, M. (1857). The Bakerian Lecture: Experimental relations of gold (and other metals) to light. *Philosophical Transactions of the Royal Society of London* 147: 145-181.

Gadd, G. M. (2010). Metals, minerals and microbes: geomicrobiology and bioremediation. *Microbiology* 156: 609-643.

Gericke, M. and Pinches, A. (2006). Biological synthesis of metal nanoparticles. *Hydrometallurgy* 83: 132-140.

Graham, T. (1861). Liquid diffusion applied to analysis. *Philosophical Transactions of the Royal Society of London* 151: 183-224.

Grzelczak, M., Perez-Juste, J., Mulvaney, P. and Liz-Marzan, L. M. (2008). Shape control in gold nanoparticle synthesis. *Chemical Society Review* 37: 1783-1791.

Gupta, S. and Bector, S. (2013). Biosynthesis of extracellular and intracellular gold nanoparticles by *Aspergillus fumigatus* and *A. flavus*. *Antonie Van Leeuwenhoek* 103: 1113-1123.

Iwashita, K. (2002). Recent studies of protein secretion by filamentous fungi. *Journal of Bioscience and Bioengineering* 94: 530-535.

Jain, N., Bhargava, A., Majumdar, S., Tarafdar, J. C. and Panwar, J. (2011). Extracellular biosynthesis and characterization of silver nanoparticles using *Aspergillus flavus* NJP08: A mechanism perspective. *Nanoscale* 3: 635-641.

Jiang, J., Oberdörster, G. and Biswas, P. (2009). Characterization of size, surface charge, and agglomeration state of nanoparticle dispersions for toxicological studies. *Journal of Nanoparticle Research* 11: 77-89.

Kitching, M., Ramani, M. and Marsili, E. (2015). Fungal biosynthesis of gold nanoparticles: mechanism and scale up. *Microbial Biotechnology* 8: 904-917.

Korbekandi, H., Ashari, Z., Iravani, S. and Abbasi, S. (2013). Optimization of biological synthesis of silver nanoparticles using *Fusarium oxysporum*. *Iranian Journal of Pharmaceutical Research* 12: 289-298.

Korbekandi, H., Iravani, S. and Abbasi, S. (2009). Production of nanoparticles using organisms. *Critical Reviews in Biotechnology* 29: 279-306.

Laemmli, U. K. (1970). Cleavage of structural proteins during the assembly of the head of bacteriophage T4. *Nature* 227: 680-685.

Lengke, M. F., Ravel, B., Fleet, M. E., Wanger, G., Gordon, R.A. and Southam, G. (2006). Mechanisms of gold bioaccumulation by filamentous cyanobacteria from gold(III)-chloride complex. *Environmental Science and Technology* 40: 6304-6309.

Liu, X., Dai, Q., Austin, L., Coutts, J., Knowles, G., Zou, J., Chen, H. and Huo, Q. (2008). A one-step homogeneous immunoassay for cancer biomarker detection using gold nanoparticle probes coupled with dynamic light scattering. *Journal of American Chemical Society* 130: 2780-2782.

Macdonald, I. D. G. and Smith, W. E. (1996). Orientation of cytochrome c adsorbed on a citrate-reduced silver colloid surface. *Langmuir* 12: 706-713.

McCotter, S. W., Horianopoulos, L. C. and Kronstad, J. W. (2016). Regulation of the fungal secretome. *Current genetics* 62:553-545.

Mukherjee, P., Ahmad, A., Mandal, D., Senapati, S., Sainkar, S. R., Khan, M. I., Ramani, R., Parischa, R., Ajayakumar, P. V., Alam, M., Sastry, M. and Kumar, R. (2001). Bioreduction of AuCl$_4^-$ ions by the fungus, *Verticillium* sp. and surface trapping of the gold nanoparticles formed. *Angewandte Chemie International Edition* 40: 3585-3588.

Mulvaney, P. (1996). Surface plasmon spectroscopy of nanosized metal particles. *Langmuir* 12: 788-800.

Noguez, C. (2007). Surface plasmons on metal nanoparticles: the influence of shape and physical environment. *Journal of Physical Chemistry C* 111: 3806-3819.

Patterson, A. L. (1939). The Scherrer formula for X-ray particle size determination. *Physical Review Letters* 56: 978-982.

Parikh, R. Y., Singh, S., Prasad, B. L. V., Patole, M. S., Sastry, M. and Shouche, Y. S. (2008). Extracellular synthesis of crystalline silver nanoparticles and molecular evidence of silver resistance from *Morganella* sp.: towards understanding biochemical synthesis mechanism. *ChemBioChem* 9: 1415-1422.

Peberdy, J. F. (1994). Protein secretion in filamentous fungi-trying to understand a highly productive black box. *Trends in Biotechnology* 12: 50-57.

Pimprikar, P. S., Joshi, S. S., Kumar, A. R., Zinjarde, S. S. and Kulkarni, S. K. (2009). Influence of biomass and gold salt concentration on nanoparticle synthesis by the tropical marine yeast *Yarrowia lipolytica* NCIM 3589. *Colloids and Surfaces B: Biointerfaces* 74: 309-316.

Polte, J., Erler, R., Thünemann, A. F., Sokolov, S., Ahner, T. T., Rademann, K., Emmerling, F. and Kraehnert, R. (2010). Nucleation and growth of gold nanoparticles studied via *in situ* small angle X-ray scattering at millisecond time resolution. *ACS Nano* 4: 1076-1082.

Prozorov, T., Mallapragada, S. K., Narasimhan, B., Wang, L., Palo, P., Nilsen-Hamilton, M., Williams, T. J., Bazylinski, D. A., Prozorov, R. and Canfield, P. C. (2007). Protein-mediated synthesis of uniform superparamagnetic magnetite nanocrystals. *Advanced Functional Materials* 17: 951-957.

Sambrook, J., Fritsch, E. F. and Maniatis, T. Eds. (1989). *Molecular Cloning: A Laboratory Manual*, Cold Spring Harbour Laboratory Press, New York, pp. 545.

Sanghi, R., Verma, P. and Puri, S. (2011). Enzymatic formation of gold nanoparticles using *Phanerochaete chrysosporium*. *Advances in Chemical Engineering and Science* 1: 154-162.

Sathishkumar, M., Sneha, K., Won, S. W., Cho, C. W., Kim, S. and Yun, Y. S. (2009). *Cinnamon zeylanicum* bark extract and powder mediated green synthesis of nano-crystalline silver particles and its bactericidal activity. *Colloids and Surfaces B: Biointerface* 73: 332-338.

Schöttler, S., Klein, K., Landfester, K. and Mailänder, V. (2016). Protein source and choice of anticoagulant decisively affect nanoparticle protein corona and cellular uptake. *Nanoscale* 8:5526-5536.

Shankar, S. S., Ahmad, A., Pasricha, R. and Sastry, M. (2003). Bioreduction of chloroaurate ions by geranium leaves and its endophytic fungus yields gold nanoparticles of different shapes. *Journal of Material Chemistry* 13: 1822-1826.

Shankar, S. S., Rai, A., Ankamwar, B., Singh, A., Ahmad, A. and Sastry, M. (2004). Biological synthesis of triangular gold nanoprisms. *Nature Materials* 3: 482-488.

Sharma, N. C., Sahi, S. V., Nath, S., Parsons, J. G., Gardea-Torresde, J. L. and Pal, T. (2007). Synthesis of plant-mediated gold nanoparticles and catalytic role of biomatrix-embedded nanomaterials. *Environmental Science and Technology* 41: 5137-5142.

Simpson, R. J. Ed. (2004). *Purifying proteins for proteomics: a laboratory manual*. Cold Spring Harbor Laboratory Press, New York, pp.750.

Song, J. Y., Jang, H. K. and Kim, B. S. (2009). Biological synthesis of gold nanoparticles using *Magnolia kobus* and *Diopyros kaki* leaf extracts. *Process Biochemistry* 44: 1133-1138.

Sun, Y. and Xia, Y. (2002). Shape-controlled synthesis of gold and silver nanoparticles. *Science* 298: 2176-2179.

Thakkar, K. N., Mhatre, S. S. and Parikh, R. Y. (2010). Biological synthesis of metallic nanoparticles. *Nanomedicine: Nanotechnology Biology and Medicine* 6: 257-262.

Tripathy, A., Raichur, A., Chandrasekaran, N., Prathna, T. C. and Mukherjee, A. (2010). Process variables in biomimetic synthesis of silver nanoparticles by aqueous extract of *Azadirachta indica* (Neem) leaves. *Journal of Nanoparticle Research* 12: 237-246.

Vigneshwaran, N., Kathe, A. A., Varadarajan, P., Nachane, R. P. and Balasubramanya, R. (2006). Biomimetics of silver nanoparticles by white rot fungus, *Phaenerochaete chrysosporium. Colloids and Surfaces B: Biointerfaces* 53: 55-59.

Wang, C., Zhang, Y., Seng, H. S. and Ngo, L. L. (2006). Nanoparticle-assisted micropatterning of active proteins on solid substrate. *Biosensors and Bioelectronics* 21: 1638-1643.

Yang, T., Li, Z., Wang, L., Guo, C. and Sun, Y. (2007). Synthesis, characterization, and self-assembly of protein lysozyme monolayer-stabilized gold nanoparticles. *Langmuir* 23: 10533-10538.

Yeh, Y. C., Creran, B. and Rotello, V. M. (2012). Gold nanoparticles: preparation, properties, and applications in bionanotechnology. *Nanoscale* 4: 1871-1880.

Zhang, Y. X., Zheng, J., Gao, G., Kong, Y. F., Zhi, X., Wang, K., Zhang, X. Q. and Cui, D. X. (2011). Biosynthesis of gold nanoparticles using chloroplasts. *International Journal of Nanomedicine* 6: 2899.

Chapter V

Catalytic Applications of Gold Nanoparticles

Preface

This chapter discusses various catalytic applications of gold nanoparticles (Au NPs). Supported and unsupported Au NPs synthesized using fungi (discussed in chapter IV) were used as heterogeneous and homogenous catalyst. The catalytic efficiency of fungal biomass supported Au NPs was tested by catalysing the A^3 coupling reactions to synthesize propargylamine. The as-synthesized nanoparticle-fungal hybrid was also found to catalyse sodium borohydride mediated reduction reaction of 4-nitrophenol and hexacyanoferrate (III). Free and unsupported protein capped Au NPs were employed for reduction of environmentally hazardous organic dyes viz., rhodamine B, bismark brown, methyl orange and methylene blue.

5.1 Introduction

The term catalysis was first coined by Berzelius in the year 1830, who minutely studied the role of catalytic materials in chemical reactions mainly the one with decomposition (Wisniak 2000). It originates from the Greek 'kata'- meaning 'down', and 'lysis'-meaning 'to loosen' or 'to break'. Catalyst significantly increases the probability of interaction between two or more reactant molecules by providing a localised surface upon which the molecules may reside for some time. It speeds up a chemical reaction without being consumed substantially during the reaction. Presence of a catalyst opens up an alternative reaction mechanism involving transitional states wherein a catalyst works by forming chemical bonds with reactants, generating intermediates that react more readily to give products than the reactants would alone. As a result of such bonding, the adsorbed molecules have a lower associated potential energy, allowing for a reaction pathway with reduced activation energy. In this way, catalyst affects the rate of approach to equilibrium of a reaction but not the position of the equilibrium.

The alchemist's trying to produce gold from other cheap metals like lead by using philosopher's stone, is a story we all must have heard. But, no one at that period thought of using gold as catalyst to produce other chemicals. Even though gold was one of the oldest known elements to the mankind, it has recently been investigated as a catalyst. The neglect towards the catalytic potential of gold was due to two prejudices: First, the assumption that gold is so expensive that it is practically unaffordable as a catalyst and second, the inertness of gold, as it has the highest electrode potential (1.48 V) amongst all metals (Corti and Holliday 2004). However, these assumptions were subsequently proved to be wrong. For example, catalyst metals like rhodium and platinum are technically more expensive. Also, as compared to the other more expensive metals, every year thousands of tons of gold is extracted from mines apart from its recycling from various applications which tend to regulate its price. The discovery of gold ions forming complexes under many organic reactions and its ability to behave as a soft Lewis acid has helped to break the viewpoint about gold's inertness. Due to these characteristics, gold is able to activate unsaturated chemical moieties such as alkynes, alkenes, and allenes, thus forming carbon-carbon and carbon-heteroatom bonds under extremely mild conditions (Hashmi and Hutchings 2006). Additionally, the pre-coordination chemistry of gold helps it to activate sp, sp^2, and sp^3 carbon-hydrogen bonds efficiently. These findings opened arsenal of new conversions and reactions featuring gold as an efficient catalyst. "So, while the ancient alchemist's investigated the question of how to make gold, now the question is what to make with gold".

Selecting the right catalyst for a chemical reaction has numerous benefits. One of the key parameters in selecting a catalyst is its size which in fact decides the available surface area for reactions to proceed. In addition, as the size of a catalyst decreases, its physico-chemical properties change significantly such as (a) the number of surface atoms and their mobility increases, (b) surface atoms behaves more independently, (c) a larger fraction of the atoms comes into contact with the reactant and (d) more steps, edge and kink sites are formed on the catalyst particles (Moshfegh 2009). Considering the

advantages provided by catalyst with smaller size and larger surface area, nanoparticles serve as an excellent option as they have high surface area to volume ratio. Using nanoscale form of precious metal like gold as catalyst not only reduces the requirement of precious metal, but also improves the efficiency and selectivity (chemoselectivity, regioselectivity, and/or enantioselectivity) (Zhang 2011).

Catalysis reactions can be divided into two categories, heterogeneous and homogeneous (Astruc et al. 2005). In heterogeneous catalysis, the catalyst is present in a different phase than the reactants. Typically, a heterogeneous catalyst usually consist of either a solid catalyst itself or a matrix on which the actual catalyst is supported, which then offers adsorption sites for incoming reactant molecules. Heterogeneous catalyst offers advantages of recovery from the reaction mixture, recyclability and higher stability. Whereas, in homogeneous catalysis reactions, a catalyst is present in the same phase as the reactants. Typically, a homogenous catalyst is co-dissolved with the reactants into a suitable solvent. Homogeneous catalysts provide advantage of increased activity as all catalytic sites are accessible because the catalyst is usually a dissolved metal complex.

In context to nanocatalyst, shortcomings like agglomeration and subsequent precipitation of synthesized nanoparticle may limit their use as promising catalyst (Bell 2003). Recent improvement in catalyst engineering and nanotechnology have solved these issues by either impregnating/synthesizing the nanoparticles on a suitable matrix or stabilizing them by a suitable capping agent to prevent agglomeration. Therefore, matrix supported Au NPs can be used as heterogeneous catalyst while capped nanoparticles make them an efficient homogenous catalyst.

The present study demonstrates the catalytic efficacy of biosynthesized Au NPs. On-cell synthesized nanoparticles (discussed in chapter IV) which resulted in fabrication of fungal biomass supported Au NPs were utilized as a natural heterogeneous catalyst for the chemical synthesis of propargylamine; reduction of nitrophenols and ferricyanides. Whereas, free and unsupported protein capped Au NPs obtained by exposing gold to fungal extracellular metabolites (detailed in chapter IV) were employed for the remediation of environmentally hazardous organic dyes.

5.2 Materials and methods

5.2.1 Heterogeneous catalysis

The fungal biomass supported Au NPs (discussed in chapter IV) were used as heterogeneous catalyst. Following catalytic reactions were tested.

5.2.1.1 Synthesis of propargylamine

Scheme 1 represents the synthesis of propargylamines by A^3 coupling of a variety of aromatic aldehydes (R = H, CH_3, Cl), secondary amine and alkyne under inert nitrogen atmosphere (Wei and Li 2003). For this purpose, the supported Au NPs were thoroughly

washed with tetrahydrofuran to ensure aqueous free environment and removal of all traces of unbound gold. The excess tetrahydrofuran was removed by keeping the fungal biomass impregnated with Au NPs on an absorbent paper. Briefly, 40 mg of supported Au NPs was added to the reaction mixture composed of substituted benzaldehyde (1 mmol), piperidine (1.1 mmol), phenyl acetylene (1.2 mmol) and 5 mL of tetrahydrofuran in a 50 mL round bottom flask equipped with a reflux condenser. The contents were heated at 80 °C using an oil bath with constant stirring at 1200 rpm. The progress of reaction was monitored by thin layer chromatography (TLC) using silica gel plates till completion. The crude reaction mixture was chromatographed using silica gel (100-200) column and the as-formed propargylamine was eluted using 50% chloroform/hexane to quantify its percent yield.
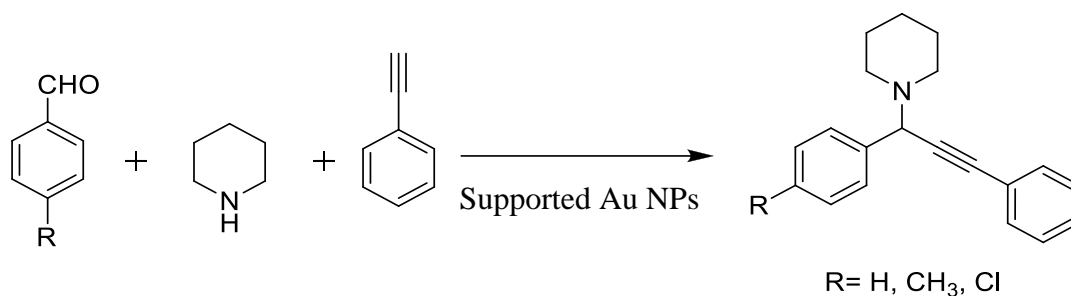
Scheme 1: Supported Au NPs mediated A^3 coupling of aldehyde, secondary amine and alkyne for the synthesis of propargylamine

Structures of all the derivatives (R = H, CH$_3$, Cl) were identified on the basis of their spectral analysis (^{1}H nuclear magnetic resonance (NMR) and matrix assisted laser desorption/ionisation mass spectrometry (MALDI-MS) mass spectral data). ^{1}H NMR and MALDI-MS spectra were recorded on Bruker Avance II 500 MHz and Waters Micromass Q-TOF spectrometer, respectively. In order to explore the possibility to reuse the catalyst for next cycle of reaction, the supported Au NPs were recovered from the earlier reaction mixture by centrifugation (3000 rpm, 5 min) and washed thoroughly with tetrahydrofuran before further use.

5.2.1.2 Reduction of 4-nitrophenol and hexacyanoferrate (III)

The reduction reaction of 4-nitrophenol was performed using NaBH$_4$ in presence of supported Au NPs. The progress of reaction was monitored by recording the absorption spectrum at one minute interval on a V-630 UV-visible spectrophotometer instrument (Jasco Corporation, Japan). Briefly, the reduction reaction of 4-nitrophenol was performed by adding 2885 µl of water, 15 µl of 4-nitrophenol (0.01 M) and 100 µl of aqueous NaBH$_4$ (0.1 M) to a 3 mL quartz cuvette containing 6 mg of supported Au NPs.

Reduction reaction of hexacyanoferrate (III) was performed by adding 2670 µl of water, 30 µl of potassium ferricyanide (8.33 x 10^{-2} M) and 300 µl of aqueous NaBH$_4$ (0.1 M) to a 3 mL quartz cuvette containing 6 mg of supported Au NPs. In order to rule out the possibility of reduction reaction by fungal mycelia, the biomass without Au NPs was used as negative control in both these reactions.

5.2.2 Homogeneous catalysis

The catalytic efficacy of biosynthesized unsupported protein capped Au NPs (discussed in chapter IV) was tested by the reduction of various organic dyes in comparison to the chemically synthesized Au NPs

5.2.2.1 Reduction of organic dyes

Reduction of various organic dyes (rhodamine B, methyl orange, methylene blue and bismark brown) was carried out. Briefly, 0.015 mL of unsupported Au NPs were added to a quartz cuvette containing 1×10^{-4} M aqueous solution of respective dye and 5×10^{-3} M freshly prepared aqueous $NaBH_4$ to achieve a final reaction volume of 3 mL. The reactions were performed at 25 ˚C under dark conditions to eliminate any disturbance due to temperature and light on the reaction kinetics. The dye degradation was monitored spectroscopically by obtaining absorption spectrum at pre-defined time interval using a Jasco V-630 UV-visible spectrophotometer. Controls containing dye without AuNPs and dye without $NaBH_4$ were also run simultaneously along with experimental reactions.

5.2.2.2 Role of nanoparticle capping material on catalytic activity

To examine the effect of nanoparticle capping material on dye degradation, two separate experiments were performed by taking rhodamine B (2.5×10^{-5} M) as a representative dye. In the first experiment, instead of protein capped unsupported Au NPs, chemically synthesized citrate capped nanoparticles (chem Au NPs) were used as catalyst for the reduction of rhodamine B in presence of $NaBH_4$ under similar experimental conditions as described above. In the second experiment, "bare Au NPs" (devoid of any protein capping) were prepared and used as catalyst for the reduction of rhodamine B under similar experimental conditions.

5.2.2.2.1 Preparation of "chem Au NPs"

For the synthesis of chem Au NPs, standard Turkevich method was followed which involve chemical reduction of gold ions by citrate at 100 °C (Frens 1973). Empirically, 2 mL of 1% trisodium citrate dihydrate was added to 20 mL of 1.0 mM $HAuCl_4.3H_2O$ solution vigorously stirred on a thermostat dry bath at 100 °C,. After 15 min, the solution was removed from the stirrer and allowed to cool down.

Change in the colour of reaction mixture was closely monitored visually during the reaction. Characterization of synthesized nanoparticles was performed by recording absorption spectrum of nanoparticle solution using V-630 UV-visible spectrophotometer (Jasco Corporation, Japan) at a resolution of 1 nm with a scan speed of 400 nm min^{-1} in a 1 cm path length quartz cuvette. Sample for transmission electron microscopy (TEM) imaging was prepared by drop coating of the nanoparticle solution on to a carbon coated copper grid. The extra solution was removed by a lint free blotting paper, and the grid was vacuum dried overnight before visualization. TEM micrographs were captured on a H-

7650 transmission electron microscope (Hitachi High-Technologies Corporation, Japan) instrument operated at an accelerating voltage of 80 kV.

5.2.2.2.2 Preparation of "bare Au NPs"

For preparation of bare Au NPs, the protocol was adapted from our previous report (Jain et al. 2015) with minor modifications as detailed below. Autoclaved Milli-Q water filtered through a 100 nm syringe driven PVDF membrane was used for preparing reagents as well as for treatments. All the steps including centrifugation (12000 rpm; 30 min) were carried out at 25 ˚C. In order to remove any unbound protein molecules, the biosynthesized unsupported protein-capped Au NPs solution was centrifuged and the pellet was washed thrice with water keeping intermittent vortexing and centrifugation. Two different strategies were followed for the removal of capping proteins. In the first one, the obtained pellet was suspended in copious volume of 1 % (w/v) sodium dodecyl sulphate (SDS) and boiled for 30 min followed by centrifugation. The resulting pellet was boiled in 1 mL of Tris-Cl (pH 8.0) in water bath for 10 min to eliminate the possibility of SDS binding to the nanoparticles, if any. To ensure the complete removal of SDS, dialysis was carried out against water with four changes followed by centrifugation. In the second strategy, nanoparticle pellet was boiled in copious volume of Milli-Q water for 30 min followed by centrifugation. The obtained bare Au NPs pellet was re-suspended in water and sonicated for 3 h before their use in catalysis reaction. In both the strategies, final volume of bare nanoparticle solution was adjusted accordingly to equalize nanoparticle concentration as discussed in the next section (5.2.2.3). The presence of proteins (amino acids) in the supernatant and their absence in the re-suspended solution of bare AuNPs was confirmed by UV-visible spectroscopy.

5.2.2.3 Equalization of nanoparticle concentration

In order to achieve nearly equal concentration of various nanoparticles (unsupported Au NPs, chem Au NPs and bare Au NPs), the as-synthesized nanoparticle solutions were diluted to obtain optical density value of 1.0 by adding required volume of autoclaved Milli-Q water filtered through a 100 nm syringe driven PVDF membrane filter. UV-visible spectrum of the diluted nanoparticle solutions were recorded to confirm the optical density value.

5.3 Results and discussion

5.3.1 Synthesis of propargylamine
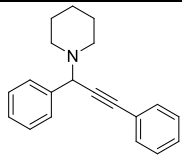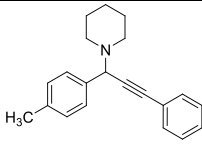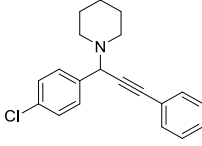
Attempts were made to explore the catalytic ability of as-synthesized supported Au NPs in organometallic reaction like A^3 coupling. The significance of A^3 coupling process can be realized by its potential for the synthesis of diverse heterocyclic frameworks due to its multi-component character (Peshkov et al. 2012). Studies carried out using homogenous

gold catalyst showed that ionic gold in the form of Au (I) and Au (III) oxidation state is predominantly responsible for the synthesis of propargylamines by A^3 coupling reaction (Zhang et al. 2011; Peshkov et al. 2012). As discussed in chapter IV, the fungal biomass supported Au NPs apart from having primarily Au (0) showed the presence of an additional doublet of much weaker intensity towards the higher binding energy value in the X-ray photoelectron spectroscopy measurement. As the doublet peaks were found to be centred around 86.05 eV and 89.45 eV, they were attributed to be the resultant of spin-orbit splitting of Au (I) state. Quantitatively, using integral intensity ratio calculation, it was estimated that the supported nanoparticles consist of ~10 ± 3 % gold in its Au (I) oxidation state. Aguilar et al. (2010) have speculated the strong role of Au (I) in the initiation of propargylamine synthesis reaction catalysed by Au NPs. The reaction of Au (I) species with terminal alkyne leads to formation of alkynyl-Au (I) intermediate which reacts with solvent like dichloromethane giving rise to Au (III) species. The reductive eliminations on alkynyl-gold (III) derivatives directs the synthesis of propargylchloride which further reacts with amine to form the final product and reformation of Au (I) species susceptible to re-start the catalytic cycle.

In order to examine the possibility of using the supported Au NPs which has Au (0) along with considerably less percentage of Au (I), synthesis of propargylamines was attempted (Scheme 1). The TLC analysis confirmed the synthesis of propargylamines. The biomass in absence of gold however failed to synthesise propargylamine as ensured by TLC. Table 5.1 represents the catalytic versatility of the supported Au NPs wherein a variety of aromatic aldehydes (R = H, CH₃, Cl) were coupled with secondary amine and alkynes giving satisfactory yield within 24 h of reaction time.

The remarkable catalytic performance of the supported Au NPs as observed with yields over 80 % of various propargylamine derivatives led us to examine the possibility of its recyclability. As catalytic efficiency is directly proportional to the surface area, significant improvement in the rate of reaction was observed when the catalyst framework was disintegrated by high speed stirring. However, the recovery of supported Au NPs was not affected due to disintegration as equivalent weight of the catalyst was easily recovered by simple centrifugation after completion of reaction. The recovered nanocatalyst was found to be successful in catalysing these reactions repeatedly for two additional cycles. However, a significant increase in the reaction time (first cycle: 48.60%; second cycle: 52.35%) with a decrease in the product yield (first cycle: 26.11%; second cycle: 37.45%) was observed with each subsequent cycle. Problems associated with gradual leaching of active gold species from the supported Au NPs into the solution might have adversely influenced the repeated catalytic activity (Astruc et al. 2005).

Table 5.1 Products synthesized using supported Au NPs in A^3 coupling.

Entry	R	Product	1st Cycle		2nd Cycle		3rd Cycle	
			Time (h)	Yield (%)	Time (h)	Yield (%)	Time (h)	Yield (%)
1	H		24	89	34	67	52	42
2	CH$_3$		24	84	36	61	55	39
3	Cl		24	80	37	59	56	36

The ^{1}H NMR and MALDI-MS data of the synthesized derivatives were found to be in good agreement with those available in the literature and all the products were known compounds. The results for ^{1}H NMR and MALDI-MS are as follows:

Entry 1: ^{1}**H NMR** (500 MHz, CDCl$_3$): δ 7.51–7.32 (m, 1H), 7.35–7.29 (m, 1H), 7.24 (t, J = 7.2 Hz, 2H), 5.22 (s, 1H), 2.71 (t, J = 5.3 Hz, 1H), 2.36 (t, J = 5.3 Hz, 1H), 1.66 (p, J = 5.5 Hz, 2H), 1.60–1.53 (m, 1H). **MALDI-MS**: m/z calcd. 275.1674, found 275. 1855 [M]$^+$.

Entry 2: ^{1}**H NMR** (500 MHz, CDCl$_3$): δ 7.42–7.25 (m, 1H), 7.24–7.14 (m, 1H), 7.02–6.87 (m, 1H), 5.15 (s, 1H), 4.02 – 3.59 (m, 1H), 2.89 – 2.55 (m, 1H), 2.53–2.24 (m, 1H), 1.80–1.57 (m, 1H). **MALDI-MS**: m/z calcd. 289.1830, found 289. 1918 [M]$^+$.

Entry 3: ^{1}**H NMR** (500 MHz, CDCl$_3$): δ 7.51–7.35 (m, 1H), 7.34–7.29 (m, 1H), 7.27–7.21 (m, 1H), 7.16 (d, J = 7.5 Hz, 1H), 5.23 (s, 1H), 2.71 (t, J = 5.3 Hz, 1H), 2.52–2.20 (m, 1H), 1.77–1.20 (m, 1H). **MALDI-MS**: m/z calcd. 309.1284, found 309.1366 [M]$^+$.

5.3.2 Reduction of 4-nitrophenol and hexacyanoferrate (III)

Phenol and phenolic compounds like nitrophenols are one of the major refractory pollutants, released into water bodies from industries manufacturing pesticides, herbicides, insecticides and synthetic dyes. The degradation of these pollutants has received immense attention due to increased environmental concerns (Panigrahi et al. 2007). One of the well-known ways for the remediation of nitrophenol is its reduction by NaBH$_4$. Even though NaBH$_4$ mediated reduction of 4-nitrophenol to 4-aminophenol is a thermodynamically favourable process, a large potential difference between donor and acceptor molecules decreases the feasibility of this reaction (Gangula et al. 2011). This can be overcome by

use of Au NPs which facilitates efficient electron transfer from the donor borohydride ions to acceptor 4-nitrophenol. Empirically, aqueous solution of 4-nitrophenol exhibits a distinct peak at 317 nm in the UV-visible absorption spectrum that shifts to 400 nm in the presence of NaBH$_4$ due to the formation of 4-nitrophenolate ion in the alkaline medium which act as an intermediate in the conversion of 4-nitrophenol to 4-aminophenol (Pradhan et al. 2002).

Based on the above mentioned literature, the reduction reaction of 4-nitrophenol was carried out to test the catalytic efficiency of the supported Au NPs. Figure 5.1 depicts a rapid decrease in the intensity of 4-nitrophenolate absorption peak validating the successful reduction of 4-nitrophenol by the supported Au NPs. It can be clearly observed that more than 90% reduction was completed within 5 min of the reaction with ~58% reduction within the first one minute. The simultaneous development of another peak at ~305 nm (Figure 5.2) confirmed the formation of reduction product (4-aminophenol; 4-AP) in the reaction mixture (Narayanan et al. 2011). It is generally advocated that Au (0) oxidation state in Au NPs acts as active component for the efficient reduction of 4-nitrophenol by NaBH$_4$ (Sharma et al. 2007; Panigrahi et al. 2007).
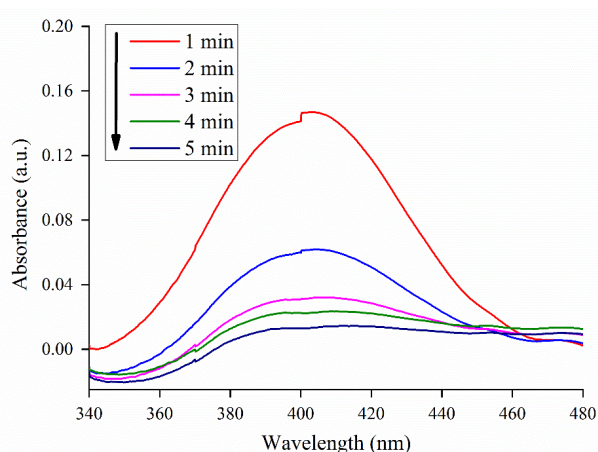
Figure 5.1 Reduction of 4-NP by NaBH$_4$ in presence of supported Au NPs
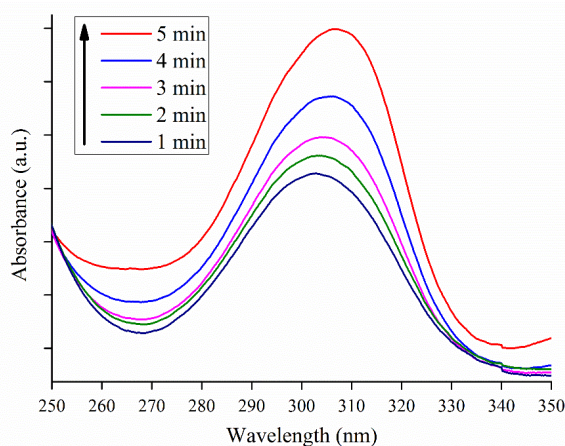
Figure 5.2 Spectra showing gradual formation of 4-AP as a function of time

Another electron transfer reaction which primarily requires Au (0) oxidation state in Au NPs as active catalyst is the reduction of hexacyanoferrate (III) into hexacyanoferrate (II) by NaBH$_4$. In absence of a suitable catalyst, this reaction is found to be very slow (half-life around 5000 s) and follows zero-order kinetics (Herves et al. 2012). However, in presence of a suitable catalyst like Au NPs the same reaction follows first-order kinetics with typically a much shorter half-life of 7.48 s under similar conditions (Carregal-Romero et al. 2009). In the present study, the as-synthesized supported Au NPs initiated the reduction of hexacyanoferrate (III) in the reaction system as observed by a rapid decrease in the intensity of its absorption peak at 420 nm (Figure 5.3). It was observed that more than 78 % of hexacyanoferrate (III) was reduced within 10 min of the reaction with an average reduction rate of 14.28% per min.
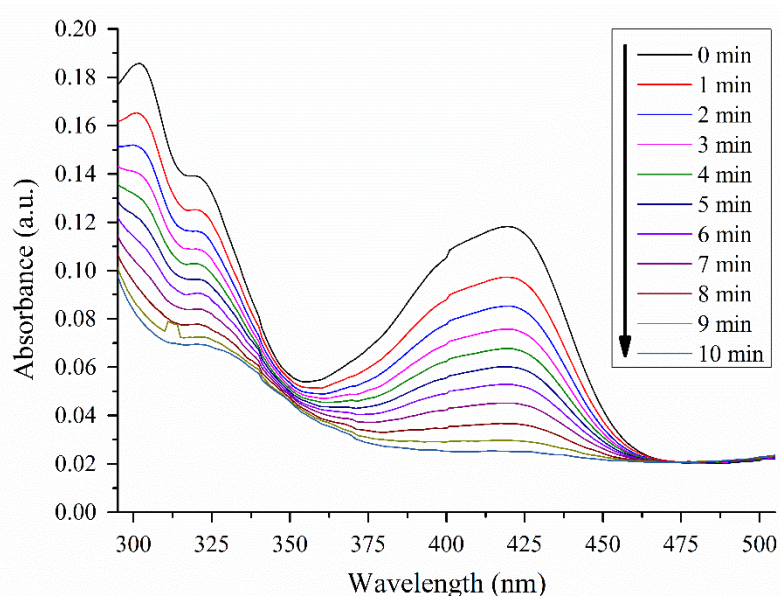
Figure 5.3 Reduction of hexacyanoferrate (III) by NaBH$_4$ in presence of supported Au NPs

Noticeably, in both the above mentioned reactions the colour of supported Au NPs remained unchanged which indicated that the Au NPs were coloidally stable and did not react with any reactants. Negative controls in the both the reactions did not show any reduction reaction.

5.3.3 Reduction of organic dyes

Dyes are important class of synthetic organic compounds which have received particular attention as prominent environmental contaminant owing to their non-biodegradability and carcinogenic effect on humans. Effluent of various industries particularly printing/dyeing units, is often rich in colour and contains residues of organic dyes. It requires proper treatment before being released into the environment. Dyes when disposed in water bodies elevate water pollution, eutrophication, and perturbations of aquatic life (Sharma et al. 2015). There are several ways by which organic dyes cause

problems in water, viz, (i) depending on exposure time and dye concentration, dyes can have acute and/or chronic effects on exposed organisms (ii) although visibility of dyes in rivers depends on their colour, extinction coefficient and on the clarity of the water, they are inherently highly visible. This means that even minor releases of effluents may cause abnormal coloration of surface waters which captures the attention of both the public and the authorities (iii) neglecting the aesthetic problem, the greatest environmental concern with dyes is their absorption and reflection of sunlight entering the water. This interferes with the growth of bacteria to levels sufficient to biologically degrade impurities in the water and start unwanted food chains (Forgacs et al. 2004).

Most of the dyes are difficult to degrade due to their complex structure and synthetic origin. Various methods adopted for dye degradation viz., flocculation, adsorption, membrane filtration, ion exchange, irradiation, ozonation, fenton reduction, photo/electro-chemical destruction and biodegradation have their respective disadvantages, thus leaving a void for an ideal method (Chaudhari et al. 2011). Application of metallic nanoparticles has been most pronounced in photocatalytic degradation of organic dyes which has gained significant research interest in the past decade. However slow reaction rate, requirement of stringent irradiation conditions and high concentration of photocatalyst have limited their applicability (Akpan and Hameed 2009). Alternative practical approach include effective degradation of organic dyes by using strong reducing agent like $NaBH_4$, wherein the rate of reaction can be drastically increased by the incorporation of nanocatalysts (Panacek et al. 2014).

In order to test the efficacy of unsupported Au NPs in catalysing $NaBH_4$ mediated reduction, four common organic dyes viz., rhodamine B, bismark brown, methylene blue and methyl orange were chosen. Rhodamine B is a nitrogen containing cationic dye which is commonly used as colourant in textile industries and as a fluorescent tracer (Kim et al. 2008). Bismarck brown, methyl orange and methylene blue are azo dyes which are certified biological stain, for microscopy, histology and cytology, and also used in textile industries (Ginimuge and Jyothi 2010; Hussein et al. 2010; Robati et al. 2016). All these dyes pose great risk as they undergo natural reductive anaerobic degradation to yield potentially carcinogenic aromatic amines in aquatic ecosystem (Fu et al., 2005). These dyes are reported to cause irritation of skin, eyes and respiratory tract; and may show carcinogenic, reproductive and developmental toxicity in human beings and animals (Lee et al., 2013; Gupta et al. 2015). Owing to their recalcitrant, xenobiotic and harmful nature, these dyes were used as model dyes.

Empirically, the reaction was initiated by the addition of the nanocatalyst (unsupported Au NPs; OD 1.0) to the cuvette containing dye and reducing agent. The characteristic absorption maxima of these dyes (Table 5.2) was used to periodically monitor the course of the reaction which resulted in decolourization of the dye. It was

evident on the basis of UV-visible spectrometric analysis that unsupported Au NPs resulted in complete degradation of all the tested dyes (Figure 5.4).

Table 5.2 Absorption maxima of various organic dyes.

S. No.	Organic Dye	Absorption maxima (λ_{max})
1	Rhodamine B	554 nm
2	Bismarck Brown	457 nm
3	Methyl Orange	464 nm
4	Methylene Blue	609 and 668 nm

Among the various dyes tested, unsupported Au NPs resulted in tremendously fast reduction of rhodamine B within 7 mins. Noticeably more than 50 % of rhodamine B reduced in the initial 3 min. Slightly slower rate of reduction was observed in case of bismark brown and methyl orange, wherein complete degradation took place in 10 min. Methylene blue showed the slowest reduction (19 min) among the tested dyes (Table 5.3). Controls containing dye without nanocatalyst and dye without $NaBH_4$ failed to show any reaction signifying that reduction is solely catalysed by nanoparticles and is not result of a thermal or temporal process.
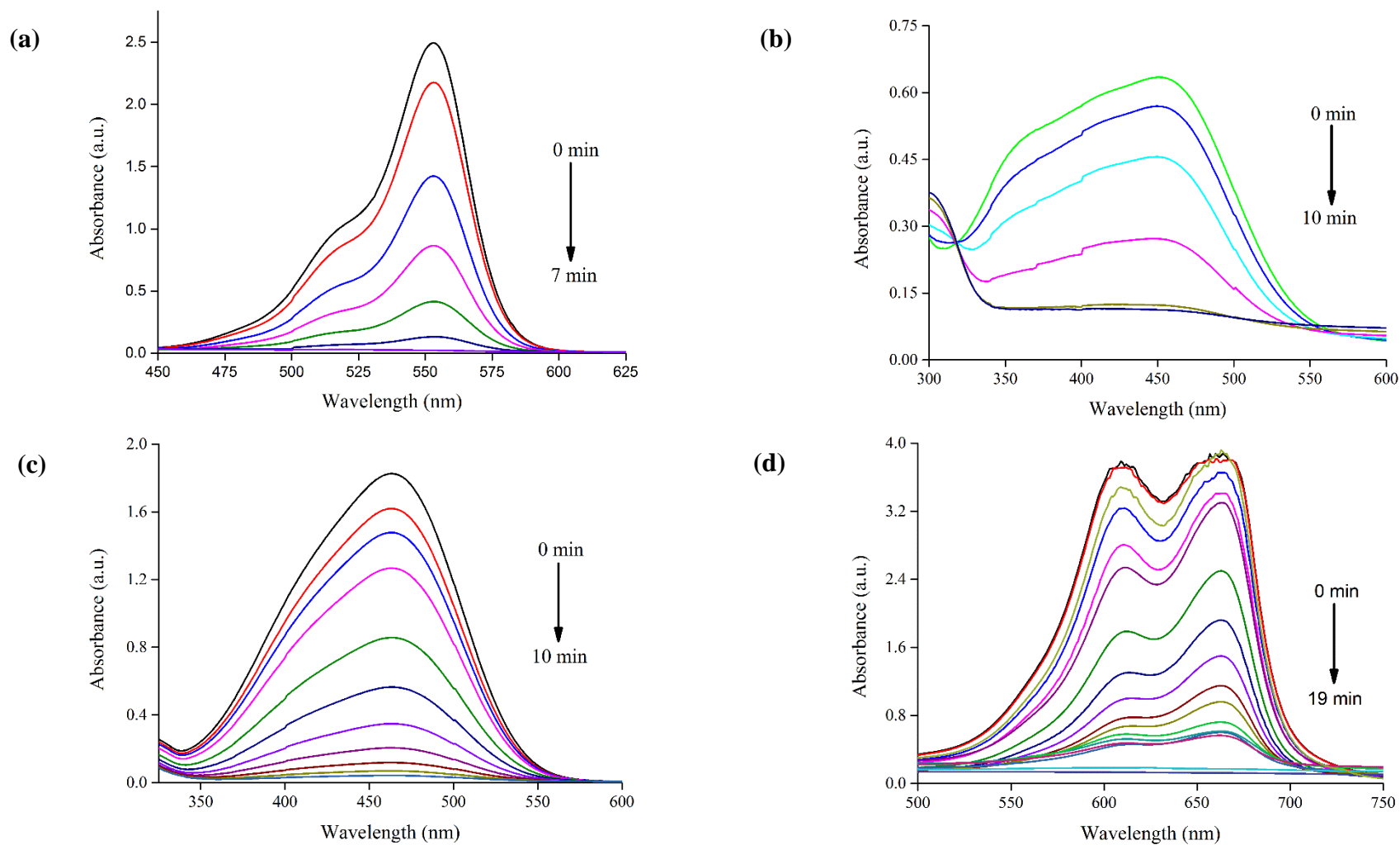
Figure 5.4 UV-visible absorption spectra of unsupported Au NPs catalysed NaBH$_4$ mediated reduction of (a) rhodamine B (recorded at every 1 min) (b) bismark brown (recorded at every 2 min) (c) methyl orange (recorded at every 1 min) (d) methylene blue (recorded at every 1 min)

Table 5.3 Time based percent reduction of various organic dyes catalysed by unsupported Au NPs.

Dyes/percent reduction	25 %	50 %	75 %	100 %
Rhodamine B	< 2 min	< 3 min	< 4 min	< 7 min
Bismarck Brown Y	< 2 min	< 5 min	< 8 min	< 10 min
Methyl Orange	< 3 min	< 4 min	< 6 min	< 10 min
Methylene Blue	< 4 min	< 5 min	< 9 min	< 19 min

Based on the most impressive results, Rhodamine B was selected for further studies to check the effect of capping material on reduction reaction by conducting two separate experiments. In first experiment, instead of protein capped unsupported Au NPs, chemically synthesized citrate capped nanoparticles (chem Au NPs) were used as catalyst for rhodamine B reduction in presence of $NaBH_4$ under the similar experimental conditions.

The chem Au NPs were synthesized using standard Turkevich method (Frens 1973). The reduction of gold ions and subsequent synthesis of nanoparticles was monitored by the progressive change in the colour of reaction mixture from pale yellow to deep red owing to the surface plasmon resonance (SPR) phenomenon of nanogold. (Figure 5.5 inset). The SPR band was further quantitatively measured by recording the UV-visible absorption spectra of the reaction mixture. Emergence of a strong absorption peak at 528 nm reflected the synthesis of gold nanoparticles (Figure 5.5). The size and morphology of nanoparticles were confirmed by TEM imaging (Figure 5.6). TEM micrograph revealed the particles to be quasi spherical with an average particle size of 25.92 ± 4.20 nm.
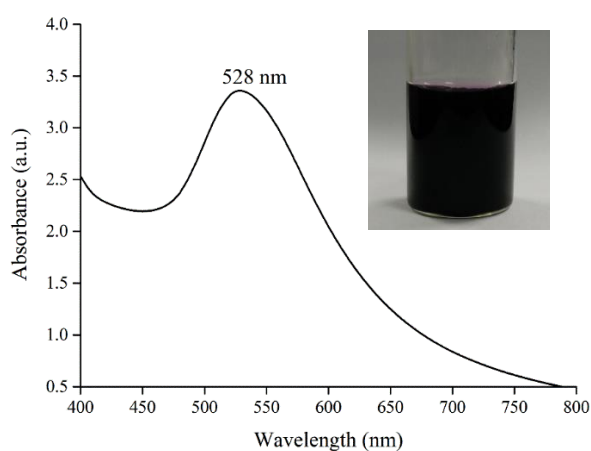
Figure 5.5 UV-visible absorption spectrum of as-synthesized chem Au NPs. Inset shows tube containing nanoparticle solution
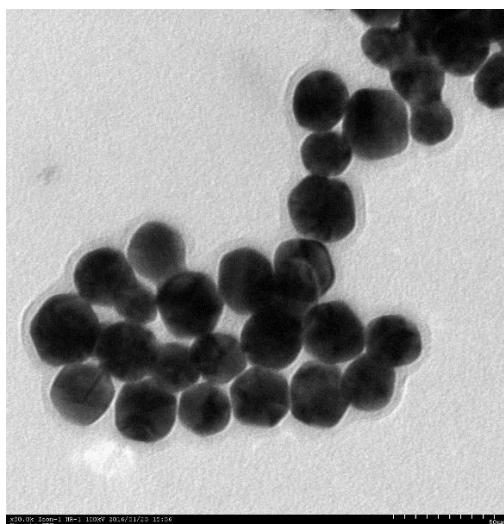
Figure 5.6 TEM micrograph of chem Au NPs (Scale bar equivalent to 50 nm)

The concentration of chem Au NPs was adjusted to equalize with protein capped unsupported Au NPs by diluting the former to obtain optical density value of 1.0 (Figure 5.7). In comparison to protein capped unsupported Au NPs which resulted in tremendously fast reduction of rhodamine B within 7 min, much slower reduction was observed in case of chem Au NPs (Figure 5.8). Although, nearly equal concentration of both type of nanoparticles were used in the reaction system, the reaction rate (k) was found to be dramatically higher for protein capped unsupported Au NPs (12.7×10^{-3} s^{-1}) as compared to chem Au NPs (1.3×10^{-3} s^{-1}) in reducing 2.5×10^{-5} M of rhodamine B (Figure 5.9). These results reflect the significance of protein capping present on the biosynthesized nanoparticles which facilitated the catalytic efficiency of nanoparticles.
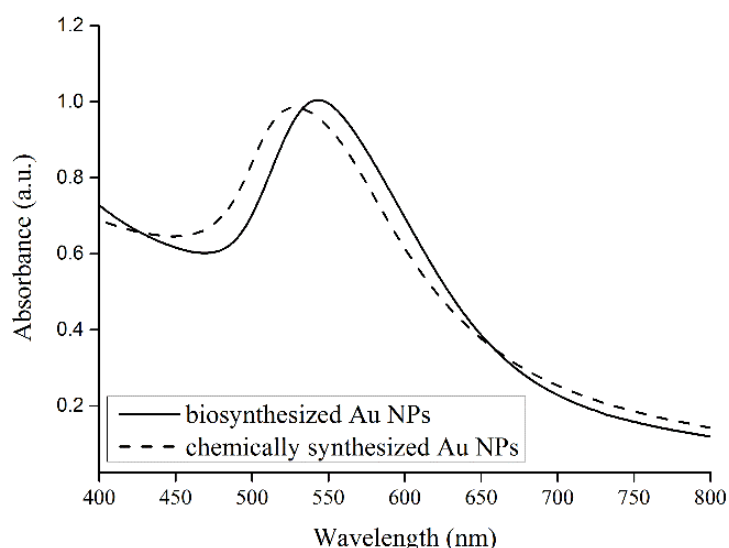
Figure 5.7 UV-visible absorption spectrum of equalized nanoparticle concentration
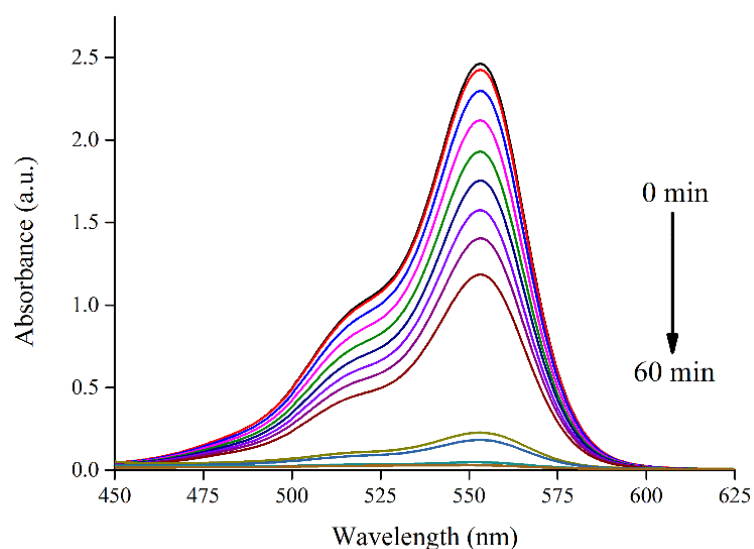
Figure 5.8 UV-visible absorption spectra of NaBH$_4$ mediated reduction of rhodamine B dye catalysed by chem Au NPs (recorded at every 5 min)
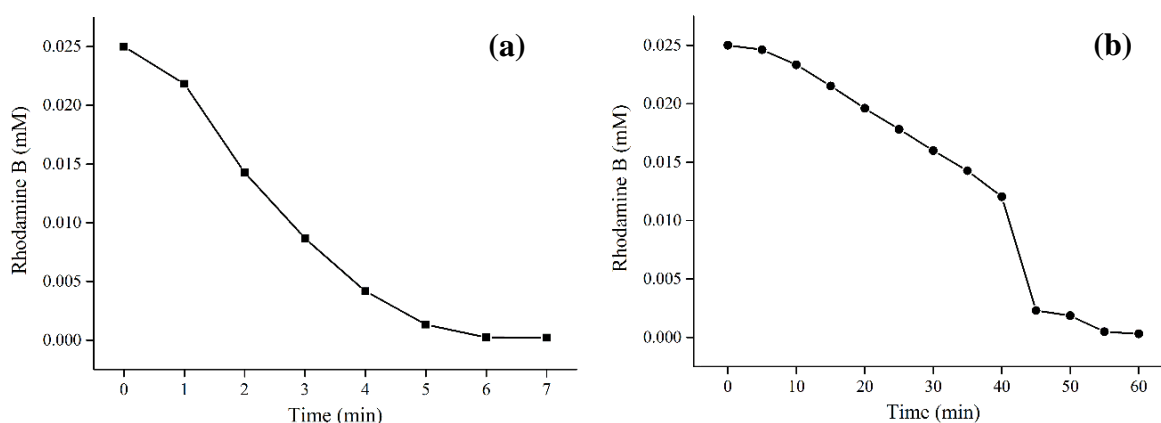
Figure 5.9 Time dependent decrease in the concentration of rhodamine B due to NaBH$_4$ mediated reduction catalysed by (a) biologically synthesized protein capped unsupported Au NPs (b) chemically synthesized citrate capped nanoparticles

Bastus et al. (2014) postulated the reduction mechanism to be a two-step process involving firstly, the accumulation of electrons from borohydride ion onto the surface of nanoparticles and secondly, the diffusion of rhodamine B molecules towards the nanoparticle surface and their subsequent reduction induced by excess surface electrons. As the reaction takes places on the surface of the nanocatalyst, the nature of capping molecules significantly affects the reaction kinetics. In order to prove the role of protein capping in enhanced catalytic efficiency, another experiment was performed. Herein, the reduction of rhodamine B was performed under similar experimental conditions using bare Au NPs which were devoid of any protein cap (prepared using two separate strategies

detailed in section 5.2.2.4). The removal of protein capping was checked by UV-visible spectroscopy (Figure 5.10).
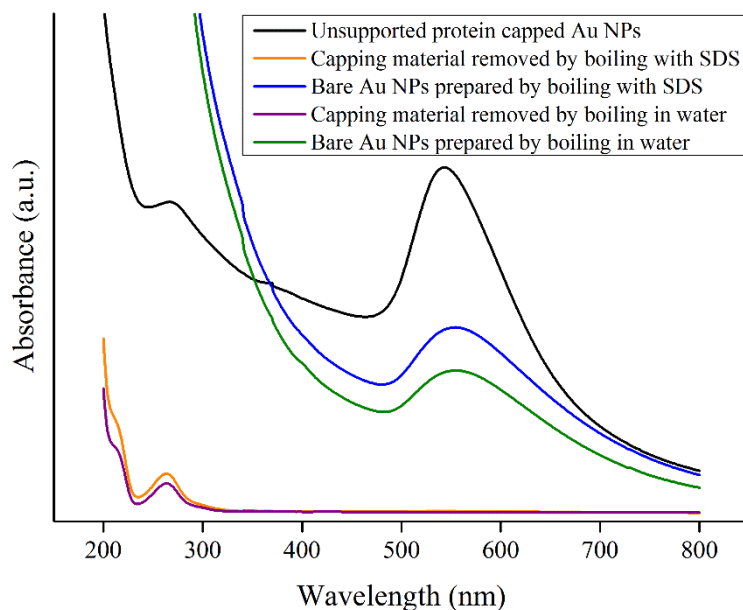
Figure 5.10 UV-visible absorption spectra showing presence of proteins (amino acids) in the supernatant and their absence in the re-suspended nanoparticle solution

The presence of absorption peak at 280 nm corresponding to aromatic amino acids in the supernatant and their absence in the re-suspended solution of Au NPs confirmed the preparation of bare nanoparticles. Noticeably, among the two strategies used for removal of protein cap, boiling with SDS resulted in higher protein content in the supernatant as observed in the UV-visible absorption spectrum in comparison to boiling with water. This may be due to the specific binding of SDS to proteins and their subsequent denaturation (Jain et al. 2015).

Both types of as-prepared bare Au NPs (boiling with and without SDS) resulted in less than 50 % reduction of the dye even after 3 hours of reaction time. Based on the results obtained, it can be hypothesized that proteins present on the surface of unsupported Au NPs may facilitate adsorption of rhodamine B as amino acids containing aromatic rings create hydrophobic spaces which may augment the efficient binding of dye molecules (Baruah et al., 2009; Jain et al., 2014). Further, as compared to other capping molecules like citrate, proteins are more efficient in binding of the dye.

5.4 Conclusions

The present chapter discusses various catalytic application of biosynthesized gold nanoparticles. Chemical synthesis of propargylamine by A^3 coupling was carried out by reacting aromatic aldehydes (R = H, CH_3, Cl), secondary amine and alkyne in presence of fungal biomass supported Au NPs. The nanocatalyst showed remarkable yield and

recyclability. The heterogeneous catalyst was also found to reduce nitrophenol and ferricyanide in presence of NaBH$_4$ within 5 and 10 min, respectively. Free and unsupported protein capped Au NPs (homogeneous catalyst) successfully reduced the environmentally hazardous organic dyes (rhodamine B, bismarck brown, methyl orange and methylene blue) in presence of NaBH$_4$ as reducing agent. The fastest catalytic efficiency was observed in case of rhodamine B wherein, the complete decolourization was achieved within 7 min of reaction time. The significance of protein capping on the catalytic efficiency was confirmed by catalysing the same reaction using chemically synthesized Au NPs and bare Au NPs (devoid of protein capping).

5.5 References

Aguilar, D., Contel, M. and Urriolabeitia, E. P. (2010). Mechanistic insights into the one-pot synthesis of propargylamines from terminal alkynes and amines in chlorinated solvents catalyzed by gold compounds and nanoparticles. *Chemistry-A European Journal* 16: 9287-9296.

Akpan, U. G. and Hameed, B. H. (2009). Parameters affecting the photocatalytic degradation of dyes using TiO$_2$-based photocatalysts: a review. *Journal of Hazardous Materials* 170: 520-529.

Astruc, D., Lu, F. and Aranzaes, J. R. (2005). Nanoparticles as recyclable catalysts: the frontier between homogeneous and heterogeneous catalysis. *Angewandte Chemie International Edition* 44: 7852-7872.

Baruah, S., Sinha, S. S., Ghosh, B., Pal, S. K., Raychaudhuri, A. K. and Dutta, J. (2009). Photoreactivity of ZnO nanoparticles in visible light: Effect of surface states on electron transfer reaction. *Journal of Applied Physics* 105: 074308.

Bastus, N. G., Merkoçi, F., Piella, J. and Puntes, V. (2014). Synthesis of highly monodisperse citrate-stabilized silver nanoparticles of up to 200 nm: kinetic control and catalytic properties. *Chemistry of Materials* 26: 2836-2846.

Bell, A. T. (2003). The impact of nanoscience on heterogeneous catalysis. *Science* 299: 1688-1691.

Carregal-Romero, S., Perez-Juste, J., Herves, P., Liz-Marzan, L. M. and Mulvaney, P. (2009). Colloidal gold-catalyzed reduction of ferrocyanate (III) by borohydride ions: a model system for redox catalysis. *Langmuir* 26: 1271-1277.

Chaudhari, K., Bhatt, V., Bhargava, A. and Seshadri, S. (2011). Combinational system for the treatment of textile waste water: a future perspective. *Asian Journal of Water, Environment and Pollution* 8: 127-136.

Corti, C. W. and Holliday, R. J. (2004). Commercial aspects of gold applications: from materials science to chemical science. *Gold Bulletin* 37: 20-26.

Forgacs, E., Cserhati, T. and Oros, G. (2004). Removal of synthetic dyes from wastewaters: a review. *Environment International* 30: 953-971.

Frens, G. (1973). Controlled nucleation for the regulation of the particle size in monodisperse gold suspensions. *Nature* 241: 20-22.

Fu, H., Pan, C., Yao, W. and Zhu, Y. (2005). Visible-light-induced degradation of rhodamine B by nanosized Bi_2WO_6. *The Journal of Physical Chemistry B* 109: 22432-22439.

Gangula, A., Podila, R., Karanam, L., Janardhana, C. and Rao, A. M. (2011). Catalytic reduction of 4-nitrophenol using biogenic gold and silver nanoparticles derived from Breynia rhamnoides. *Langmuir* 27: 15268-15274.

Ginimuge, P. R. and Jyothi, S. D. (2010). Methylene blue: revisited. *Journal of Anaesthesiology, Clinical Pharmacology* 26: 517-525.

Gupta, V. K., Khamparia, S., Tyagi, I., Jaspal, D. and Malviya, A. (2015). Decolorization of mixture of dyes: A critical review. *Global Journal of Environmental Science and Management* 1: 71-94.

Hashmi, A. S. K. and Hutchings, G. J. (2006). Gold catalysis. *Angewandte Chemie International Edition* 45: 7896-7936.

Herves, P., Perez-Lorenzo, M., Liz-Marzan, L. M., Dzubiella, J., Lu, Y. and Ballauff, M. (2012). Catalysis by metallic nanoparticles in aqueous solution: model reactions. *Chemical Society Reviews* 41: 5577-5587.

Hussein, F. H., Halbus, A. F., Hassan, H. A. and Hussein, W. A. (2010). Photocatalytic degradation of bismarck brown G using irradiated ZnO in aqueous solutions. *Journal of Chemistry* 7: 540-544.

Jain, N., Bhargava, A. and Panwar, J. (2014). Enhanced photocatalytic degradation of methylene blue using biologically synthesized "protein-capped" ZnO nanoparticles. *Chemical Engineering Journal* 243: 549-555.

Jain, N., Bhargava, A., Rathi, M., Dilip, R. V. and Panwar, J. (2015). Removal of protein capping enhances the antibacterial efficiency of biosynthesized silver nanoparticles. *PloS one* 10: e0134337.

Kim, H. N., Lee, M. H., Kim, H. J., Kim, J. S. and Yoon, J. (2008). A new trend in rhodamine-based chemosensors: application of spirolactam ring-opening to sensing ions. *Chemical Society Reviews* 37: 1465-1472.

Lee, H., Park, S. H., Park, Y. K., Kim, B. H., Kim, S. J. and Jung, S. C. (2013). Rapid destruction of the rhodamine B using TiO$_2$ photocatalyst in the liquid phase plasma. *Chemistry Central Journal* 7: 156-159.

Moshfegh, A. Z. (2009). Nanoparticle catalysts. *Journal of Physics D* 42: 233001.

Narayanan, K. B. and Sakthivel, N. (2011). Synthesis and characterization of nano-gold composite using *Cylindrocladium floridanum* and its heterogeneous catalysis in the degradation of 4-nitrophenol. *Journal of Hazardous Materials* 189: 519-525.

Panacek, A., Prucek, R., Hrbac, J., Nevecna, T. J., Steffkova, J., Zboril, R. and Kvitek, L. (2014). Polyacrylate-assisted size control of silver nanoparticles and their catalytic activity. *Chemistry of Materials* 26: 1332-1339.

Panigrahi, S., Basu, S., Praharaj, S., Pande, S., Jana, S., Pal, A. and Pal, T. (2007). Synthesis and size-selective catalysis by supported gold nanoparticles: study on heterogeneous and homogeneous catalytic process. *The Journal of Physical Chemistry C* 111: 4596-4605.

Peshkov, V. A., Pereshivko, O. P. and Van der Eycken, E. V. (2012). A walk around the A[3]-coupling. *Chemical Society Reviews* 41: 3790-3807.

Pradhan, N., Pal, A. and Pal, T. (2002). Silver nanoparticle catalyzed reduction of aromatic nitro compounds. *Colloids and Surfaces A* 196: 247-257.

Robati, D., Mirza, B., Rajabi, M., Moradi, O., Tyagi, I., Agarwal, S. and Gupta, V. K. (2016). Removal of hazardous dyes-BR 12 and methyl orange using graphene oxide as an adsorbent from aqueous phase. *Chemical Engineering Journal* 284: 687-697.

Sharma, N. C., Sahi, S. V., Nath, S., Parsons, J. G., Gardea-Torresde, J. L. and Pal, T. (2007). Synthesis of plant-mediated gold nanoparticles and catalytic role of biomatrix-embedded nanomaterials. *Environmental Science & Technology* 41: 5137-5142.

Sharma, K., Singh, G., Kumar, M. and Bhalla, V. (2015). Silver nanoparticles: facile synthesis and their catalytic application for the degradation of dyes. *RSC Advances* 5: 25781-25788.

Wei, C. and Li, C. J. (2003). A highly efficient three-component coupling of aldehyde, alkyne, and amines via CH activation catalyzed by gold in water. *Journal of the American Chemical Society* 125: 9584-9585.

Wisniak, J. (2000). Jons Jacob Berzelius a guide to the perplexed chemist. *The Chemical Educator* 5: 343-350.

Zhang, Y., Cui, X., Shi, F. and Deng, Y. (2011). Nano-gold catalysis in fine chemical synthesis. *Chemical Reviews* 112: 2467-2505.

Chapter VI

Assessment of Iron Oxide Nanoparticle as Potential Nano-fertilizer

Preface

This chapter discusses assessment of iron oxide nanoparticle as a source of micronutrient in plants. For this, a systematic comparison of various iron forms viz., ionic, bulk and nanoparticles (chemically and biologically synthesised) at different metal concentrations were made using wheat and spinach as test plants. Seed germination and a sub pilot experimental field study was conducted using foliar spray approach to determine the effect of various iron forms on wheat plant growth and grain yield. In addition, pot study was carried out to determine the effect of foliar spray of various iron forms on plant growth and biomass production of spinach. The results advocated the possibility of using biologically synthesized iron oxide nanoparticles as potential nano-fertilizers.

6.1 Introduction

The growth and development of plants essentially require sunlight, water, CO_2 and many chemical elements. Among these components, chemical elements can be acquired by plants either from the soil through roots or through the aerial parts (Loneragan 1968). Chemical elements acquired by the plants from the soil are called as mineral nutrients. Out of the 16 essential elements required for the growth of plants, those required in trace amount are called as micronutrients while those required in large quantities are called macronutrients (Macy 1936). The mineral nutrients present in the soil must be in bioavailable form, so that the plant can take them up easily (Clarkson and Hanson 1980). Availability of nutrients to the plant depends on their amount, nature and association with other nutrients in the solid phase. The concentration of minerals in soil varies and depends on a number of factors like soil moisture, soil depth, pH, cation exchange capacity, redox potential, quantity of organic matter, microbial activity, etc. (Clarkson 1985). After getting absorbed by plant roots, mineral nutrients are distributed to various plant parts and utilized in various metabolic functions.

The Iron Paradox:

Iron is one of the most essential micronutrients required for the growth of plants (Guerinot and Yi 1994). Apart from involvement in electron transport chain, it plays a significant role in the biochemical processes of photosynthesis, N_2 fixation and cellular respiration. Iron is also involved in the production and detoxification of oxygen radicals, oxygen transport, numerous reduction and monooxygenase reactions. As heme, it acts as cofactor for enzymes like catalases, peroxidases and cytochrome oxidases. Plants absorb iron in its more soluble form (Fe^{+2}) as compared to less soluble form (Fe^{+3}) which constitutes most of the iron in the earth crust. At higher soil pH, iron tends to precipitate into insoluble hydroxides and converts into less available Fe^{+3}, resulting in iron deficiency (Romheld 1987).

Iron deficiency affects overall plant growth and yield. Under iron deficient conditions, leaves develop a characteristic greenish-yellow colour referred to ''chlorosis'' resultant of decreased synthesis of the light-harvesting pigment "chlorophyll". This leads to marked reduction in the photosynthetic rates (Briat and Lobreaux 1997). Deficiency does not directly indicate insufficient iron supply as mostly it is the outcome of various conditions that may affect iron availability for plants. Interestingly, plants have evolved various mechanisms to counteract iron limitation up to an extent (Guerinot and Yi 1994). One of the well-known mechanisms involves "chelation" by siderophores which are mainly produced by rhizospheric bacteria and fungi. Siderophores bind to iron making it available for plant uptake. Another mechanism involves the function of reductases in reducing Fe^{+3} at the plasma membrane of cells on root surfaces to Fe^{+2} for efficient uptake. Roots can also release protons as root extrude, lowering the rhizosphere pH to increase iron solubility.

In spite of these mechanisms, severe iron deficiencies do occur in plants and can be managed for short term by applying iron in terms of fertilizers (Table 6.1; Rawashdeh and Florin 2015). Among the various types of iron supplements used to tackle deficiency, foliar application of ferrous sulphate (0.5-2.0 % or 5,000-20,000 mg L^{-1}) 2-3 times at weekly intervals during the crop life cycle has shown satisfactory results. As compared to other modes of supplementing iron, foliar spray shows quick response often in few days and minimizes formation of oxy-hydrides due to limited soil contact (Boynton 1954).

Table 6.1 Various types of commonly used iron fertilizers.

S. No.	Source	Formula	Percent Iron	Mode of application
1	Chelates	FeDTPA	10	Soil/Foliar
2	Chelates	FeEDTA	9-12	Soil/Foliar
3	Chelates	FeEDDHA	6	Soil/Foliar
4	Salt	$(NH_4)_2Fe(SO_4)_2.6H_2O$	14	Foliar
5	Salt	$FeSO_4.7H_2O$	20	Foliar

Sadly, excess iron is also toxic to plants (Foy et al. 1978). For example, while iron deficiency results in chlorosis, its excess leads to generation of oxidative stress. Under normal conditions the damaging action of ROS (inevitable by-products of biological oxidations) is counteracted by presence of anti-oxidant enzymes like catalase, peroxidase etc. Excess iron accelerates the production of ROS by an iron dependent reaction causing severe damage on membranes, proteins and DNA. Although iron ranks fourth among elements in terms of abundance, cellular iron concentrations are tightly regulated by sophisticated mechanisms that control its acquisition, distribution and utilization (Hell and Stephan 2003). In soil, iron is found mostly as a constituent of insoluble oxy-hydroxide "FeOOH" produced majorly by the weathering of rock. As these oxides are not very soluble at neutral pH, iron rather remains less available for plant uptake. Additionally, plants increase abundance of oxygen derived from photosynthesis in its rhizospheric region which further makes iron unavailable due to the formation of highly insoluble ferric oxides. In India, iron deficiency in agricultural soil has emerged as one of the major constraints to crop productivity. As per the report of National Food Security Mission, Ministry of Agriculture, Govt. of India, iron deficiency majorly occurred in calcareous and alkaline soils of Rajasthan, Haryana, Punjab, Uttar Pradesh, Gujarat, Bihar, Andhra Pradesh, Maharashtra, Karnataka and Tamil Nadu (www.nfsm.gov.in/Micronutrient.pdf).

In contrast to low lands and regions with higher annual rainfall, wherein acidic pH of the soil results in iron toxicity due to large concentrations of readily available reduced

Fe^{2+} form in the soil, arid regions have soil with relatively higher pH facing iron unavailability as a major problem (Lindsay and Schwab 1982). Another problem which leads to iron limitation in arid soil is the binding of iron with phosphates, carbonates, calcium, magnesium and hydroxide ions. Repeated use of fertilizers containing nitrate enhances the release of hydroxide ions, causing further increase in pH at the root zone and limits efficient iron uptake (Mortvedt 1986). Thus, innovative technologies are need of the hour that can carefully manage the nutrient delivery to plants and provide required amount of minerals such as iron.

Application of conventional fertilizers enhances the plant productivity. However, the available nutrients present in the bulk chemical forms in these fertilizers are not fully accessible to plants. A survey on crop plants reported that they could typically use less than half of the chemical fertilizers applied to them (Matson et al. 1998). The remaining minerals may leach down and/or become fixed in the soil contributing to pollution. These problems have initiated repeated use of fertilizers which adversely affects the inherent nutrient balance of the soil (Singh and Ryan 2015). Excess use of chemical fertilizers cause an irreparable damage to the soil structure, mineral cycles, soil microbial flora, plants and even more to the food chains across ecosystems leading to heritable mutations in future generations of consumers (Mortvedt 1994; Geisseler and Scow 2014). Thus, the use of large scale application of chemical fertilizers to increase plant productivity is not a suitable option for long run as these are double edged swords, which on one side increases plant productivity but on the other side disturbs the soil mineral balance and decreases soil fertility (Tisdale and Nelson 1966). Hence, it is very important to optimize the use of chemical fertilization to minimize damage to soil mineral balance and avoid mineral toxicity to plants (Shaviv and Mikkelsen 1993). Accordingly, it can be favorable that other methods of fertilization shall also be tested and developed while keeping the soil structure in good shape and the environment clean (Miransari 2011).

Nanotechnology has provided the feasibility of exploring nanoscale or nanostructured materials as smart carrier or controlled-release vectors for a variety of applications (Figure 6.1). They have been utilized in agriculture for developing systems involving controlled release and targeted delivery of agrochemicals, improved pest and disease resistance, efficient fertilizer delivery vehicles etc. (De Rosa et al. 2010). Presently, the major focus of the scientific community is towards establishing the hazardous outcome of incredibly high concentration of nanomaterial exposure to living systems. Nevertheless, nanotechnology also holds the key for modernizing current agricultural practices in pursuit of higher agricultural productivity (Ditta 2012). Nanoparticles, one of the building blocks of nanotechnology, bear unique structural and functional properties which makes them highly useful. Little interest is paid towards exploring the use of metal and metal oxide nanoparticles as direct source of nutrient for plant growth and development.
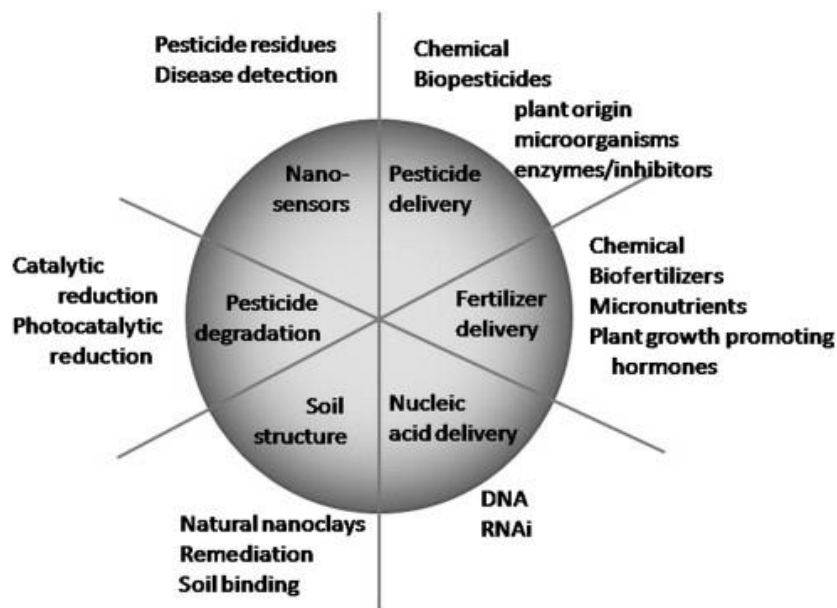
Figure 6.1 Applications of nanotechnology in plant sciences and agriculture (Adapted with permission from Ghormade et al. 2011)

For higher agricultural productivity, nanotechnology based research should focus on enhancing the bioavailability of minerals (macro and micronutrients) supplemented in the form of fertilizers to the field. In this prospect, metal and metal oxide nanoparticles can dynamically fulfill plant mineral requirement by preserving the beneficial effects of conventional fertilizers while preventing any long term damage to soil structure. In these scenarios, nanotoxicity is a major concern which limits the use of so called "nano-fertilizers" (Stampoulis 2009). Before actively utilizing the potential of nano-fertilizers for agronomic productivity, it is pre-requisite to conduct studies that alleviate the fear of associated nanotoxicity (Ma et al. 2010). As plants need only trivial amounts of micronutrients to maintain normal physiological activities, it is obvious that extremely high concentrations of any micronutrient would cause phytotoxicity (Naderi and Danesh-Shahraki 2013). Therefore, it is very important to identify the optimum concentration of nano-fertilizers that a plant requires.

The aim of the present study was to assess the agricultural potential of iron oxide nanoparticles (IONPs) to replace the conventional iron fertilizers. In this regard, different concentrations of IONPs in the form of maghemite and magnetite (chemically and biologically synthesized) were used as supplements to check their effects on the growth and biomass production of wheat and spinach plants. The effect of IONPs on these plants was compared with conventional fertilizer "ferrous sulphate" and bulk iron oxide (maghemite).

6.2 Materials and methods

6.2.1 Materials

The iron compounds used as treatments were procured from Sigma-Aldrich (Sigma-Aldrich USA). All others chemicals were purchased from Merck Chemicals (Merck KGaA, Germany) unless otherwise stated. Wheat seeds were procured from Seed Bank, Central Research Farm, Central Arid Zone Research Institute (CAZRI), Jodhpur, India. Spinach seeds were purchased from the local market of Jaipur, Rajasthan, India. Seeds were stored in a dry and dark place at ambient conditions until use. The *in vivo* studies were carried out at an artificial farming facility of Birla Institute of Technology and Science (BITS) Pilani (28° 21' 50.05", 75° 35' 9.26"). The plants were grown in *rabi* season with average air temperature of 16.0 °C during the span of study. The soil parameters were analysed at CAZRI Jodhpur. All the spectrophotometric analysis were conducted on a V-630 UV-visible spectrophotometer (Jasco Corporation, Japan) using a 1 cm path length quartz cuvette.

6.2.2 Preparation and characterization of various treatment solutions

Stock solutions of all the treatments viz., ferrous sulphate ($FeSO_4$), bulk maghemite (Fe_2O_3), maghemite nanoparticles ($N-Fe_2O_3$) and magnetite nanoparticle ($N-Fe_3O_4$) were prepared in autoclaved Milli-Q water with a final iron concentration of 1000 mg L^{-1}. Further concentrations were obtained by carefully diluting the stock solution. An indigenous protocol as described in section 3.2.2 was used for obtaining biosynthesized magnetite nanoparticle ($B-Fe_3O_4$). After synthesis, the $B-Fe_3O_4$ solution was filtered through a 0.22 µm nylon-66 membrane (HiMedia Laboratories, India) using a vacuum filter (in order to remove fungal spores) and stored at 4°C until use. During the study, $B-Fe_3O_4$ was used as-synthesized without any modification.

An aliquot from various stock solutions was sonicated for 60 mins and later used for the determination of pH, mean particle diameter by Transmission Electron Microscopy (TEM), average hydrodynamic diameter and electrophoretic mobility by dynamic light scattering and zeta-potential measurement respectively. For all these analysis, stock solution was diluted 10 times except for $B-Fe_3O_4$ wherein no dilution was made.

Samples for TEM imaging were prepared on a carbon-coated TEM grid by drop coating of the treatment solutions after 30 min sonication in a water bath sonicator (Thermo Scientific, USA). After few minutes, extra solution was removed using lint free blotting paper and the grids were kept in a vacuum desiccator prior to measurement. TEM measurement were carried out on a JEM-2100 instrument (JEOL, Japan) operated at an accelerating voltage of 80 kV.

Average hydrodynamic diameter and electrophoretic mobility was determined by dynamic light scattering and zeta-potential measurement, respectively recorded using Zetasizer Nanoseries compact scattering spectrometer (Malvern Instruments Ltd, UK).

Measurements were recorded at 25 °C ± 1 °C, in triplicates; and each measurement was the average of 20-30 data sets acquired for 10 seconds each. Hydrodynamic diameter and polydispersity index (PDI) were calculated using the Zetasizer software.

6.2.3 Studies on wheat (*Triticum aestivum* L.)

6.2.3.1 *In vitro* studies

In vitro seed germination assay was performed to evaluate the effect of various iron salts on germination of wheat seeds at a final iron concentration of 0 (control), 100, 250, 500, 750 and 1000 mg L^{-1}. B-Fe$_3$O$_4$ was used at its as-synthesized concentration of 100 mg L^{-1}. Healthy wheat seeds were surface sterilized by treating with 0.1% mercuric (II) chloride for 1 min. The sterilizing agent were drained off aseptically, and the seeds were washed 10-12 times with sterilized Milli-Q water to remove all traces of the chemical. For seed germination assay, ten surface sterilized seeds were uniformly placed on a steamed filter paper in a sterilized petri dish (90 mm × 10 mm) and supplemented with 3 mL of test solution. Controls were supplemented with similar amount of sterilized Milli-Q water. The petri dishes were sealed with parafilm, placed in a dark chamber for 4 days and further shifted to a plant growth chamber maintained at 16/8 h (light/dark) period at 28 °C. The solution was equally replenished as required with the appropriate solution. The experiment was performed in triplicate.

Germination was recorded when the root lengths were greater than 5 mm, as per the standard guidelines (US-EPA 1996). In order to assess the effect of different treatments, analysis was carried out on the basis of change in the shoot and root length after 7 days which were measured using standard procedure. Measurements of the five seeds per petridish was recorded neglecting the outliers.

6.2.3.2 *In vivo* studies

6.2.3.2.1 Soil

The *in vivo* study was carried out at an artificial farm facility of BITS Pilani. Native farm soil without any modification was used for the experiment. Representative soil sample was collected from the site and analysed for determination of various physico-chemical parameters viz., soil pH, electrical conductivity (EC), organic carbon, available nitrogen, inorganic phosphorus (Olsen's P), exchangeable nutrients (potassium, calcium, magnesium) and DTPA extractable nutrients (copper, manganese, zinc and iron).

6.2.3.2.2 Plant growth conditions

The seeds of wheat cv. DBW 16, were sown at 6-7 cm depth and cultivated under artificial irrigation during Rabi season of year 2012. The experiment was conducted using randomized design with three replicates. The plot size of each replicate was 5 × 4 ft. The seeds were sown in starting of first week of November 2012 in 5 rows with equal distance. After the germination of seeds (usually within 7-10 days) and development of small

plantlets, each row was thinned to keep healthy and almost equal sized plantlets at an equal distance. No fertilizer was applied during the entire crop period. The irrigation was applied at its optimum (usually every 20th day) by a small overhead sprinkler irrigation system till the milk stage of the plant growth.

Solution of various salts at a final iron concentration of 0 (control), 100, 250, 500, 750 and 1000 mg L^{-1} (B-Fe_3O_4 was used at its as-synthesized iron concentration of 100 mg L^{-1}) were sprayed on leaves with a hand held sprayer after four weeks of seed sowing. Based on the plant vigour, three consecutive foliar sprays (1st spray @ 2 L ha^{-1}, 2nd spray @ 4 L ha^{-1} and 3rd spray @ 6 L ha^{-1}) were performed at an interval of 2 weeks till the end of vegetative stage before the onset of flowering. Prior to spraying, the treatment stock solutions were sonicated for 60 mins followed by appropriate dilution to obtain desired concentration of iron. For efficient entry of nanoparticles inside plants, the spraying was carried after sunset preventing evaporation of aqueous phase. Maximum exposure to leaves was ensured during spraying with minimal spillage of solution on the soil. The plants were harvested at maturity and various parameters were determined.

6.2.3.2.3 Post-harvest analysis

Above ground plant biomass were uprooted from each plot and carefully piled separately in labelled bunches. It was duly ensured that the plants do not suffer any damage during transport to the analysis site. Three representative plants (without cobs) were selected from each bunch, packed in pre-weighed labelled paper envelope and oven dried at 65 ˚C for 3 days to determine the above ground plant biomass (plant dry weight). The dried plant samples were also used for quantification of iron by atomic absorption spectroscopy (AAS). Like-wise three representative cobs from each plot were also subjected to dry weight analysis following similar procedure as described above. Grain yield was quantified by collecting and recording the test weight of 100 grains from the dried cobs. Grain samples obtained were also analysed for the estimation of iron by AAS (data not shown). All the post-harvest analysis were done in triplicate.

6.2.3.2.4 Atomic absorption spectroscopy

AAS analysis was carried out to estimate the concentration of iron. Oven dried plants were properly crushed using an electric grinder and 0.2 gram of representative sample was used for di-acid digestion. The content of iron was determined in the grains as well. For this, 1.0 g of wheat seeds were carefully weighed and subsequently digested.

For digestion, 3 mL of conc. HNO_3 was added to the sample and incubated in a sealed glass container for 6 h at room temperature for pre-digestion. 2 mL of conc. HNO_3 and 1 mL of $HClO_4$ were added to the pre-digested sample and heated at 200 °C for 2 h on a hot plate. Later, the temperature was raised to 300 °C and heated till the white fumes started generating and a clear solution was left (less than 1 mL). To solubilize the sample, 5 mL of was Milli-Q water was added following by heating at 150 °C for 10 mins. Finally,

the content within the container was washed repeatedly with Milli-Q water and the washing was filtered through 0.22 µm nylon-66 membrane and collected in a volumetric flask to achieve final volume of 50 mL. The filtered solution was subjected to AAS analysis on an AA-7000 series spectrophotometer (Shimadzu Corporation, Japan).

6.2.4 Study on spinach (*Spinacia oleracea* L.)

6.2.4.1 Soil

The soil (3 parts sand and 1 part clay) used in present study was obtained from nearby organic farm. The soil was sieved using a 2 mm sieve, sundried and stored at 4°C until use in sealed plastic bags. Representative soil sample was used to determine various physico-chemical parameters as discussed in section 6.2.3.2.1.

6.2.4.2 Plant growth conditions

A pot scale experiment was conducted at the artificial farming facility of BITS Pilani during Rabi season 2012. Plastic pots (11 cm height and 12.5 cm/9.5 cm top/bottom diameter) were filled with 2.5 kg (dry weight) soil up to 9.5 cm of pot height. Eight surface sterilized spinach seeds (Dhanuka Agritech Limited, New Delhi) were sown in each pot and the pots were laid out under complete randomized design. The pots were irrigated at regular intervals using equal volume of distilled water. No fertilizer was applied during the study period. After 2 week of seed sowing, seedlings were ranked according to their size and thinned to four plants per pot keeping almost equal plant height per pot.

For this study, the final iron concentration of all the treatments were kept at 100 and 1000 mg L^{-1} in order to get contrasting yet easily comparable results except B-Fe_3O_4 which was sprayed at its as-synthesized concentration (100 mg L^{-1}). Foliar spray of various treatment solutions was carried out on leaves after 3 weeks of seed germination. Five consecutive foliar sprays were carried out at intervals of 5 days. Prior to spraying, the treatment stock solutions were sonicated for 60 mins followed by appropriate dilution to obtain desired concentration of iron. On the basis of leaf surface area, initial two sprays were performed using 5 ml of solution after which the volume was subsequently increased to 10 mL. Plants were sprayed with distilled water as control. Three replicate pots were maintained for each treatment. At 45 day post seed germination, one representative pot with average plant height and health among the three replicate pots was chosen for photography. Harvesting was performed 5 days after the last foliar spray.

6.2.4.3 Post-harvest analysis

Plants including their roots were carefully removed by loosening the soil and were washed thoroughly under running distilled water to remove adhered dirt and all traces of salts present on the leaf surface. Rhizospheric soil for each treatment was collected carefully. The plants from each pot within a treatment were divided to carry out various analysis viz., Scanning Electron Microscopy (SEM), quantification of iron by AAS,

measurement of growth (shoot length, root length and fresh weight) and various physiological and biochemical parameters. All post-harvest analysis were done in triplicate neglecting the outliers.

6.2.4.3.1 Scanning Electron Microscopy

In order to determine the presence of nanoparticles on the sprayed leaves, SEM was performed in combination with energy dispersive spectroscopy (EDS) for metal localization before washing. The leaves were partially freeze dried immediately after harvesting to retain their native structure. The leaves were then fixed overnight at 4°C in 2.5 % (v/v) glutaraldehyde in 0.1 M sodium phosphate buffer, pH 7.2. The specimen was then rinsed with the same buffer, dehydrated in a series of 30–100 % ethanol and dried in a desiccator under vacuum. An automatic E-1010 sputter coater instrument (Hitachi High-Technologies Corporation, Japan) was used for coating the samples with gold particles. The samples were examined using Hitachi S-3400N Scanning Electron microscope with Noran^{TM} System SIX (Thermo Fisher Scientific, USA) EDS attachment.

6.2.4.3.2 Atomic Absorption Spectroscopy

Three plants from each replicate were packed in pre-weighed paper envelopes and oven dried at 65 °C for 3 days. The dried plants were properly crushed using an electric grinder and 0.1 g of crushed material was digested for AAS analysis using di-acid digestion method as discussed in section 6.2.3.2.4.

6.2.4.3.3 Biochemical analysis

All assays were done at 25°C following standard protocols with slight modifications. Fresh leaves were used for the estimation of various physiological parameters (viz., total chlorophyll, sugar, protein) and biochemical/enzymatic parameters (viz., catalase, peroxidase, superoxide dismutase). Acid/alkaline phosphatase and dehydrogenase activity were measured in the rhizospheric soil samples of each treatment. Three replicates were maintained throughout and measurement for each replicate was performed thrice. Enzyme activity estimated from the crude enzyme extract was expressed per gram fresh weight of plant material.

Total sugar content: Total sugar in plant sample was determined by the standard method of Yemm and Willis (1954) with minor modifications. Briefly, plant leaves (0.2 g) were homogenized in 10 mL of 80 % (v/v) ethanol and the homogenate was filtered through Whatman No. 42 filter paper (Whatman Inc., USA). The volume of recovered filtrate was made up to 25 mL using the same solvent. Using a water bath, 0.2 mL of the obtained alcoholic extract was evaporated to dryness in a test tube followed by addition of 1.0 mL of Milli-Q water and 4.0 mL of freshly prepared 0.2 % Anthrone reagent. Tubes were incubated for 8-10 mins in a boiling water bath. The absorbance of the solution was read at 620 nm against blank (1.0 mL 80 % ethanol and 4.0 mL 0.2 % Anthrone reagent). The

total sugar content was calculated by plotting the obtained absorbance against a standard curve of glucose and expressed as mg of carbohydrate/ g fresh weight of leaf.

Total protein content: Total protein content of plants was determined by Bradford (1976) method with slight modification. Plant leaves (0.2 g) were homogenized in 10 mL of phosphate buffer (0.05 M, pH 8) and the homogenate was filtered through Whatman No. 42 filter paper. The volume of recovered filtrate was made up to 10 mL using the same buffer. The assay mixture consisting of 100 µL of filtrate and 3.0 mL of Coomassie Brilliant Blue solution was incubated for 15 mins. The absorbance was read at 595 nm against blank containing buffer instead of filtrate.

Total chlorophyll content: Total chlorophyll content was estimated using the standard method of Arnon (1949). Fresh leaves (0.2 g) were thoroughly grounded in 10 mL of 80 % (v/v) chilled acetone to extract chlorophyll in the solvent. The solution was filtered through Whatman No. 42 filter paper and volume of recovered filtrate was made up to 50 mL with the same solvent. The absorbance of the solution was read at 663 nm (chlorophyll a) and 645 nm (chlorophyll b) against black containing 80 % acetone.

Catalase activity: Catalase (EC 1.11.1.6) activity was determined by the method of Beers and Sizer (1952) with slight modifications. Plant leaves (0.2 g) were homogenized in 10 mL of chilled phosphate buffer (0.1 M, pH 6.4) and the homogenate was filtered through Whatman No. 42 filter paper. The volume of recovered crude enzyme extract was made up to 10 mL using the same buffer. The assay mixture consisted of 2.5 mL of 0.1 M phosphate buffer, 0.1 mL of 1% hydrogen peroxide (H_2O_2) and 0.2 mL of crude enzyme extract. The change in the absorbance at 230 nm was recorded for 180 s at every 30 s interval. Cuvette containing phosphate buffer and crude enzyme extract was used as blank. The enzyme activity was expressed as change of 0.5 a.u. in absorbance/min/g fresh weight of leaf.

Peroxidase activity: Peroxidase (EC 1.11.1.6) activity was determined by method of Egley et al. (1983) with slight modification. Plant leaves (0.2 g) were homogenized in 10 mL of chilled phosphate buffer (0.1 M, pH 6.8) and the homogenate was filtered through Whatman No. 42 filter paper. The volume of recovered crude enzyme extract was made up to 10 mL using the same buffer. The assay mixture consisted of 2.0 mL of 0.1 M phosphate buffer, 1.0 mL of 0.001 M pyrogallol, 1.0 mL of 0.005 M H_2O_2 and 1.0 mL of crude enzyme extract. The assay mixture was incubated for 5 mins at 25 °C for reaction to proceed after which 1.0 mL of 2.5 N H_2SO_4 was added to stop the reaction. The absorbance was read at 420 nm against black containing water instead of enzyme extract.

Superoxide dismutase activity: The assay for superoxide dismutase (EC 1.15.1.1) was carried out by following the method of Beyer and Fridovich (1987) which is based on the reduction of nitroblue tetrazolium to water insoluble blue formazan. Fresh leaves (0.2 g) were homogenized in 10 mL of chilled phosphate buffer (0.1 M, pH 6.8) and the

homogenate was filtered through Whatman No. 42 filter paper. The volume of recovered crude enzyme extract was made up to 10 mL using the same buffer. The assay mixture consisted of 50 µL of enzyme extract, 1.232 mL of 50 mM phosphate buffer, 150 µL of 0.75 mM NBT, 38 µL of 55 mM Methionine and 30 µL of 0.1 mM riboflavin. Blank was prepared using 50 µL of distilled water instead of enzyme extract. The assay mixture was incubated at room temperature under two fluorescent tubes (6000 lux) for 10 minutes to allow the development of purple colour formazan which was then measured at 560 nm against the blank. Units of the enzyme activity were expressed as the amount of enzyme required to inhibit the reduction of NBT by 50 % and the enzyme activity was expressed as units per mg of protein.

Acid phosphatase activity: Acid phosphatase (EC 3.1.3.2) activity was determined in the rhizospheric soil adopting the standard procedure of Tabatabai and Bremner (1969) with minor modifications. Rhizospheric soil from respective replicates was pooled and homogenized and 1.0 g of soil sample was taken in a screw cap test tube (15 mL capacity). 4.0 mL of 0.25 % p-nitrophenyl phosphate freshly prepared in 0.2 M sodium acetate buffer (pH 5.4) was added and the tubes were incubated for 1 h at 35 °C followed by addition of 1 mL 0.5 M calcium chloride solution and 4.0 mL 0.5 M sodium hydroxide solution. The contents were filtered through Whatman No. 42 filter paper and the absorbance of filtrate was measured at 420 nm against blank containing 1 mL Milli-Q water instead of soil sample. The activity was expressed in terms of enzyme unit (EU). One enzyme unit corresponds to the amount of enzyme required for producing 1.0×10^{-5} µmol of p-nitro phenol per second per gram of soil at pH 5.4 and 35 °C.

Alkaline phosphatase activity: Alkaline phosphatase (EC 3.1.3.1) activity was determined in the rhizospheric soil adopting the standard procedure of Tabatabai and Bremner (1969) with minor modifications. Rhizospheric soil from respective replicates was pooled and homogenized and 1.0 g of soil sample was taken in a screw cap test tube (15 mL capacity). 4.0 mL of 0.25 % p-nitrophenyl phosphate freshly prepared in 0.05 M borax buffer (pH 9.4) was added and the tubes were incubated for 1 h at 35 °C followed by addition of 1 mL 0.5 M calcium chloride solution and 4.0 mL 0.5 M sodium hydroxide solution. The contents were filtered through Whatman No. 42 filter paper and the absorbance of filtrate was measured at 420 nm against blank containing 1 mL Milli-Q water instead of soil sample. The activity was expressed in terms of enzyme unit (EU). One enzyme unit corresponds to the amount of enzyme required for producing 1.0×10^{-5} µmol of p-nitro phenol per second per gram of soil at pH 9.4 and 35 °C.

Dehydrogenase activity: Dehydrogenase (EC 1.1.1) activity, a measure of microbial activity was assayed by the method of Tabatabai (1982). Rhizospheric soil from respective replicates was pooled in screw cap test tube to obtain 1.0 g of sample. To this, 0.5 mL of 1.0 % glucose and 0.2 mL of 3 % 2,3,5-triphenyl tetrazolium chloride was added. The tubes were incubated for 24 h at 37 °C. After incubation, 10 mL of methanol was added,

the contents were mixed well and placed in refrigerator for 3 h. After incubation, the content was filtered through Whatman No. 42 filter paper and the triphenyl formazon formed was measured at 485 nm wavelength against blank containing Milli-Q water instead of soil sample.

6.2.5 Data Analysis

The data obtained were analysed using the Prism$^{®}$ software (Version 6.0; GraphPad Software Inc., USA). The effect of various treatments were statistically analysed using one way ANOVA (Stoline 1981). When ANOVA revealed significant differences among treatments, post-hoc test was conducted using Dunnett's method, which demonstrates pair wise differences between each treatment and the control (Dunnett 1955). Symbol *ns* used in the graphs shall be interpreted as statistically non-significant at P > 0.05. All data points represent the mean of independent measurements. Uncertainties were represented as standard deviations.

6.3 Results and discussion

The effect of nanoparticles on growth and development of plants is an important aspect as it holds great economic prospects. In this regard, the uptake, translocation and ultimate fate (response) of nanoparticles within plants must be carefully assessed before deciding their applicability as "nano-fertilizers". Factors that govern the behaviour of nanoparticles in plant system include their size, chemical composition, functionalization, stability along with the type of plant species (Nair et al. 2010). Keeping these facts in mind, the present study was aimed to investigate the effect of foliar spray of various iron forms viz., ionic, bulk and nanoparticle on two different plant species i.e. wheat (*Triticum aestivum* L.) and spinach (*Spinacia oleracea* L.). Foliar application has been reported to be an effective way to deliver nutrients to plants (Hong et al. 2014; Raliya et al. 2015).

The treatments were judiciously selected in order to study the effect of iron in its:

(a) Different physical states i.e. nano (IONPs), bulk (Fe_2O_3) and ionic ($FeSO_4$)

(b) Different chemical states i.e. maghemite (N-Fe_2O_3) and magnetite (N-Fe_3O_4) nanoparticles

(c) Presence of biological capping material on IONPs i.e. uncapped N-Fe_3O_4 and protein capped B-Fe_3O_4

(d) Various concentrations on plant growth and development

6.3.1 Characterization of various treatment solutions

The unexpected physico-chemical properties and complexity of nanoparticles in different environments makes the nanoparticle characterization a necessary pre-requisite step (Luyts et al. 2013). The stability of nanoparticles (i.e. their dispersion and persistence)

is considered as a key parameter for the risk assessment of their biological activity and toxicity (Oberdörster et al. 2005). The physico-chemical properties viz., pH, average particle size calculated from TEM measurement, hydrodynamic diameter and zeta potential of all the treatment solutions were determined (Table 6.2).

Table 6.2 Characteristics of various iron salt solutions used for study.

	$FeSO_4$	Fe_2O_3	$N-Fe_2O_3$	$N-Fe_3O_4$	$B-Fe_3O_4$
pH	2.0	5.0	5.0	5.0	6.5
Mean particle size (nm)*	N.A.	183.75	28.11	36.56	82.25
Average hydrodynamic size (nm)	1.56	2134	276.43	313.78	240
Zeta potential (mV)	(-) 0.18	(-) 2.06	2.92	1.77	(-) 32.22

*As per TEM measurement

As depicted in table, aqueous $FeSO_4$ solution showed highly acidic pH (< 3.0) which is due to the release of enormous number of H^+ ions resultant of the salt dissociation in water as compared to the little production of free OH^- ions (Cameron 1930). This makes $FeSO_4$ solution too acidic. As compared to $FeSO_4$, mild acidic pH (5.5-6.5) was recorded for the iron oxide compounds. Similar observation for pH of iron oxides was reported elsewhere in the literature (Baalousha 2008). Near to neutral pH was recorded for as-synthesized $B-Fe_3O_4$ solution. The near neutral pH of $B-Fe_3O_4$ solution is due to the presence of protein cap on the nanoparticles, which provide a buffered environment (Pfeiffer et al. 2014).

The average particle size calculated from the TEM micrographs revealed maximum size in case of Fe_2O_3 (bulk material) which was found in the order of micrometer as compared to other treatments (Figure 6.2). Evidently, $FeSO_4$ showed no distinct microarchitecture in TEM analysis (data not shown) while $N-Fe_2O_3$ and $N-Fe_3O_4$ were found to be of almost similar size, less than 50 nm. Interestingly, among both the commercially available nanoparticles, more polydispersity was observed in $N-Fe_2O_3$. In case of $B-Fe_3O_4$, average size of 82.25 ± 5 nm was obtained with least aggregation in comparison to other treatment solutions.

The hydrodynamic diameter, a value that refers to particle diffusion within a fluid determined by DLS for all the treatments was in accordance with the pattern of average particle size as observed through TEM measurements except in case of $B-Fe_3O_4$. However, the hydrodynamic diameter was found to be much larger than the actual particle size determined by TEM measurements (Gittings and Saville 1998). The stability of various iron salt solutions was evaluated by the measurement of zeta potential. Particles with zeta potentials more positive than +30 mV or more negative than -30 mV are normally

considered stable as large negative or positive zeta potential indicates higher tendency of particles to repel each other rather than aggregate (Clogston and Patri 2011). Even though all the treatments showed instability at their innate pH, B-Fe$_3$O$_4$ was found to be stable with zeta potential of (-) 32.22 mV (Lynch and Dawson 2008). As speculated, the presence of protein coat in B-Fe$_3$O$_4$ provided increased nanoparticle stability by preventing aggregation (Chithrani and Chan 2007).
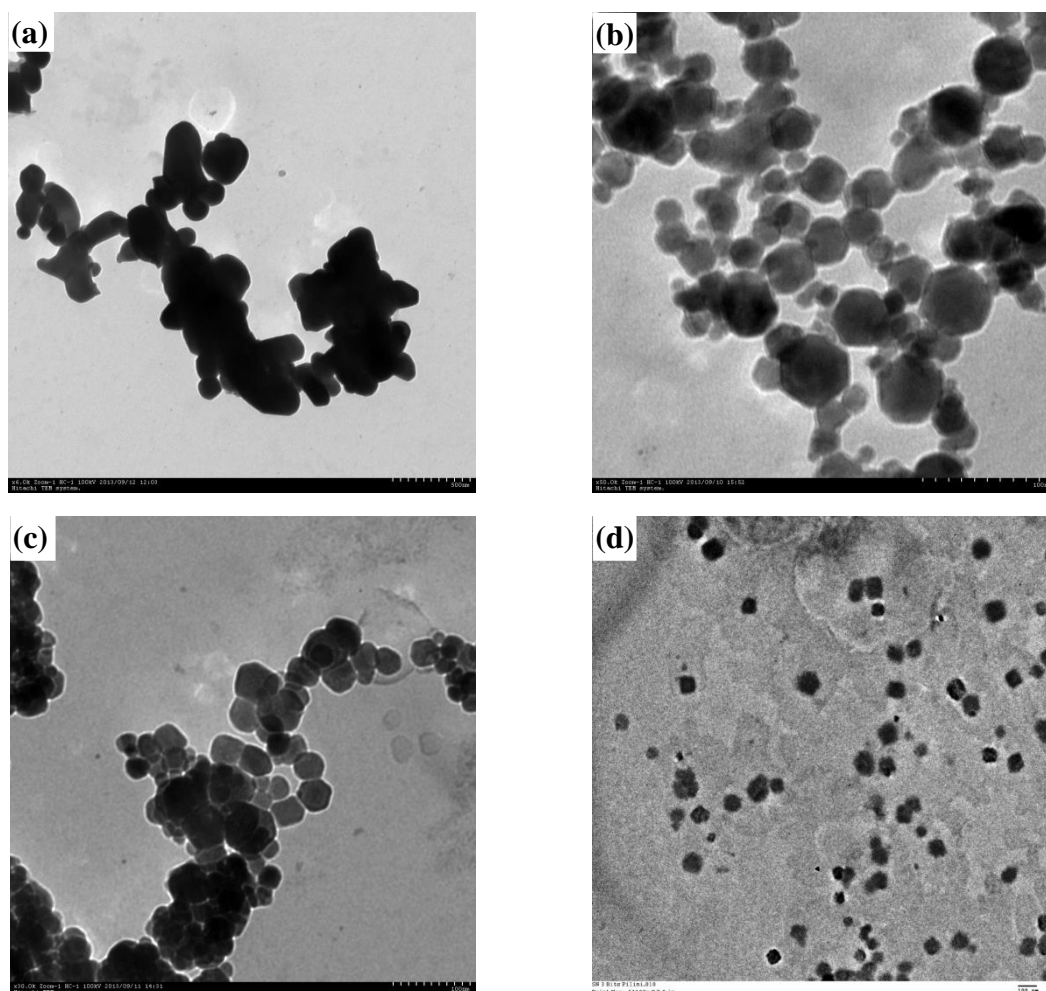
Figure 6.2 TEM micrograph of various treatments (a) Fe$_2$O$_3$ (scale bar equivalent to 500 nm); (b) N-Fe$_2$O$_3$; (c) N-Fe$_3$O$_4$ and (d) B-Fe$_3$O$_4$ (scale bar equivalent to 100 nm)

6.3.2 Studies on wheat

Wheat (*Triticum aestivum* L.) has been recommended as a test plant for studying the response of chemicals and evaluation of their phytotoxicity, if any, as per guideline No. 208 and 227 (Terrestrial Plant Test) drafted by the Organization for Economic Co-operation and Development (OECD 2006 a,b). Additionally, wheat is an extensively grown cereal crop especially in Indian subcontinent with an estimated worldwide production of 714 million tons in the year 2014 (FAOSTAT 2015). Such a mass cultivation of wheat makes it persuasive to study its response alongside nanoparticles as a micronutrient source.

6.3.2.1 Seed germination assay

Seed germination assay is widely employed as a first step to assess the phytotoxicity of any chemical substance and the results can be extrapolated to decide future exposure scenarios and hazards (US-EPA 1996). The effect of various iron salts (as discussed earlier) were tested in a broad range of iron concentration viz., 0, 100, 250, 500, 750, 1000 mg L^{-1}. However, for B-Fe_3O_4, the effect was studied at its as-synthesized iron concentration of 100 mg L^{-1}. The response was assessed by measuring the percent seed germination and seedling growth (root and shoot length) in the treatment populations as compared to control.

In general, apart from $FeSO_4$, all the other treatments showed no sign of dose-dependent phytotoxicity in terms of percent seed germination (Table 6.3). The results clearly indicated that the exposure of $FeSO_4$ at higher concentrations was more toxic than other tested iron salts (both nanoparticle and bulk forms). At iron concentration of 1000 mg L^{-1} nearly 50 % seeds exposed to $FeSO_4$ failed to germinate. Wei et al. (2013) reported similar trend during their study on effect of $FeSO_4$ fortification in brown rice. A decrease of 35 % in seed germination was observed by them at a salt exposure of 1000 mg L^{-1}. The toxic effect of $FeSO_4$ on soybean has also been reported in literature as well, wherein enhanced level of ferritin, an antioxidant that protects cells against toxic iron concentration, was observed when seeds were treated with $FeSO_4$ (Zielińska-Dawidziak and Siger 2012). In all other treatments, almost all seeds (> 90 %) germinated successfully. This observation can be attributed to the presence of thick seed coat in wheat, which has selective permeability making it a very effective barrier for salt particles to enter (Mabille et al. 2001). The importance of seed coat has been studied by creating mutants with compromised permeability facilitating the entry of chemicals inside the seeds which are naturally impermeable (Di Salvatore et al. 2008). In our study, both bulk and nanoparticle iron oxide form were unable to cause any significant effect on seed germination because they may be unable to traverse the mature seed coat.

Table 6.3 Percent seed germination of wheat seeds in response to various iron salts.

Concentration (mg L^{-1})	$FeSO_4$	Fe_2O_3	N-Fe_2O_3	N-Fe_3O_4	B-Fe_3O_4
0	> 90 %				
100	< 90 %				> 90 %
250	< 90 %				NA
500	< 70 %	> 90 %	> 90 %	> 90 %	NA
750	< 70 %				NA
1000	< 50 %				NA

To develop a deep understanding of possible phytotoxicity of iron salts on wheat, their effect on seedling growth were investigated. A juvenile seedling can be divided into two parts viz. shoot and root. Roots play an important role in uptake of water and nutrients from the environment and thus can be considered as highly prone to the exposure of any chemical. On the other hand, nanoparticle toxicity on hypocotyl relies on uptake and translocation of the chemical. Thus, we separately investigated the effect of various concentrations of selected iron salts on the growth of root and shoot (hypocotyl) parts (Figure 6.3).

(g) (h) (i)
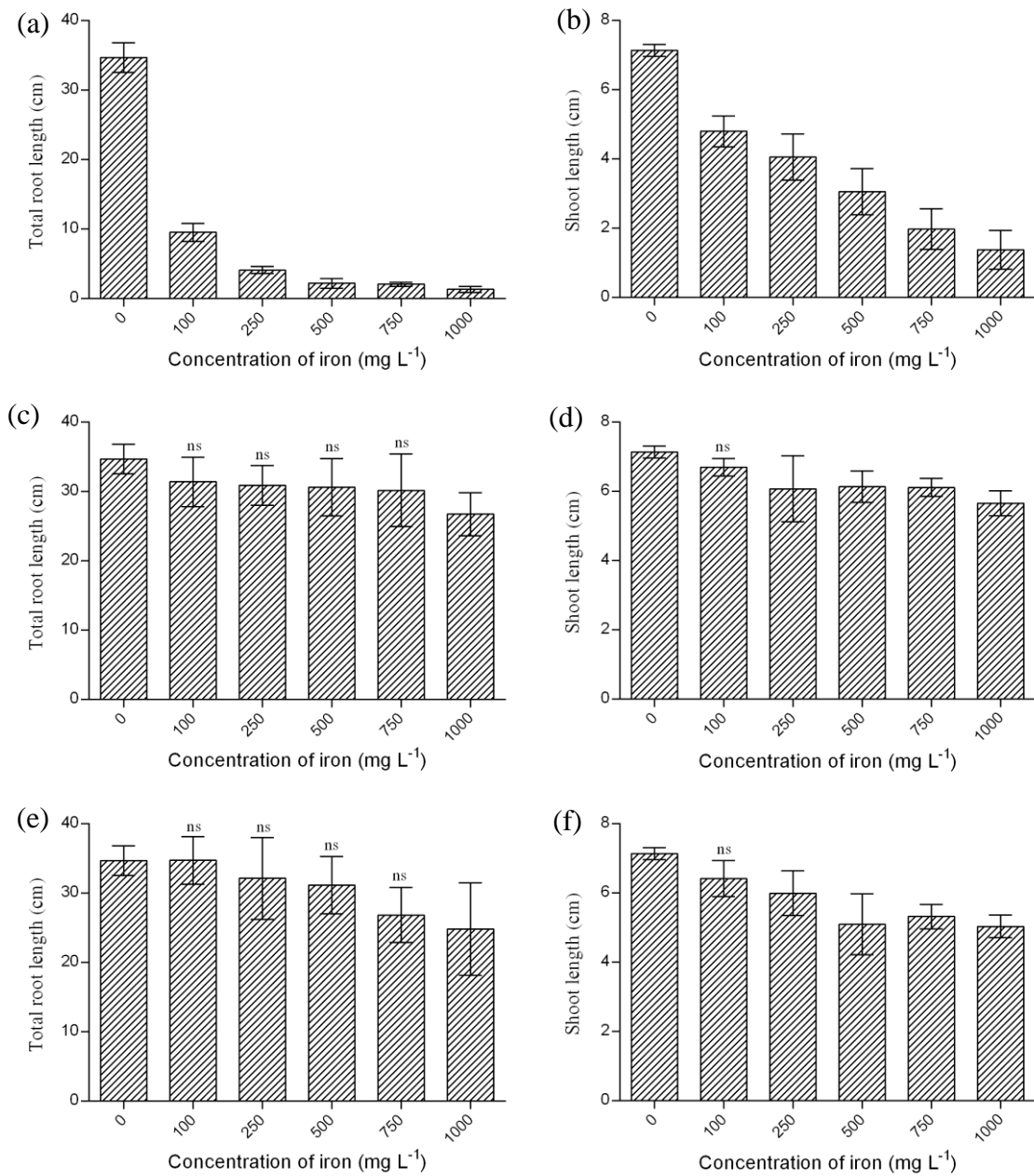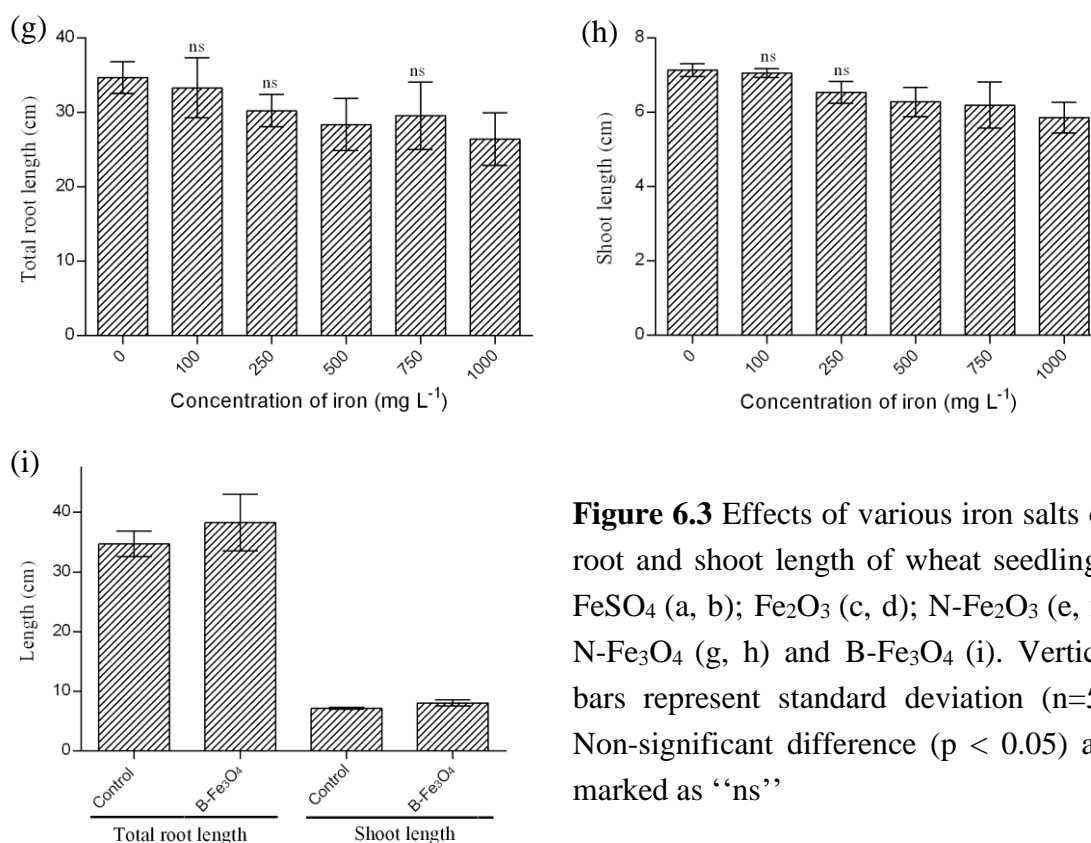
Figure 6.3 Effects of various iron salts on root and shoot length of wheat seedlings. $FeSO_4$ (a, b); Fe_2O_3 (c, d); $N-Fe_2O_3$ (e, f); $N-Fe_3O_4$ (g, h) and $B-Fe_3O_4$ (i). Vertical bars represent standard deviation (n=5). Non-significant difference (p < 0.05) are marked as ''ns''

As expected, owing to its highly acidic pH, $FeSO_4$ showed significantly decreased root length at higher iron concentrations. A percent reduction of 73.86 % in the root length was observed at 100 mg L^{-1}, as compared to control which increased upto 96.30 % in case of 1000 mg L^{-1}. Compared to the detrimental effect of $FeSO_4$ on seed germination, the results on seedling growth were found to be more pronounced as seedlings were more vulnerable because of their ability to absorb various iron salts through root system. Bulk Fe_2O_3, $N-Fe_2O_3$ and $N-Fe_3O_4$ showed milder and less damaging effects on root growth. All three forms of iron oxide resulted in 5.9 - 9.3 % reduction in root length at 100 mg L^{-1} as compared to 22.44 - 27.55 % at 1000 mg L^{-1}. However, the decrease was found to be insignificant as per the statistical analysis. Similar results were observed by Lee et al. (2010) during their study on effect of magnetite nanoparticles on seed germination and growth in *Arabidopsis thaliana*. They showed no toxicity in seed germination as well as very negligible toxicity on root elongation at 400 and 2000 mg L^{-1} concentration of nanoparticles. Treatment of $B-Fe_3O_4$ showed growth promoting effect wherein 13.63 % increase was witnessed in the root length as compared to control. The most obvious reason for the increased root length is the efficient uptake of nanoparticles which is facilitated by the presence of protein capping (corona) on the biologically synthesized nanoparticles (Judy et al. 2012). Various studies have suggested possible interactions between the biomolecules in the corona and corresponding receptors in the cell membrane of any tissue

that may trigger biological recognition and uptake of the functionalized nanoparticle (Monopoli et al. 2011; Lesniak et al. 2013; Fleischer and Payne 2014)

The dose dependent toxicity of $FeSO_4$ was also witnessed in case of wheat seedling shoot length. A decreased shoot length ranging from 29.57 % (100 mg L^{-1}) to 78.87 % (1000 mg L^{-1}) was observed at all the tested concentration of $FeSO_4$. The effect of $FeSO_4$ on shoot elongation was found to be less detrimental as compared to its effect on root elongation. The reason may be due to the fact that roots serve as the major source of nutrient uptake. Similar results were obtained in a study conducted to check the effect of iron on rye grass seeds germination and growth (Wong and Bradshaw 1982). The effect of bulk Fe_2O_3, $N-Fe_2O_3$ and $N-Fe_3O_4$ on shoot growth were more evident and statistically conclusive as compared to roots. No toxicity was observed at the lowest tested concentration (100 mg L^{-1}). However, detrimental effects were observed as we moved to higher concentrations (250, 500, 750 and 1000 mg L^{-1}). In terms of percent reduction in shoot length as compared to control, significant change of 8.45-14.08 % (250 mg L^{-1}), 15.49-23.49 % (500 mg L^{-1}), 12.67-25.3 % (750 mg L^{-1}) and 16.90-30.98 % (1000 mg L^{-1}) was calculated in various iron salts. As nanoparticle translocation is essential to cause any toxic effect, the results obtained in our study support the observation made by Zhu et al. (2008), who showed the translocation of magnetite particles in pumpkin, and their accumulation near the roots and leaves of a matured plant. In contrast to other nanoparticles, protein capped $B-Fe_3O_4$ exerted positive effect on shoot development with a significant increase of 12.67 % in shoot length as compared to control. On the basis of seed germination assay of wheat, it was evident that among various tested iron salts, IONPs were neither convincingly growth promoting nor heavily toxic to the seeds. In addition, they can surely be beneficial at lower iron concentrations such as 100 mg L^{-1} particularly the ones coated with biomolecules like proteins. However, at higher iron concentrations above 500 mg L^{-1} they may exert detrimental effect.

6.3.2.2 Field study

The assessment of plant response to nanoparticles is critically important not only from the point of using them as potential nano-fertilizers but also from the fact that these nanoparticles, if found toxic to plants, may also pose serious threat to human beings and livestock by entering the food chain (Rico et al. 2011). In order to further confirm the seed germination experiment results results and identify the border line concentration that segregates nanoparticle's positive and negative consequence on plants, their effect on the growth and development of wheat were for the entire plant life cycle. For this, various iron salts ($FeSO_4$, bulk Fe_2O_3, $N-Fe_2O_3$ and $N-Fe_3O_4$) were foliar sprayed at different iron concentrations (0, 100, 250, 500, 750 and 1000 mg L^{-1}) during the vegetative phase of wheat grown in an artificial farming facility. The iron concentration, above ground biomass, cob and grain weight, grain protein and carbohydrate contents were studied.

Various physico-chemical characteristics of experimental field soil are shown in Table 6.4. The experimental field at Pilani falls in Jhunjhunu district of Rajasthan and has coarse textured, light brown, fine sand to clay loam, very deep and non-calcareous soil. The soils are classified under Typic Torripsamments and Typic Haplocambids (Kumar et al. 2014). Apart from serious zinc deficiency, substantial deficiency of iron was observed in the experimental field soil. Moreover, alkaline pH of the soil limits the availability of iron to the plants.

Table 6.4 Physico-chemical characteristics of experimental field soil (n=3).

Parameters	Mean ± S.D.
pH	8.067 ± 0.033
Electrical conductivity (EC)	0.030 ± 0.000
K (mg Kg^{-1})	133.300 ± 1.528
N (mg Kg^{-1})	13.483 ± 0.136
Olsen's P (mg Kg^{-1})	36.087 ± 1.545
Organic carbon (%)	0.640 ± 0.020
Ca (mg g^{-1})	0.053 ± 0.003
Mg (mg g^{-1})	0.017 ± 0.003
Cu (µg g^{-1})	0.200 ± 0.044
Mn (µg g^{-1})	19.800 ± 8.325
Zn (µg g^{-1})	0.640 ± 0.151
Fe (µg g^{-1})	2.810 ± 1.005

Iron supplementation has been known to induce morphological and physiological changes in plants (Rout and Sahoo 2015). Phenotypic changes, such as plant growth and biomass production are valuable parameters used to assess the effect of any treatment. Figure 6.4 shows impact of various iron salts at different iron concentrations on the dry weight of above ground biomass of wheat plants.
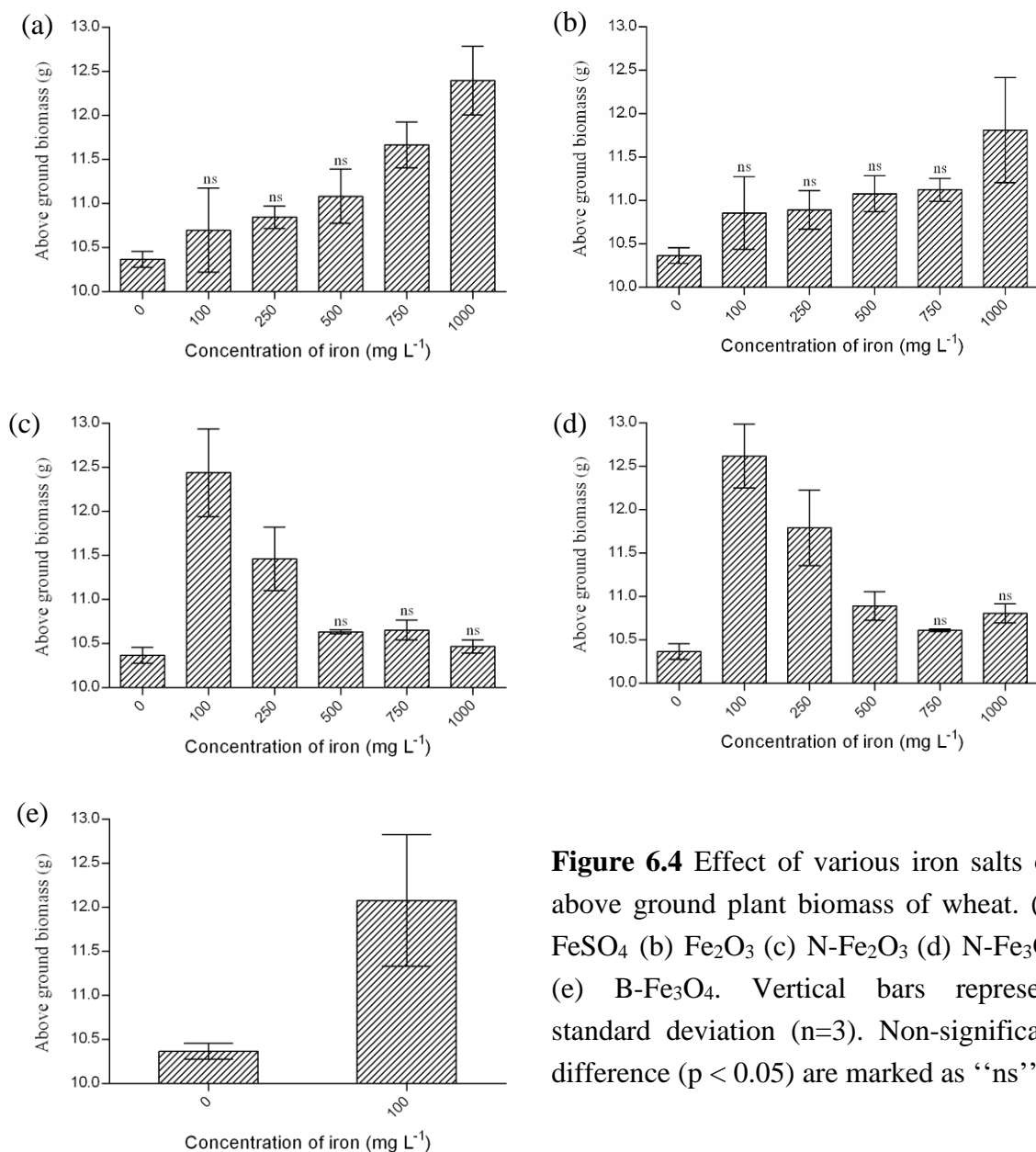
Figure 6.4 Effect of various iron salts on above ground plant biomass of wheat. (a) $FeSO_4$ (b) Fe_2O_3 (c) $N-Fe_2O_3$ (d) $N-Fe_3O_4$ (e) $B-Fe_3O_4$. Vertical bars represent standard deviation (n=3). Non-significant difference ($p < 0.05$) are marked as ''ns''

The minimum plant biomass was observed in case of control plants. Due to the substantial variation observed within replicates of each treatments, majority of the vegetative growth data (plant biomass) were not statistically significant. Noteworthy, the ionic ($FeSO_4$) and bulk (Fe_2O_3) forms of iron could enhance the plant biomass at their higher concentrations i.e. 750 and 1000 mg L^{-1}, respectively. Whereas, the nano iron forms ($N-Fe_2O_3$, $N-Fe_3O_4$ and $B-Fe_3O_4$) exerted significant impact on plant biomass production at their lowest tested concentration (100 mg L^{-1}). $N-Fe_2O_3$ and $N-Fe_3O_4$ were also stimulatory at 250 mg L^{-1} and 500 mg L^{-1}, respectively. Among the nanoparticles, $N-Fe_3O_4$ resulted in maximum increase in plant biomass. Non-significant changes at other tested concentrations among various treatments confirm the non-toxicity of tested iron salts.

Figure 6.5 shows concentration of iron in the above ground plant biomass sprayed with tested iron salt concentrations. No significant change ($p < 0.05$) in the iron concentration was observed in case of bulk Fe_2O_3 treatment as compared to control plants. It can be deduced that due to larger particle dimensions and high aggregation nature in aqueous solutions, bulk form lacks the capability of cell penetration and may be temporarily adsorbed on the leaf surface (Luyts et al. 2013). In contrast, significant increase in a dose-dependent manner was observed in plants sprayed with nanoparticle treatments ($FeSO_4$, $N-Fe_2O_3$, $N-Fe_3O_4$ and $B-Fe3O_4$) which may be due to their surface adsorption properties (Verma and Stellacci 2010). However, this increase in iron content in a dose dependent manner cannot be correlated with the entry and uptake of nanoparticles in the plants. Noteworthy, treatment of $B-Fe_3O_4$ at 100 mg L^{-1} concentration resulted in marginally higher concentration as compared to its uncapped counterparts at similar concentrations. This might be due to their easy entry in plants in presence of biomolecules on their surface (Nair et al. 2010).
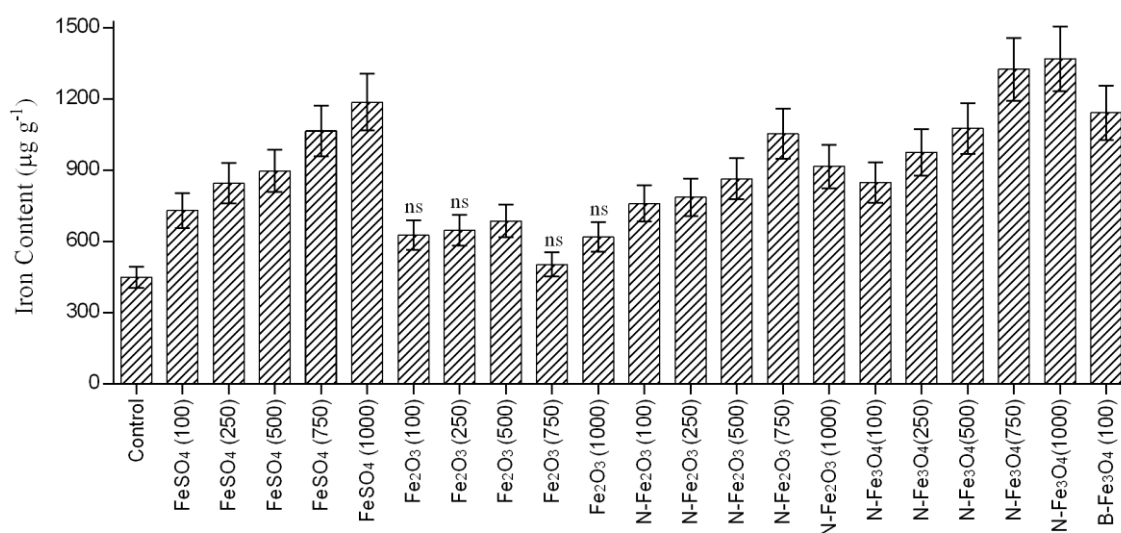
Figure 6.5 Iron concentration in the above ground plant biomass of wheat after treatment with various iron salts. Vertical bars represent standard deviation (n=3). Non-significant differences ($p < 0.05$) are marked as ''ns''

Application of various iron salt concentrations failed to show any substantial effect on wheat grain yield as evaluated by the dry weight of cobs as well as hundred grains (Test weight). As shown in Figure 6.6 and 6.7, in all the concentrations of tested iron salts, a statistically non-significant change (increase or decrease) was obtained as compared to control. This may be due to the large difference within each replicate which is a characteristic feature of field studies involving large experimental area (Kravchenko et al. 2005). Absence of any salt dependent and dose dependent trend in the cob and grain weight revealed the non-toxic effect of IONPs on wheat plant up to tested iron

concentration of 1000 mg L^{-1}. Likewise a statistically non-significant change in the total sugar and protein content in wheat grains was observed (data not shown).

(a)

(b)

(c)

(d)

(e)
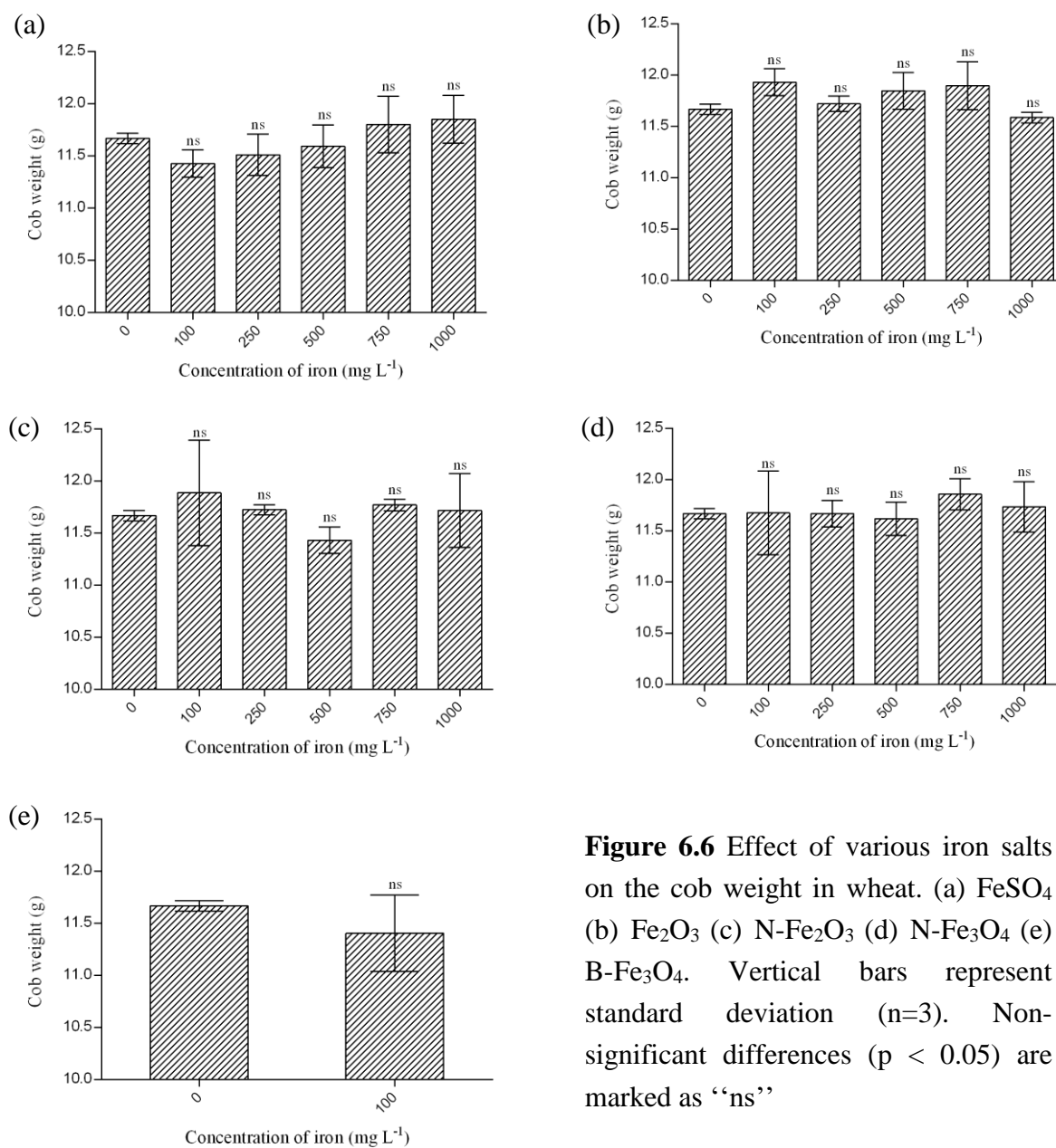
Figure 6.6 Effect of various iron salts on the cob weight in wheat. (a) $FeSO_4$ (b) Fe_2O_3 (c) $N-Fe_2O_3$ (d) $N-Fe_3O_4$ (e) $B-Fe_3O_4$. Vertical bars represent standard deviation (n=3). Non-significant differences ($p < 0.05$) are marked as ''ns''
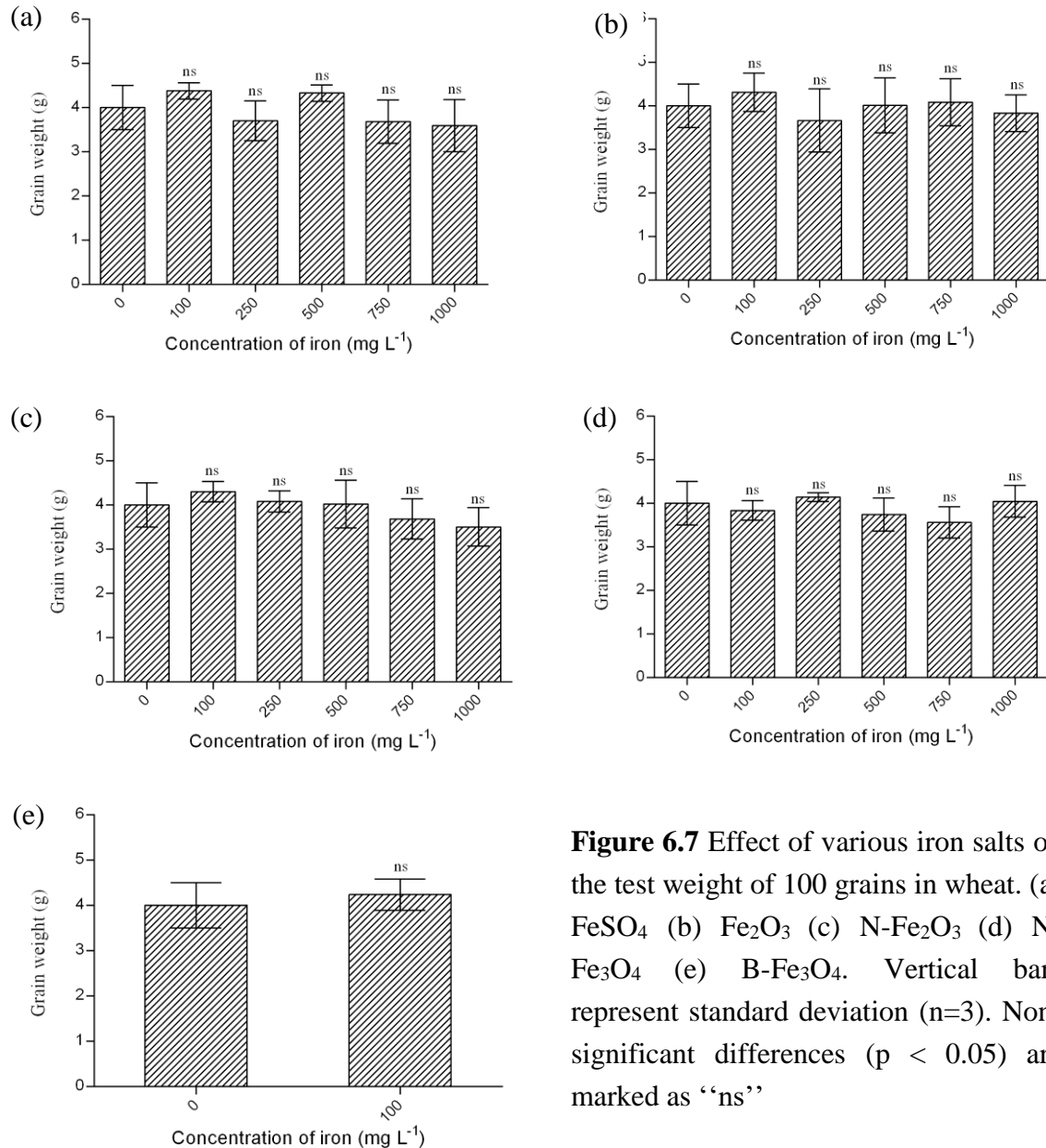
Figure 6.7 Effect of various iron salts on the test weight of 100 grains in wheat. (a) $FeSO_4$ (b) Fe_2O_3 (c) $N-Fe_2O_3$ (d) $N-Fe_3O_4$ (e) $B-Fe_3O_4$. Vertical bars represent standard deviation (n=3). Non-significant differences ($p < 0.05$) are marked as ''ns''

Figure 6.8 shows the concentration of iron in the grain obtained from wheat plants sprayed with tested iron salts. As expected, grains obtained from $FeSO_4$ sprayed plants showed substantial increase in the iron content especially at higher concentration (750 and 1000 mg L^{-1}). Majority of studies carried out to prove the beneficial role of $FeSO_4$ fertilization have also showed the increment (biofortification) of iron in the grains (Aciksoz et al. 2011; Murgia et al. 2012; Wei et al. 2012). Interestingly, grains obtained from plants exposed to IONPs also showed a marginal yet statistically significant increase in the iron content particularly at lower concentrations (100, 250 and 500 mg L^{-1}). An important point to be noted while analysing these results is that, the sprays were carried out only during the vegetative phase (milk stage) of wheat. Therefore, the increase of iron content in the grain obtained from plants exposed to IONPs can be either due to

translocation of nanoparticle from the foliar sprayed leaves to the fruiting body and subsequently to the grains or due to their ability to follow a slow dissociation kinetics to release ions within the cells for prolonged time (Liu and Hurt 2010). After entering the cell, nanoparticles can be transported apoplastically or symplastically. They may also be transported via plasmodesmata from one cell to the other (Rico et al. 2011). In the cytoplasm, nanoparticles approach different cytoplasmic organelles and interfere with different metabolic processes of the cell. The translocation and accumulation of nanoparticles in edible plant parts has been experimentally supported by various studies reported in the literature (Miralles et al. 2012). Cifuentes et al. (2010) experimentally proved the translocation of carbon coated IONPs in wheat seedlings. Likewise, the translocation of IONPs was also reported in pumpkin plants and its fruit using magnetization studies (Zhu et al. 2008). In another study, micro-XRF and micro-XANES analysis of transverse sections of cucumber of root and leaf proved that titanium oxide nanoparticles are absorbed by roots and transported to the aboveground plant parts via vascular tissues (Servin et al. 2012). They found the presence of titanium in the dermis, mesophyll, vascular system, and trichomes of leaves in the treated plants. Many reports also suggest the accumulation (biofortification) of metals in the pods and grains. For example, increased content of cerium and zinc was measured in soybean pods during the treatments wherein 500 and 1000 mg of ZnO and CeO_2 nanoparticles, respectively were mixed per kilogram of soil (Peralta-Videa et al. 2014). Rico et al. (2013) demonstrated higher cerium content in rice grains when the plants were exposed to 500 mg L^{-1} of CeO_2 nanoparticles. In contrast, the same group also reported lack of any nanoparticle (CeO_2) translocation to the above ground biomass in wheat (Rico et al. 2014). Recently, Zhao et al. (2015) experimentally proved the successful translocation of ZnO nanoparticles to the corn cob resulting in higher zinc content.
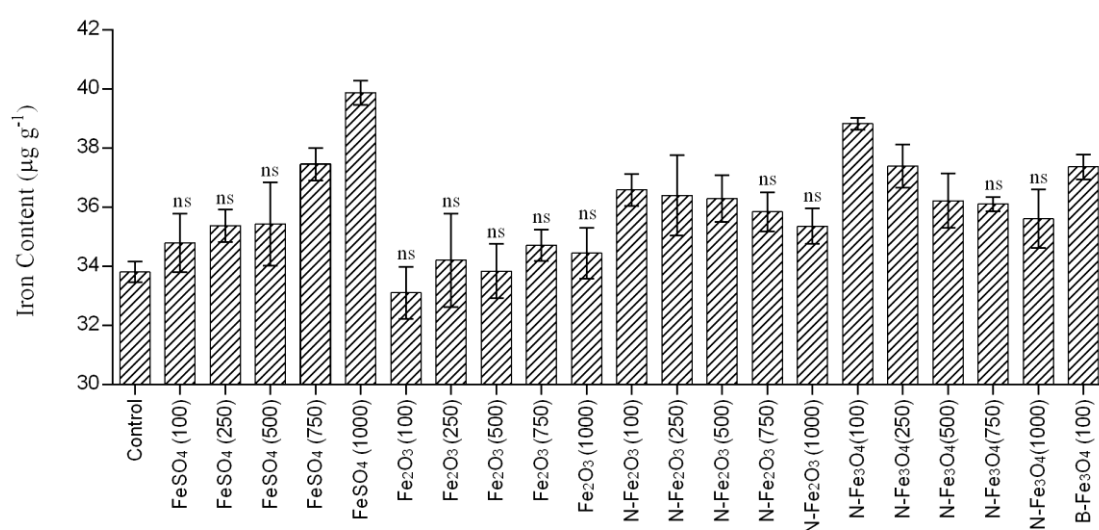
Figure 6.8 Iron concentration in wheat grain obtained from plants treated with various iron salts. Vertical bars represent standard deviation (n=3). Non-significant differences (p < 0.05) are marked as ''ns''

The present study revealed that foliar application of tested iron salts upto a 1000 mg L^{-1} concentration exerted positive effects on plant growth as demonstrated by increased plant weight. However, no significant change in the grain yield and nutritional quality was witnessed. At lower concentrations, IONPs (N-Fe$_2$O$_3$, N-Fe$_3$O$_4$ and B-Fe3O$_4$) were particularly found to stimulate biomass as well as iron content in plants and grains. Most striking was the evidence showing translocation and accumulation of iron in the grain especially in plants treated with IONPs.

6.3.3 Studies on spinach

The pot study on spinach (*Spinacia oleracea* L.) was executed simultaneously along with experiments on wheat. Spinach was chosen as model plant to assess the effect of various iron forms on its growth and development. Spinach is a leafy vegetable widely used as supplement for anaemic patients due to its high iron content (Zhang et al. 1985). According to U.S. Department of Agriculture's National Nutrient Database, 100 g of fresh raw spinach provides as much as 2.71 mg of iron (https://ndb.nal.usda.gov), which is extremely high in comparison to other vegetables (Chiplonkar et al. 1999). Owing to its remarkable ability to sequester and accumulate iron, spinach was chosen as a model plant (Schmidt 1999). The soil used for spinach pot experiment was formulated by mixing three parts sand with one part clay. Various physico-chemical characteristics of the soil are shown in table 6.5.

Table 6.5 Physico-chemical characteristics of the soil used for spinach pot study.

Parameters	Mean ± S.D.
pH	8.193 ± 0.026
Electrical conductivity (EC)	0.065 ± 0.001
K (mg Kg^{-1})	102.433 ± 4.045
N (mg Kg^{-1})	19.117 ± 0.213
Olsen's P (mg Kg^{-1})	68.893 ± 1.729
Organic carbon (%)	1.100 ± 0.072
Ca (mg g^{-1})	0.069 ± 0.003
Mg (mg g^{-1})	0.058 ± 0.005
Cu (µg g^{-1})	3.240 ± 0.289
Mn (µg g^{-1})	45.180 ± 0.566
Zn (µg g^{-1})	5.660 ± 1.016
Fe (µg g^{-1})	7.740 ± 0.150

Germination of spinach seeds started within 3-4 of sowing with a high germination rate (~85%) and within 2 weeks most of the seedlings attained a height of 7-8 cm with decent variation. After 2 weeks of seed sowing, evenly sized plants were selected by thinning and the pots were divided into various treatment populations including control as described earlier. A total of five sprays of selected iron salts at respective concentrations were carried out at regular intervals of 120 h. The volume of spray solution was increased from 5 mL to 10 mL after the initial two sprays to keep in pace with the increasing plant dimensions. Adequate precautions were practiced to prevent the wastage of iron salt solutions due to improper spraying and subsequent contamination of the soil. Harvesting was performed 5 days after the last spray. Most of the analysis were performed immediately to prevent any time dependent variation (Figure 6.9).
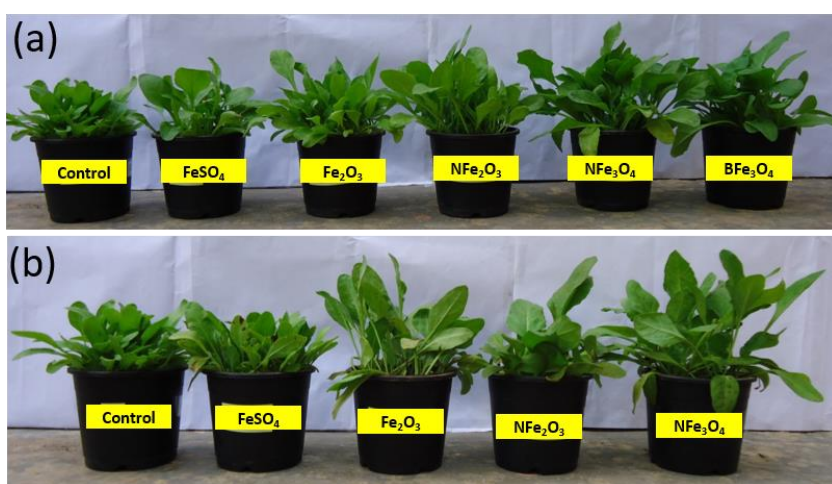
Figure 6.9 Representative photograph showing spinach plants sprayed with ionic, bulk and nanoparticle forms of iron at (A) 100 mg L^{-1} and (b) 1000 mg L^{-1} concentrations. Control plants were sprayed with distilled water

The SEM micrograph revealed interesting insights regarding the possible mode of entry of nanoparticles within plant. As seen in Figure 6.10, stomata openings on the surface of plant leaves may serve as possible gateway for the nanoparticles to enter the leaves. Various other studies have also reported that nanoparticles could enter through stomata or through the base of trichome in leaf (Eichert et al. 2008; Fernandez and Eichert, 2009; Uzu et al. 2010). Although the inherent aggregation property of nanoparticles increases their dimension, the stomatal opening provides sufficient space for the entry of nanoparticles. Another suggested way of nanoparticle entry into the plant system is by forming complexes with membrane transporters (Kurepa et al. 2010). Once inside the plant system, their entry and distribution to other cells through the cell wall directly depends on the pore diameter of cell wall. Hence, nanoparticles and their aggregates with diameter less than the pore size of plant cell wall could easily enter and translocate (Moore 2006; Navarro et al. 2008). Functionalized nanoparticles facilitate the enlargement of pore size or induction of new cell wall pore to enhance the uptake of nanoparticles. Several reports

have discussed the uptake of functionalized nanoparticles into plant cell via binding to carrier proteins, through aquaporin, ion channels or endocytosis (Nair et al. 2010). The presence of iron on the IONPs sprayed leaves was confirmed by EDS analysis (Figure 6.11). The distribution of nanoparticles on the leaf surface surrounding the stomata was visualized by EDS mapping showing the spatial distribution of iron.
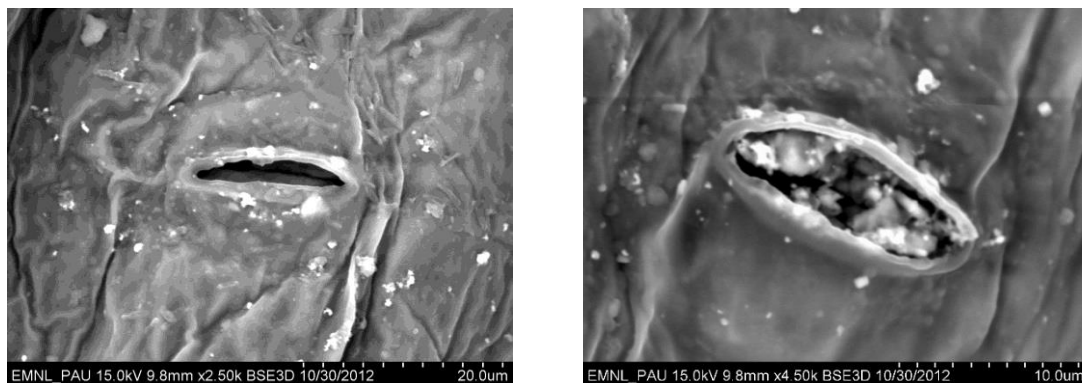
Figure 6.10 SEM micrograph showing stomatal openings on the surface of IONPs sprayed plant leaves (a) ×2500 (scale bar equal to 20 µm) (b) ×4500 (scale bar equal to 10 µm)

Atomic %	C	O	Na	Mg	Al	Si	Cl	K	Fe
Spot 1	41.0	36.8	2.6	0.5	0.5	1.6	1.5	0.7	**14.5**
Spot 2	35.4	36.4	2.7	0.5	0.7	2.1	1.6	0.5	**19.6**
Spot 3	52.8	26.0	4.8	0.5	0.3	0.4	3.5	1.1	**10.6**
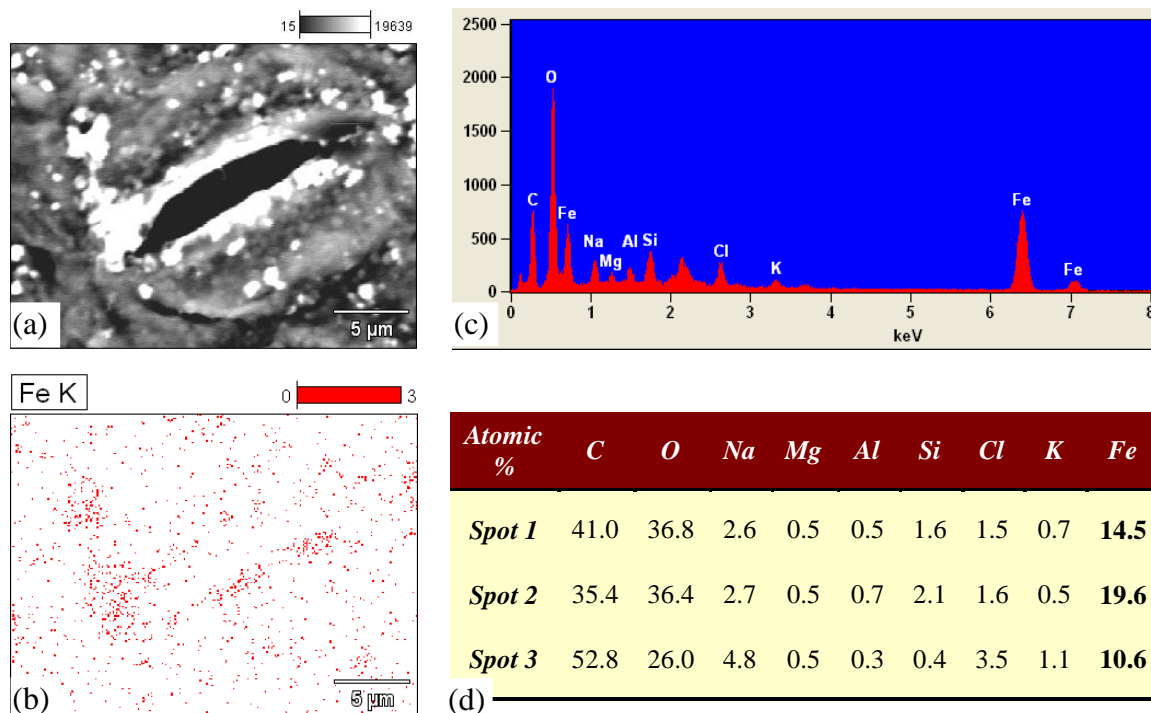
Figure 6.11 EDS analysis of spinach leaf sprayed with IONPs (a) area selected for analysis (b) EDS mapping showing spatial distribution of iron (c) localized chemical composition as determined by EDS mapping (d) quantitative chemical composition of three different spots in terms of atomic percentage

The concentration of iron within plants was estimated by AAS measurements. As demonstrated in Figure 6.12, control plants were found to have natural iron concentration of 270 ± 15 µg g^{-1} which underwent highest fold increase of 2.16 fold in the plants treated with 1000 mg L^{-1} concentration of FeSO$_4$. Comparable results were obtained for plants treated with N-Fe$_3$O$_4$ (1000 mg L^{-1}) and N-Fe$_2$O$_3$ (1000 mg L^{-1}) with 1.98 and 1.72 fold increase, respectively. In general, a dose dependent uptake of iron was observed within all the treatment groups. As expected, the uptake of bulk form of iron i.e. Fe$_2$O$_3$ was least efficient.
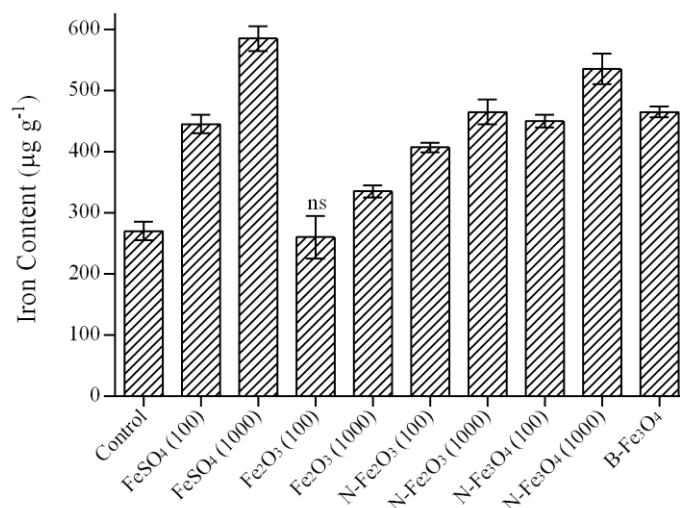
Figure 6.12 Iron content of spinach plants measured by AAS. Vertical bars represent standard deviation (n=3). Non-significant differences ($p < 0.05$) are marked as ''ns''

Plant shoot length, root length and fresh weight were measured to determine the effect of various iron salt concentrations on plant growth (Figure 6.13). All treatments showed significant increase in the shoot length as compared to control except for the 1000 mg L^{-1} concentration of FeSO$_4$ (1000) which showed an insignificant increase (13.9 %). The reason for diminished growth observed in plants treated with FeSO$_4$ (1000 mg L^{-1}), may be the toxicity of iron as it accounted for highest iron uptake (Figure 6.12). Closer inspection of plants exposed to FeSO$_4$ (1000 mg L^{-1}) revealed that the treatment is actually causing detrimental effects in plant as the signs of toxicity were clearly evident (Figure 6.14). Iron is reported to be toxic when it accumulates to high levels as it can act catalytically via the Fenton reaction to generate hydroxyl radicals, which can damage lipids, proteins and DNA (Connolly and Guerinot 2002). In general, elevated shoot growth was observed with the increase in concentration of various iron salts from 100 to 1000 mg L^{-1}. N-Fe$_3$O$_4$ and N-Fe$_2$O$_3$ treatments resulted in highest increase of 46.8 and 40.14 % in shoot length at 1000 mg L^{-1} concentrations, respectively. Surprisingly, no marked effect on the plant root length was observed in response to foliar spray. All the treatments, except Fe$_2$O$_3$ (1000 mg L^{-1}) showed a statistically non-significant change in the root length as compared to control. Fresh weight of the plants measured soon after harvesting, exhibited

noticeable homology with the results of plant shoot length. Except for FeSO$_4$ (1000), all other treatment resulted increase in fresh weight with a highest fold increase in case of N-Fe$_3$O$_4$ (1000 mg L^{-1}). Substantial variation was observed among the replicates.

(a)

(b)

(c)
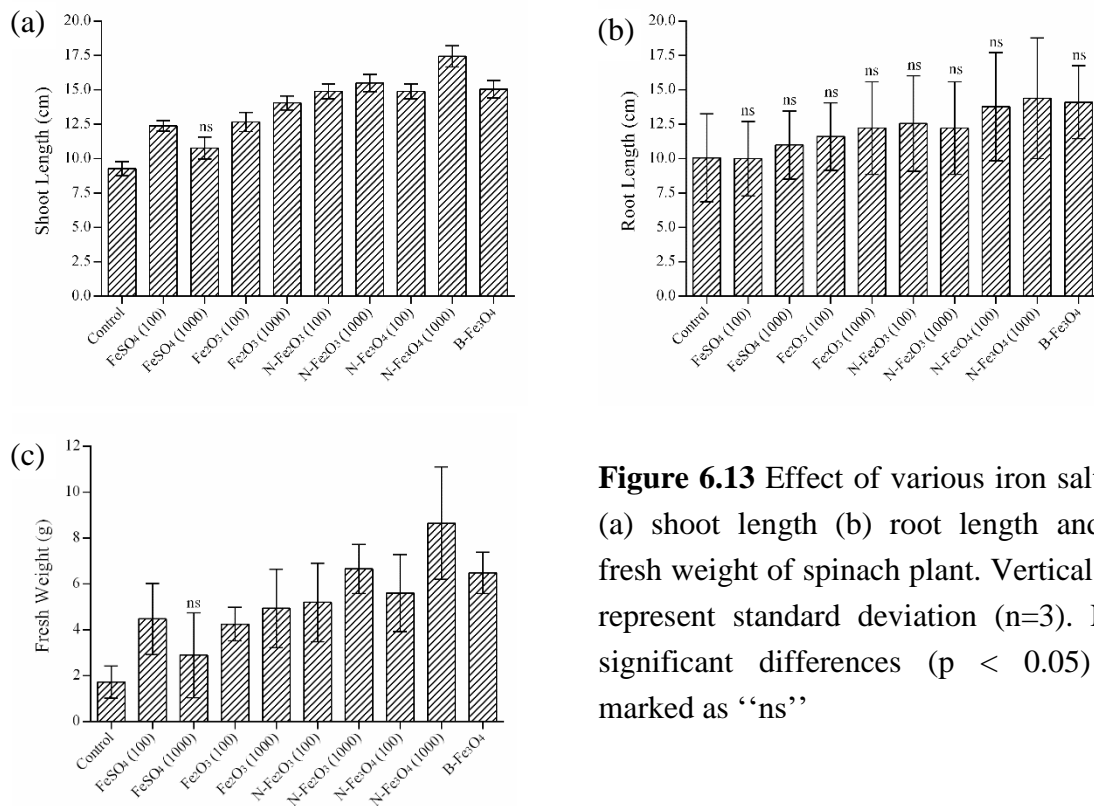
Figure 6.13 Effect of various iron salts on (a) shoot length (b) root length and (c) fresh weight of spinach plant. Vertical bars represent standard deviation (n=3). Non-significant differences (p < 0.05) are marked as ''ns''
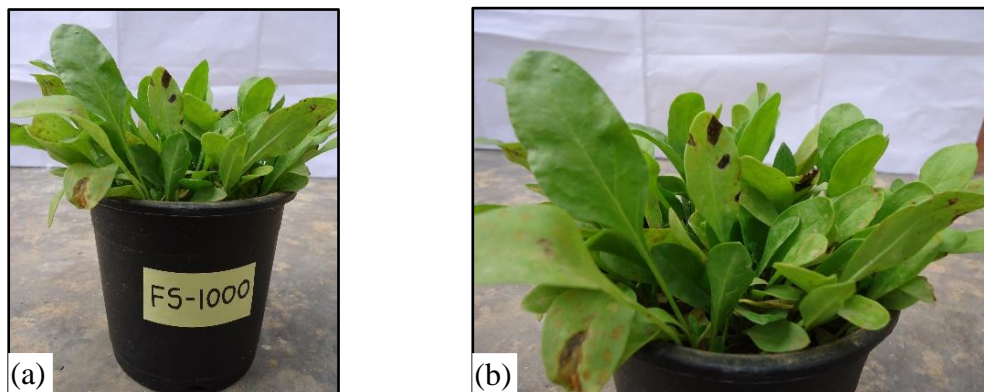
Figure 6.14 FeSO$_4$ induced toxicity in spinach plants sprayed with 1000 mg L^{-1} concentration

Plant health in terms of total chlorophyll, sugar and protein were measured across all treatments (Figure 6.15). Chlorophyll content has always been one of the most trusted parameter for analysing the effect of iron in any plant. As the photosynthetic ability of higher plants can be adversely affected by iron deficiency, the primary response associated is the loss of chlorophyll (Pushnik et al. 1984). Iron plays an integral role in the formation of δ-aminolevulinic acid, the initial committed step in chlorophyll formation (Beale 1978).

In the present study, although all the treatments except $FeSO_4$ (1000 mg L-1) showed significant increase in total chlorophyll content, plants sprayed with 100 mg L^{-1} of iron synthesized higher chlorophyll. It has been observed that higher iron accumulation in plants may lead to decreased chlorophyll synthesis resultant of iron toxicity and its associated oxidative stress (Kuzhandaivel and Venkatesan 2011). Within various treatments, B-Fe_3O_4 (171.53 %) and N-Fe_3O_4 (141.71 %) were the most effective in triggering the chlorophyll biosynthesis. Ghafariyan et al. (2013) also studied the effect of IONPs (60 mg L^{-1}) on chlorophyll biosynthesis and showed the entry and translocation of nanoparticles in soybean which resulted in increased chlorophyll levels with no trace of toxicity.

The treatment and dose dependent trend observed in total sugar and protein content were considerably similar to that of chlorophyll. As expected, plants sprayed with 100 mg L^{-1} of iron showed higher sugar content as compared to 1000 mg L^{-1} concentration. Highest increase in sugar content was observed in plants sprayed with B-Fe_3O_4 (56.22 %) followed by N-Fe_3O_4 (44.41 %) and N-Fe_2O_3 (22.81 %). Contrary to the results obtained for plant sugar, significant increase in protein content was found consistent across all the treatments. Reiterating the above mentioned trends, B-Fe_3O_4 showed highest increase of 119.05 % in total protein content followed by N-Fe_3O_4 (96.24 %) and N-Fe_2O_3 (94.43 %) at 100 mg L^{-1} concentration.
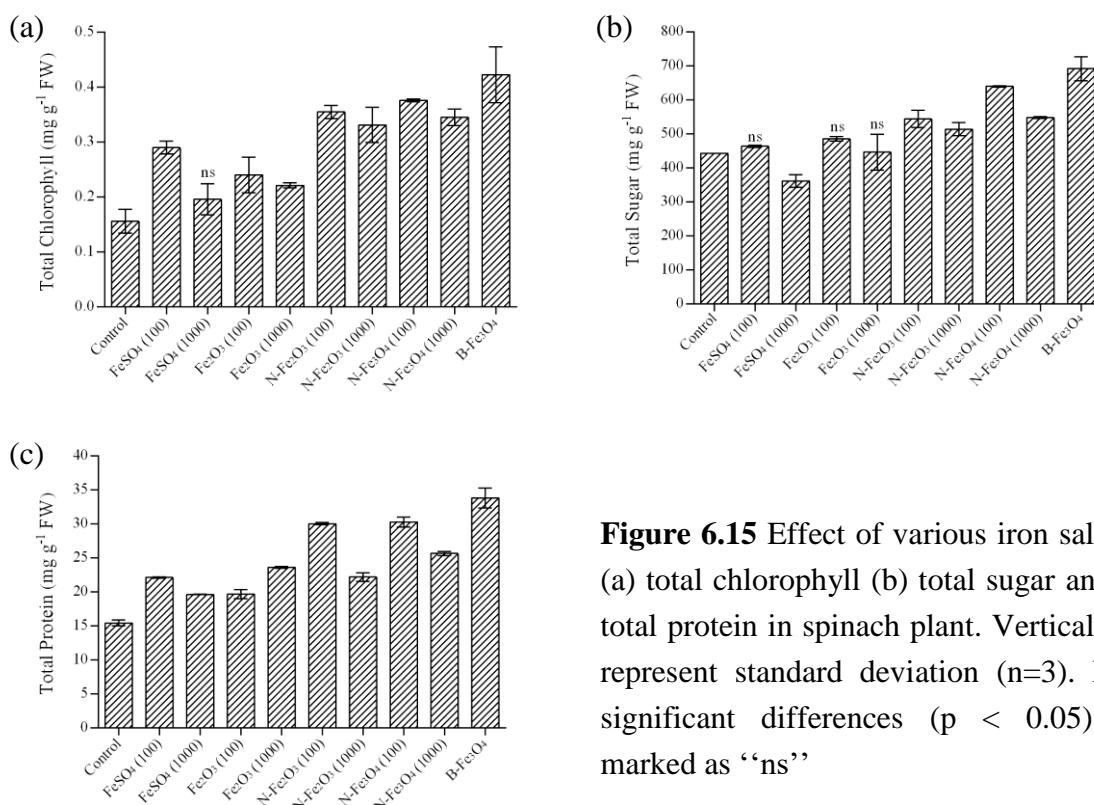
Figure 6.15 Effect of various iron salts on (a) total chlorophyll (b) total sugar and (c) total protein in spinach plant. Vertical bars represent standard deviation (n=3). Non-significant differences ($p < 0.05$) are marked as ''ns''

The obtained results indicate that IONPs promote plant growth and do not show any sign of toxicity up to the tested iron concentration of 1000 mg L^{-1}. Many reports suggest the beneficial role of other nanoparticles on plant growth and development. Yang et al. (2007) demonstrated the improvement in the rate of photosynthesis in spinach chloroplast with the treatment of nanoanatase-TiO$_2$ as compared to no significant effect observed in treatment with bulk TiO$_2$. Smaller size, higher penetrability and increased reactivity of the nanoanatase-TiO$_2$ were responsible for these observations. Similar kind of results were observed in *Arabidopsis thaliana* treated with different concentrations of TiO$_2$ nanoparticles (Ze et al. 2011). They reported improvement in the mean germination time and growth of wheat seedling with lower concentration of TiO$_2$ nanoparticles as compared to bulk TiO$_2$ which showed inversed results. In another study, ZnO nanoparticles were found to be effective in increasing the growth of *Vigna radiata* and *Cicer arietinum* seedlings below a concentration of 20 and 1 mg L^{-1} respectively. Beyond these concentrations, the plant growth was inhibited as observed by Mahajan et al (2011). Priester et al (2012) reported the effect of ZnO nanoparticles on Soybean plant. They reported slight improvement in aboveground biomass, soyabean pod biomass and pod count under ZnO nanoparticles treatment. Burman et al. (2013) suggested improved biomass production in chickpea seedlings when treated with ZnO nanoparticles at a concentration of 1.5 mg L^{-1}. Beneficial role of multi walled carbon nanotubes and its oxidized form on seed germination rate and growth of mustard plant was reported by Mondal et al. (2011).

Iron is one of the most notorious elements since it has a pivotal and dual role in free radical chemistry in all organisms. On one side, iron in its free and unbounded form can participate in Fenton reactions and catalyse the generation of hydroxyl radical and other toxic oxygen species which can cause catastrophes (cellular damage). Whereas on the other side, iron is a constituent of the variety of antioxidant enzymes like catalase, ascorbate/guaiacol peroxidase and ferro-superoxidase dismutase (Morrissey and Guerinot 2009). Healthy plants growing in an unstressed environment avoid the interaction of free iron and peroxides by disposing the metal in vacuoles and apoplast, sequestering in ferritin and by having high levels of antioxidant enzymes and metabolites in most subcellular compartments (Becana et al. 1998). In stress involving excess uptake of iron, the metal can displace the cell redox balance toward a pro-oxidant state, causing alterations in the morphologic, biochemical and physiological characteristics of the plants, generating oxidative stress (Ravet and Pilon 2013).

Accordingly, we measured the catalase, peroxidase and superoxide dismutase activity in leaves of spinach plants sprayed with different iron salts in comparison to the control plants (Figure 6.16a). Increased activity of these enzymes in plants may indicate oxidative stress resulting in an elevation of ROS levels. Significantly increased catalase activity was observed in plants treated with 1000 mg L^{-1} dose of FeSO$_4$ (56.89 %), N-Fe$_2$O$_3$ (47.87) and N-Fe$_3$O$_4$ (69.27 %) as compared to control. Across all the treatments,

only N-Fe$_3$O$_4$ at 100 mg L^{-1} concentration exhibited increase of 24.39 % in level of catalase.

(a)

(b)

(c)
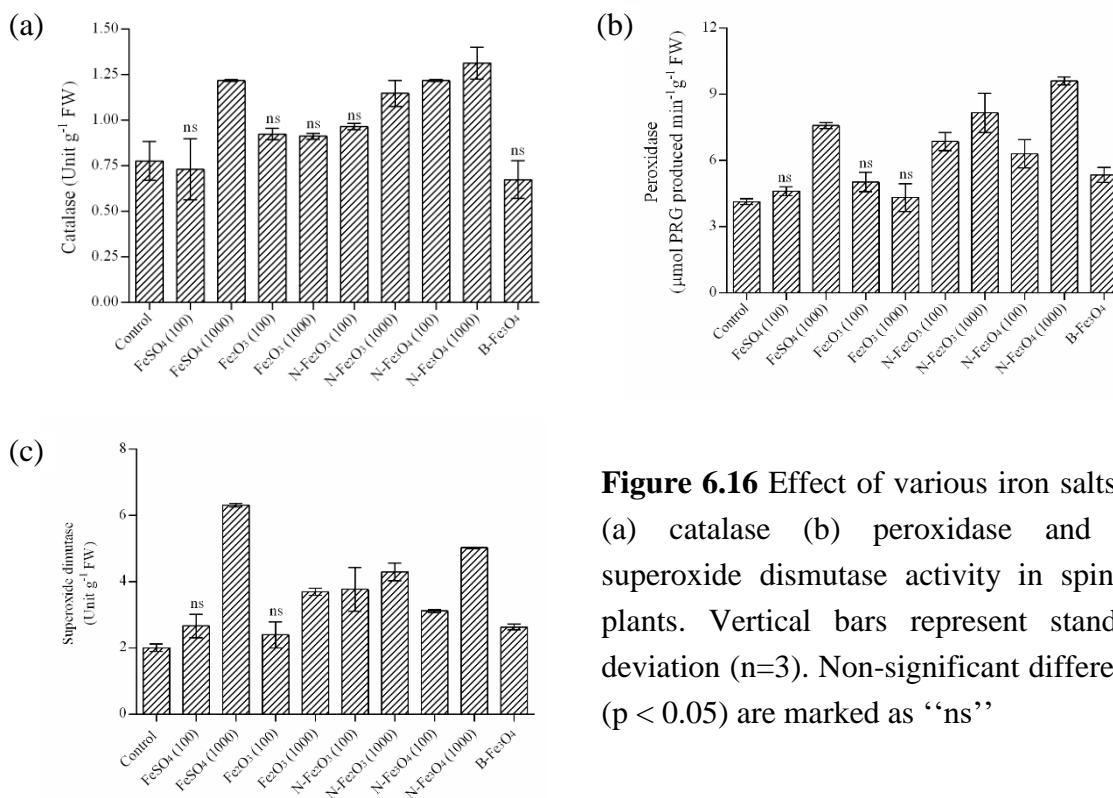
Figure 6.16 Effect of various iron salts on (a) catalase (b) peroxidase and (c) superoxide dismutase activity in spinach plants. Vertical bars represent standard deviation (n=3). Non-significant difference (p < 0.05) are marked as ''ns''

Similar trend was observed in peroxidase activity (Figure 6.16 b). A significant increase in the peroxidase activity was observed in all the IONPs (N-Fe$_2$O$_3$, N-Fe$_3$O$_4$ and B-Fe$_3$O$_4$). The highest increase of 132.43 % was observed in plants treated with N-Fe$_3$O$_4$ (1000 mg L^{-1}) while lowest significant increase of 29.43% was observed for B-Fe$_3$O$_4$.

As compared to control plants, except FeSO$_4$ and Fe$_2$O$_3$, all the other treatments exhibited a significant increase in the superoxide dismutase activity (Figure 6.16c). Highest increase of 215.13 % and 150.90 % in the superoxide dismutase activity was observed in plants treated with 1000 mg L^{-1} concentration of FeSO$_4$ and N-Fe$_3$O$_4$, respectively.

Interestingly, in all above three assays performed to understand the effect of various iron salts on antioxidant level in spinach, we have documented following observations. Firstly, across all the treatments Fe$_2$O$_3$ showed least response which may be due to its limited ability to penetrable inside plant cells. Secondly, the higher tested concentration of any treatment lead to an increased activity of these antioxidant enzymes. Thirdly, among the IONPs, B-Fe$_3$O$_4$ can be considered as the safest because it stimulated lesser antioxidant enzymatic activity as compared to its counterparts. Analogous results were obtained by the other research groups. Wang et al. (2011) reported dose dependent increase in catalase and superoxide dismutase activity in ryegrass and pumpkin plants after

being exposed to Fe_3O_4 nanoparticles. In a similar study on maize, Fe_3O_4 nanoparticles increased the catalase and peroxidase activity (Jalali et al. 2016).

In addition to effects on plants, nanoparticles may also have profound effects on the soil microbial community (Collins et al. 2012; Dinesh et al. 2012). As the rhizospheric microorganisms play a significant role in supporting its host's well-being it is essential to analyse the effect of iron in its ionic, bulk and nanoparticle form on the health of soil microbiome (Gadd 2010). In this regard, dehydrogenase activity was measured for the quantitative determination of soil microbial population (Figure 6.17a). Among the tested iron salts, only $B-Fe_3O_4$ showed significant increase of nearly 50 % in the dehydrogenase activity. This may be due to the higher secretion of photosynthetic leachates by these plants owing to their improved metabolism as mentioned earlier. A significant decrease in the dehydrogenase activity was witnessed in case of Fe_2O_3 treatment. The most possible reason may be the fallout of the salt to the soil as the plants were unable to absorb most of the salt. The heavy load of residual salt would have been washed out during watering thus getting accumulated in the soil, resulting in decreased microbial population. All the other treatments showed statistically non-significant change in the dehydrogenase activity.
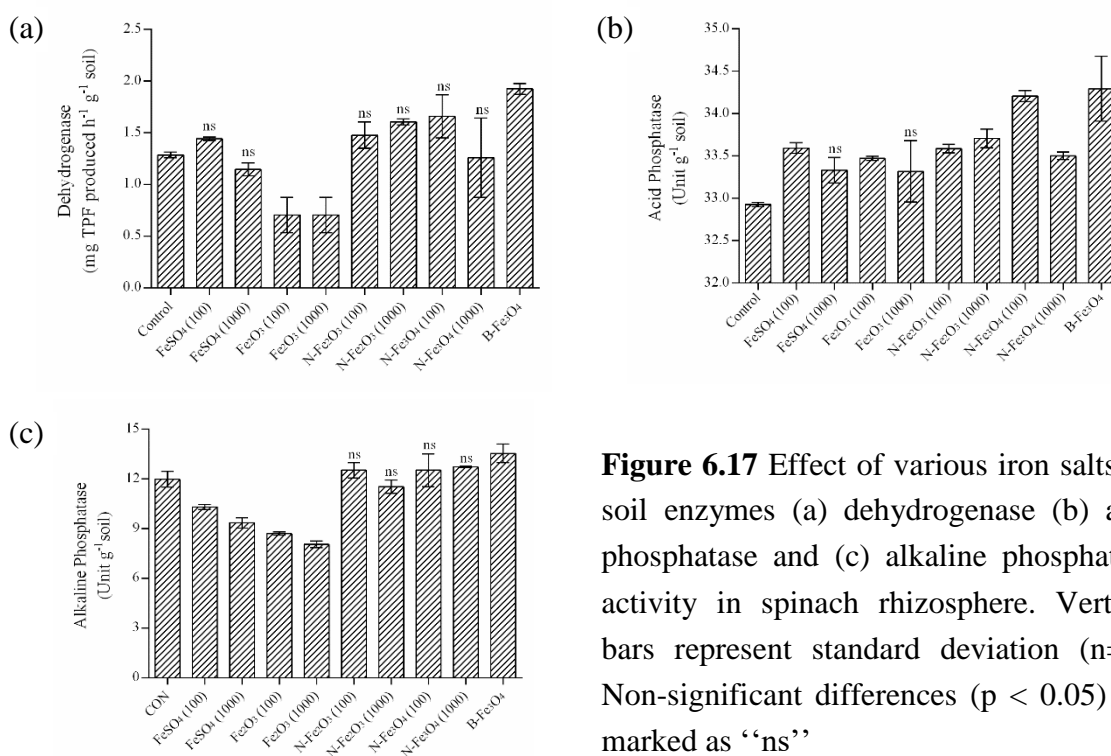
Figure 6.17 Effect of various iron salts on soil enzymes (a) dehydrogenase (b) acid phosphatase and (c) alkaline phosphatase activity in spinach rhizosphere. Vertical bars represent standard deviation (n=3). Non-significant differences (p < 0.05) are marked as ''ns''

The phosphorus mobilization is very important aspect for the proper plant growth and development. Unlike the soils having neutral pH, alkaline soils as used in the present study suffers from high deficiency of available phosphorus for plant uptake (Hopkins and Ellsworth 2005). At pH above 7.5, phosphate ions tend to react quickly with calcium and magnesium to form less soluble compounds. Acid and alkaline phosphatases are enzymes

that catalyse reactions involving the release of free phosphorus and help in phosphorus mobilization in soil for plant uptake (Richardson et al. 2011). While acid phosphatase has been reported to be secreted by plants roots as well as by many microorganisms, alkaline phosphatase is exclusively contributed by soil microflora (Tadano et al. 1991; Duff et al. 1994). The results obtained in our study correlate this phenomenon as increase in the soil acid phosphatase activity was observed for those treatments which showed higher plant growth as well (Figure 16.17b). The highest increase in the acid phosphatase activity was detected in B-Fe$_3$O$_4$ and N-Fe$_3$O$_4$ at 100 mg L^{-1}. However, a non-significant increase was observed in Fe$_2$O$_3$ (1000 mg L^{-1}) as compared to control. Contrasting results were obtained in the alkaline phosphatase activity of various rhizospheric soil samples of treated plants (Figure 16.17c). While treatments like FeSO$_4$ and Fe$_2$O$_3$ showed significant decrease in the enzymatic activity as compared to control, soil samples of IONPs exposed plants showed non-significant increase in the alkaline phosphatase activity. A marginally significant increase was observed in case of B-Fe$_3$O$_4$. The obtained results for soil enzyme activities are in harmony with the other tested plant growth parameters as described earlier.

6.4 Conclusions

The present chapter discusses the experimental assessment of IONPs to be used as a micronutrient source in plants. A systematic comparison of various iron forms viz., ionic (FeSO$_4$), bulk (Fe$_2$O$_3$) and nanoparticle [chemically synthesized (N-Fe$_2$O$_3$ and N-Fe$_3$O$_4$) and biologically synthesized (B-Fe$_3$O$_4$)] at different metal concentrations were made using wheat and spinach as test plants. Characterization of various treatment solutions revealed increase in particle size in order of N-Fe$_2$O$_3$, N-Fe$_3$O$_4$ and B-Fe$_3$O$_4$ and Fe$_2$O$_3$. Due to its bulk nature, Fe$_2$O$_3$ was in micrometer size. Studies on wheat were performed in two separate experiments. First experiment was carried out to test the effect of various iron salt at different concentrations (100, 250, 500, 750 and 1000 mg L^{-1}; B-Fe$_3$O$_4$ only at 100 mg L^{-1}) on seed germination and seedling growth of wheat. The results suggest that IONPs are not toxic; instead if used at lower optimum concentration, they can be beneficial.

Following this, another experiment was executed to study the effect of these treatments on growth, biomass production and grain yield in wheat at a sub-pilot field level. The obtained results strongly supported our hypothesis that IONPs can promote the plant growth especially at lower iron concentration (100 mg L^{-1}). Among IONPs, the level of growth promoting response was in the following order B-Fe$_3$O$_4$ < N-Fe$_2$O$_3$ < N-Fe$_3$O$_4$. All plants were found to accumulate iron supplemented to them in various forms. No change in the grain yield was observed. As presumed on the basis of available literature, FeSO$_4$ treatment showed substantial increase in the iron content of the grains. Interestingly, IONPs treatment also showed significant increase in the iron content particularly at lower tested concentrations (100, 250 and 500 mg L^{-1}).

Another experiment using spinach as model plant was carried out simultaneously. In this study, similar treatments were included at 100 and 1000 mg L^{-1} concentrations. The obtained results strongly advocated the growth promoting effect of B-Fe$_3$O$_4$ as it not only stimulated higher growth but also increased plant metabolism and lower antioxidant levels in treated plants. B-Fe$_3$O$_4$ also showed non-toxic effect on the soil microflora and could marginally improve the phosphate mobilization in soil. The results obtained in the spinach study indicated the importance of surface modification and biocompatible nature of protein shell present on the surface of biologically synthesized nanoparticles.

6.5 References

Aciksoz, S. B., Yazici, A., Ozturk, L. and Cakmak, I. (2011). Biofortification of wheat with iron through soil and foliar application of nitrogen and iron fertilizers. *Plant and Soil* 349: 215-225.

Arnon, D. I. (1949). Copper enzymes in isolated chloroplasts. Polyphenol oxidase in Beta vulgaris. *Plant Physiology* 24: 1-15.

Baalousha, M., Manciulea, A., Cumberland, S., Kendall, K. and Lead, J. R. (2008). Aggregation and surface properties of iron oxide nanoparticles: influence of pH and natural organic matter. *Environmental Toxicology and Chemistry* 27: 1875-1882.

Beale, S. I. (1978). δ- Aminolevulinic acid in plants: its biosynthesis, regulation, and role in plastid development. *Annual Review of Plant Physiology* 29: 95-120.

Becana, M., Moran, J. F. and Iturbe-Ormaetxe, I. (1998). Iron-dependent oxygen free radical generation in plants subjected to environmental stress: toxicity and antioxidant protection. *Plant and Soil* 201: 137-147.

Beers, R. F. and Sizer, I. W. (1952). A spectrophotometric method for measuring the breakdown of hydrogen peroxide by catalase. *Journal of Biological Chemistry* 195: 133-140.

Beyer, W. F. and Fridovich, I. (1987). Assaying for superoxide dismutase activity: some large consequences of minor changes in conditions. *Analytical Biochemistry* 161: 559-566.

Boynton, D. (1954). Nutrition by foliar application. *Annual Review of Plant Physiology* 5: 31-54.

Bradford, M. M. (1976). A rapid and sensitive method for the quantitation of microgram quantities of protein utilizing the principle of protein-dye binding. *Analytical Biochemistry* 72: 248-254.

Briat, J. F. and Lobréaux, S. (1997). Iron transport and storage in plants. *Trends in Plant Science* 2: 187-193.

Burman, U., Saini, M. and Kumar, P. (2013). Effect of zinc oxide nanoparticles on growth and antioxidant system of chickpea seedlings. *Toxicological & Environmental Chemistry* 95: 605-612.

Cameron, F. K. (1930). The solubility of ferrous sulphate. *The Journal of Physical Chemistry* 34: 692-710.

Chiplonkar, S. A., Tarwadi, K. V., Kavedia, R. B., Mengale, S. S., Paknikar, K. M. and Agte, V. V. (1999). Fortification of vegetarian diets for increasing bioavailable iron density using green leafy vegetables. *Food Research International* 32: 169-174.

Chithrani, B. D. and Chan, W. C. (2007). Elucidating the mechanism of cellular uptake and removal of protein-coated gold nanoparticles of different sizes and shapes. *Nano Letters* 7: 1542-1550.

Cifuentes, Z., Custardoy, L., de la Fuente, J. M., Marquina, C., Ibarra, M. R., Rubiales, D. and Pérez-de-Luque, A. (2010). Absorption and translocation to the aerial part of magnetic carbon-coated nanoparticles through the root of different crop plants. *Journal of Nanobiotechnology* 8: 1-8.

Clarkson, D. T. and Hanson, J. B. (1980). The mineral nutrition of higher plants. *Annual Review of Plant Physiology* 31: 239-298.

Clarkson, D. T. (1985). Factors affecting mineral nutrient acquisition by plants. *Annual Review of Plant Physiology* 36: 77-115.

Clogston, J. D. and Patri, A. K. (2011). Zeta potential measurement. *Characterization of Nanoparticles Intended for Drug Delivery* 697: 63-70.

Collins, D., Luxton, T., Kumar, N., Shah, S., Walker, V. K. and Shah, V. (2012). Assessing the impact of copper and zinc oxide nanoparticles on soil: a field study *PLoS One*, 7: e42663.

Connolly, E. L. and Guerinot, M. (2002). Iron stress in plants. *Genome Biology* 3: 1024-1028.

De Rosa, M. C., Monreal, C., Schnitzer, M., Walsh, R. and Sultan, Y. (2010). Nanotechnology in fertilizers. *Nature Nanotechnology* 5: 91-91.

Di Salvatore, M., Carafa, A. M. and Carratù, G. (2008). Assessment of heavy metals phytotoxicity using seed germination and root elongation tests: a comparison of two growth substrates. *Chemosphere* 73: 1461-1464.

Dinesh, R., Anandaraj, M., Srinivasan, V. and Hamza, S. (2012). Engineered nanoparticles in the soil and their potential implications to microbial activity. *Geoderma* 173, 19-27.

Ditta, A. (2012). How helpful is nanotechnology in agriculture? *Advances in Natural Sciences: Nanoscience and Nanotechnology* 3: 033002.

Duff, S. M., Sarath, G. and Plaxton, W. C. (1994). The role of acid phosphatases in plant phosphorus metabolism. *Physiologia Plantarum* 90: 791-800.

Dunnett, C. W. (1955). A multiple comparison procedure for comparing several treatments with a control. *Journal of the American Statistical Association* 50: 1096-1121.

Egley, G. H., Paul Jr, R. N., Vaughn, K. C. and Duke, S. O. (1983). Role of peroxidase in the development of water-impermeable seed coats in *Sida spinosa* L. *Planta* 157: 224-232.

Eichert, T., Kurtz, A., Steiner, U. and Goldbach, H. E. (2008). Size exclusion limits and lateral heterogeneity of the stomatal foliar uptake pathway for aqueous solutes and water-suspended nanoparticles. *Physiologia Plantarum* 134: 151-160.

FAOSTAT, 2015. FAO Database, Food and Agriculture Organization of the United Nations, available at http://faostat.fao.org

Fernández, V. and Eichert, T. (2009). Uptake of hydrophilic solutes through plant leaves: current state of knowledge and perspectives of foliar fertilization. *Critical Reviews in Plant Sciences* 28: 36-68.

Fleischer, C. C. and Payne, C. K. (2014). Nanoparticle–cell interactions: molecular structure of the protein corona and cellular outcomes. *Accounts of Chemical Research* 47: 2651-2659.

Foy, C. D., Chaney, R. T. and White, M. C. (1978). The physiology of metal toxicity in plants. *Annual Review of Plant Physiology* 29: 511-566.

Gadd, G. M. (2010). Metals, minerals and microbes: geomicrobiology and bioremediation. *Microbiology* 156: 609-643.

Geisseler, D. and Scow, K. M. (2014). Long-term effects of mineral fertilizers on soil microorganisms–A review. *Soil Biology and Biochemistry* 75: 54-63.

Ghafariyan, M. H., Malakouti, M. J., Dadpour, M. R., Stroeve, P. and Mahmoudi, M. (2013). Effects of magnetite nanoparticles on soybean chlorophyll. *Environmental Science & Technology* 47: 10645-10652.

Ghormade, V., Deshpande, M. V. and Paknikar, K. M. (2011). Perspectives for nano-biotechnology enabled protection and nutrition of plants. *Biotechnology Advances* 29: 792-803.

Gittings, M. R. and Saville, D. A. (1998). The determination of hydrodynamic size and zeta potential from electrophoretic mobility and light scattering measurements. *Colloids and Surfaces A: Physicochemical and Engineering Aspects* 141: 111-117.

Guerinot, M. L. and Yi, Y. (1994). Iron: nutritious, noxious, and not readily available. *Plant Physiology* 104: 815.

Hell, R. and Stephan, U. W. (2003). Iron uptake, trafficking and homeostasis in plants. *Planta* 216: 541-551.

Hong, J., Peralta-Videa, J. R., Rico, C., Sahi, S., Viveros, M. N., Bartonjo, J. and Gardea-Torresdey, J. L. (2014). Evidence of translocation and physiological impacts of foliar applied CeO_2 nanoparticles on cucumber (*Cucumis sativus*) plants. *Environmental Science & Technology* 48: 4376-4385.

Hopkins, B. and Ellsworth, J. (2005, March). Phosphorus availability with alkaline/calcareous soil. *Western Nutrient Management Conference* 6: 88-93.

Jalali, M., Ghanati, F. and Sanavy, S. A. M. M. (2016). Effects of Fe_3O_4 nanoparticles and iron chelate on the antioxidant capacity and nutritional value of soil cultivated maize (*Zea mays*) plants. *Crop and Pasture Science* (Just Accepted)

Judy, J. D., Unrine, J. M., Rao, W., Wirick, S. and Bertsch, P. M. (2012). Bioavailability of gold nanomaterials to plants: importance of particle size and surface coating. *Environmental Science & Technology* 46: 8467-8474.

Kravchenko, A. N., Robertson, G. P., Thelen, K. D. and Harwood, R. R. (2005). Management, topographical, and weather effects on spatial variability of crop grain yields. *Agronomy Journal* 97: 514-523.

Kumar, M., Moharana, P. C., Raina, P. and Kar, A. (2014). Spatial Distribution of DTPA-Extractable Micronutrients in Arid Soils of Jhunjhunun District, Rajasthan. *Annals of Arid Zone* 53: 9-15.

Kurepa, J., Paunesku, T., Vogt, S., Arora, H., Rabatic, B. M., Lu, J. and Smalle, J. A. (2010). Uptake and distribution of ultrasmall anatase TiO_2 Alizarin red S nanoconjugates in *Arabidopsis thaliana*. *Nano Letters* 10: 2296-2302.

Kuzhandaivel, H. and Venkatesan, S. (2011). Impact of iron toxicity on certain enzymes and biochemical parameters of tea. *Asian Journal of Biochemistry* 6: 223-233.

Lee, C. W., Mahendra, S., Zodrow, K., Li, D., Tsai, Y. C., Braam, J. and Alvarez, P. J. (2010). Developmental phytotoxicity of metal oxide nanoparticles to *Arabidopsis thaliana*. *Environmental Toxicology and Chemistry* 29: 669-675.

Lesniak, A., Salvati, A., Santos-Martinez, M. J., Radomski, M. W., Dawson, K. A. and Åberg, C. (2013). Nanoparticle adhesion to the cell membrane and its effect on nanoparticle uptake efficiency. *Journal of the American Chemical Society* 135: 1438-1444.

Lindsay, W. L. and Schwab, A. P. (1982). The chemistry of iron in soils and its availability to plants. *Journal of Plant Nutrition* 5: 821-840.

Liu, J. and Hurt, R. H. (2010). Ion release kinetics and particle persistence in aqueous nano-silver colloids. *Environmental Science & Technology* 44: 2169-2175.

Loneragan, J. F. (1968). Nutrient requirements of plants. *Nature* 220: 1307-1308.

Luyts, K., Napierska, D., Nemery, B. and Hoet, P. H. (2013). How physico-chemical characteristics of nanoparticles cause their toxicity: complex and unresolved interrelations. *Environmental Science: Processes & Impacts* 15: 23-38.

Lynch, I. and Dawson, K. A. (2008). Protein-nanoparticle interactions. *Nano Today* 3: 40-47.

Ma, X., Geiser-Lee, J., Deng, Y. and Kolmakov, A. (2010). Interactions between engineered nanoparticles (ENPs) and plants: phytotoxicity, uptake and accumulation. *Science of the Total Environment* 408: 3053-3061.

Mabille, F., Gril, J. and Abecassis, J. (2001). Mechanical properties of wheat seed coats. *Cereal Chemistry* 78: 231-235.

Macy, P. (1936). The quantitative mineral nutrient requirements of plants. *Plant Physiology* 11: 749.

Mahajan, P., Dhoke, S. K. and Khanna, A. S. (2011). Effect of nano-ZnO particle suspension on growth of mung (*Vigna radiata*) and gram (*Cicer arietinum*) seedlings using plant agar method. *Journal of Nanotechnology* 2011: 696535

Matson, P. A., Naylor, R. and Ortiz-Monasterio, I. (1998). Integration of environmental, agronomic, and economic aspects of fertilizer management. *Science* 280: 112-115.

Miralles, P., Church, T. L. and Harris, A. T. (2012). Toxicity, uptake, and translocation of engineered nanomaterials in vascular plants. *Environmental Science & Technology* 46: 9224-9239.

Miransari, M. (2011). Soil microbes and plant fertilization. *Applied Microbiology and Biotechnology* 92: 875-885.

Mondal, A., Basu, R., Das, S. and Nandy, P. (2011). Beneficial role of carbon nanotubes on mustard plant growth: an agricultural prospect. *Journal of Nanoparticle Research* 13: 4519-4528.

Monopoli, M. P., Walczyk, D., Campbell, A., Elia, G., Lynch, I., Baldelli Bombelli, F. and Dawson, K. A. (2011). Physical-chemical aspects of protein corona: relevance to *in vitro* and *in vivo* biological impacts of nanoparticles. *Journal of the American Chemical Society* 133: 2525-2534.

Moore, M. N. (2006). Do nanoparticles present ecotoxicological risks for the health of the aquatic environment? *Environment International* 32: 967-976.

Morrissey, J. and Guerinot, M. L. (2009). Iron uptake and transport in plants: the good, the bad, and the ionome. *Chemical Reviews* 109: 4553-4567.

Mortvedt, J. J. (1986). Iron sources and management practices for correcting iron chlorosis problems. *Journal of Plant Nutrition* 9: 961-974.

Mortvedt, J. J. (1994). Needs for controlled-availability micronutrient fertilizers. *Fertilizer Research* 38: 213-221.

Murgia, I., Arosio, P., Tarantino, D. and Soave, C. (2012). Biofortification for combating 'hidden hunger' for iron. *Trends in Plant Science* 17: 47-55.

Naderi, M. R. and Danesh-Shahraki, A. (2013). Nanofertilizers and their roles in sustainable agriculture. *International Journal of Agriculture and Crop Sciences* 5: 2229.

Nair, R., Varghese, S. H., Nair, B. G., Maekawa, T., Yoshida, Y. and Kumar, D. S. (2010). Nanoparticulate material delivery to plants. *Plant Science* 179: 154-163.

Navarro, E., Baun, A., Behra, R., Hartmann, N. B., Filser, J., Miao, A. J. and Sigg, L. (2008). Environmental behavior and ecotoxicity of engineered nanoparticles to algae, plants, and fungi. *Ecotoxicology* 17: 372-386.

Oberdörster, G., Oberdörster, E. and Oberdörster, J. (2005). Nanotoxicology: an emerging discipline evolving from studies of ultrafine particles. *Environmental Health Perspectives* 113: 823-839.

OECD. (2006a). *Test No. 208: Terrestrial Plant Test: Seedling Emergence and Seedling Growth Test*, OECD Guidelines for the Testing of Chemicals, Section 2, OECD Publishing, Paris.

OECD. (2006b). *Test No. 227: Terrestrial Plant Test: Vegetative Vigour Test*, OECD Guidelines for the Testing of Chemicals, Section 2, OECD Publishing, Paris.

Peralta-Videa, J. R., Hernandez-Viezcas, J. A., Zhao, L., Diaz, B. C., Ge, Y., Priester, J. H. and Gardea-Torresdey, J. L. (2014). Cerium dioxide and zinc oxide nanoparticles alter the nutritional value of soil cultivated soybean plants. *Plant Physiology and Biochemistry* 80: 128-135.

Pfeiffer, C., Rehbock, C., Hühn, D., Carrillo-Carrion, C., de Aberasturi, D. J., Merk, V. and Parak, W. J. (2014). Interaction of colloidal nanoparticles with their local environment: the (ionic) nanoenvironment around nanoparticles is different from bulk and determines the physico-chemical properties of the nanoparticles. *Journal of the Royal Society Interface* 11: 20130931.

Priester, J. H., Ge, Y., Mielke, R. E., Horst, A. M., Moritz, S. C., Espinosa, K. and Schimel, J. P. (2012). Soybean susceptibility to manufactured nanomaterials with

evidence for food quality and soil fertility interruption. *Proceedings of the National Academy of Sciences* 109: 2451-2456.

Pushnik, J. C., Miller, G. W. and Manwaring, J. H. (1984). The role of iron in higher plant chlorophyll biosynthesis, maintenance and chloroplast biogenesis. *Journal of Plant Nutrition* 7: 733-758.

Raliya, R., Nair, R., Chavalmane, S., Wang, W. N. and Biswas, P. (2015). Mechanistic evaluation of translocation and physiological impact of titanium dioxide and zinc oxide nanoparticles on the tomato (*Solanum lycopersicum* L.) plant. *Metallomics* 7: 1584-1594.

Ravet, K. and Pilon, M. (2013). Copper and iron homeostasis in plants: the challenges of oxidative stress. *Antioxidants & Redox Signaling* 19: 919-932.

Rawashdeh, H. M. and Florin, S. (2015). Foliar application with iron as a vital factor of wheat crop growth, yield quantity and quality: a review. *International Journal of Agriculture Pollution Research* 3: 368-376.

Richardson, A. E., Lynch, J. P., Ryan, P. R., Delhaize, E., Smith, F. A., Smith, S. E. and Oberson, A. (2011). Plant and microbial strategies to improve the phosphorus efficiency of agriculture. *Plant and Soil* 349: 121-156.

Rico, C. M., Hong, J., Morales, M. I., Zhao, L., Barrios, A. C., Zhang, J. Y. and Gardea-Torresdey, J. L. (2013). Effect of cerium oxide nanoparticles on rice: a study involving the antioxidant defence system and in vivo fluorescence imaging. *Environmental Science & Technology* 47: 5635-5642.

Rico, C. M., Lee, S. C., Rubenecia, R., Mukherjee, A., Hong, J., Peralta-Videa, J. R. and Gardea-Torresdey, J. L. (2014). Cerium oxide nanoparticles impact yield and modify nutritional parameters in wheat (*Triticum aestivum L.*). *Journal of Agricultural and Food Chemistry* 62: 9669-9675.

Rico, C. M., Majumdar, S., Duarte-Gardea, M., Peralta-Videa, J. R. and Gardea-Torresdey, J. L. (2011). Interaction of nanoparticles with edible plants and their possible implications in the food chain. *Journal of Agricultural and Food Chemistry* 59: 3485-3498.

Römheld, V. (1987). Different strategies for iron acquisition in higher plants. *Physiologia Plantarum* 70: 231-234.

Rout, G. R. and Sahoo, S. (2015). Role of iron in plant growth and metabolism. *Reviews in Agricultural Science* 3: 1-24.

Schmidt, W. (1999). Mechanisms and regulation of reduction-based iron uptake in plants. *New Phytologist* 141: 1-26.

Servin, A. D., Castillo-Michel, H., Hernandez-Viezcas, J. A., Diaz, B. C., Peralta-Videa, J. R. and Gardea-Torresdey, J. L. (2012). Synchrotron micro-XRF and micro-XANES confirmation of the uptake and translocation of TiO_2 nanoparticles in cucumber (*Cucumis sativus*) plants. *Environmental Science & Technology* 46: 7637-7643.

Shaviv, A. and Mikkelsen, R. L. (1993). Controlled-release fertilizers to increase efficiency of nutrient use and minimize environmental degradation-A review. *Fertilizer Research* 35: 1-12.

Singh, B. and Ryan, J. (2015). Managing Fertilizers to Enhance Soil Health. *International Fertilizer Industry Association, Paris*, 1-24.

Stampoulis, D., Sinha, S. K. and White, J. C. (2009). Assay-dependent phytotoxicity of nanoparticles to plants. *Environmental Science & Technology* 43: 9473-9479.

Stoline, M. R. (1981). The status of multiple comparisons: simultaneous estimation of all pairwise comparisons in one-way ANOVA designs. *The American Statistician* 35: 134-141.

Tabatabai, M. A. (1982). Soil enzymes. In Page, A. L. (Ed.) *Methods of soil analysis, Part 2, chemical and microbiological properties*, American Society of Agronomy, Madison WI, p. 903-947.

Tabatabai, M. A. and Bremner, J. M. (1969). Use of p-nitrophenyl phosphate for assay of soil phosphatase activity. *Soil Biology and Biochemistry* 1: 301-307.

Tadano, T. and Sakai, H. (1991). Secretion of acid phosphatase by the roots of several crop species under phosphorus-deficient conditions. *Soil Science and Plant Nutrition* 37: 129-140.

Tisdale, S. L. and Nelson, W. L. (1966). Soil fertility and fertilizers. *Soil Science* 101:346.

US-EPA (U.S. Environmental Protection Agency), 1996. Ecological Effects Test Guidelines (OPPTS 850.4200) Seed germination/root elongation toxicity test, available at http://www.epa.gov

Uzu, G., Sobanska, S., Sarret, G., Munoz, M. and Dumat, C. (2010). Foliar lead uptake by lettuce exposed to atmospheric fallouts. E*nvironmental Science & Technology* 440: 1036-1042.

Verma, A. and Stellacci, F. (2010). Effect of surface properties on nanoparticle–cell interactions. *Small* 6: 12-21.

Wang, H., Kou, X., Pei, Z., Xiao, J. Q., Shan, X. and Xing, B. (2011). Physiological effects of magnetite (Fe_3O_4) nanoparticles on perennial ryegrass (Lolium perenne L.) and pumpkin (Cucurbita mixta) plants. *Nanotoxicology* 5: 30-42.

Wei, Y., Shohag, M. J. I., Yang, X. and Yibin, Z. (2012). Effects of foliar iron application on iron concentration in polished rice grain and its bioavailability. *Journal of Agricultural and Food Chemistry* 60: 11433-11439.

Wei, Y., Shohag, M. J. I., Ying, F., Yang, X., Wu, C. and Wang, Y. (2013). Effect of ferrous sulfate fortification in germinated brown rice on seed iron concentration and bioavailability. *Food Chemistry* 138: 1952-1958.

Wong, M. H. and Bradshaw, A. D. (1982). A comparison of the toxicity of heavy metals, using root elongation of rye grass, *Lolium perenne*. *New Phytologist* 91: 255-261.

Yang, F., Liu, C., Gao, F., Su, M., Wu, X., Zheng, L. and Yang, P. (2007). The improvement of spinach growth by nano-anatase TiO_2 treatment is related to nitrogen photoreduction. *Biological Trace Element Research* 119: 77-88.

Yemm, E. W. and Willis, A. J. (1954). The estimation of carbohydrates in plant extracts by anthrone. *Biochemical Journal* 57: 508.

Ze, Y., Liu, C., Wang, L., Hong, M. and Hong, F. (2011). The regulation of TiO_2 nanoparticles on the expression of light-harvesting complex II and photosynthesis of chloroplasts of *Arabidopsis thaliana*. *Biological Trace Element Research* 143: 1131-1141.

Zhang, D., Hendricks, D. G., Mahoney, A. W. and Cornforth, D. P. (1985). Bioavailability of iron in green peas, spinach, bran cereal, and cornmeal fed to anemic rats. *Journal of Food Science* 50: 426-428.

Zhao, L., Sun, Y., Hernandez-Viezcas, J. A., Hong, J., Majumdar, S., Niu, G. and Gardea-Torresdey, J. L. (2015). Monitoring the environmental effects of CeO_2 and ZnO nanoparticles through the life cycle of corn (*Zea mays*) plants and *in situ* μ-XRF mapping of nutrients in kernels. *Environmental Science & Technology* 49: 2921-2928.

Zhu, H., Han, J., Xiao, J. Q. and Jin, Y. (2008). Uptake, translocation, and accumulation of manufactured iron oxide nanoparticles by pumpkin plants. *Journal of Environmental Monitoring* 10: 713-717.

Zielińska-Dawidziak, M. and Siger, A. (2012). Effect of elevated accumulation of iron in ferritin on the antioxidants content in soybean sprouts. *European Food Research and Technology* 234: 1005-1012.

Chapter VII
Toxicological Assessment of Nanotechnology Derived Food

Preface

This chapter discusses assessment of toxicological potential of nanotechnology derived food in rodents. In a 90-day sub-acute repeated dose oral toxicity experiment, the effect of magnetite nanoparticles (100 mg L^{-1}) sprayed wheat on female wistar rats was evaluated. The toxicity of test substance was compared with other experimental variables. Essential checkpoints like monitoring of health status, food and water intake by animals were carried out throughout the feeding trial followed by measurement of haematological and clinical biochemistry parameters. Examination of gross necroscopy and histopathology of selected tissues at terminal sacrifice were also performed. The obtained results show no toxicity of nanotechnology derived food under experimental conditions.

7.1 Introduction

The science of nanotechnology has incredible potential to revolutionize many aspects of human life. However, the benefits may come with some price. One of the major questions faced by the world before accepting nanotechnology is "Whether the unknown risks of nanoparticles including their environmental and health impact, prevail over their potential benefits". The risks associated with application of nanoparticles are yet to be evaluated. This consideration has developed the field of 'nanotoxicology', which is responsible for assessing the toxicological potential as well as promoting safe design and use of nanoparticles (Oberdörster et al. 2005). Therefore, a systematic and thorough quantitative analysis regarding the potential health impacts, environmental clearance and safe disposal of nanoparticles can lead to improvements in designing further applications of nanotechnology (Meng et al. 2009).

Although no direct human diseases have been linked to nanoparticles so far, early experimental studies indicate that nanoparticles could initiate adverse biological responses that can lead to toxicological outcomes (Nel et al. 2006). Nanoparticles which constitute a part of ultrafine particulate matter, can enter in human/ animal system through oral, respiratory or intra-dermal routes. Currently, there is a common assumption that the small size of nanoparticles allow them to easily enter cells, tissues, cells, organelles and interact with functional biomolecular structures (i.e. DNA, ribosomes) since the actual physical size of an engineered nanostructure is similar to many biological molecules (e.g. antibodies, proteins) and structures (e.g. viruses). A corollary is that the entry of the nanoparticles into vital biological systems could cause damage, which could subsequently cause harm to human health (Xia et al. 2009).

One of the most disgustful scenarios is the lack of concrete technical data on toxicological aspect of nanoparticles giving opportunity to both nanotechnology proponents and opponents to make contradictory, unscientific and sweeping conclusions about the safety of nanoparticles. This atmosphere of uncertainty is precisely the feature of nanotechnology that causes cynics the greatest concern (Colvin 2003). Herein, arises a need for proper physico-chemical characterization, determination of appropriate exposure protocols and reliable methods for assessing nanoparticle's outcome in environment, their internalization and kinetics in living organisms. Once these issues are addressed, optimal experimental conditions could be established in order to identify if a particular nanoparticle poses a threat to human health (Thomas and Sayre 2005). Multidisciplinary research between materials scientists, environmentalists and life scientists should overcome these limitations in identifying the true hazards of nanotechnology. Sadly, the risk assessments of nanotechnology are partly subjective and likely to be highly politicized.

Disastrously, no single scenario for describing risks and controls can be universally applied to conclude the outcome due to the heterogeneous and developmental nature of nanotechnology. Also, an absence of standardized methodologies and guidelines makes it

difficult to compare the safety/ toxicity assessments from different research groups (Dhawan et al. 2009). The ethical issues will be specific only for the knowledge base at a given time and for a specified product and its exposure scenario. Moreover, maintaining utmost specificity regarding design of experiments, alternative assessments are needed to take into consideration ethical, social and political values that relate policies such as those involving nanotechnology (Schulte and Salamanca-Buentello 2007). Before interpreting toxicological data, it is thus essential to calculate and determine the expected concentrations of nanoparticles that may be exposed to the biological system or present in the ecosystem.

The use of nanotechnology in agriculture is significantly important as it directly affects humans (Bouwmeester et al. 2009). Nano-fertilizers enable nanoparticles to enter in the food chain allowing their distribution in every organism related to the food chain. As all substances, from arsenic to table salt are toxic to plants, animals or humans at some exposure level; this would not limit their use in various applications which are designed keeping in mind the critical exposure concentration. As discussed in most of the studies regarding use of nanoparticles for promoting growth of plants focus on using lower concentration of nanoparticle, it can be argued that it will pose insignificant health and environmental damage (Colvin 2003).

Many countries have identified the potential of nanotechnology in the food and agriculture sectors and are investing significantly in its applications to food production. However, owing to our limited knowledge of the human health effects of these applications, these countries recognize the need for early consideration of the food safety implications of the nanotechnology. As suggested by scientific committee of European Food Security Authority (EFSA), "the risk assessment paradigm (hazard identification, hazard characterization, exposure assessment and risk characterization) is applicable for nanoparticles (EFSA Scientific Committee 2011). However, risk assessment of these nanoparticles in the food and feed area should consider the specific properties of the subject (tested) nanoparticles in addition to those common to the equivalent non-nanoforms". It is most likely that different types of nanoparticles vary as to their toxicological properties. The available data on oral exposure to specific nanoparticles and any consequent toxicity are extremely limited; the majority of the available information on toxicity of nanoparticles is from *in vitro* or *in vivo* studies using other routes of exposure. The risk assessment of nanoparticles has to be performed on a case-by-case basis. Various parameters may be included in deciding the risk associated with use of any particular nanoparticle in food and feed. These include physio-chemical characterization of nanoparticles, its stability in the food and feed, exposure scenario of the nanoparticles from food and feed, toxico-kinetics (absorption, distribution, metabolism/ biotransformation, excretion/ elimination) within the human and animal systems. The Nanotechnology Regulatory Science Research Plan of United States Food and Drug Administration (FDA) lays out a framework and implementation plan to provide coordinated leadership on regulatory science activities and

issues related to FDA-regulated products that either contain nanoparticles or otherwise involve the application of nanotechnology to address key scientific gaps in knowledge, methods, or tools needed to make regulatory assessments of these products (Chaudhry and Castle 2011).

Based on the importance of biological risk assessment of crop and/ or food either grown or developed using nanoparticle or nanotechnology henceforth called as "nanotechnology derived food", a first of its kind study was planned as described in the present chapter. The wheat crop treated with iron oxide nanoparticles (IONPs) as discussed in chapter VI was used as "nanotechnology derived food" and its toxicity was assessed on female wistar rat. Among the various types of IONPs used, magnetite nanoparticles (N-Fe_3O_4) showed highest increase in plant growth and grain iron content and at iron concentration of 100 mg L^{-1}, thus was selected as test substance for the study. Based on the available guidelines, a 90-day sub-acute repeated dose oral toxicity study was performed. Various checkpoints like monitoring of health status, food and water intake by animals was carried out throughout the feeding trial followed by the measurement of haematological as well as clinical biochemistry parameters and examination of gross necroscopy and histopathology of selected tissues at terminal sacrifice.

7.2 Materials and methods

7.2.1 Permissions and experimental guidelines

The experimental procedures on animals were carried out with permission from "Institutional Animal Ethics Committee" of Birla Institute of Technology & Science, Pilani, India (Protocol No. IAEC/RES/16/02). The study proposal was in compliance with the relevant and latest available scientific opinion by EFSA entitled "Guidance on the risk assessment of the application of nanoscience and nanotechnology in the food and feed chain" compiled by EFSA Scientific Committee (2011). Based on EFSA suggestions, guideline No. 408 (Repeated dose 90-day oral toxicity study in rodents) issued by Organisation for Economic Co-operation and Development (OECD) was followed for drafting the experimental design with justifiable modifications (OECD 1998).

7.2.2 Materials

The magnetite nanoparticles (N-Fe_3O_4) used in the present study were procured from Sigma-Aldrich (Sigma-Aldrich USA). All others chemicals were purchased from Merck Chemicals (Merck KGaA, Germany) unless otherwise stated. Diagnostic kits used for the biochemical estimation were procured from commercial manufacturer Spinreact, Spain. The spectrophotometric observations were recorded on a Multiscan Go plate reader (Thermo Scientific, USA).

7.2.3 Feed preparation and analysis

As the study was designed to assess the toxicity of nanotechnology derived food, wheat plants obtained from the sub-pilot field experiment mentioned in Chapter VI was used as feed. Among the various treatments evaluated to study the effect of IONPs on wheat, plants foliar sprayed with N-Fe_3O_4 (100 mg L^{-1}) resulted in highest increase in plant biomass as well as seed iron content. Therefore, the harvested plants of this treatment including grains were used as test substance. The effect of test substance was compared with similar concentrations of its non-nanoform counterpart i.e. ferrous sulphate ($FeSO_4$) sprayed wheat along with control wheat plants and feed with Fe_3O_4 nanoparticles. Animals fed with routine rat chow were used as control treatment. In each case, the wheat plant with grains were finely crushed and grounded and mixed with powdered rat chow to obtain 33 % (w/w) of the additive/ supplement. The formulation was moulded in the form of small balls (20-30 mm) using 1 % (w/v) carboxymethyl cellulose as binding agent. Fresh feed balls were prepared weekly, dried at 40° C and stored in dry place until these were used as feed to the animals.

Iron content in feed sample groups was estimated using Atomic Absorption Spectroscopy (AAS). For this purpose, 1 g of formulated feed was acid digested by di-acid method. Briefly, 3 mL of conc. HNO_3 was added to the sample (1.0 g) and incubated in a sealed glass container for 6 h at room temperature for pre-digestion. After which, 2 mL of conc. HNO_3 and 1 mL of $HClO_4$ was added to the pre-digested sample and heated at 200 °C for 2 h on a hot plate. Later, the temperature was raised to 300 °C and heated till the white fumes started generating and remaining sample volume becomes less than 1 mL. Finally, the contents within the container was washed repeatedly with Milli-Q water and the washings were filtered through 0.22 µm nylon-66 membrane and collected in a volumetric flask to achieve final volume of 50 mL. The resulting solution was subjected for AAS analysis on an AA-7000 series spectrophotometer (Shimadzu Corporation, Japan).

7.2.4 Animals and housing

The feeding trials were performed in compliance with good laboratory practices at BITS Pilani Animal House facility using female Wistar Rats (*Rattus norvegicus*). The animals were purchased from Chaudhary Charan Singh Haryana Agricultural University, Hisar, India. The animals were housed under same room of 23 ± 2 °C with relative humidity under $60 \pm 5\%$. Light and dark period were maintained on 12:12 h light/ dark cycle and each animal was provided free access to food and filtered water. The experiment as discussed in the later sections was started after 10 days (acclimatization period) of their delivery to the animal testing facility (i.e. 3rd September, 2013). All experiments using live animal were carried out between 09.00 A.M. to 03.00 P.M.

7.2.5 Study design

In order to decide the number of animals to be placed in each group, a crude formula based on the law of diminishing return known as "resource equation" method used rather the robust power analysis method (Charan and Kantharia 2013). The reason for choosing the crude method was inability to assume the expected outcome and standard deviation in various analysis as no similar previous study findings were available to be used as reference. In resource equation method, using one way ANOVA, degree of freedom "E value" (total number of animals - total number of groups) was calculated. Theoretically, any sample size with "E value" between 10 and 20 shall be considered as adequate. In our study, we found that keeping a minimum of five animals per group would solve our purpose. However, after meticulous discussion and study based on the available literature on toxicity, we decided to use ten animals per group. Later on, after successful completion of the study and analysis of results, back calculation was carried out using power analysis by taking mean value of various parameters with their respective standard deviations and p value (0.05) (http://www.biomath.info/power/ttest.htm). As determined, 6-8 animals were required as minimum sample size for each group which was lower than the number of animals used by us in the present study.

As per the OECD guideline 408, 7-8 weeks old rats with an average weight of 170 ± 23 g were selected for the 90-day repeated dose oral toxicity study. The percent variation in the weight of selected rats was calculated to be 13.5 % of the mean value which was far less than the maximum permitted value of 20 %. Out of ten animals per group, three to four animals were caged together in such a way that the average weight between groups was similar. The animals were subjected to their respective diet by placing the freshly prepared feed balls (pre-weighed) in cages (Table 7.1). The animals were allowed to eat *ad libitum*. Fresh food was made available after every 24 hours unless required.

Table 7.1 Details of the experimental groups included in the study.

Groups	Diet Description	
	Base	Additive (33 % w/w)
A	Animal Chow	---
B	Animal Chow	Control wheat plant
C	Animal Chow	Wheat plants sprayed with N-Fe_3O_4 [100 mg (Fe) L^{-1}]
D[*]	Animal Chow	Commercially available Fe_3O_4 nanoparticle
E	Animal Chow	Wheat plants sprayed with $FeSO_4$ [100 mg (Fe) L^{-1}]

[*]Fe_3O_4 nanoparticle mixed in animal chow to achieve iron concentration of 100 mg L^{-1}.

7.2.6 Pre-sacrifice analysis

7.2.6.1 Periodical health status

Each animal was weighed at the onset as well as end of the study in addition to the routine weighing at every seventh day. Apart from this, rats were inspected (*in cage*) daily for mortality, morbidity, changes in skin, fur, eyes, occurrence of secretions and excretions as well as activity level and behaviour. After every seventh day, detailed physical examination of each rat was conducted by taking the animal outside its cage. The examinations included changes in skin, fur, mucous membranes, secretions and excretions, gait, posture, response to handling, bizarre behaviour and autonomic activity such as lacrimation, piloerection, pupil size, unusual respiration.

7.2.6.2 Food and water intake

As the test substance was administered orally as diet/feed, it was particularly essential to determine the average food consumption by animals within each group. In this regard, the weight of consumed food was recorded daily by subtracting the weight of leftover food in the cage out of the available food. Similarly, water consumption was also monitored.

7.2.6.3 Haematology analysis

One week before the terminal sacrifice, blood samples were collected from each animal using tail vein bleeding for haematological analysis. Parameters viz., red blood cell (RBC), white blood cell (WBC), blood platelet (PLT), mean corpuscle volume (MCV), mean corpuscle haemoglobin concentration (MCHC), haemoglobin (HGB) and haematocrit (HCT) were measured by using a K-4500 automatic blood cell counter (Sysmex Corporation Ltd, Japan).

7.2.6.4 Clinical biochemistry

Blood samples from each animal three days before the terminal sacrifice was collected by retro-orbital bleeding under short influence of general anaesthesia (diethyl ether). The choice of the method for bleeding was chosen as a large blood volume (1.5-1.75 mL) was required for various clinical biochemistry tests (Parasuraman et al. 2010). In order to avoid the severity of the adverse effects that can occur during this bleeding technique, the collection was carried out under the supervision of an authorized and expert veterinarian. Blood was collected in 2 mL micro-centrifuge tubes with or without disodium EDTA for the recovery of plasma and serum, respectively. The aliquots of plasma and serum were immediately stored at -80 ˚C till further use. All the assays mentioned below were performed in technical replicates of three at 25 ˚C room temperature with 48 hours of blood collection. The animals were closely monitored for next 24 hours after anaesthetic recovery.

Creatinine: The concentration of creatinine in plasma was quantified using commercially available kit (Spinreact Reference No. 1001113). The assay was based on the Jaffe reaction wherein creatinine reacted with sodium picrate (alkaline picrate) forming a red colour

complex (Vasiliades 1976). The rate and intensity of the complex formation, measured spectrophotometrically was proportional to the creatinine concentration in the sample. Manufacturer's protocol was followed as such for the assay.

Urea: The concentration of urea in plasma was quantified using commercially available kit (Spinreact Reference No. 1001325). The assay was based on the reaction of urea with o-phthalaldehyde forming a coloured complex (Jung et al. 1975). The intensity of complex formation, measured spectrophotometrically was proportional to the urea concentration in the sample. Manufacturer's protocol was followed as such for the assay.

Alanine aminotransferase (ALT): ALT activity in plasma was detected using commercially available kit (Spinreact Reference No. 1001171). The estimation was based of reversible transfer of an amino group from alanine to α-ketoglutarate forming glutamate and pyruvate by the enzyme. The pyruvate produced was further reduced to lactate by lactate dehydrogenase (LDH) and NADH. The rate of decrease in concentration of NADH, measured spectrophotometrically, was proportional to the catalytic concentration of ALT present in the sample (Wilkinson et al. 1972). Manufacturer's protocol was followed as such for the assay.

Aspartate aminotransferase (AST): AST activity in plasma was detected using commercially available kit (Spinreact Reference No. 1001161). The estimation was based on the reversible transfer of an amino group from aspartate to α-ketoglutarate forming glutamate and oxaloacetate. The oxaloacetate produced was further reduced to malate by malate dehydrogenase (MDH) and NADH. The rate of decrease in concentration of NADH, measured spectrophotometrically, was proportional to the catalytic concentration of AST present in the sample (Wilkinson et al. 1972). Manufacturer's protocol was followed as such for the assay.

Albumin: The concentration of albumin in plasma was quantified using commercially available kit (Spinreact Reference No. 1001020). The estimation was based on reaction of albumin with bromocresol green at a slightly acid pH, producing a colour change of the indicator from yellow-green to green-blue (Doumas et al. 1971). The intensity of the colour formed was proportional to the albumin concentration in the sample. Manufacturer's protocol was followed as such for the assay.

Alkaline phosphatase (ALP): ALP activity in the serum was detected using commercially available kit (Spinreact Reference No. 1001131). The reaction was based on the activity of ALP which catalysed the hydrolysis of p-nitrophenyl phosphate at pH 10.4, liberating p-nitrophenol and phosphate (Bessey et al. 1946). The rate of p-nitrophenol formation, measured spectrophotometrically, was proportional to the catalytic concentration of ALP present in the sample. Manufacturer's protocol was followed as such for the assay.

Antioxidant assay: The total antioxidant capacity of the plasma obtained from rats of various groups was measured by a commercially available antioxidant assay kit (Item No.

709001; Cayman Chemical Company, USA). As per the manufacturers information, the kit was capable of measuring the total/combined antioxidant capacity (aqueous and lipid soluble antioxidants) of plasma generated by antioxidant activities of all its constituents including vitamins, proteins, lipids, glutathione, uric acid, etc. The assay relied on the ability of antioxidants in the sample to inhibit the oxidation of ABTS$^{\circledR}$ (2,2'-Azino-di-[3-ethylbenzthiazoline sulphonate]) to ABTS$^{\circledR \bullet +}$ by metmyoglobin (Re et al. 1999). The amount of ABTS$^{\circledR \bullet +}$ produced was monitored by reading the absorbance at 750 nm. The degree of suppression of absorbance was proportional to the antioxidant's concentration. The capacity of the antioxidants in the sample to prevent ABTS$^{\circledR}$ oxidation was compared with the stabdard graph obtained using Trolox, a water-soluble tocopherol analogue.

7.2.7 Post-sacrifice analysis

Terminal sacrifice in a humane manner of all the animals was done on the ninetieth day of the study. Animals were anesthetized with diethyl ether and killed by cervical dislocation under the supervision of an authorized veterinarian. Liver and kidney tissues from each animal were collected and processed immediately. The extracted tissue samples were washed thrice with chilled phosphate buffered saline (PBS; 1×, pH 7.4). One part of the tissue was used for iron quantification while other part was used for gross necroscopy and histopathology.

7.2.7.1 Iron accumulation in tissues

Level of accumulated iron, if any in liver and kidney samples was determined by atomic absorption spectroscopy (AAS). For this purpose, freshly extracted, PBS washed tissue samples (1.0 g) were acid digested using di-acid method as described in section 7.2.3.

7.2.7.2 Histopathology

Tissue samples obtained from the scarified rats after washing with PBS were fixed in 10 % buffered formalin for 12 hours. After fixation, the tissues were subjected to dehydration with 30 % ethanol (15 min) followed by 50 % ethanol treatment for 15 min. Later on, final dehydration was carried by treating tissue with 70 % ethanol twice for 15 min each. The as-dehydrated samples were sent to National Institute of Pathology, New Delhi for further sample processing and analysis. The tissues were carefully processed for paraffin embedding in a tissue processor. Blocks were made using plastic moulds and incubated at low temperature which resulted in solidification of paraffin. Sections precisely 3 µm thick were sectioned using a microtome. The sections were stained with haematoxylin and eosin (H & E) and mounted in DPX for visualization under light microscope. Assistance of a professional histopathologist was employed to study the architectural changes in liver and kidney across all groups. The pathologist performing the histological evaluations was masked to the treatment allocations to reduce biasness.

7.2.8 Data analysis

The obtained data were analysed using Prism® software (Version 6.0; GraphPad Software Inc., USA). Outliers (animals showing minimum and maximum value in each assay) were neglected from the final calculations. The effect of various treatments were statistically analysed using one way ANOVA (Stoline 1981). When ANOVA revealed significant differences among treatments, post-hoc test was conducted with Dunnett's method, which demonstrates pair wise differences between each treatment and the control (Dunnett 1955). Symbol *ns* used in the graphs shall be interpreted as statistically non-significant at $P > 0.05$ as compared to control. All data points represent the mean of independent measurements. Uncertainties were represented as standard deviations.

7.3 Results and discussion

The effect of nanoparticles on growth and development of plants is an important aspect as it holds great ecological as well as economic prospects (Solanki et al. 2015). Although a considerable increase in the above ground biomass was observed in the wheat sprayed with a lower concentration of IONPs, a non-significant change (neither increase nor decrease) was found in the yield and nutritional quality of grains during field study (details in chapter VI). Noticeably, a significant increase was observed in the grain iron content of plants sprayed with lower concentrations of IONPs with the highest recorded content at 100 mg (Fe) L^{-1} concentration. These results were very much to our surprise as during the experiment, the sprays were carried out only in the vegetative phase (milk stage) of wheat with no chance of direct nanoparticle exposure to grains. This increased grain iron content can only be a consequence of nanoparticles or IONPs sourced iron translocation from the foliar sprayed leaves to the fruiting body and subsequently to the grains. However, the increased iron content in the above ground biomass (without cob) with the treatments at higher concentrations during the field study would have been due to the deposition of IONPs on the plant surface, because of their strong surface adsorption property rather than their uptake within the plant tissues (Verma and Stellacci 2010).

These results encouraged us to design an elaborative and convincing experiment to assess the toxicity of food, in present case wheat derived using IONPs as source of nutrient "nano-fertilizer". Among the various type of tested IONPs viz., maghemite (N-Fe_2O_3), magnetite (N-Fe_3O_4) and biosynthesized magnetite (B- Fe_3O_4) nanoparticles, on the basis of results obtained it was deduced that N-Fe_3O_4 at lowest tested concentration (100 mg L^{-1}) resulted in maximum increase in the grain iron content. Hence, it was used as the test substance. Toxicity of test substance (wheat sprayed with 100 mg (Fe) L^{-1} of N-Fe_3O_4) mixed with rat chow (@ 33% w/w) was compared with chow containing control wheat; 100 mg (Fe) L^{-1} N-Fe_3O_4 as such and wheat sprayed with 100 mg (Fe) L^{-1} of $FeSO_4$ (Table 7.1). The notion behind inclusion of a group consisting of animals fed on a diet supplemented directly

with Fe_3O_4 nanoparticles was to mimic the maximum possible exposure scenario, wherein none of the sprayed nanoparticles were converted to non-nano forms and were still present in their native state in the test substance. For the utilization of nano-form in the plant metabolism, the dissociation of metal oxide nanoparticles in their respective ions is necessary. Therefore, a group consisting of animals fed on a diet supplemented with $FeSO_4$ sprayed wheat was included in order to relate the nano-form toxicity to ionic form, if any. Commercially available routine animal chow was used as control in the study. The study was planned on rats, keeping in mind the natural scenario where the rats rather than eating only the grain portion actually consume the whole plant, the overall dried plant including its cob containing grains was used as additive in the diet.

Various studies related to the assessment of toxicity of genetically modified (GM) food were considered in designing the experiment (Schrøder et al. 2007; Zeljenková et al. 2014). Based on the thorough literature search, the 90 day repeated dose oral toxicity study as per OECD guideline no. 408 was selected. It is known to be the most appropriate test study for the detection of a wide range of toxicological endpoints (Séralini et al. 2011; Delaney 2015). The guideline was also suggested by European Food safety Authority (EFSA), the only appropriate risk assessment guide for nanotechnology derived food (EFSA Scientific Committee 2011). The experiment was executed as a 90-day sub-chronic oral toxicity study using repeated dosing of the test substance. The aim of the present study was to assess the risk of nanotechnology derived food in rodents rather than establishing a formal dose-response curve. Thus, the proportion of test substance or additive to be mixed in animal chow was selected at 33 % (w/w) based on thorough review of several reports on GM food risk assessment. Majority of the studies reported incorporation of GM food at 33 % (w/w) as the highest level in the animal feed so as to prevent the nutritional distortion in rodent's natural diet (EFSA 2008).

7.3.1 Food iron content

A detailed quantitative analysis of the iron in the formulated diet groups used in the feeding trial was performed by AAS analysis. The animal chow used in the present study was found to contain 239 ± 0.82 mg kg^{-1} of iron. Control wheat plant mixed with animal chow resulted in slight increase in iron content (256 ± 2.46 mg kg^{-1}). However, addition of wheat sprayed with $FeSO_4$ and N-Fe_3O_4 lead to significant increase in the iron i.e. 281 ± 6.83 mg kg^{-1} and 301 ± 7.39 mg kg^{-1}, respectively. The highest increase of nearly 41 % (337 ± 9.64 mg kg^{-1}) was due to the addition of Fe_3O_4 nanoparticles (as such) in the animal chow. The content of iron in the routine animal chow was in accordance with the reported values (Reeves et al. 1993).

7.3.2 Periodical health status

All the animals irrespective of their group managed to survive till the end of the study with no adverse effect on animal health. All the rats were carefully monitored for behaviour,

appearance, infections and palpable health issues. The daily clinical observations did not reveal any signs of functional deficits, morbidity and mortality in the animals.

7.3.3 Body weight and feed consumption

Animal body weight was measured weekly. During the experiment, a time dependent increase in the average body weight of all the animals in various experimental groups was observed and reached upto maximum of 240 g at 9th week of the study (Figure 7.1a). The time dependent increase in body weight observed during the present study is in accordance with the published reports (Poulsen et al. 2007; Schrøder et al. 2007). However, diet dependent variation between experimental groups was found to be non-significant during the study period (90 days).
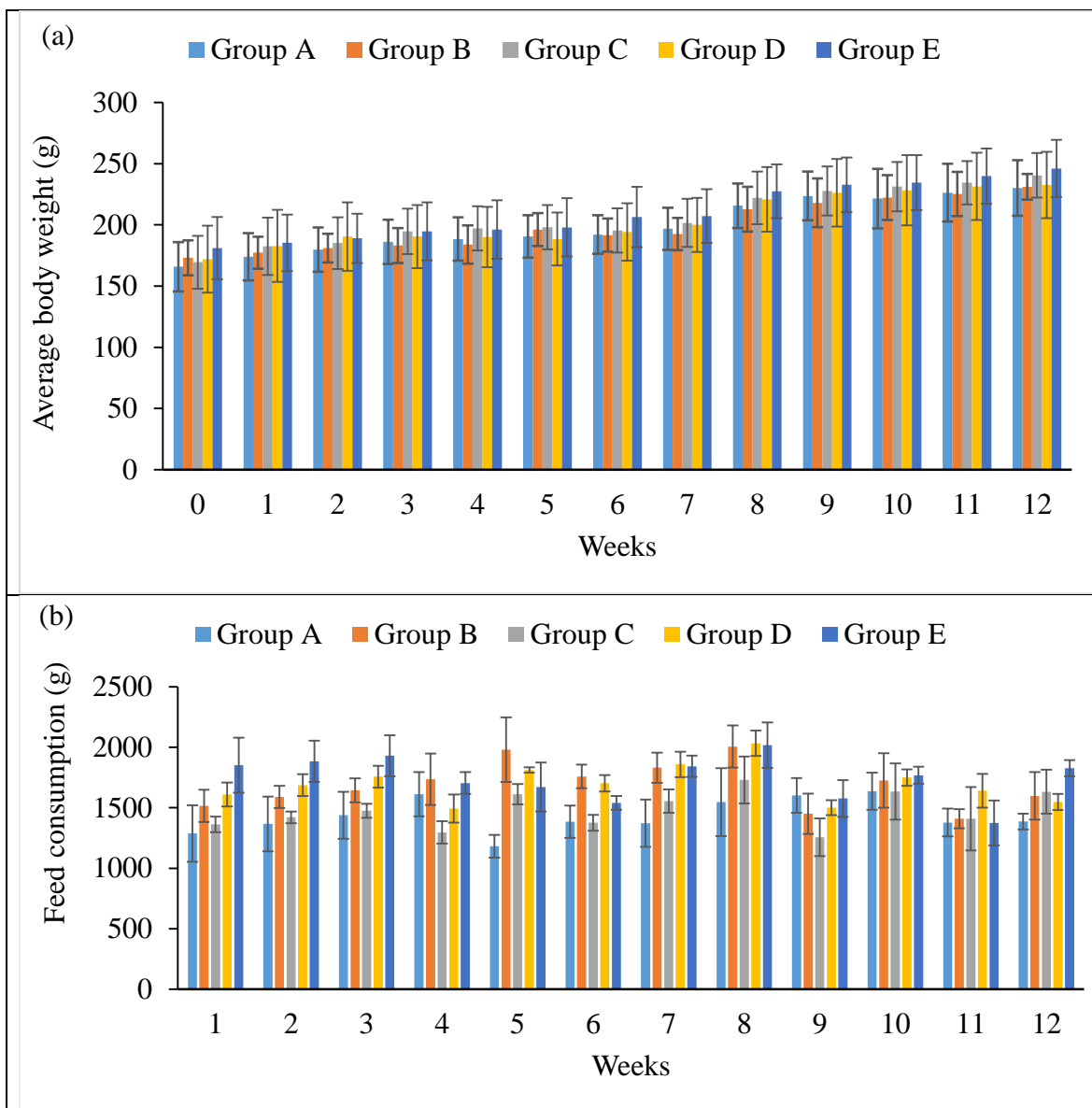

Figure 7.1 (a) Average weekly body weights of animals in different groups (b) Average feed consumption per week per group. Vertical bars represent standard deviation (n=8)

None of the animals showed any rejection to the given diet. The average food consumption rate per day was recorded the data are represented as average food consumption per week per group. In general, feed consumption remained statistically constant throughout the study for all the animals irrespective of their groups (Figure 7.1b). No significant change in the water consumption rate was observed throughout the study (data not shown). The average food and water consumption rate was in agreement with published literature (Vickery 1984; Zeljenková et al. 2014). The uneven trend observed in the average food consumption rate may be due to the eccentric eating habits of a single animal within a group even for some time.

7.3.4 Haematological parameters

Haematology parameters such as RBC, WBC and PLT count, measurement of MCV, MCHC, HGB and HCT were analysed near the end of the study (Table 7.2). Marginal yet statistically significant increase in WBC count was observed in animals of group D. However, all other tested parameters were found to be non-significant as compared to control (Group A) Furthermore, the obtained values were within the range described for individual parameters in other animals of same strain, age and sex (Schrøder et al. 2007; Zeljenková et al. 2014).

Table 7.2 Haematological parameters of animals in various experimental groups (n=8).

Parameter	Group A	Group B	Group C	Group D	Group E
RBC $(10^6 \ \mu L^{-1})$	7.23 ± 0.32	7.05 ± 0.29	6.89 ± 0.38	6.81 ± 0.42	6.95 ± 0.35
WBC $(10^3 \ \mu L^{-1})$	9.99 ± 1.44	10.17 ± 1.24	10.41 ± 1.33	$10.86* \pm 1.67$	10.33 ± 1.29
PLT $(10^3 \ \mu L^{-1})$	739 ± 34	745 ± 29	752 ± 32	749 ± 44	750 ± 37
MCV (fL)	55.32 ± 0.82	55.26 ± 1.02	55.35 ± 0.78	55.23 ± 1.22	55.29 ± 0.96
MCHC $(g \ dL^{-1})$	33.81 ± 0.61	33.92 ± 0.59	34.03 ± 0.62	34.07 ± 0.60	33.98 ± 0.55
HGB $(g \ dL^{-1})$	14.37 ± 0.47	14.24 ± 0.38	14.42 ± 0.51	14.80 ± 0.57	14.29 ± 0.42
HCT (%)	43.63 ± 1.38	43.68 ± 1.25	43.81 ± 1.19	43.92 ± 1.43	43.75 ± 1.21

± represent standard deviation (n=8); *Significant difference ($p < 0.05$)

7.3.5 Clinical biochemistry

Measurement of various clinical biochemistry parameters viz., creatinine, urea, ALT, AST, albumin, APL and total anti-oxidant capacity (TAC) were recorded in the blood serum and plasma were carried in order to assess the effect of various diet groups on renal and hepatic functions (Figure 7.2).
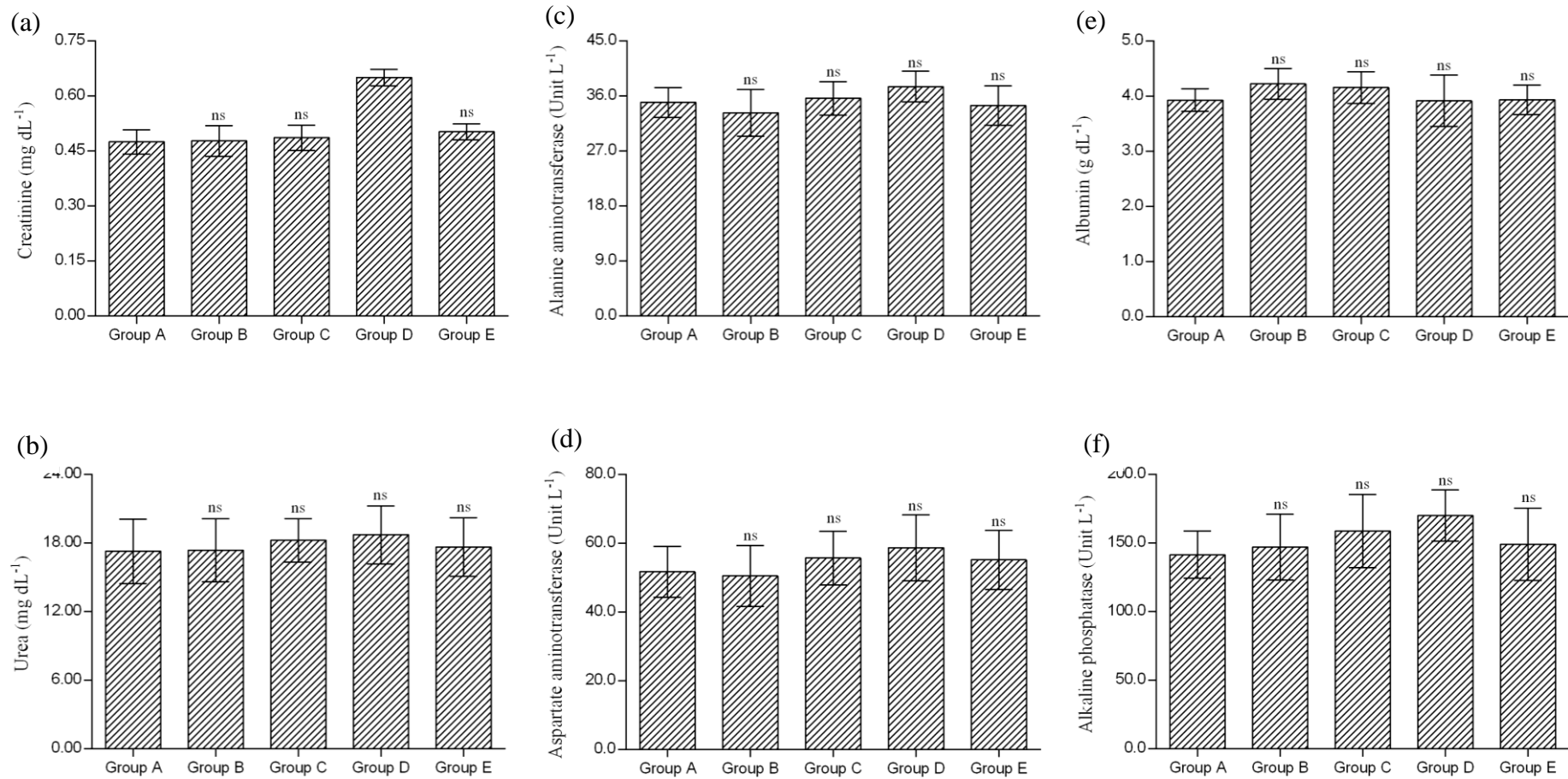
Figure 7.2 Clinical biochemistry parameters measured in the blood of experimental animals (a) Creatinine (b) Urea (c) Alanine amino transferase (d) Aspartate amino transferase (e) Albumin (f) Alkaline phosphatase. Vertical bars represent standard deviation (n=8). Non-significant difference ($p < 0.05$) as compared to control are marked as "ns"

Creatinine is a breakdown product of creatine phosphate, an energy reservoir molecule in muscles. The creatinine production depends on the muscular mass and usually its level in the blood is maintained. Creatinine is removed from the blood mainly by the kidneys, primarily by glomerular filtration. If the filtration by the kidney is deficient, creatinine level in the blood rises. Therefore, creatinine levels in blood were used to check the effect of various diet on renal efficiency (Gowans and Fraser 1988). In the present study, a non-significant change in the plasma creatinine level, which is considered as a marker of kidney function was observed in all the treatments except in the group directly fed with N-Fe_3O_4 nanoparticles as compared to control. Elevated level of creatinine in animals of group D indicated that nanoparticles (mixed in food) may be negatively effecting the renal efficiency. On thorough literature survey, we were unable to come across any report suggesting elevation in creatinine level after exposure to IONPs, whereas many reports suggested that creatinine level remained unchanged (non-significant change) as compared to control animals (Tate et al. 2009; Wang et al. 2010; Uchiyama et al. 2015). Thus, we expect this rise in creatinine level to be an experimental error.

Urea is a waste product of breakdown of proteins and is usually excreted out from the body through urine. A high blood level of urea indicates renal dysfunction and thus may serve as an important parameter (Carvounis et al. 2002). In the present study, a non-significant change was found in the blood urea level in animals of various groups. However, unlike the creatinine assay, measurement of blood urea did not show corresponding (elevated) level in animals of group D. Therefore, the observed difference in the creatinine level cannot be related to clinical or pathological toxicity and thus considered insignificant (Uchino et al. 2012).

The level of serum transaminases (AST and ALT) were also analysed in animals. ALT and AST are found abundantly in the cytosol of hepatocytes. Their activity in the liver is tremendously high as compared to blood. However, conditions pertaining to hepatocellular injury or death releases these transaminases from damaged liver cells which increases their measured level/activity in the blood. Thus, the increased levels of ALT/ AST are sensitive indicators of hepatic injury (Kim et al. 2008). Elevated activities of ALT and AST in animals of group C and D were observed during the analysis. However, the changes were found to be statistically non-significant as compared to control.

The liver is a major producer for most of the blood proteins like albumin and its level in the blood may serve as a liver function test. Albumin acts as a carrier protein for fatty acids, steroids, hormones in the blood and plays a major role in stabilizing oncotic pressure. Variation in the albumin level indicates disturbance in the hepatic activity (Doumas and Peters 1997. The measured values of blood albumin across various treatment groups were within or close to the range observed in the control group describing no effect of the various diet.

Similarly, an increase in ALP level in the blood reflects damage to the integrity of the hepatobiliary system and the flow of bile into the small intestine. Phosphatase is actually

a group of enzymes that hydrolyse monophosphate ester at an alkaline pH. ALP is primarily secreted by the mucosal cells lining the bile system of liver. The proper maintenance of ALP level in the blood indicated free flow of bile through the liver into the biliary tract to the gallbladder. Conditions with improper functioning of liver, bile ducts or gallbladder system results in an increase ALP level in the blood stream (Kaplan 1972). Similar to other liver parameter (ALT, AST and Albumin), non-significant variation was observed in the blood ALP level in various treatment as compared to control.

Reactive oxygen species (ROS) are produced as a consequence of normal aerobic metabolism (Murphy 2009). In general, ROS include the superoxide radical ($O_2\bullet^-$), hydroxyl radical (OH•), hydroperoxyl radical (HO$_2$•), hydrogen peroxide (H_2O_2), alkoxy radical (RO•), peroxy radical (ROO•), singlet oxygen ($^1O_2$) and excited carbonyl (RO*), all of which are cytotoxic to cells (Singh 1982). Unstable free radical species attack cellular components causing damage to lipids, proteins, and DNA which can initiate a chain of events resulting in the onset of a variety of diseases (Rahman 2007). In living systems, the control of oxidative stress and their resulting damage is controlled by the antioxidative systems. These antioxidant systems include enzymes such as superoxide dismutase, catalase, and glutathione peroxidase; macromolecules such as albumin, ceruloplasmin, and ferritin; and an array of small molecules, including ascorbic acid, α-tocopherol, β-carotene, reduced glutathione, uric acid, and bilirubin (Cao and Prior 1998). The sum of endogenous and food-derived antioxidants represents the total antioxidant activity of the system. The cooperation among different antioxidants provides greater protection against attack by reactive oxygen or nitrogen species, than any single compound alone. Thus, the overall antioxidant capacity was determined using commercially available antioxidant assay kit (Cayman Chemical Company, USA) as it provide more relevant biological information as compared to the measurement of individual components.
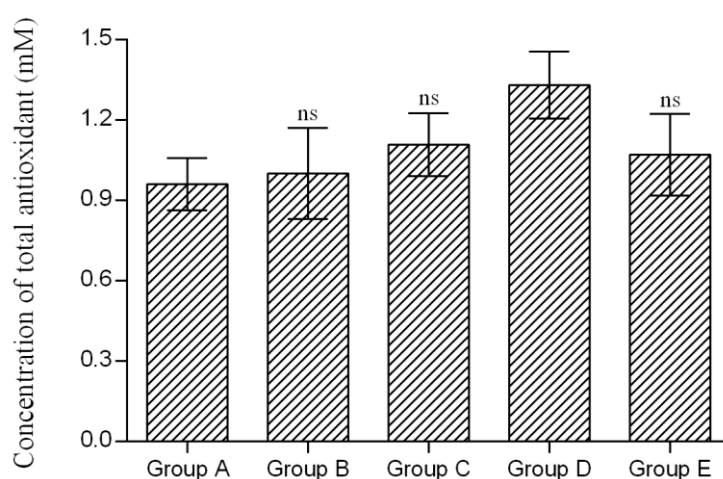

Figure 7.3 Changes in the total antioxidant capacity in various groups. Vertical bars represent standard deviation (n=8). Non-significant difference (p < 0.05) marked as ''ns''

As depicted in Figure 7.3, the total antioxidant capacity in animals across various groups showed an increase. However, except for group D the changes was statistically non-significant. The result obtained in group D was inevitable, as the rise in ROS levels and associated antioxidants on metal or metal oxide nanoparticle exposure is a well-known observation found almost universally in various *in vitro* and *in vivo* studies (Kim et al. 2008; Jain et al. 2008; Iversen et al. 2013; Milto et al. 2014).

7.3.6 Iron accumulation in tissues

Liver and kidney are reported as primary accumulation sites for metal ions and/ or nanoparticles. In order to detect the accumulation of iron in response to various diet groups, liver and kidney samples of the sacrificed animals were subjected to AAS analysis after di-acid digestion (Table 7.3). Iron accumulation in liver and kidney were found to be in accordance to the results obtained in the total antioxidant assay. Liver and kidney samples of group D animals showed significant increase in the iron content as compared to control. This might have triggered higher production of ROS as described earlier (Weissleder et al. 1989; Briley-Saebo et al. 2004). Many other reports regarding *in vivo* toxicity of IONPs in rodent models have also indicated accumulation of these nanoparticles in tissues especially liver and kidney (Kim et al. 2008; Jain et al. 2008; Iversen et al. 2013; Milto et al. 2014).

Table 7.3 Iron content in liver and kidney of animals in various experimental groups.

Group	Liver ($\mu g\ g^{-1}$)	Kidney ($\mu g\ g^{-1}$)
A	398.4 ± 43.16	151.7 ± 15.67
B	404.6 ± 42.43	153.9 ± 16.48
C	432.0 ± 41.31	154.1 ± 11.39
D	$497.2^* \pm 40.93$	$175.8^* \pm 12.26$
E	430.9 ± 40.27	153.6 ± 13.60

$\pm$ represents standard deviation (n=8)

*Significant difference ($p < 0.05$)

7.3.7 Histopathology

Gross necroscopy examination of liver and kidney samples revealed no sign of diet dependent changes. The H & E staining provided a comprehensive microanatomical picture of the liver and kidney (Figure 7.4). Hematoxylin precisely stains nuclear components, including heterochromatin and nucleoli while eosin stains cytoplasmic components including cytoplasmic granules; and extracellular components including collagen & elastic fibres, muscle fibres; and red blood cells (Bancroft and Gamble 2008).

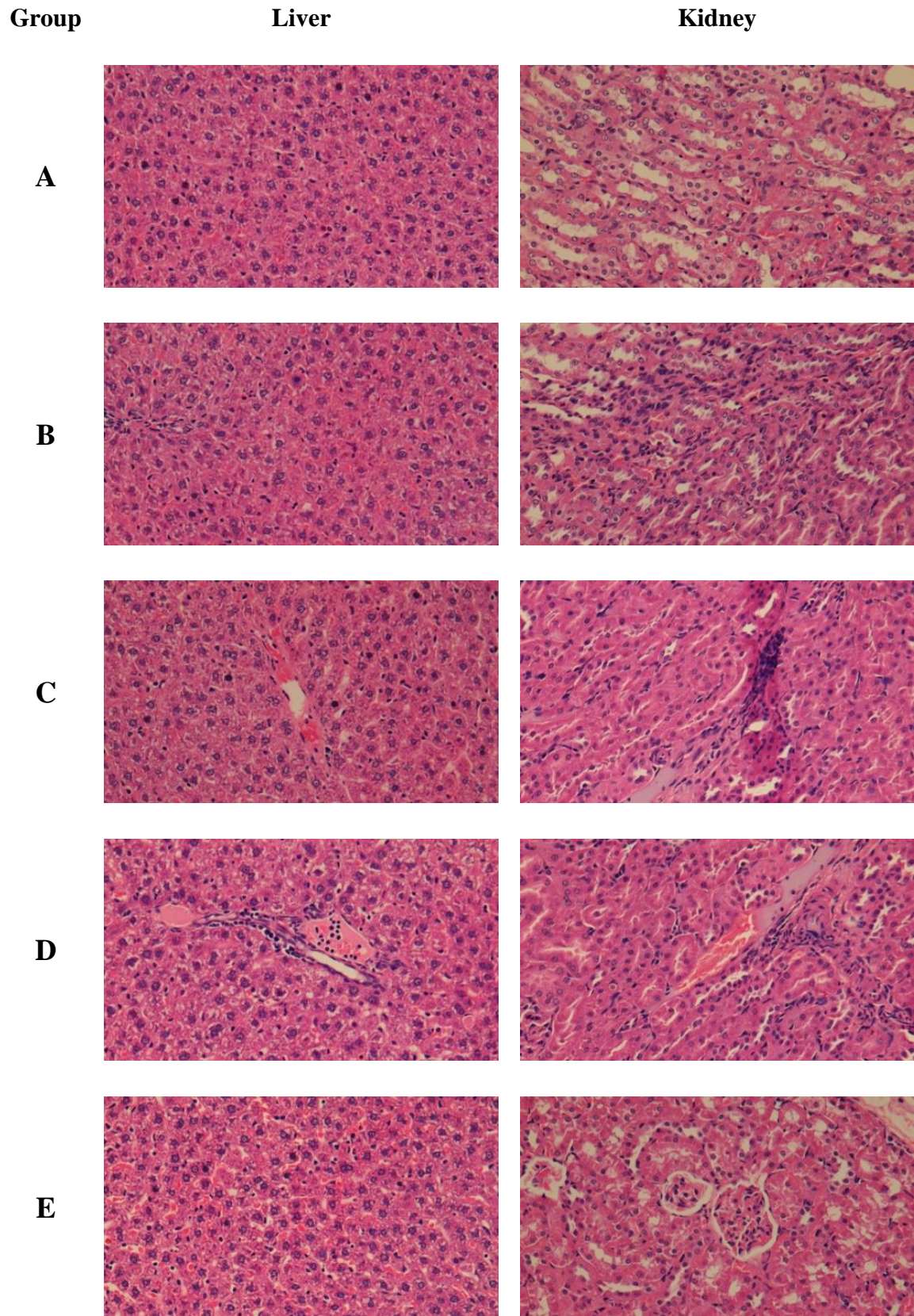| Group	Liver	Kidney
A		
B		
C		
D		
E		

Figure 7.4 Histopathological microscopic view of H & E stained tissues of liver and kidney of animals in various experimental groups (x40 magnification)

Histopathology analysis of liver and kidney tissues revealed no significant adverse effects of the test substances (group B to E) as evidenced by the normal tissue architecture observed in the animals. Mild inflammation resultant of acute biological response was observed at many sites within liver and kidney as shown by the noticeable abundance of lymphocytes. However these histological alterations cannot be pronounced as an indication of cell injury due to test substance, because similar results were witnessed in control groups as well. Overall analysis of all the histopathological samples leads to the conclusion that the gross architecture was intact with no noticeable necrosis or fibrosis within the analysed tissue.

7.4 Conclusions

The present chapter discusses first of a kind study towards safety assessment of nanotechnology derived food using rodent model. In a 90-day sub-acute repeated dose oral toxicity experiment, the effect of wheat sprayed with N-Fe_3O_4 (100 mg L^{-1}), as discussed in chapter VI,was evaluated. The toxicity of test substance on female Wistar rats was compared with judiciously decided experimental variables viz., control wheat, Fe_3O_4 nanoparticles and $FeSO_4$ sprayed wheat at similar concentrations. The measurements were statistically validated as compared to control (routine animal chow). No adverse effect on animal behaviour, general health and body weight were observed during the study. Weekly recording of food and water consumption was also normal across various groups. Blood samples collected near the end of the study were analysed for haematological and clinical biochemistry parameters. A few parameters in animals fed with Fe_3O_4 nanoparticles were significantly different (creatinine and total antioxidant capacity), while all others were within normal reference range of this breed, age and sex of rats, thus may not conclude to any pathological disturbance. At terminal sacrifice, liver and kidney from animals belonging to various groups were isolated and subjected to AAS analysis for determination of iron content, gross necroscopy and histopathological analysis. Iron content in liver and kidney of animals fed with Fe_3O_4 nanoparticles showed significant increase. Moreover, pathologically unrelated and minor changes were observed in histopathology analysis. In conclusion, the wheat plants grown using three consecutive foliar sprays (2-6 L ha^{-1}) of solution with 100 mg L^{-1} iron concentration of commercially available and chemically synthesized Fe_3O_4 nanoparticle suspension exert no toxic effect on female Wistar rat in a feeding trial based on 90-day sub-acute repeated dose oral toxicity test under experimental conditions as evaluated by selected physical, hematological, biochemical and histopathological examinations. Further studies are required in this direction which might support our results or will rather add conclusive experimental data regarding risk assessment of nanotechnology derived food.

7.5 References

Bancroft, J. D. and Gamble, M. (2008). *Theory and practice of histological techniques.* Churchill Livingstone, London, 6th Edition, pp. 744.

Bessey, O. A., Lowky, O. H. and Brock, M. J. (1946). A method for the rapid determination of alkaline phosphatase with five cubic millimeters of serum. *Journal of Biological Chemistry* 164: 321-329.

Bouwmeester, H., Dekkers, S., Noordam, M. Y., Hagens, W. I., Bulder, A. S., De Heer, C. and Sips, A. J. (2009). Review of health safety aspects of nanotechnologies in food production. *Regulatory Toxicology and Pharmacology* 53: 52-62.

Briley-Saebo, K., Bjørnerud, A., Grant, D., Ahlstrom, H., Berg, T. and Kindberg, G. M. (2004). Hepatic cellular distribution and degradation of iron oxide nanoparticles following single intravenous injection in rats: implications for magnetic resonance imaging. *Cell and Tissue Research* 316: 315-323.

Cao, G. and Prior, R. L. (1998). Comparison of different analytical methods for assessing total antioxidant capacity of human serum. *Clinical Chemistry* 44: 1309-1315.

Carvounis, C. P., Nisar, S. and Guro-Razuman, S. (2002). Significance of the fractional excretion of urea in the differential diagnosis of acute renal failure. *Kidney International* 62: 2223-2229.

Charan, J. and Kantharia, N. D. (2013). How to calculate sample size in animal studies? *Journal of Pharmacology and Pharmacotherapeutics* 4: 303-306.

Chaudhry, Q. and Castle, L. (2011). Food applications of nanotechnologies: an overview of opportunities and challenges for developing countries. *Trends in Food Science and Technology* 22: 595-603.

Colvin, V. L. (2003). The potential environmental impact of engineered nanomaterials. *Nature Biotechnology* 21: 1166-1170.

Delaney, B. (2015). Safety assessment of foods from genetically modified crops in countries with developing economies. *Food and Chemical Toxicology* 86: 132-143.

Dhawan, A., Sharma, V. and Parmar, D. (2009). Nanomaterials: A challenge for toxicologists. *Nanotoxicology* 3: 1-9.

Doumas, B. T., Watson, W. A. and Biggs, H. G. (1971). Albumin standards and the measurement of serum albumin with bromcresol green. *Clinica Chimica Acta* 31: 87-96.

Doumas, B. T. and Peters, T. (1997). Serum and urine albumin: a progress report on their measurement and clinical significance. *Clinica Chimica Acta* 258: 3-20.

Dunnett, C. W. (1955). A multiple comparison procedure for comparing several treatments with a control. *Journal of the American Statistical Association* 50: 1096-1121.

EFSA Scientific Committee. (2011). Guidance on the risk assessment of the application of nanoscience and nanotechnologies in the food and feed chain. *EFSA Journal* 9: 2140-2176.

EFSA, GMO. (2008). Safety and nutritional assessment of GM plants and derived food and feed: the role of animal feeding trials. *Food and Chemical Toxicology* 46: S2.

Gowans, E. M. and Fraser, C. G. (1988). Biological variation of serum and urine creatinine and creatinine clearance: ramifications for interpretation of results and patient care. *Annals of Clinical Biochemistry* 25: 259-263.

Iversen, N. K., Frische, S., Thomsen, K., Laustsen, C., Pedersen, M., Hansen, P. B. and Wang, T. (2013). Superparamagnetic iron oxide polyacrylic acid coated γ-Fe_2O_3 nanoparticles do not affect kidney function but cause acute effect on the cardiovascular function in healthy mice. *Toxicology and Applied Pharmacology* 266: 276-288.

Jain, T. K., Reddy, M. K., Morales, M. A., Leslie-Pelecky, D. L. and Labhasetwar, V. (2008). Biodistribution, clearance, and biocompatibility of iron oxide magnetic nanoparticles in rats. *Molecular pharmaceutics* 5: 316-327.

Jung, D., Biggs, H., Erikson, J. and Ledyard, P. U. (1975). New Colorimetric reaction for end-point, continuous-flow, and kinetic measurement of urea. *Clinical Chemistry* 21: 1136-1140.

Kaplan, M. M. (1972). Alkaline phosphatase. *New England Journal of Medicine* 286: 200-202.

Kim, W., Flamm, S. L., Di Bisceglie, A. M. and Bodenheimer, H. C. (2008). Serum activity of alanine aminotransferase (ALT) as an indicator of health and disease. *Hepatology* 47: 1363-1370.

Meng, H., Xia, T., George, S. and Nel, A. E. (2009). A predictive toxicological paradigm for the safety assessment of nanomaterials. *ACS Nano* 3: 1620-1627.

Milto, I. V., Grishanova, A. Y., Klimenteva, T. K., Suhodolo, I. V., Vasukov, G. Y. and Ivanova, V. V. (2014). Iron metabolism after application of modified magnetite nanoparticles in rats. *Biochemistry* 79: 1245-1254.

Murphy, M. P. (2009). How mitochondria produce reactive oxygen species. *Biochemical Journal* 417: 1-13.

Nel, A., Xia, T., Mädler, L. and Li, N. (2006). Toxic potential of materials at the nanolevel. *Science* 311: 622-627.

Oberdörster, G., Oberdörster, E. and Oberdörster, J. (2005). Nanotoxicology: an emerging discipline evolving from studies of ultrafine particles. *Environmental Health Perspectives* 113: 823-839.

OECD. (1998). Test No. 408: Repeated Dose 90-Day Oral Toxicity Study in Rodents, *OECD Guidelines for the Testing of Chemicals*, Section 4, OECD Publishing, Paris.

Parasuraman, S., Raveendran, R. and Kesavan, R. (2010). Blood sample collection in small laboratory animals. *Journal of Pharmacology and Pharmacotherapeutics* 1: 87-93.

Poulsen, M., Kroghsbo, S., Schrøder, M., Wilcks, A., Jacobsen, H., Miller, A. and Emami, K. (2007). A 90-day safety study in Wistar rats fed genetically modified rice expressing snowdrop lectin *Galanthus nivalis* (GNA). *Food and Chemical Toxicology* 45: 350-363.

Rahman, K. (2007). Studies on free radicals, antioxidants, and co-factors. *Clinical Interventions in Aging* 2: 219-236.

Re, R., Pellegrini, N., Proteggente, A., Pannala, A., Yang, M. and Rice-Evans, C. (1999). Antioxidant activity applying an improved ABTS radical cation decolorization assay. *Free Radical Biology and Medicine* 26: 1231-1237.

Reeves, P. G., Nielsen, F. H. and Fahey Jr, G. C. (1993). AIN-93 purified diets for laboratory rodents: final report of the American Institute of Nutrition ad hoc writing committee on the reformulation of the AIN-76A rodent diet. *Journal of Nutrition* 123: 1939-1951.

Schrøder, M., Poulsen, M., Wilcks, A., Kroghsbo, S., Miller, A., Frenzel, T. and Shu, Q. (2007). A 90-day safety study of genetically modified rice expressing Cry1Ab protein (*Bacillus thuringiensis* toxin) in Wistar rats. *Food and Chemical Toxicology* 45: 339-349.

Schulte, P. A. and Salamanca-Buentello, F. (2007). Ethical and scientific issues of nanotechnology in the workplace. *Ciência & Saúde Coletiva* 12: 1319-1332.

Séralini, G. E., Mesnage, R., Clair, E., Gress, S., De Vendômois, J. S. and Cellier, D. (2011). Genetically modified crops safety assessments: present limits and possible improvements. *Environmental Sciences Europe* 23: 1-10.

Singh, A. (1982). Chemical and biochemical aspects of superoxide radicals and related species of activated oxygen. *Canadian Journal of Physiology and Pharmacology* 60: 1330-1345.

Solanki, P., Bhargava, A., Chhipa, H., Jain, N. and Panwar, J. (2015). Nano-fertilizers and their smart delivery system. In Rai, M., Ribeiro, C., Mattoso, L. and Duran, N. (Eds.) *Nanotechnologies in Food and Agriculture*, Springer International Publishing, Switzerland. p. 81-101.

Stoline, M. R. (1981). The status of multiple comparisons: simultaneous estimation of all pairwise comparisons in one-way ANOVA designs. *The American Statistician* 35: 134-141.

Tate, J. A., Ogden, J. A., Strawbridge, R. R., Pierce, Z. E. and Hoopes, P. J. (2009). Toxicity and biodistribution of activated and non-activated intravenous iron oxide nanoparticles. *SPIE BiOS: Biomedical Optics* 1: 71810-71810

Thomas, K. and Sayre, P. (2005). Research strategies for safety evaluation of nanomaterials, Part I: evaluating the human health implications of exposure to nanoscale materials. *Toxicological Sciences* 87: 316-321.

Uchino, S., Bellomo, R. and Goldsmith, D. (2012). The meaning of the blood urea nitrogen/creatinine ratio in acute kidney injury. *Clinical Kidney Journal* 5: 187-191.

Uchiyama, M. K., Toma, S. H., de Paula Rodrigues, S. F., Shimada, A. L. B., Loiola, R. A., Rodríguez, H. J. C. and Farsky, S. H. P. (2015). Ultrasmall cationic superparamagnetic iron oxide nanoparticles as nontoxic and efficient MRI contrast agent and magnetic-targeting tool. *International Journal of Nanomedicine* 10: 4731-4738.

Vasiliades, J. (1976). Reaction of alkaline sodium picrate with creatinine: I. Kinetics and mechanism of formation of the mono-creatinine picric acid complex. *Clinical Chemistry* 22: 1664-1671.

Verma, A. and Stellacci, F. (2010). Effect of surface properties on nanoparticle–cell interactions. *Small* 6: 12-21.

Vickery, W. L. (1984). Optimal diet models and rodent food consumption. *Animal Behaviour* 32: 340-348.

Wang, L., Wang, L., Ding, W. and Zhang, F. (2010). Acute toxicity of ferric oxide and zinc oxide nanoparticles in rats. *Journal of Nanoscience and Nanotechnology* 10: 8617-8624.

Weissleder, R. A., Stark, D. D., Engelstad, B. L., Bacon, B. R., Compton, C. C., White, D. L. and Lewis, J. (1989). Superparamagnetic iron oxide: pharmacokinetics and toxicity. *American Journal of Roentgenology* 152: 167-173.

Wilkinson, J. H., Baron, D. N., Moss, D. W. and Walker, P. G. (1972). Standardization of clinical enzyme assays: a reference method for aspartate and alanine transaminases. *Journal of Clinical Pathology* 25: 940-944.

Xia, T., Li, N. and Nel, A. E. (2009). Potential health impact of nanoparticles. *Annual Review of Public Health* 30: 137-150.

Zeljenková, D., Ambrušová, K., Bartušová, M., Kebis, A., Kovrižnych, J., Krivošíková, Z. and Szabová, E. (2014). Ninety-day oral toxicity studies on two genetically modified maize MON810 varieties in Wistar Han RCC rats (EU 7th Framework Programme project GRACE). *Archives of Toxicology* 88: 2289-2314.

Chapter VIII

Summary and Future Scope

Preface

This chapter summarizes the significant features of the work presented in this thesis and emphasizes on potential avenues for future endeavours.

8.1 Summary of accomplished work

The impact of nanotechnology is increasing at tremendous pace due to its remarkable potential. Most of the nanotechnology applications are based on the fact that nanoscale provides great freedom for manipulation. Using nanotechnology, it is possible to manipulate the bulk material and make them stronger, lighter, durable, extremely conductive and reactive. Nanoparticles are considered as the protagonist of the nanotechnology revolution. Amid nanoparticles, inorganic (metal and metal oxides) nanoparticles are of special interest due to their unique and tuneable properties, flexibility in functionalization and supple biological interactivity.

Ever increasing use of nanoparticles in various fields is escalating their demand. Technologies for synthesis of nanoparticles are undergoing constant development to cope up with the demand in the present scenario, and recent synthesis methods are replacing the conventional methods. Increasing awareness towards ecosystem restoration has influenced researchers to develop eco-friendly yet cost effective and efficient methodologies for nanoparticle synthesis. Biological methods for nanoparticle synthesis particularly using microorganisms, presents a desirable alternate to the conventional physical and chemical synthesis methods. Translating the knowledge gained by understanding natural biomineralization process at laboratory scale, the potential of microorganisms isolated from metal rich regions for the synthesis of metal and metal oxide nanoparticles can be harnessed. Among various microorganisms, fungi represents a favourable natural machinery due to its large and most diverse secretome making it highly anticipated for on-cell/ extracellular synthesis of nanoparticles.

Working in this direction, mycosynthesis of iron oxide nanoparticles (IONPs) and gold nanoparticles (Au NPs) was attempted. The selection for efficient fungal isolate(s) for the nanoparticle synthesis was accomplished by isolating fungi from soil samples collected from metal rich regions of Nathara Ki Pal, Udaipur and Sonshi Mine, Goa. A total of 11 morphologically distinct fungi were isolated and identified at molecular level. All the fungal isolates were screened for their metal tolerance ability against iron and gold ions. *Aspergillus japonicus* AJP01 was found to be the most tolerant fungus against iron while *Cladosporium oxysporum* AJP03 and *Lichtheimia ramosa* AJP11 exhibited highest metal tolerance against gold ions. In addition to iron, *Aspergillus japonicus* AJP01 also showed reasonably high gold metal tolerance. Hence, these fungal isolates were further utilized as potential candidates for respective nanoparticle synthesis.

For the extracellular mycosynthesis of IONPs, an indigenous protocol was developed. *Aspergillus japonicus* AJP01 successfully synthesised IONPs by hydrolysing precursor salt solution (a mixture of potassium ferricyanide and potassium ferrocyanide). The IONPs were characterized using standard techniques viz. UV-visible spectroscopy, TEM, SAED, EDS and XRD. SEM analysis of fungal biomass exposed to precursor salt solution confirmed that the nanoparticle synthesis was exclusively extracellular since no

particles were found bounded to the fungal biomass surface. FTIR analysis revealed that the mycosynthesised IONPs were coated with proteins, which confers their stability. SDS-PAGE analysis of extracellular proteins demonstrated the possibility of role of one or more proteins in coprecipitation, controlled nucleation and/or stabilization of nanoparticles.

Fungal isolates showing metal tolerance against gold were screened to test their potential for on-cell and/ or extracellular synthesis of Au NPs. On-cell synthesis of Au NPs was achieved using *Aspergillus japonicus* AJP01. The dual role of this fungal isolate in synthesis as well as immobilization of nanoparticles was the remarkable feature. The attractiveness of the approach lied in its simplicity and one-step procedure for the synthesis of nanoparticle-fungal hybrid which can be used in various applications like catalysis. *Cladosporium oxysporum* AJP03 and *Lichtheimia ramosa* AJP11 showed potential for extracellular synthesis of Au NPs. The protocol which utilizes fungal extracellular metabolites (cell-free filtrate) for reduction, nucleation and stabilization of nanoparticles. In order to obtain nanoparticles with well-defined properties and high yield, optimization of process parameters viz., concentration of extracellular metabolites and precursor salt; and reaction pH was carried out. The morphology, composition and crystallinity of nanoparticles were confirmed using standard techniques. The underlying mechanism involved in synthesis of Au NPs by *Lichtheimia ramosa* AJP11 was also investigated. The obtained results indicated the possibility of ~14 kDa protein to be the "active" biomolecule involved in extracellular synthesis.

Once synthesized, the commercial efficacy of mycosynthesized Au NPs were explored in the field of catalysis. On-cell synthesized nanoparticles which resulted in fabrication of fungal biomass supported Au NPs were utilized as a natural heterogeneous catalyst for the chemical synthesis of propargylamine; reduction of nitrophenols and ferricyanides. Whereas, extracellularly synthesized free and unsupported protein capped Au NPs were employed for the remediation of environmentally hazardous organic dyes. Owing to the presence of surface proteins, mycosynthesized Au NPs exhibited excellent dye degradation efficiency.

Increased use of nanoscale material in present times, has increased the chances of exposure of nanoparticles to plants. Incorporation of nanoparticles in food chain is a considerable threat to eco-system and should be investigated critically. Although, nanoparticles of toxic and heavy elements have negative effect on plants as reported by many studies, nanoparticles of physiologically important elements can have positive and growth promoting effect on plants, if applied thoughtfully. In this regard, a comprehensive study was executed to assess the agricultural potential of IONPs as nano-fertilizers. Different concentration of IONPs in the form of maghemite and magnetite (chemically and biologically synthesized) along with ionic ($FeSO_4$) and bulk (Fe_2O_3) forms were used as supplements to check their effects on the growth and biomass production of wheat and

spinach plants. The results suggested that IONPs are not toxic to the tested plants and instead if used at lower optimum concentration, can be beneficial.

In order to test the safety of nanotechnology derived food, a first of its kind study was carried out using rodent model. The toxicity of wheat crop grown using IONPs was assessed using a 90-day sub-acute repeated dose oral toxicity study in female wistar rats involving various examinations. The obtained results showed no sign of toxicity of the test substance under experimental conditions.

8.2 Potential for future work

The simplicity and versatility of present "biosynthesis" approach for nanoparticle synthesis allows its utilization for production of various other metal and metal oxide nanoparticles. However, biological approaches are still practised at laboratory level and have not been profitably scaled-up to the industrial level. Therefore, attempts are required to make the process more efficient and cost effective. These objectives can be fulfilled not only by selecting suitable organisms but also by understanding the factors that affect yield and properties of nanoparticles. In present study, the preliminary knowledge obtained for the mechanism involved in the synthesis of IONPs and Au NPs has just opened the door for a whole new domain of sophisticated molecular (genetic and proteomic) alterations which if successful will help in achieving mass scale production of nanoparticles with desired properties.

The excellent efficiency of mycosynthesized Au NPs in catalysis as observed in the present work has marked the importance of protein cap on nanoparticle surface. The efficacy of these protein capped nanoparticles can also be utilized for various other applications like molecular and chemical sensing, remediation and biomedical therapies. Further, these nanoparticles can be immobilized in suitable matrices for their repeated use in applications involving harsh conditions.

In the present work, use of IONPs as potential nano-fertilizers has been shown with experimental evidences. However, much more work at molecular level is still required to prove this notion. Experiments involving similar plants (wheat and spinach) at different geographical locations as well as using other plant species shall be carried out to ascertain the beneficial role of IONPs as well as other particles as nano-fertilizers.

The risk assessment of nanotechnology/ nano-fertilizers in agriculture is significantly important as it directly affects humans. Nano-fertilizers enable nanoparticles to enter in the food chain allowing their distribution in every organism related to the food chain. Also, it is most likely that different types of nanoparticles may exert varying toxicological response. Thus, it is very essential to execute further *in vivo* studies on oral exposure of nanotechnology derived food and check for any consequent toxicity as risk assessment of nanoparticles has to be performed on a case-by-case basis.

APPENDICES

LIST OF PUBLICATIONS

From the thesis

Research Papers

- ❖ **Bhargava, A.**, Jain, N., Barathi L., M., Akhtar, M.S., Yun, Y.S. and Panwar, J. 2014. Synthesis, characterization and mechanistic insights of mycogenic iron oxide nanoparticles. *Journal of Nanoparticle Research*, 15, 2031-2042.

- ❖ **Bhargava, A.**, Jain, N., Gangopadhyay, S. and Panwar, J. 2015. Development of gold nanoparticle -fungal hybrid based heterogeneous interface for catalytic applications. *Process Biochemistry*, 50, 1293-1300.

- ❖ **Bhargava, A.**, Jain, N., Dilip, R. V., Pareek, V., Khan, Mohd. A. and Panwar, J. 2016. Utilizing metal tolerance potential of soil fungus for efficient synthesis of gold nanoparticles with superior catalytic activity for degradation of rhodamine B. *Journal of Environmental Management* (DOI: 10.1016/j.jenvman.2016.08.021).

Book Chapters

- ❖ **Bhargava, A.**, Jain, N. and Panwar, J. 2011. Synthesis and application of magnetic nanoparticles: a biological perspective. In: Current topics in biotechnology and microbiology: recent trends. (Dhingra H. K., Jha P. N., Bajpai P., Eds.), Lap Lambert Academic Publishing AG & Co Kg, Colne, Germany, pp. 117-155.

- ❖ Solanki, P., **Bhargava, A.**, Chhipa, H., Jain, N. and Panwar, J. 2014. Nano-fertilizers and their smart delivery system. In: Emerging Nanotechnologies in Agriculture, Rai, M., Ribeiro, C., Mattoso, L. and Duran, N. (Eds.), Springer, Germany, pp. 81-101.

Conference Papers/ Abstract

- ❖ **Bhargava, A.**, Jain, N. and Panwar, J. 2010. Biogenic synthesis of iron nanoparticles. In: Contemporary Trends in Biological and Pharmaceutical Research (CTBPR), March 12-13, 2011, BITS Pilani, Pilani Campus, India.

- ❖ **Bhargava, A.**, Jain, N., Barathi, M.L. and Panwar, J. 2011. Fungal mediated synthesis of iron oxide nanoparticles and their characterization. In: 52nd Annual conference of AMI on international conference on microbial biotechnology for sustainable development, November 3-6, 2011, Panjab University, Chandigarh, India.

- ❖ Barathi, M.L., **Bhargava, A.**, Jain, N. and Panwar, J. 2012. Rapid biosynthesis of gold nanoparticles using *Aspergillus japonicus* isolate AJP01 and their characterization. In: International Conference on Nanoscience and Technology (ICONSAT), January 20-23, 2012, Hyderabad, India.

- ❖ **Bhargava, A.**, Jain, N. and Panwar, J. 2013. Gold nanoparticle-fungal hybrid: Synthesis, characterization and catalytic applications. In: 3rd Nano Today Conference, December 8-11, Biopolis, Singapore.

- ❖ Solanki, P., **Bhargava, A.**, Jain, N. and Panwar, J. 2014. Catalytic efficacy of biosynthesized gold nanoparticles. In: National conference on Nano-Functional Material (NFM-2014), November 7-8, 2014, BITS Pilani, Pilani Campus, Pilani, p. 90.

- ❖ **Bhargava, A.**, Solanki, P., Jain, N. and Panwar, J. 2014. Effect of iron oxide nanoparticles on the growth and biomass. In: International Conference on Emerging Trends in Biotechnology (ICETB-2014), November 6-9, 2014, Jawaharlal Nehru University, New Delhi, India.

- ❖ Pareek, V., **Bhargava, A.**, Khan, M.A., Dilip, R.V., and Panwar, J. 2015. Enhanced catalytic degradation of rhodamine B using mycogenic gold nanoparticles. In: 4th International Conference on Advanced Nanomaterials and Nanotechnology, December 8-11, 2015, Indian Institute of Technology, Guwahati.

From additional work during Ph.D. tenure

Research Papers

- ❖ Jain, N., **Bhargava, A.**, Majumdar, S., Tarafdar, J.C. and Panwar, J. 2011. Extracellular biosynthesis and characterization of silver nanoparticles using *Aspergillus flavus* NJP08: A mechanism perspective. *Nanoscale*, 3, 635-641.

- ❖ Jain, N., **Bhargava, A.**, Tarafdar, J.C., Singh, S.K. and Panwar, J. 2012. A biomimetic approach towards synthesis of zinc oxide nanoparticles. *Applied Microbiology and Biotechnology*, 97, 859-869.

- ❖ Jain, N., **Bhargava, A.**, and Panwar, J. 2014. Enhanced photocatalytic degradation of methylene blue using biologically synthesized "protein-capped" ZnO nanoparticles. *Chemical Engineering Journal*, 243, 549-555.

- ❖ Jain, N., **Bhargava, A.**, Sabat, D. and Panwar, J. 2014. Unveiling the potential of metal-tolerant fungi for efficient enzyme production. *Process Biochemistry,* 49, 1858-1866.

- ❖ Jain, N., **Bhargava, A.**, Dilip, R. V., Rathi, M. and Panwar, J. 2015. Removal of protein capping enhances the antibacterial efficiency of biosynthesized silver nanoparticles. *PLoS ONE*, 10, e0134337.

Conference Papers/ Abstract

- ❖ Jain, N., **Bhargava, A.** and Panwar, J. 2010. Biosynthesis of silver nanoparticles: A green chemistry approach. In: National Conference on Green and Sustainable Chemistry, February 19-21, 2010, BITS Pilani, Pilani Campus, India.

- ❖ Jain, N., **Bhargava, A.** and Panwar, J. 2011. Improved antimicrobial efficacy of biogenic silver nanoparticles. In: International Conference on Nanomaterial and Nanotechnology (ICNANO), December 18-21, 2011, University of Delhi, Delhi, India.

- ❖ Jain, N., **Bhargava, A.**, Akhtar, M.S., Yun, Y.S. and Panwar, J. 2012. Positive effect of zinc oxide nanoparticles on tomato plants: a step towards developing "Nano-fertilizers". In: International Conference on Nanoscience and Technology (ICONSAT), January 20-23, 2012, Hyderabad, India.

- ❖ Dey, D. **Bhargava, A.**, Jain, N. and Panwar, J. 2012. Phytosynthesis of silver nanoparticles from *Prosopis cineraria* leaf extract and evaluation of their antimicrobial activity. In: International Conference on Industrial Biotechnology, November 21-23, 2012, Punjabi University, Patiala, India.

- ❖ Jain, N., Sabat, D., **Bhargava, A.** and Panwar, J. 2013. Purification and characterization of alkaline protease from metal tolerant fungus Aspergillus flavus NJP08. In: International Conference on Health, Environment and Industrial Biotechnology (BioSangam), November 21-23, 2013, Motilal Nehru National Institute of Technology, Allahabad, India.

- ❖ Jain, N., **Bhargava, A.**, and Panwar, J. 2013. Biomimetics at nanoscale: Utilizing metal tolerant fungal isolate to fabricate ZnO nanoparticles. In: Asian Congress on Biotechnology, December 15-19, 2013, Indian Institute of Technology, Delhi, p. 88-89.

- ❖ Jain, N. **Bhargava, A.**, and Panwar, J. 2014. Protease-assisted synthesis and stabilization of spherical silver nanoparticles: a novel template to study protein-nanoparticle interactions. In: International Conference on Nanotechnology in the Service of Health, Environment & Safety (NanoSciTech 2014), February 13-15, 2014, Panjab University, Chandigarh, India.

- ❖ Jain, N., **Bhargava, A.** and Panwar, J. 2014. Mycogenic protein-capped zinc oxide nanoparticles and their photocatalytic activity. In: International conference on Biotechnology & Bioengineering (ICBB-2014), October 29-30, 2014, BITS Pilani, Dubai Campus, Dubai, p. 18.

- ❖ Dilip, R.V., **Bhargava, A.**, Pareek, V. and Panwar, J. 2015 Rapid and efficient synthesis of silver nanoparticles by metal tolerant fungus. In: 4th International Conference on Advanced Nanomaterials and Nanotechnology, December 8-11, 2015, Indian Institute of Technology, Guwahati.

Patent: Jain, N., **Bhargava, A.** and Panwar, J. Biosynthesis of Zinc Oxide Nanoparticles, Indian Patent Application No: 1439/DEL/2011A. Date of filing: 19/5/2011, Date of Publication: 17/05/2013

BIOGRAPHY

Prof. Jitendra Panwar

Prof. Jitendra Panwar has completed his Doctoral degree in the area of Mycorrhizal Biotechnology in 2000 from Jai Narain Vyas University, Jodhpur. After Ph.D., he moved to Division of Soil-Water-Plant Relationship, Central Arid Zone Research Institute (ICAR), Jodhpur for Post-Doctoral studies where he worked in the area of Soil Fertility, Microbiology and Plant Physiology. Subsequently, he has been awarded Young Scientist Project by Department of Science & Technology, New Delhi, India. He joined Department of Biological Sciences, BITS Pilani, Pilani Campus as Assistant Professor in October 2005 and became Associate Professor in February 2013. He served as Head of the Department during September 2012 to August 2014. He has handled several research projects in the field of Microbial Biotechnology and Nanobiotechnology, funded by DST, ICAR, UGC and Aditya Birla Group. Prof. Panwar has 18 years of teaching and research experience as in 2016.

Prof. Panwar is also a recipient of "Visiting Professor Fellowship" to visit South Korea for a period of three months under INSA-NRF International Bilateral Exchange/ Collaboration Programme 2011-12. Recently, he has been nominated to visit Czech Republic for one month under INSA-CAS Exchange Programme 2016. He has successfully completed four research projects funded by Department of Science & Technology (DST), New Delhi; Aditya Birla Group, Mumbai; Indian Council of Agricultural Research (ICAR), New Delhi; and University Grant Commission (UGC), New Delhi. Currently, he is working on a research project funded by DST, New Delhi under its Nano-Mission programme which has been extended for its 4th year. As a result of his research accomplishments, he has published more than 45 research papers in peer reviewed journals. In addition, Prof. Panwar has presented papers and delivered lectures in several National & International conferences and organizations. His current research interest lies in the area of nano-biotechnology, nano-fertilizers and protein-nanoparticle interactions.

BIOGRAPHY

Arpit Bhargava

Mr. Arpit Bhargava did his graduation in Bachelor of Science (B.Sc.) from Bangalore University, Karnataka and Masters in Science (M.Sc.) with specialization in Biotechnology from Nirma University, Ahmedabad in the year 2007 and 2009, respectively. In the year 2010 he joined Birla Institute of Technology and Science, Pilani in the Ph.D. programme under the supervision of Prof. Jitendra Panwar. Later, he was recruited as a JRF in World Bank funded NAIP-ICAR project at the same Institute. In the year 2013, he was awarded prestigious Senior Research Fellowship by Council Scientific and Industrial Research (CSIR). He possesses an active research interest in the area of bio-nanotechnology with major emphasis on biomedical and environmental applications of inorganic nanoparticles and risk assessment of nanotechnology. He has published several research articles in renowned journals and also presented his research findings in various National and International conferences. He has also been consistently involved in the teaching programme at Department of Biological Sciences, BITS Pilani, Pilani Campus.

REPRINT OF PUBLICATIONS

RESEARCH PAPER

Synthesis, characterization and mechanistic insights of mycogenic iron oxide nanoparticles

**Arpit Bhargava · Navin Jain · Manju Barathi L. ·
Mohd. Sayeed Akhtar · Yeoung-Sang Yun ·
Jitendra Panwar**

Abstract In the present study, extracellular synthesis of iron oxide nanoparticles (IONPs) was achieved using *Aspergillus japonicus* isolate AJP01. The isolate demonstrated its ability to hydrolyze the precursor salt solution, a mixture of iron cyanide complexes, under ambient conditions. Hydrolysis of these complexes released ferric and ferrous ions, which underwent protein-mediated coprecipitation and controlled nucleation resulting in the formation of IONPs. Transmission electron microscopy, selected area electron diffraction pattern, energy dispersive spectroscopy and grazing incidence X-ray diffraction analysis confirmed the mycosynthesis of IONPs. The synthesized particles were cubic in shape with a size range of 60–70 nm with crystal structure corresponding to magnetite. Scanning electron microscopy analysis revealed the absence of IONPs on fungal biomass surface, indicating the extracellular nature of synthesis. Fourier transform infrared spectroscopy confirmed the presence of proteins on as-synthesised IONPs, which may confer their stability. Preliminary investigation indicated the role of proteins in the synthesis and stabilization of IONPs. On the basis of present findings, a probable mechanism for synthesis of IONPs is suggested. The simplicity and versatility of the present approach can be utilized for the synthesis of other nanomaterials.

A. Bhargava · N. Jain · M. Barathi L. · J. Panwar (✉)
Centre for Biotechnology, Department of Biological
Sciences, Birla Institute of Technology and Science,
Pilani, India
e-mail: drjitendrapanwar@yahoo.co.in

Mohd. S. Akhtar
Department of Applied Microbiology, College of Natural
Sciences, Jimma University, Jimma, Ethiopia

Y.-S. Yun
Division of Environmental and Chemical Engineering,
Chonbuk National University, Chonbuk, South Korea

Introduction

The advent of nanotechnology has revolutionized science, economy and everyday life. Intrinsic properties with respect to bulk materials change drastically in the event of reduction of size to nanoscale-like quantum confinement in semiconductors, surface plasmon resonance in some metallic nanoparticles and

superparamagnetism in magnetic nanoparticles (Noguez 2007; Jun et al. 2008; Wu et al. 2008). As compared to the larger particles of the bulk material, nanoparticles exhibit completely new or improved properties based on their size, distribution and morphology. Changes in properties at nanoscale have been thoroughly used in various interesting applications involving optoelectrical, catalytic, photochemical and electrochemical phenomena (Fedlheim and Foss 2001).

Iron oxide nanoparticles (IONPs) have been consistently used in developing technologies related to data storage, environmental remediation, energy generation, water purification, etc. (Teja and Koh 2009). Narrowing our focus to applications of IONPs in biology, their amenable properties offer very useful and attractive potentials in biomedicine, viz. biomolecular targeting, hyperthermia, cell manipulations and as carrier/delivery molecule (Bhargava et al. 2011). As evident by the importance of IONPs, their synthesis has received considerable attention. Biosynthesis of nanoparticles presents an appealing approach which integrates material science and microbial biotechnology, potentially overcoming limitations associated with conventional physical and chemical methods of nanoparticle synthesis (Laurent et al. 2008). Presently, the biological method relies on the use of plants, bacteria and fungi for the synthesis of nanoparticles and became an eco-friendly, yet cost-effective alternative with the ability of controlling synthesis at the molecular level in certain cases. Molecular control can be well appreciated in the biosynthesis of magnetosomes by magnetotactic bacteria where the overall synthesis is regulated at the genetic level by a group of genes collectively called 'magnetosome island' which is a conserved gene cluster (Komeili 2007). Recently, Parikh et al. (2011) reported the presence of a gene homolog of a putative gene of the silver-binding protein (silE) from various strains of *Morganella* spp. that were tested for silver nanoparticles synthesis.

Fungi have emerged as potential candidates for the biosynthesis of nanoparticles because of their ease in handling, low cost maintenance as well as easy downstream processing, due to the predominantly extracellular nature of nanoparticle synthesis (Gade et al. 2010). Additionally, being a eukaryotic organism, fungi have been reported to secrete a versatile range of extracellular components in higher amounts as compared to prokaryotic organisms. This might be helpful in achieving significantly higher and desired

productivity of various nanoparticles (Dhillon et al. 2011).

Appreciating the perspective that organisms isolated from metal-rich regions show improved ability for high metal tolerance as well as microbial activities that adapt to stressed environment, Jain et al. (2013) reported the efficiency of metal-tolerant fungal isolates toward extracellular synthesis of nanoparticles. In the present study, we report the mycosynthesis of IONPs utilizing *Aspergillus japonicus* isolate AJP01 isolated from iron-rich soil. The fungal isolate demonstrated its ability to hydrolyze the precursor salt solution, a mixture of iron cyanide complexes, under ambient conditions. Hydrolysis of these complexes releases ferric and ferrous ions, which possibly undergo protein-mediated coprecipitation and controlled nucleation resulting in the formation of IONPs as suggested by the experimental inferences. The IONPs were synthesised extracellularly and stabilized by proteins of fungal origin. Based on the preliminary molecular and biochemical investigations, the probable mechanism for synthesis and subsequent stabilization of IONPs is discussed.

Materials and methods

Materials

All chemicals used were of analytical grade and procured from Sigma-Aldrich (Sigma-Aldrich, St. Louis, MO, USA) or Merck Chemicals (Merck KGaA, Darmstadt, Germany) unless otherwise stated. Commercially available magnetite nanoparticles (637106) were purchased from Sigma-Aldrich. All culture media and molecular biology kits were purchased from HiMedia Laboratories (HiMedia Laboratories, Mumbai, India). Reagents and enzymes used in PCR reactions were obtained from Promega (Promega, Mannheim, Germany). The primers ITS1 and ITS4 were purchased from Sigma-Aldrich and Bt2a, Bt2b, CL1 and CL2A from Eurofins MWG Operon (Eurofins MWG Operon, Ebersberg, Germany).

Isolation and molecular identification of fungal isolate

The fungus was isolated from soil samples of iron-rich regions of Udaipur, Rajasthan, India. Briefly, the collected soil samples were serially diluted and plated

on Martin Rose Bengal Agar media (pH 7.2) supplemented with chloramphenicol at a final concentration of 30 μg/mL after autoclaving. Petri plates were incubated at 28 °C for 96 h under dark conditions. Individual and morphologically distinct fungal colonies were selected and further purified by repeated sub-culturing on potato dextrose agar (PDA) medium (pH 5.6). Glycerol stocks of the isolates were prepared and preserved at −70 °C.

Fungal DNA was extracted using HiPurA^TM plant genomic DNA miniprep purification spin kit with minor modifications. Amplification of the internal transcribed spacer (ITS) regions of ribosomal DNA was amplified using primers ITS1 (5′-TCCGTAGGT-GAACCTGCGG) and ITS4 (5′-TCCTCCGCTTATT-GATATGC) (White et al. 1990). Partial amplification of β-tubulin gene was performed using the primers Bt2a (5′-GGTAACCAAATCGGTGCTGCTTTC) and Bt2b (5′-ACCCTCAGTGTAGTGACCCTTG GC) (Glass and Donaldson 1995). In addition, partial amplification of the calmodulin gene was performed using the primers CL1 (5′-GARTWCAAGGAG GCCTTCTC) and CL2A (5′-TTTTTGCATCATGA GTTGGAC) (O'Donnell et al. 2000). PCR reactions were carried out in total volumes of 50 μL containing Taq Buffer A, 15 mM MgCl$_2$, 50 μM each of deoxynucleoside triphosphates, 50 pmol of each primers (30 pmol in case of partial β-tubulin gene amplification), 1 unit of TaqDNA polymerase and 4 μL of template genomic DNA. The reactions were carried out on a Veriti^® Thermal Cycler (Applied Biosystems, Carlsbad, CA, USA). The PCR conditions followed for amplification of ITS regions were as follows: 2 min of preheating at 94 °C followed by 30 cycles of denaturation at 94 °C for 1 min, annealing at 57 °C for 1.5 min, extension at 72 °C for 2 min and a final extension of 4 min at 72 °C. The PCR conditions followed for amplification of partial β-tubulin gene were as follows: 5 min of preheating at 94 °C followed by 35 cycles of denaturation at 94 °C for 1 min, annealing at 60 °C for 45 s, extension at 72 °C for 1 min and a final extension of 7 min at 72 °C. The PCR conditions followed for amplification of partial calmodulin gene were as follows: 10 min of preheating at 94 °C followed by 35 cycles of denaturation at 94 °C for 50 s, annealing at 58 °C for 50 s, extension at 72 °C for 1 min and a final extension of 7 min at 72 °C. The PCR products were separated on 1.0 % (w/v) agarose gel including DNA ladder SM0241

(Fermentas Life Sciences, Burlington, ON, Canada) and purified using a HiPurA^TM PCR product purification spin kit.

The purified PCR products were sequenced using an ABI prism DNA sequencer by BigDye terminator method (Applied Biosystems, Foster City, CA, USA). The resulting nucleotide sequences were compared using Basic Local Alignment Search Tool (BLAST) network services of the National Center for Biotechnology Information (NCBI) database (http://www.ncbi.nlm.nih.gov/) and the most closely related species were determined. The sequences were further submitted to GenBank and the accession numbers were obtained.

Extracellular mycosynthesis of IONPs

All the fungal isolates were screened to check their ability to hydrolyze the precursor salt solution comprising freshly prepared potassium ferricyanide K$_3$[Fe(CN)$_6$] and potassium ferrocyanide K$_4$[Fe(CN)$_6$] in a millimolar ratio of 1:0.5 (data not shown). The isolate showing maximum hydrolysis was selected for further study. The fungal isolate was maintained on PDA slants (pH 5.6) with repeated sub-culturing on fresh media. From an actively growing culture, a loopful of spores was inoculated in 80 mL of MGYP medium (0.3 % malt extract, 1.0 % glucose, 0.3 % yeast extract, 0.5 % peptone; pH 7.0) in 250 mL Erlenmeyer flasks. The inoculated flasks were incubated at 28 °C for 72 h on a rotary shaker (120 rpm) under dark conditions. After incubation, the fungal biomass was separated from the culture medium by centrifugation (5,000 rpm) at 4 °C for 15 min and washed thrice with autoclaved Milli-Q water to remove all traces of media. Typically, 20 g of biomass (fresh weight) was resuspended in 100 mL of precursor salt solution in a 250 mL Erlenmeyer flask and incubated at 28 °C for 96 h on a rotary shaker (120 rpm) under dark conditions. After incubation, the biomass was separated by filtration using Whatman grade 1 filter paper (Whatman Inc., Florham Park, NJ, USA) and the cell-free filtrate containing IONPs was obtained for further characterization. Biomass in autoclaved Milli-Q water (without precursor salt solution) as positive control and pure precursor salt solution (without biomass) as negative control were also incubated simultaneously along with the experimental flasks in three replicates.

The growth (colony forming unit, CFU) and viability of fungus before and after exposure to

precursor salt solution were checked. For determination of CFU, the fungal biomass was cut into pieces (5 × 5 mm) and shaken with 0.02 % Tween 80 for 30 min on a rotary shaker (250 rpm). Suitable dilutions were spread on the surface of PDA medium (pH 5.6). CFU on the plates were counted after incubation at 28 °C for 72 h under dark conditions (Schnurer 1993). The fungus viability was observed by inoculating the exposed fungal biomass on PDA medium (pH 5.6). The inoculated Petri plates were incubated at 28 °C for 72 h under dark conditions.

A separate experiment was performed to examine the possibility of IONPs synthesis, solely by the fungal extracellular proteins. For this, 20 g (fresh weight) of fungal biomass was suspended in 100 mL of autoclaved Milli-Q water and incubated for 72 h in an Erlenmeyer flask in similar conditions as described earlier. After incubation, the cell-free filtrate containing extracellular proteins was recovered by filtration using Whatman grade 1 filter paper. The precursor salt solution at a final millimolar ratio of 1:0.5 was added to the flask containing cell-free filtrate and incubated on a rotary shaker (120 rpm) at 28 °C for 96 h under dark conditions. Cell-free filtrate (without precursor salt solution) as positive control and pure precursor salt solution (without cell-free filtrate) as negative control were also incubated simultaneously along with the experimental flasks in three replicates.

Characterization of mycosynthesized IONPs

Hydrolysis of iron cyanide complex was monitored by taking UV–visible absorption spectra of the culture supernatant at different time intervals. UV–visible measurements were carried out on a V-630 UV–visible spectrophotometer instrument (Jasco Corporation, Tokyo, Japan) at a resolution of 1 nm with a scan speed of 400 nm/min using a 1 cm path length quartz cuvette. Samples for transmission electron microscopy (TEM) imaging and selected area electron diffraction (SAED) pattern determination were prepared on a carbon-coated TEM grid by drop coating the cell-free filtrate containing IONPs after 30 min of sonication. TEM measurement and SAED pattern determination were carried out on a JEM-2100 instrument (JEOL, Tokyo, Japan) operated at an accelerating voltage of 80 and 200 kV for low- and high-resolution imaging, respectively. Energy dispersive spectroscopy (EDS) analysis was carried out

using a H-7650 scanning electron microscope (SEM) instrument (Hitachi High-Technologies Corporation, Tokyo, Japan) equipped with Quantax EDS attachment (Bruker AXS Ltd., Coventry, UK) by freeze drying the cell-free filtrate containing IONPs followed by coating on a double-sided carbon tape attached to the grid surface. The crystalline phase of the iron oxide was identified by grazing incidence X-ray diffraction (GIXRD) measurements of thin layer of mycosynthesized IONPs on glass substrates carried out on an X'Pert PRO X-ray diffractometer instrument (PANalytical BV, Almelo, The Netherlands). The diffraction pattern was recorded between 20° and 80° (2θ) with the diffractometer operated at a voltage of 40 kV and a current of 30 mA with CuK_α radiation. The crystal phase was determined by comparing the calculated values of interplanar spacing and the corresponding intensities of diffraction peaks with theoretical values from the Joint Committee on Powder Diffraction Standards-International Centre for Diffraction Data (JCPDS-ICCD) database. Fourier transform infrared (FTIR) spectroscopy measurements of the freeze-dried IONPs diluted with potassium bromide in the ratio of 1:100 were recorded on an IR Prestige-21 FTIR instrument (Shimadzu, Nakagyo-ku, Japan) with a diffuse reflectance mode (DRS-8000) attachment. All measurements were carried out in wavenumber range of 400–4,000 cm^{-1} at a resolution of 4 cm^{-1}.

For scanning electron microscopy (SEM) analysis of the fungal biomass exposed to precursor salt solution, the biomass was fixed overnight at 4 °C with 2.5 % (v/v) glutaraldehyde in 0.1 M sodium phosphate buffer, pH 7.2. The specimen was rinsed in buffer, dehydrated in a series of 30–100 % ethanol and then dried in a desiccator under vacuum. An automatic Polaron OM-SC7640 sputter coater instrument (Quorum Technologies, Sussex, UK) was used for coating the specimens with gold particles. The specimen was examined using EVO 40 scanning electron microscope instrument (Carl Zeiss, Oberkochen, Germany).

Ferrozine assay for estimation of free iron

To estimate the free iron content in the solution after completion of reaction, ferrozine assay was performed in the cell-free filtrate (Gibbs 1976). The aliquot (1 mL) was treated with ferrozine at a final concentration of 1 mM and the absorbance was recorded at 562 nm against blank (1 mM ferrozine). Ferrous

sulfate solution (1 mM) was used as positive control, whereas cell-free filtrate (without precursor salt solution) and pure precursor salt solution (without cell-free filtrate) were used as negative controls. The experiment was performed in triplicate.

Protein purification and one-dimensional gel electrophoresis

Extracellular proteins from both the test (biomass exposed to precursor salt solution) and control (biomass in autoclaved Milli-Q water) were purified using ammonium sulfate precipitation. Solid ammonium sulfate was added slowly at a final concentration of 80 % (w/v) (Simpson 2004). The mixture was gently stirred for 4–5 h at 4 °C. The resulting precipitate was subsequently collected by centrifugation at 10,000 rpm for 20 min at 4 °C. The proteins obtained thereafter were resuspended in a minimum amount of 50 mM phosphate buffer, pH 7.2, and dialyzed using a Sigma-Aldrich 12-kDa cutoff dialysis bag pre-treated as per the manufacturer's instructions. Briefly, the precipitated protein was filled in the treated dialysis bag, which was then suspended in dialysis buffer (50 mM phosphate buffer, pH 7.2) and stirred slowly at 4 °C. The buffer was changed three to four times over a 12 h period. The total protein concentration in the dialyzed samples was estimated by the standard protocol of Lowry et al. (1951), using bovine serum albumin as standard.

The dialyzed protein fractions were separated on the basis of molecular weight by sodium dodecyl sulfate–polyacrylamide gel electrophoresis (SDS-PAGE) as per standard procedure with adequate modifications (Laemmli 1970). Samples were denatured in 2× sample buffer containing 60 mM Tris (pH 6.8), 25 % glycerol, 2 % SDS, 14.4 mM 2-mercaptoethanol and 0.1 % bromophenol blue, boiled for 5 min, followed by centrifugation at 8,000 rpm for 1 min at 4 °C. Unstained protein molecular weight marker SM0661 (Fermentas Life Sciences) was run along with samples. Electrophoresis was performed on a Mini Protean®3 Cell instrument (BioRad Laboratories, Hercules, CA, USA) at a constant voltage of 100 kV for 120 min. After electrophoresis, the gel was stained with Coomassie Brilliant blue G-250 stain and was observed in a BioRad Gel Doc™ XR imaging system.

Role of proteins in nanoparticle stability

The role of extracellular proteins in nanoparticle stabilization was investigated. For this, the cell-free filtrate containing extracellular proteins from positive control flask (without precursor salt solution) was recovered by filtration using Whatman grade 1 filter paper. The commercially available magnetite nanoparticles at a final concentration of 50 mg/mL was added to the cell-free filtrate and incubated on a rotary shaker (150 rpm) at 28 °C for 48 h under dark conditions. After this, zeta potential measurements were carried out on a Zetasizer Nano ZS (Malvern Instruments Ltd, Worcestershire, UK) at neutral pH. Magnetite nanoparticles (50 mg/mL) suspended in water were used as control.

Results

Molecular identification of fungal isolate

Fungi were isolated from soil samples of iron-rich regions of Udaipur, Rajasthan, India. Preliminary identification of fungi was performed on the basis of morphological parameters such as color, spore shape, arrangement and hyphal branching pattern after staining with cotton blue. A total of 16 fungal isolates were observed on the basis of distinct morphological parameters. After screening, the isolate showing maximum hydrolysis of precursor salt solution was identified at the molecular level by comparative sequence analysis of the ITS regions of ribosomal DNA as well as that of partial β-tubulin and partial calmodulin gene sequences. The sequencing of PCR products resulted in 540 bp (ITS region), 491 bp (partial β-tubulin gene) and 699 bp (partial calmodulin gene) long nucleotide sequences. These sequences were compared using BLAST algorithm. Isolate AJP01 showed the maximum similarity with *Aspergillus japonicus*. The derived fungal sequences were deposited in GenBank with the following accession numbers: JF770435 (ITS region), JX103558 (partial β-tubulin gene) and JX103559 (partial calmodulin gene). *Aspergillus japonicus* isolate AJP01 has been deposited in the Microbial Type Culture Collection and Gene Bank at the Institute of Microbial Technology, Chandigarh, India with the MTCC number 11733 and is available at public domain.
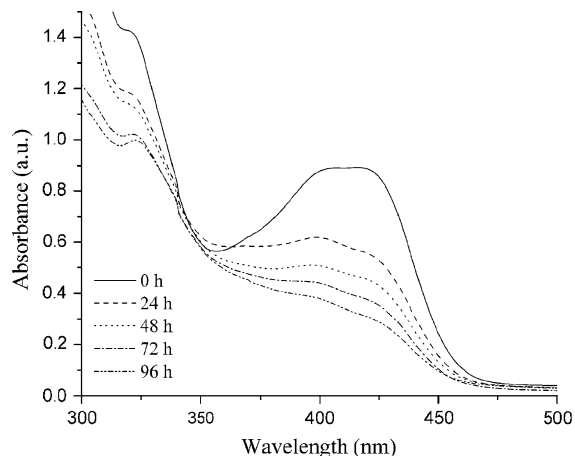
Fig. 1 UV–visible absorption spectrum of cell-free filtrate representing the gradual synthesis of IONPs as a function of time
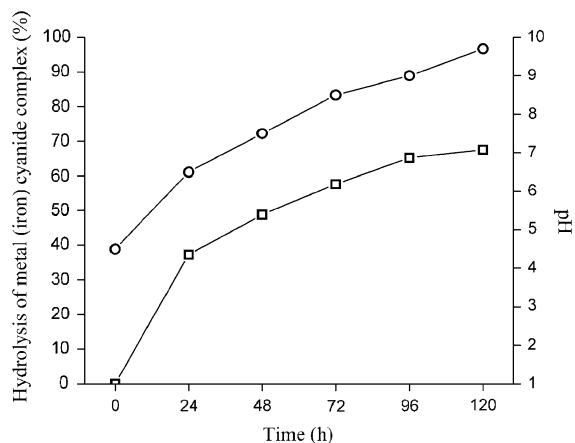

Fig. 2 Graphical representation of increase in the rate of hydrolysis of iron cyanide complex (in percent) observed at 420 nm (*open squares*) and increase in reaction pH (*open circles*) as a function of time

Fig. 3 TEM micrograph of mycosynthesized iron oxide nanoparticles (*scale bar* equivalent to 100 nm)

Characterization of mycosynthesized IONPs

The absorption spectra of precursor salt solution showed highly symmetric band absorption with peak maximum at 420 nm, which is attributed to the characteristic absorption maximum of potassium ferricyanide (Williams 1997). A steady decrease in intensity of peak as a function of time of reaction was observed during the reaction spanning 96 h (Fig. 1). The hydrolysis of iron cyanide complexes accounted for the highest magnitude (37.28 %) in the
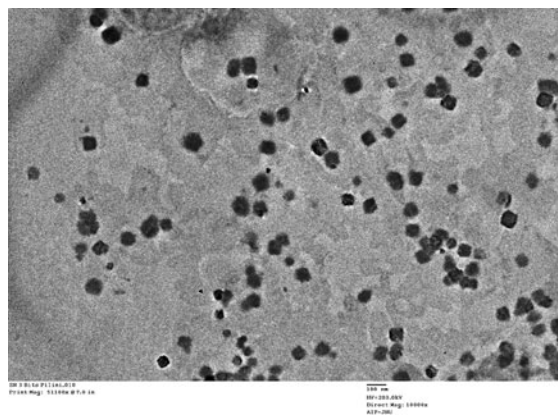
initial 24 h (Fig. 2). After 96 h of incubation, no significant increase was observed in the percent hydrolysis.

The size and morphology of mycosynthesized IONPs were determined by TEM measurements. A representative TEM micrograph (Fig. 3) revealed the particle morphology to be cubic in shape with strict control over particle size. The particle size distribution histogram obtained from TEM measurements (Fig. 4) showed that the maximum number of particles confined in the range of 60–70 nm and possessed an average size of 82.25 ± 5 nm. The SAED patterns (Fig. 5) confirmed the nanoparticles to be crystalline and the diffraction pattern data were found to be consistent with the typical structure characteristics of iron oxide (magnetite [Fe_3O_4] and maghemite [γ-Fe_2O_3]). On the basis of calculated d-values, the diffraction pattern analysis suggested that the particles belonged to magnetite (Sun et al. 2004). High-resolution TEM micrograph (Fig. 6) demonstrated the well-resolved interference fringe pattern attesting to the crystallinity of a typical magnetite nanoparticle with no sign of crystal defects. EDS analysis of freeze-dried sample was performed to determine the elemental composition of nanoparticles (Fig. 7). The EDS spectrum showed an optical absorption band at ~ 6.5 eV, which is representative of iron (Njagi et al. 2010). Figure 8 shows the XRD pattern of synthesised IONPs. Analysis of XRD spectra showed characteristic Bragg's diffraction peaks which are in good agreement with the standard magnetite pattern (JCPDS: 19-0629).
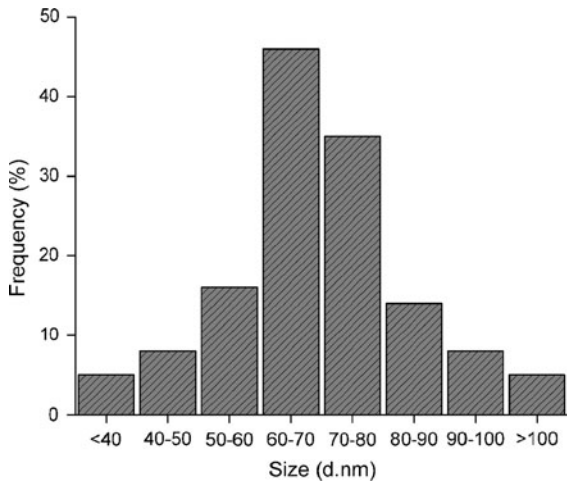
Fig. 4 Particle size distribution histogram of iron oxide nanoparticles extracted from TEM analysis
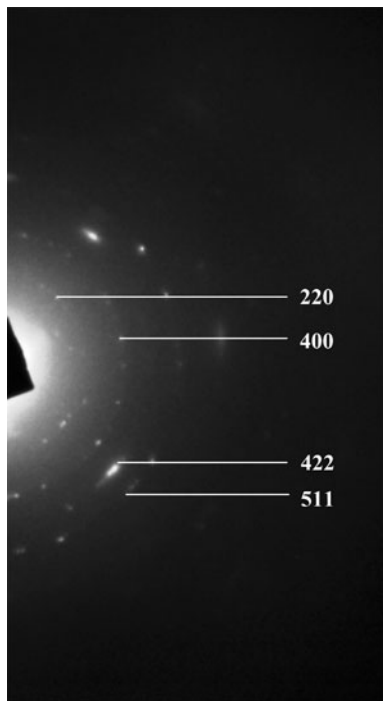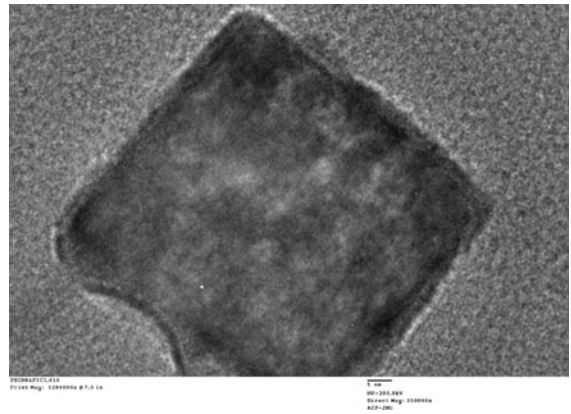

Fig. 6 High-resolution TEM micrograph of a single iron oxide nanoparticle (*scale bar* equivalent to 5 nm)

Fig. 7 EDS spectrum of freeze-dried cell-free filtrate containing mycosynthesized iron oxide nanoparticles

Fig. 5 SAED pattern from a single iron oxide nanoparticle. The diffraction rings corresponds to the allowed (511), (422), (400) and (220) Bragg's reflections

To examine the possibility of synthesis of IONPs bounded to the fungal biomass, SEM imaging of the fungal biomass exposed to the precursor salt solution was performed after completion of the reaction. A representative SEM micrograph of the exposed biomass (Fig. 9) showed the absence of IONPs on the fungal surface, signifying exclusively extracellular synthesis by this fungal isolate.

Ferrozine assay for qualitative estimation of free metal ions

The hydrolysis of the iron cyanide complex was further confirmed by the ferrozine assay, wherein ferrozine specifically binds with free ferrous ions. However, it may non-specifically bind to free ferric ions. The precursor salt solution exposed to fungal biomass for 96 h showed positive result in the ferrozine assay. However, the precursor salt solution failed to give positive results on reaction with ferrozine as metal ions were strongly bound with cyanide and remained in the form of iron cyanide complexes. In the absence of free metal ions, there was a negative result in the ferrozine assay.
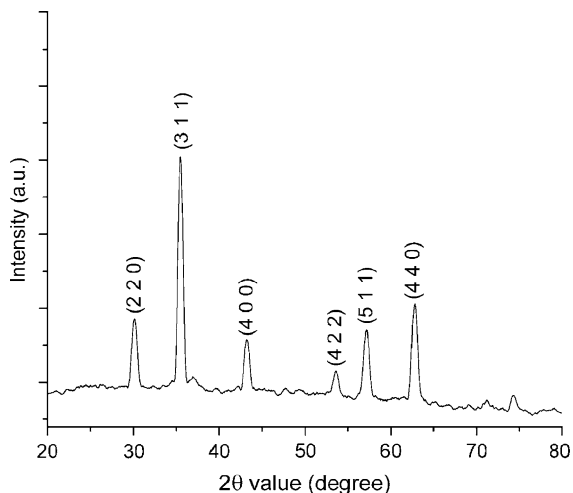
Fig. 8 Grazing incidence X-ray diffraction pattern of myco-synthesized iron oxide nanoparticles. The XRD pattern indicates Bragg's reflections corresponding to the magnetite structure
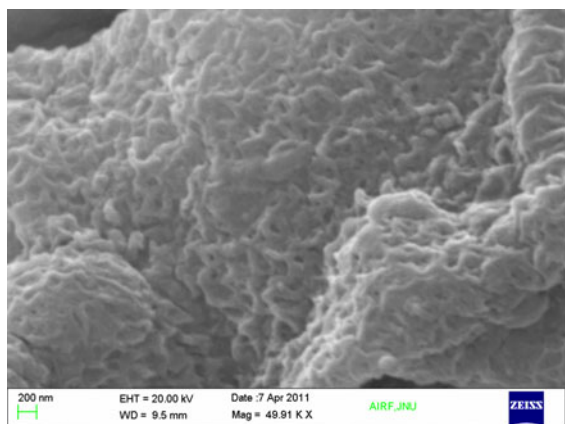

Fig. 9 SEM micrograph of fungal biomass exposed to precursor salts showing the absence of iron oxide nanoparticles on biomass surface (*scale bar* equivalent to 200 nm)

Role of fungal proteins in synthesis and stabilization

Fourier transform infrared measurements were carried out to identify the possible interaction between fungal proteins and IONPs (Fig. 10). FTIR analysis of freeze-dried samples showed a prominent vibration band at wavenumber 1,635 cm^{-1} assigned to the amide I bond of proteins arising due to carbonyl stretch in proteins, wavenumber 1,458 cm^{-1} representing –CH_2– bending mode characteristic of protein side chains and wavenumber 1,400 cm^{-1} indicating COO^- stretching
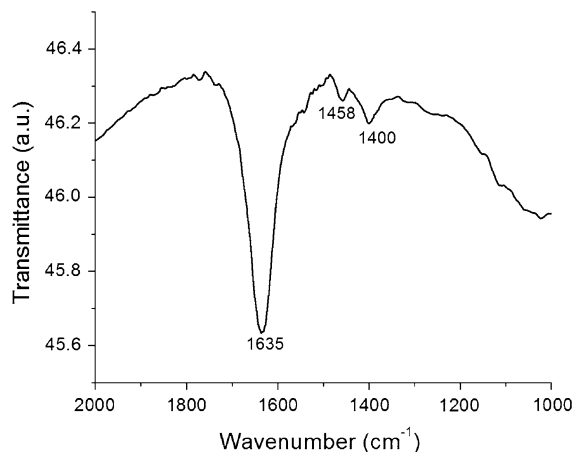

Fig. 10 FTIR spectrum of freeze-dried sample of iron oxide nanoparticles
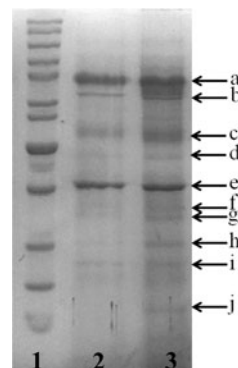

Fig. 11 SDS-PAGE analysis of purified extracellular proteins from *Aspergillus japonicus* isolate AJP01. *Lane 1* 10–200 kDa molecular size marker (Fermentas SM0661). Purified extracellular proteins obtained from unexposed (*lane 2*) and exposed (*lane 3*) fungal biomass to precursor salt solution. The *arrows* indicate extracellular proteins with molecular weight ca. 85 kDa (*a*), 76 kDa (*b*), 55 kDa (*c*), 49 kDa (*d*), 42 kDa (*e*), 38 kDa (*f*), 36.5 kDa (*g*), 31 kDa (*h*), 28 kDa (*i*) and 21 kDa (*j*)

(Macdonald and Smith 1996; Wang et al. 2006; Yang et al. 2007).

A significant difference was observed in the concentration of various extracellular proteins expressed from biomass exposed to the precursor salt solution as compared to the control (unexposed biomass). The concentration of extracellular proteins secreted by the fungal biomass exposed to the precursor salt solution was determined to be 1,125 $\pm$ 7.5 µg/mL, which was nearly twice the concentration of extracellular proteins (587 $\pm$ 2.3 µg/mL) secreted by the unexposed biomass as estimated by Lowry's assay.

To identify the active role of extracellular proteins secreted by fungal biomass in synthesis and/or stabilization of IONPs, the protein profiles were compared by one-dimensional SDS-PAGE (Fig. 11). The SDS-PAGE analysis revealed the presence of several extracellular proteins, ca. 85 kDa (a), 76 kDa (b), 55 kDa (c), 49 kDa (d), 42 kDa (e), 38 kDa (f), 36.5 kDa (g), 31 kDa (h), 28 kDa (i) and 21 kDa (j).

The role of fungal protein in stabilization was further proved in the context with commercially available magnetite nanoparticles. A zeta potential of -1.83 mV was observed in control having magnetite nanoparticles suspended in water, whereas a zeta potential value of -12.2 eV was observed for magnetite nanoparticles incubated with fungal extracellular proteins. The more negative zeta potential observed in the latter case signifies that the protein plays an important role in the stabilization of nanoparticles making them more dispersed and stable (Patil et al. 2007).

Discussion

Overall, 16 morphologically distinct fungi were isolated from iron-rich soil. In our earlier study, we have demonstrated the ability of metal-tolerant fungus in the biosynthesis of nanoparticles (Jain et al. 2013). A mixture of iron cyanide complex was chosen as the precursor salt solution for the extracellular synthesis of IONPs. All the fungal isolates were screened to check their ability to hydrolyze iron cyanide complexes. Isolate AJP01 showed the most promising results on the basis of UV–visible spectroscopic measurements and was selected for further studies. For harnessing the complete potential of the remarkable capabilities of any biological entity, it is a prerequisite to identify the organism which improves the possibility of constructive modification, both at the physiological and molecular levels (Jogler et al. 2009). On the basis of comparative sequence analysis of ITS regions of ribosomal DNA, partial β-tubulin and partial calmodulin gene sequences, isolate AJP01 was identified as *Aspergillus japonicus*.

The extracellular synthesis of IONPs was achieved by exposing fungal biomass to precursor salt solution under ambient conditions. As shown in Fig. 1, the fungus was successful in hydrolyzing iron cyanide complexes, as the intensity at 420 nm corresponding to the absorption maxima of potassium ferricyanide observed a progressive decrease as a function of time. Noteworthy is the development of a broad absorption band at ca. 330 nm corresponding to the formation of iron oxide (Sherman and Waite 1985). This indicates the concurrent synthesis of IONPs as the cell-free filtrate turned brown in color at the end of the reaction. A similar kind of observation regarding change in color of the cell-free filtrate has been reported by Bharde et al. (2006), wherein the synthesis of IONPs was achieved using *Fusarium oxysporum* and *Verticillium* species. The percent hydrolysis of iron cyanide complexes showed no increase after 96 h of reaction (Fig. 2). The subsequent decrease in the rate of hydrolysis with time may be credited to the increase in pH toward alkalinity apart from a decline in substrate concentration which might have affected fungal enzyme activity such as nitrilase/cyanide hydratase. Cyanide hydratase is primarily a fungal enzyme responsible for the hydrolysis of cyanide complexes forming formamide (Ebbs 2004). The hydrolysis may be attributed to cyanide biodegradation as a consequence of its availability as a sole source of carbon and nitrogen for the survival of fungus under nutrient-deprived stress conditions (Dumestre et al. 1997; Barclay et al. 1998).

The fungus was able to maintain its growth and viability as it showed significant increase in CFU values as well as good growth on PDA plates even after 96 h of exposure with precursor salt solution containing cyanide, proving the utilization and degradation of cyanide as an energy source (Supplementary Material, Table S1, Fig. S1).

It is notable that the size of mycosynthesized nanoparticles is less than 100 nm as characterized by TEM analysis (Fig. 3; Fig. 4). This amenable size makes them potential candidates for use in various bio-inspired applications, where particle size is an essential consideration (Arruebo et al. 2007). SAED, HR-TEM, EDS and XRD analysis in this study further confirmed the composition and crystallinity of the obtained IONPs, respectively (Figs. 5, 6, 7, 8). The SEM analysis depicts the absence of nanoparticles on fungal surface (Fig. 9). These results prove the exclusive extracellular synthesis of IONPs by *Aspergillus japonicus* isolate AJP01.

The exposure of fungal biomass to the precursor salt solution resulted in the release of metal ions from cyanide complexes, which were confirmed by the

positive results for ferrozine assay in the test samples as compared to pure precursor salt solution. In earlier reports, it has been clearly demonstrated that complexed iron does not react with ferrozine and requires to be released from its complex form (Riemer et al. 2004). Ferrozine assay clearly indicated the degradation of cyanide complexes by fungal isolate and subsequent release of free metal ions (Dumestre et al. 1997; Barclay et al. 1998).

The mycosynthesis of nanoparticles is a result of complex biochemical reactions which can be mediated by a number of metabolic intermediates (Durán et al. 2011). In an earlier study, we showed that mycosynthesized silver nanoparticles were individually coated with extracellular fungal proteins (Jain et al. 2011). In the present study, FTIR measurements showed close interactions between fungal proteins and IONPs (Fig. 10). The proteins are believed to be associated with nanoparticles in their native secondary structure, as indicated by the vibration band at wavenumber 1,635 cm^{-1} (Takekiyo et al. 2009). The concentration of extracellular proteins secreted by fungal biomass

exposed to precursor salt solution was nearly twice the concentration of extracellular proteins secreted by unexposed biomass as estimated by Lowry's assay and also observed by SDS-PAGE (Fig. 11). These results indicate the elevated expression of various extracellular proteins in the presence of precursor salt solution, which may be responsible for the coprecipitation, controlled nucleation and/or stabilization of IONPs. However, the hydrolysis of iron cyanide complexes may not be attributed to these extracellular proteins, as synthesis of IONPs using only cell-free filtrate (containing extracellular proteins) exclusive of biomass failed to give positive results for hydrolysis of iron cyanide complexes. In this case, no change in the intensity at 420 nm which is attributed to the characteristic absorption maximum of potassium ferricyanide was observed as a function of time during the course of reaction spanning 96 h. These results clearly indicate the role of fungal membrane proteins in hydrolyzing iron cyanide complexes and releasing free ferric and ferrous ions, and expectantly subsequent hydrolysis of cyanide. Fungi are well known to

Fig. 12 Possible mechanism suggesting mycosynthesis of iron oxide nanoparticles
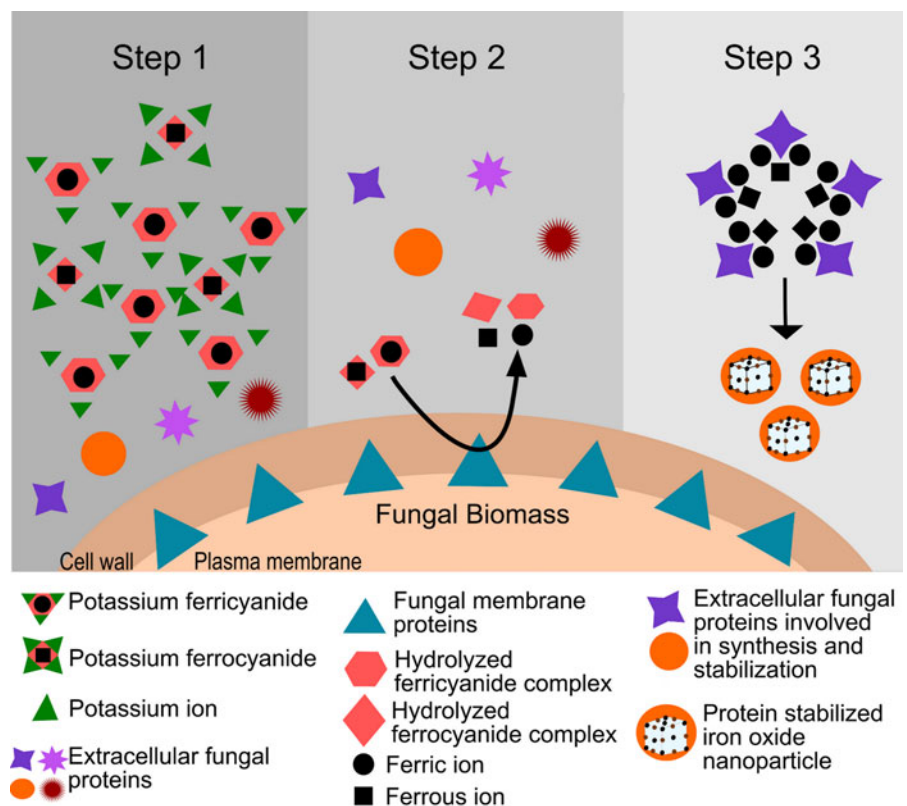
degrade (hydrolyze) metal cyanide complex by the action of enzymes such as cyanide hydratase or nitrilase, which hydrolyzes the metal cyanide bond, releasing the free metal moiety (Barclay et al. 1998; Ebbs 2004).

Based on the present experimental findings, a schematic presentation of the possible mechanism for synthesis of IONPs is speculated (Fig. 12). We hypothesized that the synthesis process occurs in three steps. The first step involves the immediate release of potassium ions from the ferricyanide and ferrocyanide complexes soon after the addition of precursor salts in solution. In the second step, the ferricyanide and ferrocyanide complexes undergo hydrolysis as supported by UV–visible spectroscopic analysis. This is possibly mediated by one or more of the fungal membrane proteins releasing ferric and ferrous ions as determined by the ferrozine assay during the present study. Expectantly, hydrolysis of cyanide may take place as being the only nutrient source for growth and survival of fungi under nutrient-deprived stress conditions during the experiment. The role of extracellular proteins in the hydrolysis of iron cyanide complexes can be disqualified as no observable results were obtained in the reaction with only cell-free filtrate. The third step involves the IONPs 'synthesis' by coprecipitation and controlled nucleation of ferric and ferrous ions available at millimolar ratio of 1:0.5, respectively. Progressing alkaline pH and interaction of one or more extracellular proteins may mediate the 'synthesis', followed by stabilization of mycosynthesized IONPs by other proteins, as suggested by the FTIR studies. The role of extracellular proteins in stabilization was further confirmed by the increase in zeta potential value of protein stabilized nanoparticles as compared to unstabilized ones.

Further investigations at the biochemical and molecular level regarding the hydrolysis of iron cyanide complexes, protein/polypeptide-mediated synthesis and stabilization of IONPs are in progress in our laboratory. Elucidation of the detailed mechanism behind biosynthesis of IONPs using fungi can lead to imperative modifications in the protocol for augmentation in the overall yield of IONPs. Genetic engineering implications to the present process can be achieved if the involved proteins and their respective genes can be identified making mycosynthesis comparable to commercially used physical and chemical methods of nanoparticle synthesis.

References

Arruebo M, Fernández-Pacheco R, Ibarra MR, Santamaría J (2007) Magnetic nanoparticles for drug delivery. Nano Today 2:22–32. doi:10.1016/S1748-0132(07)70084-1

Barclay M, Hart A, Knowles CJ, Meeussen JCL, Tett VA (1998) Biodegradation of metal cyanides by mixed and pure cultures of fungi. Enzyme Microb Technol 22:223–231. doi:10.1016/S0141-0229(97)00171-3

Bharde A, Rautaray D, Bansal V, Ahmad A, Sarkar I, Yusuf SM, Sanyal M, Sastry M (2006) Extracellular biosynthesis of magnetite using fungi. Small 2:135–141. doi:10.1002/smll.200500180

Bhargava A, Jain N, Panwar J (2011) Synthesis and application of magnetic nanoparticles: a biological perspective. In: Dhingra HK, Jha PN, Bajpai P (eds) Current topics in biotechnology and microbiology: recent trends. Lap Lambert Academic Publishing AG & Co Kg, Colne, pp 117–155

Dhillon GS, Brar SK, Kaur S, Verma M (2011) Green approach for nanoparticle biosynthesis by fungi: current trends and applications. Crit Rev Biotechnol 32:49–73. doi:10.3109/07388551.2010.550568

Dumestre A, Chone T, Portal J, Gerard M, Berthelin J (1997) Cyanide degradation under alkaline conditions by a strain of *Fusarium solani* isolated from contaminated soils. Appl Environ Microbiol 63:2729–2734

Durán N, Marcato P, Durán M, Yadav A, Gade A, Rai M (2011) Mechanistic aspects in the biogenic synthesis of extracellular metal nanoparticles by peptides, bacteria, fungi, and plants. Appl Microbiol Biotechnol 90:1609–1624. doi:10.1007/s00253-011-3249-8

Ebbs S (2004) Biological degradation of cyanide compounds. Curr Opin Biotechnol 15:231–236. doi:10.1016/j.copbio.2004.03.006

Fedlheim DL, Foss CA (2001) Metal nanoparticles: synthesis, characterization, and applications. CRC Press, Boca Raton

Gade A, Ingle A, Whiteley C, Rai M (2010) Mycogenic metal nanoparticles: progress and applications. Biotechnol Lett 32:593–600. doi:10.1007/s10529-009-0197-9

Gibbs CR (1976) Characterization and application of ferrozine iron reagent as a ferrous iron indicator. Anal Chem 48:1197–1201. doi:10.1021/ac50002a034

Glass NL, Donaldson GC (1995) Development of primer sets designed for use with the PCR to amplify conserved genes

from filamentous ascomycetes. Appl Environ Microbiol 61:1323–1330

Jain N, Bhargava A, Majumdar S, Tarafdar JC, Panwar J (2011) Extracellular biosynthesis and characterization of silver nanoparticles using *Aspergillus flavus* NJP08: a mechanism perspective. Nanoscale 3:635–641. doi:10.1039/C0NR00656D

Jain N, Bhargava A, Tarafdar JC, Singh SK, Panwar J (2013) A biomimetic approach towards synthesis of zinc oxide nanoparticles. Appl Microbiol Biotechnol 97:859–869. doi:10.1007/s00253-012-3934-2

Jogler C, Lin W, Meyerdierks A, Kube M, Katzmann E, Flies C, Pan Y, Amann R, Reinhardt R, Schüler D (2009) Toward cloning of the magnetotactic metagenome: identification of magnetosome island gene clusters in uncultivated magnetotactic bacteria from different aquatic sediments. Appl Environ Microbiol 75:3972–3979. doi:10.1128/AEM.02701-08

Jun YW, Seo JW, Cheon J (2008) Nanoscaling laws of magnetic nanoparticles and their applicabilities in biomedical sciences. Acc Chem Res 41:179–189. doi:10.1021/ar700121f

Komeili A (2007) Molecular mechanisms of magnetosome formation. Annu Rev Biochem 76:351–366. doi:10.1146/annurev.biochem.74.082803.133444

Laemmli UK (1970) Cleavage of structural proteins during the assembly of the head of bacteriophage T4. Nature 227:680–685. doi:10.1038/227680a0

Laurent S, Forge D, Port M, Roch A, Robic C, Vander Elst L, Muller RN (2008) Magnetic iron oxide nanoparticles: synthesis, stabilization, vectorization, physicochemical characterizations, and biological applications. Chem Rev 108:2064–2110. doi:10.1021/cr068445e

Lowry OH, Rosebrough NJ, Farr AL, Randall RJ (1951) Protein measurement with the folin phenol reagent. J Biol Chem 193:265–275

Macdonald IDG, Smith WE (1996) Orientation of cytochrome c adsorbed on a citrate-reduced silver colloid surface. Langmuir 12:706–713. doi:10.1021/la950256w

Njagi EC, Huang H, Stafford L, Genuino H, Galindo HM, Collins JB, Hoag GE, Suib SL (2010) Biosynthesis of iron and silver nanoparticles at room temperature using aqueous sorghum bran extracts. Langmuir 27:264–271. doi:10.1021/la103190n

Noguez C (2007) Surface plasmons on metal nanoparticles: the influence of shape and physical environment. J Phys Chem C 111:3806–3819. doi:10.1021/jp066539m

O'Donnell K, Nirenberg H, Aoki T, Cigelnik E (2000) A multigene phylogeny of the *Gibberella fujikuroi* species complex: detection of additional phylogenetically distinct species. Mycoscience 41:61–78. doi:10.1007/BF02464387

Parikh RY, Ramanathan R, Coloe PJ, Bhargava SK, Patole MS, Shouche YS, Bansal V (2011) Genus-wide physicochemical

evidence of extracellular crystalline silver nanoparticles biosynthesis by *Morganella* spp. PLoS ONE 6:e21401. doi:10.1371/journal.pone.0021401

Patil S, Sandberg A, Heckert E, Self W, Seal S (2007) Protein adsorption and cellular uptake of cerium oxide nanoparticles as a function of zeta potential. Biomaterials 28:4600–4607. doi:10.1016/j.biomaterials.2007.07.029

Riemer J, Hoepken HH, Czerwinska H, Robinson SR, Dringen R (2004) Colorimetric ferrozine-based assay for the quantitation of iron in cultured cells. Anal Biochem 331:370–375. doi:10.1016/j.ab.2004.03.049

Schnurer J (1993) Comparison of methods for estimating the biomass of three food-borne fungi with different growth patterns. Appl Environ Microbiol 59:552–555

Sherman DM, Waite TD (1985) Electronic spectra of Fe (super 3+) oxides and oxide hydroxides in the near IR to near UV. Am Mineral 70:1262–1269

Simpson RJ (2004) Purifying proteins for proteomics: a laboratory manual. Cold Spring Harbor Laboratory Press, New York

Sun YK, Ma M, Zhang Y, Gu N (2004) Synthesis of nanometer-size maghemite particles from magnetite. Colloids Surf A 245:15–19. doi:10.1016/j.colsurfa.2004.05.009

Takekiyo T, Wu L, Yoshimura Y, Shimizu A, Keiderling TA (2009) Relationship between hydrophobic interactions and secondary structure stability for trpzip β-hairpin peptides. Biochemistry 48:1543–1552. doi:10.1021/bi8019838

Teja AS, Koh PY (2009) Synthesis, properties, and applications of magnetic iron oxide nanoparticles. Prog Cryst Growth Charact Mater 55:22–45. doi:10.1016/j.pcrysgrow.2008.08.003

Wang C, Zhang Y, Seng HS, Ngo LL (2006) Nanoparticle-assisted micropatterning of active proteins on solid substrate. Biosens Bioelectron 21:1638–1643. doi:10.1016/j.bios.2005.07.008

White TJ, Bruns T, Lee S, Taylor J (1990) Amplification and direct sequencing of fungal ribosomal RNA genes for phylogenetics. In: Innis MA, Gelfand DH, Sninsky JJ, White TJ (eds) PCR protocols a guide to methods and applications. Academic Press, San Diego, pp 315–322

Williams M (1997) The Merck Index, 12th Edition. CD-Rom Version 12.1. Drug Dev Res 41:108–108. doi:10.1002/(SICI)1098-2299(199706)41:2<108::AID-DDR9>3.0.CO;2-L

Wu Z, Neaton JB, Grossman JC (2008) Quantum confinement and electronic properties of tapered silicon nanowires. Phys Rev Lett 100:e246804. doi:10.1103/PhysRevLett.100.246804

Yang T, Li Z, Wang L, Guo C, Sun Y (2007) Synthesis, characterization, and self-assembly of protein lysozyme monolayer-stabilized gold nanoparticles. Langmuir 23:10533–10538. doi:10.1021/la701649z
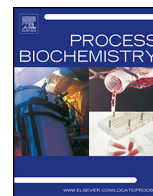
Development of gold nanoparticle-fungal hybrid based heterogeneous interface for catalytic applications

Arpit Bhargava [a], Navin Jain [a], Subhashis Gangopadhyay [b], Jitendra Panwar [a],*

[a] Centre for Biotechnology, Department of Biological Sciences, Birla Institute of Technology and Science, Pilani 333031, India
[b] Department of Physics, Birla Institute of Technology and Science, Pilani 333031, India

ABSTRACT

Unsupported and free gold nanoparticles (Au NPs) represent great potential in the field of catalysis. However, shortcomings like agglomeration and loss of the precious catalyst has encouraged the development of supported Au NPs as catalyst with increased activity, selectivity, ease of separation from the reaction mixture and recyclability. The present work demonstrates an eco-friendly, rapid and facile synthesis of catalytically active bio-supported Au NPs using a soil fungus, *Aspergillus japonicus* AJP01. The dual role of the fungal isolate in synthesis as well as immobilization of Au NPs is the remarkable feature of the study. The fungus successfully reduced Au(III) into Au NPs containing principally Au(0) with a small percentage of Au(I) as revealed by X-ray photoelectron spectroscopy. The particles were spherical in shape and well distributed on fungal mycelia with size ranging predominantly between 15 and 20 nm. The as-synthesized nanoparticle-fungal hybrid was found to be highly efficient in catalyzing sodium borohydride mediated reduction reactions of 4-nitrophenol and hexacyanoferrate(III). The versatility of the bionanocatalyst was further demonstrated by catalyzing the A^3 coupling reactions for the synthesis of propargylamines.

© 2015 Elsevier Ltd. All rights reserved.

1. Introduction

Gold is considered as the metal of beauty, commerce and pride since antiquity. In addition, gold is being used in various scientific applications viz. advanced electronics, fuel cells, coatings, dentistry and biomedicine due to its unique properties like malleability, inertness, heat and electrical conductivity [1]. Breaking the ancient viewpoint wherein gold was considered as an inert metal, later part of the 20th century witnessed the rise of gold based catalysis reactions. The stoichiometry of gold has now been employed in various chemical processes like oxidation of alcohols and aldehydes, epoxidation of propylene, hydrochlorination of ethyne, carbon–carbon bond formation and many other reactions [2]. Presently, gold in its nanoform as "gold nanoparticles (Au NPs)" is extensively used in diverse applications like electronics, sensors, photo-thermal and photo-dynamic therapy, drug and gene delivery, probe fabrication, diagnostics, cosmetics and lubricants [3]. Besides these applications, Au NPs have also become the preferred catalyst for a wide variety of chemical reactions [4]. Compared to its bulk form, Au NPs outperform as catalyst due to their increased surface area, presence of more active sites and improved reaction selectivity [5,6].

Shortcomings like agglomeration and loss of precious catalyst during harsh reaction conditions have compromised the applicability of unsupported and free Au NPs. This has encouraged researchers for the development of supported Au NPs as catalytic system. As catalysts, supported Au NPs exhibit multiple improvements over free Au NPs like increased activity, ease of separation from the reaction mixture and recyclability [7]. The on-cell synthesis of nanoparticles using microbes is an exciting eco-friendly approach which provides a low-cost nanoparticle support system and a smart heterogeneous interface for the catalytic reactions [8]. Various properties of nanoparticles including their size, shape, surface structure and composition contribute significantly to the catalytic activity, efficiency and selectivity [3]. Biological systems maintain strict control over these properties and immobilize nanoparticles on their surface either by entanglement to the cell wall or by embedment within the cell wall leading to marginal metal leaching and thus retains excellent recyclability [9,10].

Use of Au NPs in reduction reactions mediated by sodium borohydride (NaBH$_4$) has been reported by several researchers [11–14]. The reduction of 4-nitrophenol to 4-aminophenol as well as hexacyanoferrate(III) to hexacyanoferrate(II) are redox catalysed reactions wherein Au NPs transfer electrons from borohydride ion

to the reducing entity. As no chemical reaction occurs between the reactants and nanoparticles, the catalytic property and colloidal stability of participating Au NPs is retained even after reaction completion [13,14]. Considering the importance of simple separation and reusability of Au NPs, researchers have also turned to explore their use in catalyzing three component coupling reactions known as A³ coupling which were earlier mostly reported to be catalysed by the ionic form of gold [15–19]. A³ coupling reactions involve conversion of aldehyde, amine and alkyne for the synthesis of propargylamines which acts as a building block and skeleton for the synthesis of biologically active compounds [20].

The present study reports an eco-friendly and rapid synthesis of catalytically active bio-supported Au NPs using a soil fungus, *Aspergillus japonicus* AJP01. The fungal biomass played a dual role as it simultaneously synthesized and immobilized the Au NPs on its surface. The nanoparticles were characterized by scanning electron microscopy (SEM), energy dispersive spectroscopy (EDS), X-ray diffraction (XRD), X-ray photoelectron spectroscopy (XPS), UV–vis spectroscopy and transmission electron microscopy (TEM) measurements. The versatile catalytic property of the as-synthesized bionanocatalyst has also been comprehensively discussed.

2. Experimental

2.1. Chemicals

All the chemicals used were of analytical grade and procured from Sigma-Aldrich or Merck Chemicals unless otherwise stated. The culture media components were purchased from HiMedia Laboratories. Milli-Q water was obtained from a Milli-Q Biocel water purification system manufactured by Merck Millipore.

2.2. Mycosynthesis of bionanocatalyst

Soil fungus *A. japonicus* AJP01 was used for the synthesis of Au NPs. The complete details of isolation and molecular characterization of the fungal isolate can be obtained from our previous report [21]. Stock culture of the fungal isolate was maintained on potato dextrose agar (PDA) slants (pH 5.6) by repeated sub-culturing on fresh media at 28 °C. From an actively growing culture, a loopful of spore was inoculated in 100 mL of MGYP medium (0.3% malt extract, 1.0% glucose, 0.3% yeast extract, 0.5% peptone; pH 7.0) in 250 mL Erlenmeyer flask. The inoculated flask was incubated at 28 °C for 72 h on a rotary shaker (120 rpm) under dark conditions. After the incubation period, fungal biomass was separated from the culture medium by centrifugation (5000 rpm, 15 min, 4 °C) and washed thrice with autoclaved Milli-Q water to remove all traces of media from the biomass surface. Typically, 20 g (wet weight) of biomass was resuspended in 100 mL of 1.0 mM gold(III) chloride trihydrate solution in 250 mL Erlenmeyer flask and incubated for 72 h under the similar conditions described above. Biomass in autoclaved Milli-Q water (without gold(III) chloride solution) as positive control and pure gold(III) chloride solution (without biomass) as negative control were also incubated simultaneously at 28 °C for 72 h on a rotary shaker (120 rpm) under dark conditions along with the experimental flasks in three replicates. After incubation, the biomass was separated by filtration using Whatman grade 1 filter paper and washed thrice with autoclaved Milli-Q water before further characterization and use in catalytic application.

2.3. Characterization of bionanocatalyst

The amount of Au(III) ions remaining in the solution after exposure to *A. japonicus* AJP01 as a function of time was monitored by measuring the UV–vis absorption spectrum of culture supernatant using a Jasco V-630 UV–vis spectrophotometer operated at

a scan speed of 400 nm min⁻¹. The synthesis of Au NPs on the fungal biomass surface was visually validated and further confirmed by SEM imaging. Sample for SEM was prepared by fixing the fungal biomass bearing Au NPs in 2.5% (v/v) glutaraldehyde (prepared in 0.1 M sodium phosphate buffer, pH 7.2) at 4 °C for overnight. After fixation, the specimen was rinsed with phosphate buffer (pH 7.2) and dehydrated in a series of 30–100% ethanol followed by drying in a vacuum desiccator. SEM micrographs were obtained by imaging the specimen on a Hitachi S-3400N SEM instrument. EDS measurements of specimen were carried out using a Thermo Noran System SIX EDS attached with the SEM instrument. XRD measurement of the freeze dried biomass was carried out to authenticate crystallinity of Au NPs using an X'Pert PRO X-ray diffractometer operated at a voltage of 40 kV and current of 30 mA with CuK_α radiation. The crystal phase was determined by comparing the calculated values of interplanar spacing and corresponding intensities of diffraction peaks with theoretical values from the Joint Committee on Powder Diffraction Standards-International Centre for Diffraction Data (JCPDS-ICCD) database. Scherrer's equation was applied to determine the size of the Au NPs using the data acquired by XRD analysis [22].

The chemical state of gold species within the Au NPs trapped on the surface of fungal biomass was determined by XPS using an Omicron EA 125 instrument equipped with a seven-channel detection system. The sample was fixed on a small piece of conducting carbon tape and dried overnight under an ultra-high vacuum condition. Monochromatic light of Al-$K\alpha$ radiation of energy 1486.7 eV was used as X-ray source. Wide scale and high resolution XPS spectrums of Au 4f were obtained using energy steps of 0.1 and 1.0 eV, respectively. The emission current of 15 mA and chamber base pressure below 10⁻⁹ mbar was used throughout the XPS measurement.

In order to extract the trapped Au NPs, 0.1 g (wet weight) of fungal biomass was suspended in 1.0 mL Milli-Q water and sonicated for 3 h in an ultrasonic cleaner. After sonication, the fungal biomass was separated by centrifugation (3000 rpm, 5 min) and the supernatant containing extracted Au NPs was analysed by UV–vis spectroscopy and TEM. Sample for TEM was prepared by placing a drop of nanoparticle solution on to a carbon coated copper grid. The extra solution was removed using an absorbent paper and the grid was incubated overnight in vacuum desiccator prior to measurement. TEM micrographs were captured on a JEOL JEM-2100 instrument at an operating voltage of 200 kV.

2.4. Catalytic activity of bionanocatalyst

2.4.1. Reduction of 4-nitrophenol and hexacyanoferrate(III)
The reduction reaction of 4-nitrophenol as well as hexacyanoferrate(III) was performed using NaBH₄ in presence of bionanocatalyst. The progress of reaction was monitored by recording the absorption spectrum at one minute interval. Briefly, the reduction reaction of 4-nitrophenol was performed by adding 2885 µL of water, 15 µL of 4-nitrophenol (0.01 M) and 100 µL of aqueous NaBH₄ (0.1 M) to a 3 mL quartz cuvette containing 6 mg of bionanocatalyst. Similarly, reduction reaction of hexacyanoferrate(III) was performed by adding 2670 µL of water, 30 µL of potassium ferricyanide (8.33×10^{-2} M) and 300 µL of aqueous NaBH₄ (0.1 M) to a 3 mL quartz cuvette containing 6 mg of bionanocatalyst. In order to rule out the possibility of reduction reaction by fungal mycelia, the biomass without Au NPs was used as negative control in both these reactions.

2.4.2. Synthesis of propargylamines
Scheme 1 represents the synthesis of propargylamines by A³ coupling of variety of aromatic aldehydes (R = H, CH₃, Cl), secondary amine and alkyne under inert nitrogen atmosphere [19].
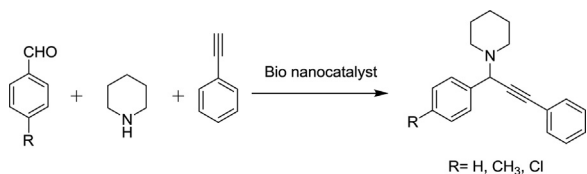
Scheme 1. Bionanocatalyst mediated A^3 coupling of aldehyde, secondary amine and alkyne for the synthesis of propargylamine (R = H, CH3, Cl).

The bionanocatalyst was thoroughly washed with tetrahydrofuran to ensure aqueous free environment and removal of all traces of unbound gold. The excess tetrahydrofuran was removed by keeping the fungal biomass on an absorbent paper. Briefly, 40 mg of bionanocatalyst was added to the reaction mixture composed of substituted benzaldehyde (1 mmol), piperidine (1.1 mmol), phenyl acetylene (1.2 mmol) and 5 mL of tetrahydrofuran in a 50 mL round bottom flask equipped with a reflux condenser. The contents were heated at 80 °C using an oil bath with constant stirring at 1200 rpm. The progress of reaction was monitored by thin layer chromatography (TLC) using silica gel plates till completion. The crude reaction mixture was chromatographed using silica gel (100–200) column and the as-formed propargylamine was eluted using 50% chloroform/hexane to quantify its percent yield. Structures of all the derivatives (R = H, CH3, Cl) were identified on the basis of their spectral analysis (^{1}H nuclear magnetic resonance (NMR) and matrix

assisted laser desorption/ionization mass spectrometry (MALDI-MS) mass spectral data). ^{1}H NMR and MALDI-MS spectrums were recorded on Bruker Avance II 500 MHz and waters micromass Q-TOF spectrometer, respectively. In order to explore the possibility to reuse the catalyst for next cycle of reaction, the bionanocatalyst was recovered from the earlier reaction mixture by centrifugation (3000 rpm, 5 min) and washed thoroughly with tetrahydrofuran before further use.

3. Results and discussion

The fungus *A. japonicus* AJP01 was isolated as a part of our previous study carried out to investigate the nanoparticle synthesis ability of fungi present in metal rich soil [21].

3.1. Characterization of bionanocatalyst

The concentration of Au(III) ions remaining in the culture supernatant was monitored by determining the absorption intensity of Au(III) at 290 nm [23]. As shown in Fig. 1a, the highest concentration of Au(III) was observed at 0 min i.e. soon after the addition of gold(III) chloride in the culture supernatant which underwent a continuous decrease as a function of time. Fig. 1b represents percent decrease in the concentration of Au(III) ions. It is clearly evident that nearly all the Au(III) ions were utilized within 60 min of biomass-salt exposure. Regardless of the rapid utilization of Au(III)
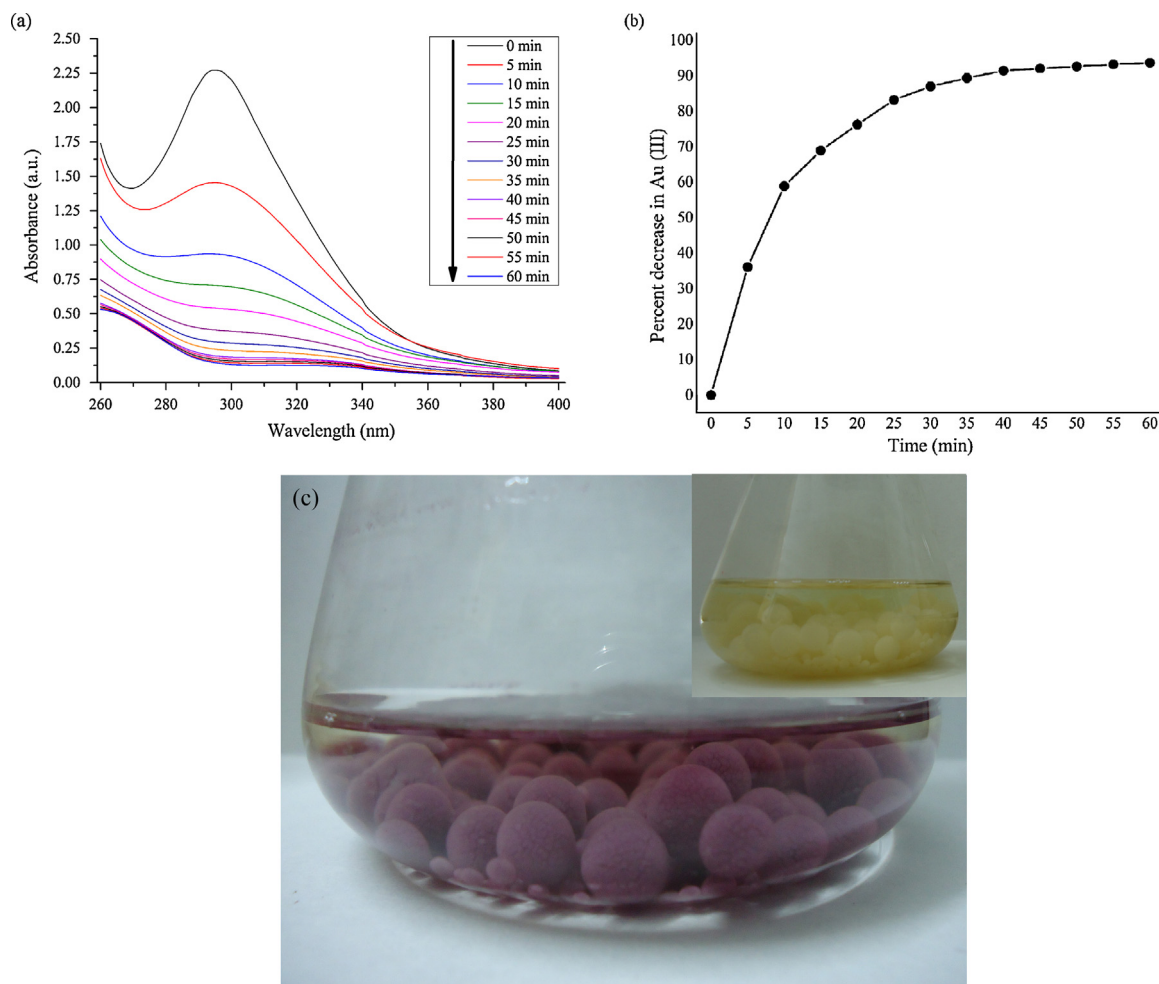

Fig. 1. (a) UV–vis spectra showing utilization of Au(III) ions from culture supernatant as a function of time (b) percent decrease in concentration of Au(III) ions with time (c) Erlenmeyer flask containing fungal biomass after 9 h exposure to gold(III) chloride (Inset shows fungal biomass before exposure). (For interpretation of the references to colour in this figure legend, the reader is referred to the web version of this article.)
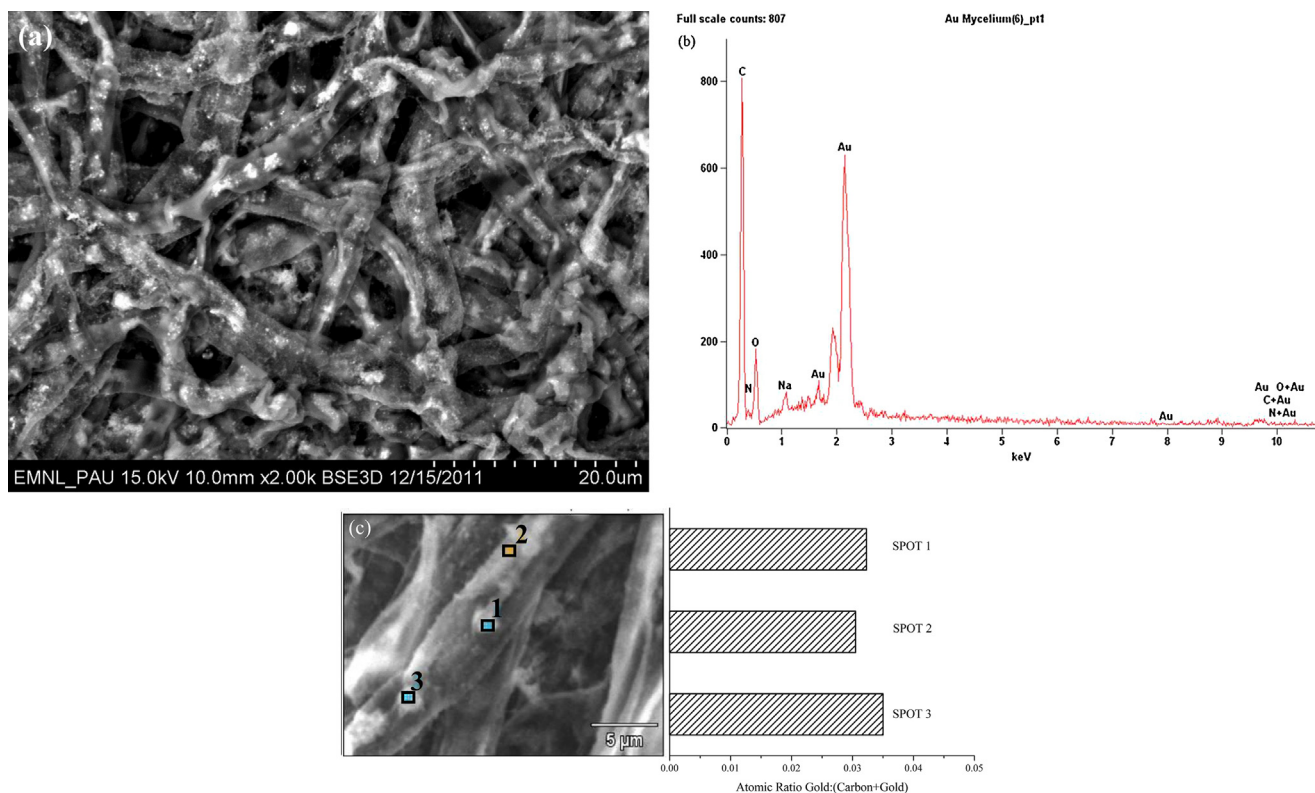
Fig. 2. (a) SEM micrograph of fungal biomass supporting Au NPs (b) EDS spectrum showing elemental composition (c) Atomic ratios of gold: (carbon + gold) obtained from EDS analysis.

ions from the culture supernatant, the synthesis of Au NPs on fungal biomass was observed much later precisely after 4 h of biomass-salt exposure as evident by the change in biomass colour from pale white to vivid purple (Fig. 1c). The development of purple colour was due to the excitation of surface plasmon vibrations that absorbed light in the visible region giving a characteristic coloured appearance to Au NPs. Similar to our observation, Mukherjee et al. [24] also reported the change in colour of fungal biomass due to surface trapping of Au NPs. Based on these results, it can be hypothesized that initially Au(III) ions were absorbed by the fungal biomass and later reduced to form Au NPs. No visual change in the colour intensity of biomass was observed after 9 h of incubation which suggested completion of nanoparticle synthesis. Notably, the reaction completion time in the present study is significantly shorter in comparison to the earlier studies on biosynthesis of Au NPs as reviewed by Lengke et al. [25]. Another distinctive feature of the present study is the exclusive surface bound synthesis of Au NPs as no purple colour was observed in the culture supernatant.

SEM was performed to confirm the synthesis and distribution of nanoparticles on biomass surface. The representative SEM micrograph (Fig. 2a) revealed omnipresence of nanoparticles with limited aggregation on the fungal mycelia. Fig. 2b shows the spot EDS spectrum of Au NPs trapped on biomass. The presence of a strong peak in the EDS spectrum at 2.1 KeV confirmed the presence of pure metallic Au NPs. Apart from this, the comparatively weaker signals for carbon (C), oxygen (O) and nitrogen (N) indicated the presence of fungal biomass in the vicinity of Au NPs [26]. Homogeneity is a highly anticipated property of any catalyst system required to achieve uniform reaction rates [5,6]. Keeping this fact in mind, EDS analysis of three distinct spots of nanoparticle aggregates were carried out to determine the atomic ratio of gold with respect to carbon content. It is clearly evident that the content of gold remained almost similar despite of the location of nanoparticle aggregates confirming the homogenous synthesis of Au NPs on fungal biomass

surface (Fig. 2c). The crystalline nature of the as-synthesized Au NPs was evaluated using XRD measurements. The observed Bragg reflections indicated in Fig. 3, exhibits fcc packing of nanoparticles with well defined peaks at 2θ value of 38.16°, 44.34°, 64.67° and 77.62° corresponding to (1 1 1), (2 0 0), (2 2 0) and (3 1 1) planes, respectively. The recorded XRD pattern was found to be in good agreement with the available JCPDS-ICCD database (JCPDS file no. 00-004-0784).

XPS analysis was employed to determine the chemical as well as the oxidation state on the surface of bionanocatalyst. The wide scale survey scan of the vacuum dried sample showed a clear existence of gold in the form of Au 4f binding energy peaks along with the C1s,
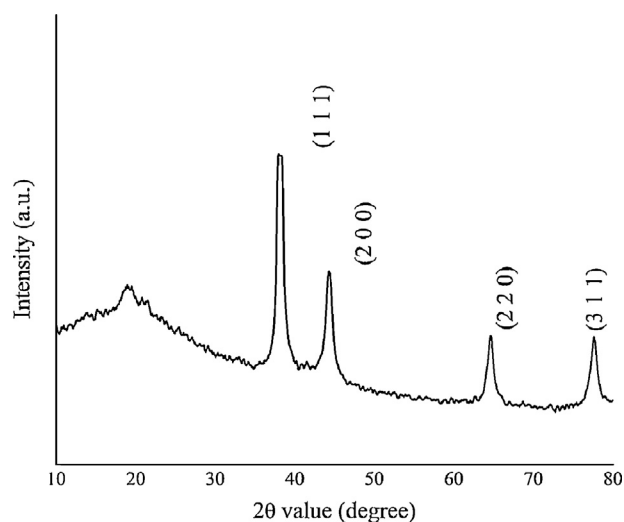

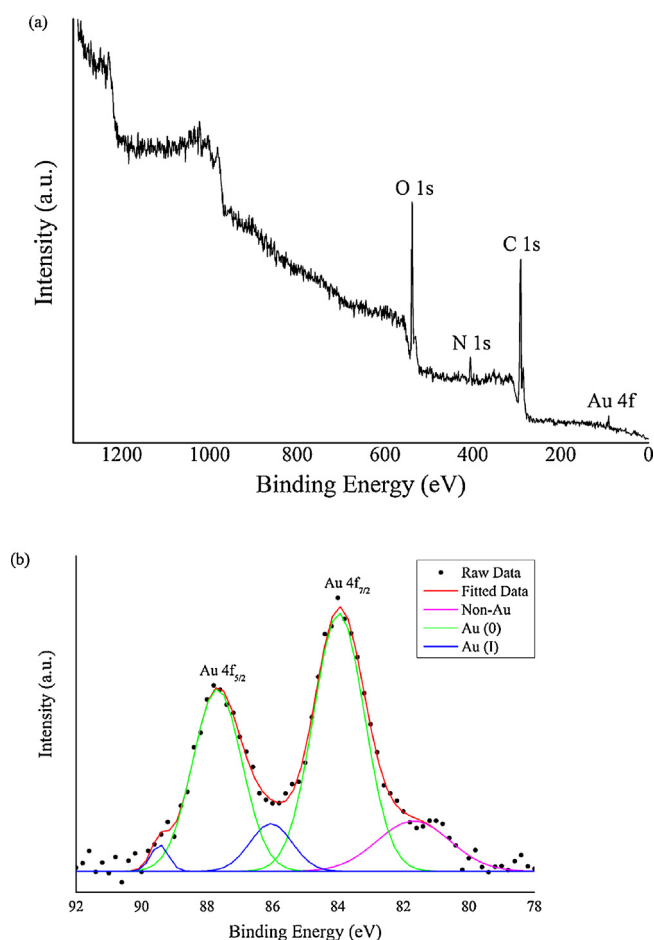Fig. 3. XRD analysis of freeze dried powdered fungal biomass supporting Au NPs.

Fig. 4. XPS analysis of bionanocatalyst (a) wide scale XPS survey spectrum of the vacuum dried fungal biomass supporting Au NPs (b) high resolution XPS spectrum of Au 4f photoelectron peaks with various deconvolution components. The scatter points refer to the raw data, while the solid lines to the curve fitting results.

N1s and O1s peaks (Fig. 4a). This finding further confirmed the formation of Au NPs on the surface of fungal biomass. To compensate any kind of energy shift due to charging effect, XPS peak positions were calibrated against C1s binding energy of 284.5 eV. Fig. 4b represents a high resolution XPS spectrum of Au 4f binding energy with its various deconvolution components. A linear background subtraction and Gaussian fitting were used for the deconvolution of Au 4f peak. The peaks centred around 84 eV and 87.6 eV corresponds to the spin-orbit splitting components Au $4f_{7/2}$ and Au $4f_{5/2}$, respectively, and represented metallic Au(0) state. The binding energy values observed are in good agreement with the reported binding energy values of Au(0) state [14,27]. Apart from this, an additional doublet of much weaker intensity towards the higher binding energy value was also observed. These doublet peaks were found to be centred around 86.05 eV and 89.45 eV and were attributed to the spin-orbit splitting of Au(I) state. From the integral intensity ratio calculation, a small fraction of ~10% ± 3% of Au(I) oxidation state was estimated. Absence of any Au(III) components (which usually appears at even higher binding energy) confirmed that the fungal isolate successfully reduced gold(III) chloride. However, a broad peak of non-gold component centred at 81.7 eV was also observed. This might be attributed to the plasmon loss of 'Bromine', a possible contaminant within the various chemicals used during the analysis. Similar to our interpretation, Das et al. (2012) also speculated the formation of Au(I) as an intermediate form during the reduction of Au(III) to Au(0) as reported in their study on the biomineralization mechanism of gold by *Rhizopous oryzae* [27].

The UV–vis spectrum of the supernatant containing the extracted Au NPs showed appearance of a single surface plasmon resonance (SPR) band at around 545 nm (Fig. 5a). As the characteristic SPR band may be influenced by size, shape and aggregation presence of a single and symmetrical SPR band during the present study suggested that the as-synthesized Au NPs were isotropic in shape and size with no significant aggregation [28,29]. In order to validate these results, TEM imaging was carried out to determine size and shape of the nanoparticles. A representative high resolution (HR)-TEM micrograph revealed that the particles were spherical in shape (Fig. 5b). The particle size histogram of Au NPs showed that the particle size ranges majorly between 15 and 20 nm, as shown in Fig. 5c. The particle size of ~22 nm as calculated using the Scherrer's equation was found to be in close agreement with the results obtained by TEM measurements.

3.2. Catalytic activity of bionanocatalyst

Phenol and phenolic compounds like nitrophenols are one of the major refractory pollutants, released into water bodies from industries manufacturing pesticides, herbicides, insecticides and synthetic dyes. The degradation of these pollutants has received immense attention due to increased environmental concerns [30]. One of the well known ways for the remediation of nitrophenols is its reduction by $NaBH_4$. Even though $NaBH_4$ mediated reduction of 4-nitrophenol to 4-aminophenol is a thermodynamically favourable process, a large potential difference between donor and acceptor molecules decreases the feasibility of this reaction [31]. This can be overcome by use of Au NPs which facilitates efficient electron transfer from the donor borohydride ions to acceptor 4-nitrophenol. Empirically, aqueous solution of 4-nitrophenol exhibits a distinct peak at 317 nm in the UV–vis absorption spectrum that shifts to 400 nm in the presence of $NaBH_4$ due to the formation of 4-nitrophenolate ion in the alkaline medium which act as an intermediate in the conversion of 4-nitrophenol to 4-aminophenol [32]. Based on the above mentioned literature, the reduction reaction of 4-nitrophenol was carried out to test the catalytic efficiency of the nanoparticle-fungal hybrid. Fig. 6a depicts a rapid decrease in the intensity of 4-nitrophenolate absorption peak validating the successful reduction of 4-nitrophenol by the bionanocatalyst. It can be clearly observed that more than 90% reduction was completed within 5 min of the reaction with ~58% reduction within the first one minute. The simultaneous development of another peak at ~305 nm (Fig. 6a inset) confirmed the formation of reduction product (4-aminophenol) in the reaction mixture [33]. It is generally advocated that Au(0) oxidation state in Au NPs acts as active component for the efficient reduction of 4-nitrophenol by $NaBH_4$ [14,30].

Another electron transfer reaction which primarily requires Au(0) oxidation state in Au NPs as active catalyst is the reduction of hexacyanoferrate(III) into hexacyanoferrate(II) by $NaBH_4$. In absence of a suitable catalyst, this reaction is found to be very slow (half-life around 5000 s) and follows zero-order kinetics [11]. However, in presence of a suitable catalyst like Au NPs the same reaction follows first-order kinetics with typically a much shorter half-life of 7.48 s under similar conditions [13]. In the present study, the as-synthesized bionanocatalyst initiated the reduction of hexacyanoferrate(III) in the reaction system as observed by a rapid decrease in the intensity of its absorption peak at 420 nm (Fig. 6b). It was observed that more than 78% of hexacyanoferrate(III) was reduced within 10 min of the reaction with an average reduction rate of 14.28% per min. Noticeably, in both the above mentioned reactions the colour of bionanocatalyst remained unchanged which indicated that the Au NPs were coloidally stable and did not react with any reactants. Negative controls in the both the reactions have not shown any reduction reaction.
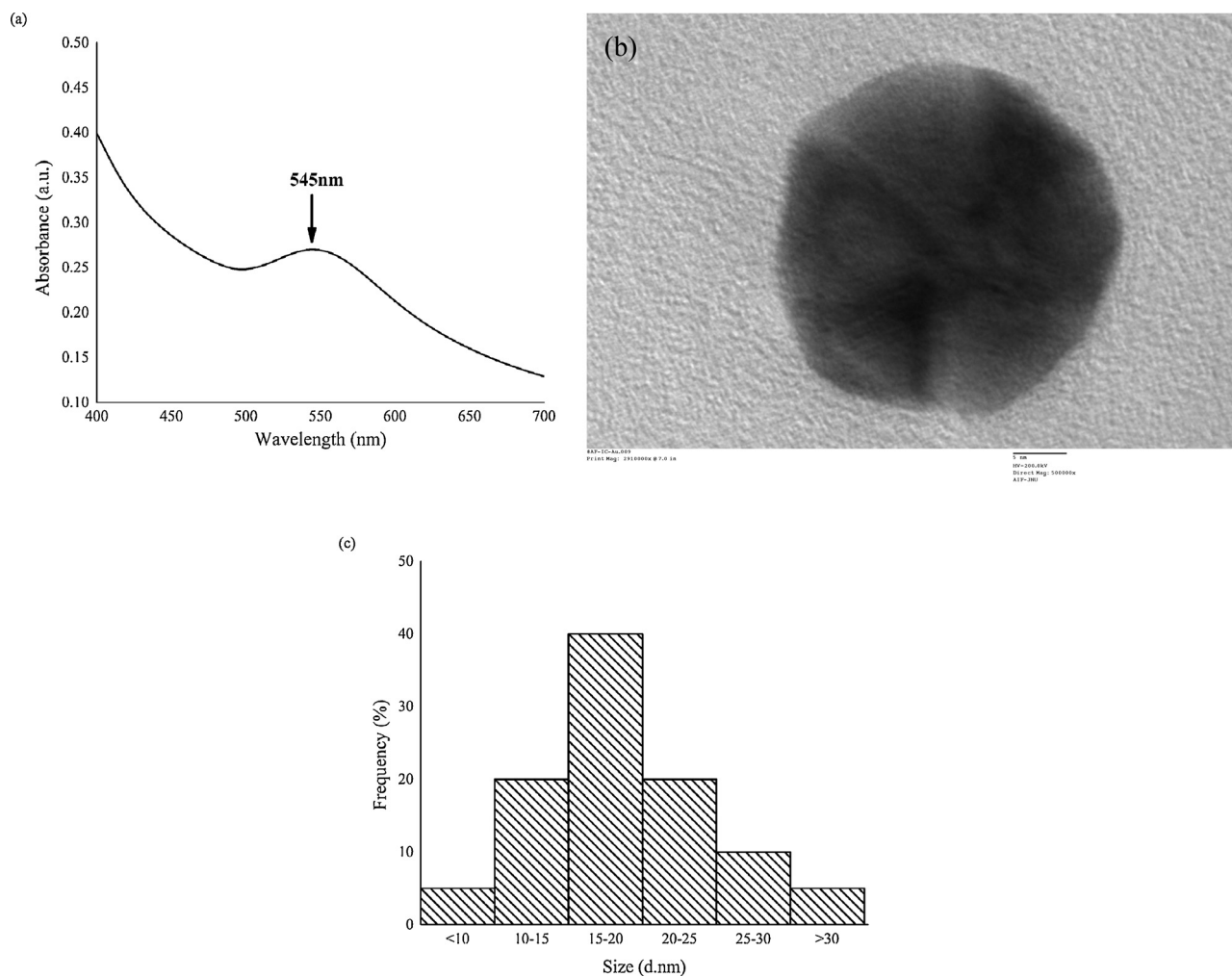
(a)

(b)

(c)

Fig. 5. (a) UV–vis spectra of Au NPs solution extracted from fungal biomass (b) HR-TEM micrograph of single Au NPs (Scale bar equivalent to 5 nm) (c) Particle size distribution histogram of Au NPs from TEM analysis.

Table 1
Bionanocatalyst mediated synthesis of propargylamine.

Entry	R	Product	1st Cycle		2nd Cycle		3rd Cycle	
			Time (h)	Yield (%)	Time (h)	Yield (%)	Time (h)	Yield (%)
1	H		24	89	34	67	52	42
2	CH₃		24	84	36	61	55	39
3	Cl		24	80	37	59	56	36

(a)

(b)
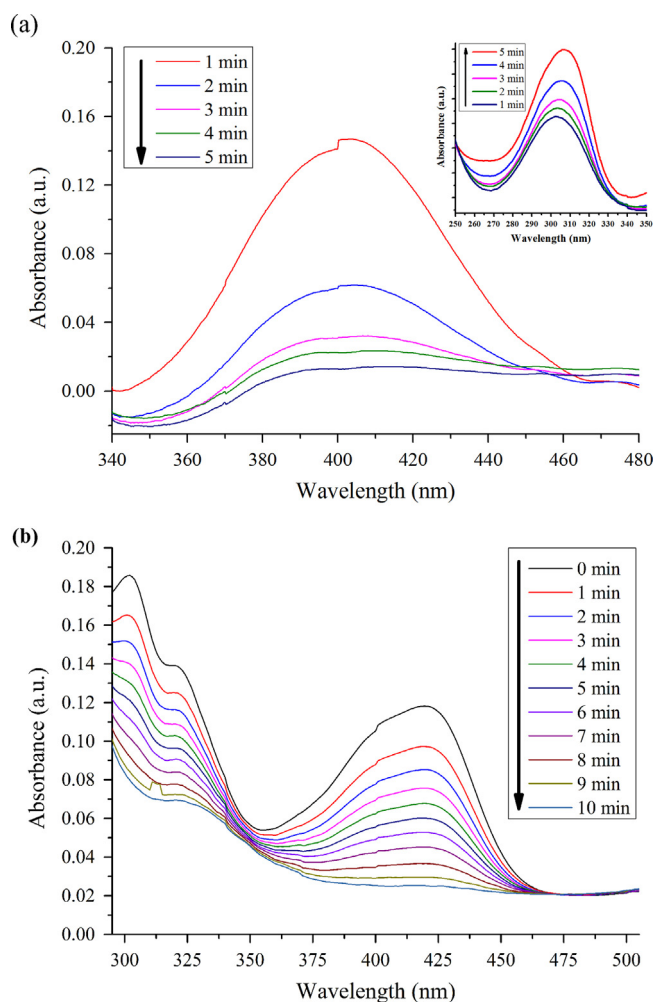
Fig. 6. (a) Reduction of 4-NP by NaBH$_4$ in presence of bionanocatalyst (Inset shows the gradual formation of 4-AP as a function of time) (b) Reduction of hexacyanoferrate(III) by NaBH$_4$ in presence of bionanocatalyst.

Considering the excellent results obtained in the above mentioned redox reactions, attempts were made to explore the catalytic ability of as-synthesized bionanocatalyst in more compelling reaction like A^3 coupling. The significance of A^3 coupling process can be realized by its potential for the synthesis of diverse heterocyclic frameworks due to its multi-component character [20]. Studies carried out using homogenous gold catalyst showed that ionic gold in the form of Au(I) and Au(III) oxidation state is predominantly responsible for the synthesis of propargylamines by A^3 coupling reaction [4,20]. In order to examine the possibility of using the as-synthesized bionanocatalyst which has Au(0) along with considerably less percentage of Au(I), synthesis of propargylamines was attempted (Scheme 1). The TLC analysis confirmed the synthesis of propargylamines. Table 1 represents the catalytic versatility of the bionanocatalyst wherein a variety of aromatic aldehydes (R = H, CH$_3$, Cl) were coupled with secondary amine and alkynes giving satisfactory yield within 24 h of reaction time. The ^{1}H NMR and MALDI-MS data of the synthesized derivatives were found to be in good agreement with those available in the literature and all the products were known compounds (see ESI). Similar to our observation Aguilar et al. [34] also speculated the strong role of Au(I) in the initiation of propargylamine synthesis reaction catalysed by gold nanoparticles. The remarkable catalytic performance of the bionanocatalyst as observed with yields over 80% of various propargylamine derivatives led us to examine the possibility of its
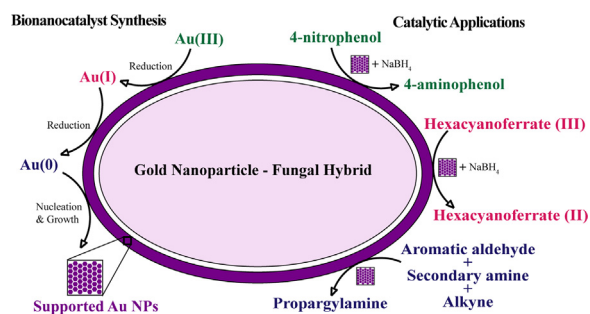

Fig. 7. Synthesis and catalytic applications of gold nanoparticle-fungal hybrid.

recyclability. The recovered bionanocatalyst was found to be successful in catalyzing these reactions repeatedly for two additional cycles however, a significant increase in the reaction time (first cycle: 48.60%; second cycle: 52.35%) with a decrease in the product yield (first cycle: 26.11%; second cycle: 37.45%) were observed with each subsequent cycle. Problems associated with gradual leaching of active gold species from the bionanocatalyst into the solution might have adversely influenced the repeated catalytic activity [35].

4. Conclusions

In conclusion, the present study demonstrates on-cell synthesis of Au NPs using a soil fungus *A. japonicus* AJP01. The attractiveness of the approach lies in its simplicity and one-step procedure for the synthesis of nanoparticle-fungal hybrid with strong catalytic activity. Another remarkable features of the synthesis is the dual role of fungal isolate in simultaneous synthesis and immobilization of Au NPs on its surface. The fungus successfully reduced Au(III) into Au NPs containing principally Au(0) with a small percentage of Au(I). The resulting nanoparticle-fungal hybrid exhibited the characteristic vivid purple colour. The as-synthesized bionanocatalyst was found to be highly efficient in carrying out NaBH$_4$ mediated reduction of 4-nitrophenol and hexacyanoferrate(III). The catalytic potential and robustness of the hybrid was further strengthened by successfully catalyzing the A^3 coupling reactions. This is the first report wherein a nanoparticle-fungal hybrid has been utilized for the synthesis of propargylamines with over 80% yield. The synthesis and catalytic applications of gold nanoparticle-fungal hybrid has been schematically presented in Fig. 7. Current investigations in our lab concentrate on the optimization of the reaction parameters to increase product yield and extend the recyclability. Besides the potential applications in heterogeneous catalysis, the present approach could be extended to check various other scientific applications like chemical and molecular sensing, bioremediation of heavy metals, anti-microbial activity and to synthesize other bio-nanocatalytic systems.

of Scientific and Industrial Research (File no.: 09/719(0062)/2013-EMR-I), Government of India for providing financial assistance in the form of Senior Research Fellowship.

Appendix A. Supplementary data

Supplementary data associated with this article can be found, in the online version, at doi:10.1016/j.procbio.2015.04.012

References

[1] Corti C, Holliday R. Commercial aspects of gold applications: from materials science to chemical science. Gold Bull (Geneva) 2004;37:20–6.
[2] Hashmi ASK, Hutchings GJ. Gold catalysis. Angew Chem Int Ed 2006;45:7896–936.
[3] Daniel M-C, Astruc D. Gold nanoparticles: assembly, supramolecular chemistry, quantum-size-related properties, and applications toward biology, catalysis, and nanotechnology. Chem Rev (Washington, DC, US) 2003;104:293–346.
[4] Zhang Y, Cui X, Shi F, Deng Y. Nano-gold catalysis in fine chemical synthesis. Chem Rev (Washington, DC, US) 2011;112:2467–505.
[5] Moshfegh AZ. Nanoparticle catalysts. J Phys D: Appl Phys 2009;42:233001.
[6] Bell AT. The impact of nanoscience on heterogeneous catalysis. Science 2003;299:1688–91.
[7] Berry V, Rangaswamy S, Saraf RF. Highly selective, electrically conductive monolayer of nanoparticles on live bacteria. Nano Lett 2004;4:939–42.
[8] Bigall NC, Reitzig M, Naumann W, Simon P, van Pée K-H, Eychmüller A. Fungal templates for noble-metal nanoparticles and their application in catalysis. Angew Chem Int Ed 2008;47:7876–9.
[9] Bennett JA, Creamer NJ, Deplanche K, Macaskie LE, Shannon IJ, Wood J. Palladium supported on bacterial biomass as a novel heterogeneous catalyst: a comparison of Pd/Al$_2$O$_3$ and bio-Pd in the hydrogenation of 2-pentyne. Chem Eng Sci 2010;65:282–90.
[10] Komeili A. Molecular mechanisms of magnetosome formation. Annu Rev Biochem 2007;76:351–66.
[11] Herves P, Perez-Lorenzo M, Liz-Marzan LM, Dzubiella J, Lu Y, Ballauff M. Catalysis by metallic nanoparticles in aqueous solution: model reactions. Chem Soc Rev 2012;41:5577–87.
[12] Stratakis M, Garcia H. Catalysis by supported gold nanoparticles: beyond aerobic oxidative processes. Chem Rev (Washington, DC, US) 2012;112:4469–506.
[13] Carregal-Romero S, Pérez-Juste J, Hervés P, Liz-Marzán LM, Mulvaney P. Colloidal gold-catalyzed reduction of ferrocyanate(III) by borohydride ions: a model system for redox catalysis. Langmuir 2009;26:1271–7.
[14] Sharma NC, Sahi SV, Nath S, Parsons JG, Gardea-Torresde JL, Pal T. Synthesis of plant-mediated gold nanoparticles and catalytic role of biomatrix-embedded nanomaterials. Environ Sci Technol 2007;41:5137–42.
[15] Skouta R, Li C-J. Gold-catalyzed reactions of C–H bonds. Tetrahedron 2008;64:4917–38.
[16] Kidwai M, Bansal V, Kumar A, Mozumdar S. The first Au-nanoparticles catalyzed green synthesis of propargylamines via a three-component coupling reaction of aldehyde, alkyne and amine. Green Chem 2007;9:742–5.
[17] Zhang X, Corma A. Supported gold(III) catalysts for highly efficient three-component coupling reactions. Angew Chem 2008;120:4430–3.
[18] Karimi B, Gholinejad M, Khorasani M. Highly efficient three-component coupling reaction catalyzed by gold nanoparticles supported on periodic mesoporous organosilica with ionic liquid framework. Chem Commun 2012;48:8961–3.
[19] Wei C, Li C-J. A highly efficient three-component coupling of aldehyde, alkyne, and amines via C–H activation catalyzed by gold in water. J Am Chem Soc 2003;125:9584–5.
[20] Peshkov VA, Pereshivko OP, Van der Eycken EV. A walk around the A3-coupling. Chem Soc Rev 2012;41:3790–807.
[21] Bhargava A, Jain N, Barathi LM, Akhtar MS, Yun Y-S, Panwar J. Synthesis, characterization and mechanistic insights of mycogenic iron oxide nanoparticles. J Nanopart Res 2013;15:1–12.
[22] Patterson AL. The Scherrer formula for X-ray particle size determination. Phys Rev 1939;56:978–82.
[23] Badwaik VD, Bartonojo JJ, Evans JW, Sahi SV, Willis CB, Dakshinamurthy R. Single-step biofriendly synthesis of surface modifiable, near-spherical gold nanoparticles for applications in biological detection and catalysis. Langmuir 2011;27:5549–54.
[24] Mukherjee P, Ahmad A, Mandal D, Senapati S, Sainkar SR, Khan MI, et al. Bioreduction of AuCl^{4-} ions by the fungus, Verticillium sp. and surface trapping of the gold nanoparticles formed. Angew Chem Int Ed 2001;40:3585–8.
[25] Lengke M, Sanpawanitchakit C, Southam G. Biosynthesis of gold nanoparticles: a review. In: Rai M, Duran N, editors. Metal nanoparticles in microbiology. Berlin: Springer; 2011. p. 37–74.
[26] Song JY, Jang H-K, Kim BS. Biological synthesis of gold nanoparticles using Magnolia kobus and Diopyros kaki leaf extracts. Process Biochem 2009;44:1133–8.
[27] Das SK, Liang J, Schmidt M, Laffir F, Marsili E. Biomineralization mechanism of gold by Zygomycete fungi Rhizopous oryzae. ACS Nano 2012;6:6165–73.
[28] Zhang YX, Zheng J, Gao G, Kong YF, Zhi X, Wang K, et al. Biosynthesis of gold nanoparticles using chloroplasts. Int J Nanomed 2011;6:2899.
[29] Polte J, Erler R, Thünemann AF, Sokolov S, Ahner TT, Rademann K, et al. Nucleation and growth of gold nanoparticles studied via in situ small angle X-ray scattering at millisecond time resolution. ACS Nano 2010;4:1076–82.
[30] Panigrahi S, Basu S, Praharaj S, Pande S, Jana S, Pal A, et al. Synthesis and size-selective catalysis by supported gold nanoparticles: study on heterogeneous and homogeneous catalytic process. J Phys Chem C 2007;111:4596–605.
[31] Gangula A, Podila RMR, Karanam L, Janardhana C, Rao AM. Catalytic reduction of 4-nitrophenol using biogenic gold and silver nanoparticles derived from Breynia rhamnoides. Langmuir 2011;27:15268–74.
[32] Pradhan N, Pal A, Pal T. Silver nanoparticle catalyzed reduction of aromatic nitro compounds. Colloids Surf A 2002;196:247–57.
[33] Narayanan KB, Sakthivel N. Synthesis and characterization of nano-gold composite using Cylindrocladium floridanum and its heterogeneous catalysis in the degradation of 4-nitrophenol. J Hazard Mater 2011;189:519–25.
[34] Aguilar D, Contel M, Urriolabeitia EP. Mechanistic insights into the one-pot synthesis of propargylamines from terminal alkynes and amines in chlorinated solvents catalyzed by gold compounds and nanoparticles. Chem—Eur J 2010;16:9287–96.
[35] Astruc D, Lu F, Aranzaes JR. Nanoparticles as recyclable catalysts: the frontier between homogeneous and heterogeneous catalysis. Angew Chem Int Ed 2005;44:7852–72.

Chapter VI

SYNTHESIS AND APPLICATION OF MAGNETIC NANOPARTICLES: A BIOLOGICAL PERSPECTIVE

Arpit Bhargava, Navin Jain and Jitendra Panwar*

Centre for Biotechnology, Department of Biological Sciences

Birla Institute of Technology & Science, Pilani-333 031

Corresponding author: Jitendra Panwar

E-mail: *drjitendrapanwar@yahoo.co.in;* *jpanwar@bits-pilani.ac.in*

ABSTRACT: The fast growing field of nanotechnology presents great potential to influence diverse areas like energy, environment, agriculture, healthcare and consumer goods and therefore building great expectations not only in the academic community but also among investors, governments and industries. This chapter deals with most recent advances in the biogenic synthesis and biological applications of magnetic iron nanoparticles [MINPs]. Owing to the limitations and drawbacks of physiochemical methods of MINP synthesis, considerable interest has been generated in biogenic synthesis methods as the later being eco-friendly and cost effective. Magnetotactic bacteria [MTB] represent a fascinating example of biologically controlled mineralization forming MINPs in the form of magnetosomes. Progress in the biological methods can be realized with the number of reports coming in the past decade on MINP synthesis using bacteria, fungi and plants. The later section of the chapter discusses various biological applications of MINPs viz. in separations of biomolecules and cells, detection and diagnostics, imaging, hyperthermia, drug and therapeutic delivery, nucleic acid delivery and transfer, cell manipulation and tissue engineering and in agriculture. Further, the chapter evaluates the advantages of biosynthesized MINPs over commercially available ones and finally concludes with the possible directions of future research in this field.

Chapter 4
Nano-fertilizers and Their Smart Delivery System

Priyanka Solanki, Arpit Bhargava, Hemraj Chhipa, Navin Jain, and Jitendra Panwar

Abstract Outburst of world population in the past decade has forced the agricultural sector to increase crop productivity to satisfy the needs of billions of people especially in developing countries. Widespread existence of nutrient deficiency in soils has resulted in great economic loss for farmers and significant decreases in nutritional quality and overall quantity of grains for human beings and livestock. Use of large-scale application of chemical fertilizers to increase the crop productivity is not a suitable option for long run because the chemical fertilizers are considered as double-edged swords, which on the one hand increase the crop production but on the other hand disturb the soil mineral balance and decrease soil fertility. Large-scale application of chemical fertilizers results in an irreparable damage to the soil structure, mineral cycles, soil microbial flora, plants, and even more on the food chains across ecosystems leading to heritable mutations in future generations of consumers.

In recent years, nanotechnology has extended its relevance in plant science and agriculture. Advancement in nanotechnology has improved ways for large-scale production of nanoparticles of physiologically important metals, which are now used to improve fertilizer formulations for increased uptake in plant cells and by minimizing nutrient loss. Nanoparticles have high surface area, sorption capacity, and controlled-release kinetics to targeted sites making them "smart delivery system." Nanostructured fertilizers can increase the nutrient use efficiency through mechanisms such as targeted delivery, slow or controlled release. They could precisely release their active ingredients in responding to environmental triggers and biological demands. In recent lab scale investigations, it has been reported that nano-fertilizers can improve crop productivity by enhancing the rate of seed germination, seedling growth, photosynthetic activity, nitrogen metabolism, and carbohydrate and protein synthesis. However, as being an infant technology, the ethical and safety issues surrounding the use of nanoparticles in plant productivity are limitless and must be very carefully evaluated before adapting the use of the so-called nano-fertilizers in agricultural fields.

P. Solanki • A. Bhargava • H. Chhipa • N. Jain • J. Panwar (✉)
Department of Biological Sciences, Centre for Biotechnology, Birla Institute of Technology and Science, Pilani 333031, India
e-mail: drjitendrapanwar@yahoo.co.in

81

Extracellular biosynthesis and characterization of silver nanoparticles using *Aspergillus flavus* NJP08: A mechanism perspective

Navin Jain,[a] Arpit Bhargava,[a] Sonali Majumdar,[a] J. C. Tarafdar[b] and Jitendra Panwar[*a]

The present study demonstrates an eco-friendly and low cost protocol for synthesis of silver nanoparticles using the cell-free filtrate of *Aspergillus flavus* NJP08 when supplied with aqueous silver (Ag^+) ions. Identification of the fungal isolate was based on nuclear ribosomal DNA internal transcribed spacer (ITS) identities. Transmission electron microscopy (TEM) and energy dispersive spectroscopy (EDS) revealed the formation of spherical metallic silver nanoparticles. The average particle size calculated using Dynamic Light Scattering measurements (DLS) was found to be 17 ± 5.9 nm. UV-Visible and Fourier transform infrared (FTIR) spectroscopy confirmed the presence of extracellular proteins. SDS-PAGE profiles of the extracellular proteins showed the presence of two intense bands of 32 and 35 kDa, responsible for the synthesis and stability of silver nanoparticles, respectively. A probable mechanism behind the biosynthesis is discussed, which leads to the possibility of using the present protocol in future "nano-factories".

Introduction

Nanotechnology has now started leaving the confines of laboratories; and conquering new applications to change our lives. Nanoparticles possess increased structural integrity as well as unique chemical, optical, mechanical, electronic and magnetic properties compared to large particles of bulk materials.[1] These unique properties are derived due to variations in specific characteristics such as size, distribution and structure of particles. Due to these incredible properties, nanoparticles have become significant in recent years and nano-products are coming to the market rapidly. The fast growing field of nanotechnology presents great potential to influence various sectors in the areas of energy, environment, agriculture, healthcare and consumer goods. Therefore, it has built great expectations not only in the academic community but also among the investors, governments, and industries. According to estimates, the worldwide nano product market is estimated to reach $1 trillion by the year 2015.[2] To compete with this tremendous demand, the synthesis of nanomaterials of specific composition, shape and size is a burgeoning area of research in the field of nanotechnology.

Among various metals, silver has been known since ancient times as effective antimicrobial agent for the treatment of diseases, for food preservation and keep water safe.[3] With the recent advancements in the field of nanotechnology, silver nanoparticles have been widely used as a novel therapeutic agent extending their use as antibacterial, antifungal, antiviral, anti-inflammatory and anti-cancerous agents. The broad-spectrum antimicrobial properties of silver nanoparticles encourage its use in a large number of biomedical and environmental applications as well as in growing list of cosmetics, clothing and numerous consumer products.[4,5]

Conventional synthesis of silver nanoparticles involves a number of chemical and physical methods including chemical reduction in aqueous or non-aqueous solution,[6] microemulsion,[7] template,[8] sonochemical,[9] and microwave-assisted[10] methods. However, all these methods are energy and capital intensive, employ toxic chemicals, and often yield particles in non-polar organic solutions, thus precluding their biomedical applications. Thus the need for the development of clean, reliable, biocompatible and benign processes to synthesize nanoparticles leads to turning of more and more researchers to exploit biological systems as possible eco-friendly "nano-factories".

It is well known that the biological systems can provide a number of metal or metal-containing particles in the nanometre range. Thus, they can be seen as a nanophase system in their own right and as the starting point for producing other novel nanophase systems. Biological methods for nanoparticle synthesis would help circumvent many of the detrimental features by enabling synthesis at mild pH, pressure and temperature and at a substantially lower cost. A number of micro-organisms have been found to be capable of synthesizing inorganic nano-composites either intra- or extracellularly. These include magnetotactic bacteria,[11,12] silica deposits by diatoms,[13] and gypsum and calcium layers by S-layer bacteria.[14] The secrets gleaned from nature combined with academic and scientific curiosity have led to the development of biomimetic approaches for the synthesis of nanoparticles.

Whilst various studies have been commenced on identification of microorganisms as possible nanofactories,[15] very little work has been conducted on the actual mechanisms of nanoparticle formation in microorganisms. The defensive mechanism of cells for silver detoxification has been suggested as a biological pathway for the synthesis of silver nanoparticles.[16] Ahmad *et al.* had shown that NADH-dependent enzymes are responsible for the biosynthesis of nanoparticles.[17] The reduction mechanism

[a]Centre for Biotechnology, Department of Biological Sciences, Birla Institute of Technology and Science, Pilani, Rajasthan, 333031, India. E-mail: drjitendrapanwar@yahoo.co.in; Fax: +911596244183; Tel: +919414411654
[b]Central Arid Zone Research Institute, Jodhpur, Rajasthan, 342003, India

ENVIRONMENTAL BIOTECHNOLOGY

A biomimetic approach towards synthesis of zinc oxide nanoparticles

Navin Jain · Arpit Bhargava · Jagadish C. Tarafdar ·
Sunil K. Singh · Jitendra Panwar

Abstract Using natural processes as inspiration, the present study demonstrates a positive correlation between zinc metal tolerance ability of a soil fungus and its potential for the synthesis of zinc oxide (ZnO) nanoparticles. A total of 19 fungal cultures were isolated from the rhizospheric soils of plants naturally growing at a zinc mine area in India and identified on the genus, respectively the species level. *Aspergillus aeneus* isolate NJP12 has been shown to have a high zinc metal tolerance ability and a potential for extracellular synthesis of ZnO nanoparticles under ambient conditions. UV–visible spectroscopy, Fourier transform infrared spectroscopy, X-ray diffraction analysis, transmission electron microscopy, and energy dispersive spectroscopy studies further confirmed the crystallinity, morphology, and composition of synthesized ZnO nanoparticles. The results revealed the synthesis of spherical nanoparticles coated with protein molecules which served as stabilizing agents. Investigations on the role of fungal extracellular proteins in the synthesis of nanoparticles indicated that the process is nonenzymatic but involves amino acids present in the protein chains.

Keywords Biomimetics · ZnO nanoparticles · Rhizosphere · Soil fungi · Metal tolerance · *Aspergillus*

N. Jain · A. Bhargava · J. Panwar (✉)
Centre for Biotechnology, Department of Biological Sciences,
Birla Institute of Technology and Science,
Pilani, India
e-mail: drjitendrapanwar@yahoo.co.in

J. C. Tarafdar · S. K. Singh
Central Arid Zone Research Institute,
Jodhpur, India

Introduction

Nature is considered as a school for material science and its associated disciplines such as chemistry, biology, physics, or engineering (Bensaude-Vincent et al. 2002). An assortment of biological entities serves as the fundamental base for solving a variety of challenges in the field of architecture, aerodynamics, and mechanical engineering, as well as in material science (Fratzl 2007). Biology is considered as the master of so-called bottom-up fabrication which includes building up nanostructures starting from basic atoms or molecules (Naik and Stone 2005). Biological systems serve as prominent source of inspiration due to their remarkable variety of complex structures and functions which confer a huge impact on material science since several decades. Some examples of natural amalgams include crustacean's carapaces, mollusk shells, bone, and tooth tissues in vertebrates (Sanchez et al. 2005). A number of single-celled organisms also produce inorganic materials of nanometer range intra- and/or extracellulary. Common examples include magnetotactic bacteria which synthesize magnetite (Lovley et al. 1987); diatoms which synthesize siliceous materials (Kröger et al. 1999), S-layer forming bacteria (Pum and Sleytr 1999), etc. These structures are highly controlled, range from macroscopic to nanometer scale, and result in intricate architectures that provide multifunctional properties.

Taking inspiration from these natural biological systems, recently, biologists were able to develop an alternative strategy for nanoparticle synthesis using microorganisms. A landmark study by Klaus et al. (1999) established an interface between material science and biological systems. They reported the synthesis of crystalline silver nanoparticles of well-defined composition and shapes using *Pseudomonas stutzeri* isolated from a silver mine. The nanoparticles were

Enhanced photocatalytic degradation of methylene blue using biologically synthesized "protein-capped" ZnO nanoparticles

Navin Jain, Aprit Bhargava, Jitendra Panwar *

Centre for Biotechnology, Department of Biological Sciences, Birla Institute of Technology and Science, Pilani 333 031, India

HIGHLIGHTS

- One pot synthesis & surface modification of ZnO nanoparticles at ambient conditions.
- Simple, low-cost & eco-friendly protocol with potential for mass scale production.
- Superior photocatalytic performance of protein-capped ZnO nanoparticles.
- Surface proteins act as an effectual host and facilitates dye absorption.
- Low recombination rate of the e^-/h^+ pairs.

ARTICLE INFO

ABSTRACT

Using the extracellular fungal proteins, a low cost and eco-friendly synthesis of zinc oxide nanoparticles has been demonstrated in aqueous solvent system. The obtained nanoparticles were characterized by transmission electron microscopy (TEM), energy dispersive X-ray spectroscopy (EDS), UV–visible spectroscopy and powder X-ray diffraction (XRD) measurements. The as-synthesized particles were quasi-spherical, symmetrical, polydisperse and well distributed without any aggregation with size predominantly ranging between 80 and 120 nm. Photoluminescence (PL) and fourier-transform infrared (FT-IR) spectroscopy studies revealed that nanoparticles were individually coated with protein molecules that may act as stabilizing agents. Photocatalytic studies for the degradation of methylene blue dye under UV irradiation revealed extremely high photocatalytic activity of protein-capped ZnO nanoparticles (nearly 90% degradation in 30 min) which clearly outperformed commercial bare ZnO nanoparticles (nearly 40% degradation in 30 min) under the same conditions. The remarkable photocatalytic performance originated mainly due to the presence of surface proteins which act as an effectual host for methylene blue dye and facilitates absorption of dye along with low recombination rate of the e^-/h^+ pairs. The low cost, simplicity and eco-friendly nature of the present protocol for "one-pot" synthesis and modification of ZnO nanoparticles could be extended to synthesize other metal nanoparticles thus expanding its applicability in various fields.

© 2013 Elsevier B.V. All rights reserved.

1. Introduction

Industrial effluents have long been a major concern among the environmental protection issues and considered as a potential threat. Organic dyes have received particular attention as prominent environmental contaminants owing to their non-biodegradability and carcinogenic effects on humans. Moreover, they drastically affect the nature of water, inhibit sunlight penetration and reduce photosynthesis resulting in severe toxicity to aquatic creatures [1,2]. Semiconductor based photocatalytic oxidation have attracted great attention for solving many current environmental issues especially removal of dye pollutants from water [3–6]. The approach is highly advantageous as it does not yield toxic intermediate products, making it suitable for cleaning polluted water bodies that contains low to medium concentration of contaminants. Various semiconductors such as TiO_2 ($E_g = 3.2$ eV), ZnO ($E_g = 3.4$ eV), ZnS ($E_g = 3.6$ eV), WO_3 ($E_g = 2.8$ eV) and $SrTiO_3$ ($E_g = 3.2$ eV) have been widely implemented as promising candidates for the photocatalytic degradation reactions.

Although TiO_2 has been universally recognized as the most efficient photocatalyst, recent reports have highlighted the effectiveness of ZnO in removing organic compounds from water matrices [7,8]. In particular, ZnO in nanoparticle regime has appeared to

* Corresponding author. Tel.: +91 1596 515250; fax: +91 1596 244183.
E-mail address: drjitendrapanwar@yahoo.co.in (J. Panwar).
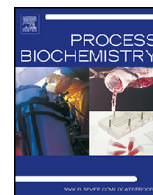
Unveiling the potential of metal-tolerant fungi for efficient enzyme production

Navin Jain, Arpit Bhargava, Debabrat Sabat, Jitendra Panwar*

Centre for Biotechnology, Department of Biological Sciences, Birla Institute of Technology and Science, Pilani 333031, India

ABSTRACT

The present study first time reports the utilization of metal tolerant fungi as a potential source for efficient enzyme production. The purification and characterization of alkaline protease from an indigenous zinc-metal tolerant fungal isolate *Aspergillus flavus* NJP08 has been demonstrated. The specific activity of enzyme was determined as $89.1 \, U \, mg^{-1}$ which is found to be the highest among the reported *Aspergillus flavus* isolates so far. The protease was purified 55.87 fold up to homogeneity and identified as "alkaline protease" with a molecular mass of 33 kDa. The N-terminal sequence was GLTTQKSAPWGLG which showed high similarity with other reported proteases of genus *Aspergillus*. Physico-chemical characterization of enzyme revealed an estimated half-life of >20 h with aliphatic and GRAVY index values of 79.65 and −0.161 respectively, depicting high thermo-stability and secretory nature of protease. The protease was active within the temperature range of 25–50 °C with an optimum temperature of 50 °C and was stable in the pH range of 6.0–11.0. The enzyme was activated by Ca^{2+} and Fe^{2+} ions, partially inhibited by Cu^{2+} ions and strongly inhibited by PMSF. High enzyme stability in presence of various detergents further strengthens enzyme applicability in industrial applications.

© 2014 Elsevier Ltd. All rights reserved.

1. Introduction

Proteases (E.C.3.4.21) are one of the three largest groups of commercial enzymes accounting approximately up to two-third share of the worldwide industrial enzyme market [1]. Among proteases, alkaline proteases are of immense economic importance as they can withstand high temperature, pH, non-aqueous and denaturing conditions. They are widely used in laundry and dish washing detergent, cosmetics and food processing with expanding research applications in diagnostic reagents, peptide synthesis and synthetic organic chemistry [2]. The protease activity affected severely by various factors such as pH, temperature, surfactants, bleach systems, and mechanical handling that eventually determine its stability.

Alkaline proteases can be obtained from a wide range of sources such as animals, plants and microorganisms (bacteria, moulds, yeasts) as well as mammalian tissues. However, from a commercial perspective, high enzyme yield and economical downstream processing are highly desirable. To compensate the industrial demand for an alkaline protease possessing properties to overcome these challenges, there is a constant need to search for new enzyme sources. In this regard, microorganisms remain the preferred choice due to high yield of purified proteases and their wide range of biochemical and catalytic properties [3]. At present, a major proportion of commercially available alkaline proteases are derived from *Bacillus* strains, although the potential of using fungi as a promising alternative is now being progressively comprehended [3,4]. Fungi are an attractive source of proteases due to their inexpensive cultivation, ease of handling and suitability for genetic manipulation. Moreover, fungi are capable to grow on economical media and often secrete bulk quantities of enzymes which offer convenient downstream processing [5–7]. Filamentous fungi have received particular attention owing to their highly diverse biochemical and enzyme systems that empowers them to survive in extreme and diverse habitats. Among filamentous fungi, genus *Aspergillus* has been recognized as one of the dominant and economically important group of fungi. Previously, we reported an abundance of the genus *Aspergillus* in zinc metal rich regions of

Removal of Protein Capping Enhances the Antibacterial Efficiency of Biosynthesized Silver Nanoparticles

Navin Jain, Arpit Bhargava, Mohit Rathi, R. Venkataramana Dilip, Jitendra Panwar*

Centre for Biotechnology, Department of Biological Sciences, Birla Institute of Technology and Science, Pilani, 333 031, India

* drjitendrapanwar@yahoo.co.in

Abstract

The present study demonstrates an economical and environmental affable approach for the synthesis of "protein-capped" silver nanoparticles in aqueous solvent system. A variety of standard techniques viz. UV-visible spectroscopy, transmission electron microscopy (TEM), energy dispersive spectroscopy (EDS) and X-ray diffraction (XRD) measurements were employed to characterize the shape, size and composition of nanoparticles. The synthesized nanoparticles were found to be homogenous, spherical, mono-dispersed and covered with multi-layered protein shell. In order to prepare bare silver nanoparticles, the protein shell was removed from biogenic nanoparticles as confirmed by UV-visible spectroscopy, FTIR and photoluminescence analysis. Subsequently, the antibacterial efficacy of protein-capped and bare silver nanoparticles was compared by bacterial growth rate and minimum inhibitory concentration assay. The results revealed that bare nanoparticles were more effective as compared to the protein-capped silver nanoparticles with varying antibacterial potential against the tested Gram positive and negative bacterial species. Mechanistic studies based on ROS generation and membrane damage suggested that protein-capped and bare silver nanoparticles demonstrate distinct mode of action. These findings were strengthened by the TEM imaging along with silver ion release measurements using inductively coupled plasma atomic emission spectroscopy (ICP-AES). In conclusion, our results illustrate that presence of protein shell on silver nanoparticles can decrease their bactericidal effects. These findings open new avenues for surface modifications of nanoparticles to modulate and enhance their functional properties.

Introduction

Over the past few years, worldwide escalation and augmentation of multi-drug resistance in microorganisms has been a serious concern for modern medicine [1–5]. The need for the development of new, low cost and effective antimicrobial agents independent of bacterialresistance has revived the interest of scientific community to explore the antimicrobial properties of